

ABSTRACT

SHEN, FEI. Affinity Interaction between Hexamer Peptide Ligand HWRGWV and Immunoglobulin G Studied by Quartz Crystal Microbalance and Surface Plasmon Resonance. (Under the direction of Dr. Ruben G. Carbonell.)

Immunoglobulins (Ig), also referred to as antibodies, act as protective agents against pathogens trying to invade an organism. Human immunoglobulin G (hIgG), as the most prominent immunoglobulin presented in serum and other human fluids, has broad applications in fields like immunotherapy and clinical diagnostics. *Staphylococcus aureus* Protein A and *Streptococcus* Protein G are the most common affinity ligands for IgG purification and detection. However, drawbacks associated with these two protein ligands have motivated searches for alternative affinity ligands. The hexamer peptide ligand HWRGWV identified from a one-bead-one-peptide combinatorial library synthesized on chromatography resins has demonstrated high affinity and specificity to the Fc fragment of hIgG. A chromatography resin with HWRGWV can purify human IgG (hIgG) from complete minimum essential medium (cMEM) with purities and yields as high as 95%, which are comparable to using Protein A as affinity ligand (4). As a short peptide ligand, HWRGWV can be produced at relatively low costs under good manufacturing practices (GMP) conditions, it is highly robust, less immunogenic and allows for milder elution conditions for the bound antibody (3, 5). Although this short peptide ligand has exhibited promising properties for IgG capture and purification, limited information is available on the intrinsic mechanisms of affinity interaction between the peptide ligand and target protein.

In this study, the affinity interaction between hIgG and peptide ligand immobilized on solid surfaces was studied by quartz crystal microbalance (QCM) and surface plasmon

resonance (SPR). Compared with previous methods employed for the peptide characterization, QCM and SPR can provide direct measurements of equilibrium adsorption isotherms and rates of adsorption, allowing a complete kinetic and thermodynamics analyses of the ligand-target interactions.

New methods were developed to modify gold and silica surfaces of QCM and SPR sensors for the immobilization of peptide ligands with low nonspecific binding. The silica surface was first modified by the formation of self-assembling monolayer (SAM) of 3-amino-propyl triethoxy silane as an anchor layer. Short chains of poly(ethylene glycol) (PEG) with Fmoc-protected amino groups at one end and carboxyl groups at the other end were then coupled through the carboxyl terminal to the amino groups on the silane. The short PEG chains served as spacer arms to reduce nonspecific binding to the substrate. The gold surface was modified by a two-component SAM using mixtures of $\text{HS}(\text{CH}_2)_{11}(\text{CH}_2\text{CH}_2\text{O})_6\text{NH}_2$ and $\text{HS}(\text{CH}_2)_{11}(\text{CH}_2\text{CH}_2\text{O})_3\text{OH}$. The advantage of using a modified silica surface is its relatively higher stability than the SAM on gold during the peptide functionalization step, however the SPR sensors do not work on silica surfaces. In addition, the modification process of the gold surface is relatively simple compared with that of the silica surface. The peptide immobilization process was optimized with silica surfaces and the best conditions were applied for the immobilization on gold surfaces. The results of surface modifications and peptide immobilizations were characterized by various surface analysis techniques including, ellipsometry, contact angle goniometer, chemical force microscopy (CFM), x-ray photoelectron spectroscopy (XPS) and time of flight secondary ion mass spectroscopy (ToF-SIMS).

QCM and SPR results indicated that this peptide ligand HWRGWV immobilized on modified silica or gold surfaces has high affinity and specificity to hIgG binding even in a complex medium such as cMEM. Both thermodynamic and kinetic parameters of affinity interaction were obtained by the analysis of QCM and SPR data. Compared with QCM, SPR is more suitable for quantitative analysis of the protein binding, which is essential for the investigation of thermodynamics and kinetics parameters. The maximum binding capacity (4.15 mg m^{-2}) and the dissociation constant ($1.83 \text{ }\mu\text{M}$) derived from SPR data are both close to those obtained with chromatography techniques. The association and dissociation rate constants ($0.68 \text{ m}^3 \text{ mol}^{-1} \text{ s}^{-1}$ and 1.24 s^{-1} respectively) were acquired for the first time for the affinity binding of IgG on peptide ligand HWRGWV functionalized surface. Although QCM is not as quantitative as SPR, it provides additional information on the status of the adsorbed layers. For instance, the dissipation measurement of QCM indicated that no significant denaturation of adsorbed hIgG occurred during the adsorption process. In addition, it was shown that the peptide ligand immobilized on modified silica surfaces has similar affinity and binding characteristics for IgG adsorption as on modified gold surfaces.

In summary, new surface modification strategies were developed to study the affinity interaction between peptide ligands and target biomolecules. The use of Fc-specific binding peptides on QCM and SPR sensors could result in new devices for IgG concentration determination and also have promise as platforms for the development of immunosensors.

Affinity Interaction between Hexamer Peptide Ligand HWRGWV and Immunoglobulin G
Studied by Quartz Crystal Microbalance and Surface Plasmon Resonance

by
Fei Shen

A dissertation submitted to the Graduate Faculty of
North Carolina State University
in partial fulfillment of the
requirements for the Degree of
Doctor of Philosophy

Chemical Engineering

Raleigh, North Carolina

2010

APPROVED BY:

Dr. Ruben G. Carbonell
(Chair of Advisory Committee)

Dr. Orlando Rojas

Dr. Jan Genzer

Dr. Jason M. Haugh

BIOGRAPHY

Fei Shen was born on May 6th, 1979 in Maanshan, Anhui Province, China, as the second child of Liangfu Shen and Guixiang Cheng. She attended elementary and high school at her hometown. In 1996, she enrolled in the School of Chemical Engineering Technology of Tianjin University and obtained the Bachelor's and Master's Degree in biochemical engineering in 2000 and 2003 respectively.

In 2004, she started her Ph.D. study in the Chemical and Biomolecular Engineering Department at North Carolina State University. One year later, she joined the bio-separation group under the direction of Dr. Ruben G. Carbonell.

ACKNOWLEDGEMENTS

A doctoral research topic should be novel, non-trivial and useful. Successfully defining, solving and presenting an understandable solution to such a research topic constitutes the accomplishments of one's research journey. There would not be such accomplishments of my research journey as a Ph.D. student without the people who supported and helped me in the past few years.

First of all, I would like to express my sincere appreciation to my advisor Dr. Carbonell. He has been always supportive and considerate through my research and studies. Influenced by his enthusiasm and sharpness for this research, I have found my research challenging yet enjoyable.

I want to thank Dr. Rojas and Dr. Genzer for providing a good working environment with equipment with which I could conduct my experiments very effectively. Their insightful discussions on my research ideas are also highly appreciated. I would also thank Dr. Haugh for his valuable comments and feedback on my work.

Special thanks also to Dr. Patrick Gurgel for all his support, encouragement, advisory discussions and help in every aspect of my PhD studies.

I would like to thank the Bioseparations Group members, Dr. Rojas' research group members and Dr. Genzer's research group members for their kindness, friendship, generous help, invaluable discussion, and the happy collaborative working environment they provided. In addition, appreciation is also expressed to Carol Carroll, Peggy Wilkins, Sandra Bailey and Ena Meng, for their help and compassion.

I wish to thank the financial support of Tosoh Bioscience, LLC, the William R. Kenan Jr. Institute for Engineering, Technology & Science at NC State, and ProMetic Biosciences, Ltd.

Last but not the least, I want to thank my husband, parents and my sister for their unconditional love, endless encouragement and support.

3.2.2	Preparation of substrates.....	50
3.2.3	Surface modification.....	51
3.2.4	Ellipsometric film thickness measurements.....	52
3.2.5	Contact-angle measurements and contact-angle titrations.....	53
3.2.6	Time of flight secondary ion mass spectroscopy.....	53
3.2.7	Quartz crystal microbalance (QCM).....	54
3.3	Results and Discussion.....	56
3.3.1	Modification of silica surface.....	56
3.3.2	Characterization of the modified silica surfaces by ToF-SIMS.....	58
3.3.3	Determination of the pKa of amine groups on surface by contact angle titration	60
3.3.4	Measurement of nonspecific protein adsorption by QCM.....	62
3.4	Conclusion.....	63
	References.....	64
	Appendix 3-1 Principle of ToF-SIMS.....	79
	Appendix 3-2 ToF-SIMS spectra around m/z 28.....	81

CHAPTER 4. STUDY OF THE AFFINITY INTERACTION BETWEEN HEXAMER PEPTIDE HWRGWV IMMOBILIZED ON MODIFIED SILICA SURFACE AND HUMAN IMMUNOGLOBULIN G BY QUARTZ CRYSTAL MICROBALANCE.....83

4.1	Introduction.....	85
4.2	Materials and methods.....	89
4.2.1	Materials.....	89
4.2.2	Surface modification.....	90
4.2.3	Peptide immobilization and protection group deprotection.....	90
4.2.4	Film-thickness measurements by ellipsometry.....	92
4.2.5	Time of flight secondary ion mass spectroscopy.....	93
4.2.6	Quartz crystal microbalance experiments and data analysis.....	94
4.3	Results and discussion.....	98
4.3.1	Grafting of peptide on modified silica surface.....	98
4.3.2	Characterization of the modified surfaces with ToF-SIMS.....	103
4.3.3	Study the affinity interaction between peptide ligand and hIgG by QCM.....	106
4.3.4	Kinetics analysis of QCM data.....	111
4.3.5	The effects of PEG spacer arm on the affinity interaction between peptide ligand and IgG.....	113
4.3.6	Dissipation analysis.....	115
4.4	Conclusions.....	116

Reference.....	117
----------------	-----

CHAPTER 5: FORMATION AND CHARACTERIZATION OF SELF-ASSEMBLED MONOLAYERS OF THIOLATE CONTAINING OLIGO(ETHYLENE GLYCOL) AND TERMINATED WITH AMINE GROUPS ON GOLD.....138

5.1 Introduction.....	140
5.2 Materials and methods.....	142
5.2.1 Materials.....	142
5.2.2 Formation of SAMs.....	142
5.2.3 Contact angle measurement.....	143
5.2.4 Chemical force microscopy experiments.....	143
5.2.5 X-ray spectroscopy experiments.....	144
5.2.6 Measurement of amine group density by radiolabeling method.....	144
5.3 Results and discussion.....	145
5.3.1 Formation of pure SAMs of EG ₆ NH ₂ and EG ₃ OH.....	145
5.3.2 Formation of mixed SAM of EG ₆ NH ₂ and EG ₃ OH.....	153
5.4 Conclusions.....	158
References.....	158
Appendix 5-1 The application and operation mode of AFM.....	170

CHAPTER 6. A FINITY INTERACTION BETWEEN HEXAMER PEPTIDE HWRGWV IMMOBILIZED ON GOLD SURFACE WITH HUMAN IMMUNOGLOBULIN G BY QUARTZ CRYSTAL MICROBALANCE AND SURFACE PLASMON RESONACE.....173

6.1 Introduction.....	175
6.2 Materials and methods.....	178
6.2.1 Materials.....	178
6.2.2 Formation of SAM of HS(CH ₂) ₁₁ (CH ₂ CH ₂ O) ₆ NH ₂	179
6.2.3 Stability of SAM under peptide immobilization and protection group deprotection conditions.....	180
6.2.4 Peptide immobilization and Fmoc Group deprotection.....	180
6.2.5 Characterization of the modified gold surface by XPS.....	181
6.2.6 Characterization of the modified gold surface by ToF-SIMS.....	182
6.2.7 Study of the affinity interaction between peptide ligand and hIgG by SPR..	182
6.2.8 Study of the affinity Interaction between peptide ligand and hIgG by QCM	187
6.2.9 Regeneration of SPR sensor online.....	188

6.3	Results and discussion.....	189
6.3.1	Immobilization of peptide on SAM of HS(CH ₂) ₁₁ (CH ₂ CH ₂ O) ₆ NH ₂	189
6.3.2	Study the protein adsorption on the modified surface with and without peptide by SPR and QCM.....	196
6.3.3	The application of peptide functionalized SPR sensor for IgG concentration determination.....	204
6.4	Conclusions.....	205
	References.....	206

CHAPTER 7. CONCLUSIONS AND RECOMMENDATIONS FOR FUTURE WORK.....228

7.1	Conclusions.....	229
7.1.1	Modification of Silica.....	229
7.1.2	Study the affinity interaction between peptide ligand HWRGWV immobilized on silica surface and immunoglobulin G (IgG) by QCM.....	229
7.1.3	Modification of gold surface.....	230
7.1.4	Study the affinity interaction between peptide ligand HWRGWV immobilized on gold surface and IgG by QCM and SPR.....	231
7.2	Recommendations for future work.....	232
7.2.1	Characterization of the peptide ligands.....	232
7.2.2	Application of the biosensor functionalized with Fc-specific binding peptide ligand.....	233
7.2.3	Application of the methodology developed in this study for the study of other peptide ligand.....	235
	References.....	235

LIST OF TABLES

Table 2.1 Comparison of QCM and SPR.....	42
Table 3.1 Thickness and contact angle measurements of modified silica surface.....	70
Table 3.2 Positive and negative ion detection mode SIMS peaks of modified silica surfaces.....	71
Table 3.3 Apparent dissociation constant and maximum capacity of the BSA adsorption on modified silica surface APTES-PEG ₃ -NH ₂	72
Table 4.1 Effect of coupling reagent and peptide concentrations on peptide immobilization density.....	126
Table 4.2 Effect of side-chain protection on peptide density.....	127
Table 4.3 Apparent dissociation constant and maximum binding capacity of the BSA and hIgG adsorption on modified silica surface APTES-PEG ₃ -NH ₂ and APTES-PEG ₃ -NH-HWRGWV-NH ₂	127
Table 4.4 Association rates and dissociation rates of hIgG adsorption on silica surface functionalized with peptide ligands.....	127
Table 4.5 Dependence of estimated association rates on the association rates on the transfer coefficient k_m value.....	128
Table 5.1 Hansen solubility parameter (HSP) values of THF and ethanol.....	163
Table 5.2 Advancing and receding contact angle measurements and contact angle hysteresis of the SAM formed under different conditions, mean value (standard deviation).....	163
Table 5.3 Radioactivity of SAM of EG ₆ NH ₂ radiolabeled by H ¹⁴ CHO.....	163
Table 5.4 The relative abundance of C, N and O estimated from the peak areas obtained from survey scan.....	164
Table 5.5 The relative abundance of difference carbon components estimated by fitting in the spectra of 1Cs narrow scan.....	164
Table 6.1 XPS atomic percentage of SAM of HS(CH ₂) ₁₁ (CH ₂ CH ₂ O) ₆ NH ₂ before and after peptide immobilization	213
Table 6.2 Comparing the normalized XPS atomic percentage of the elements excluding that of substrate with calculated stoichiometric ratios.....	213
Table 6.3 Comparing the dissociation constant and maximum capacity of the BSA and hIgG adsorption on gold surfaces measured by QCM and SPR.....	213
Table 6.4 The ratios of protein adsorption amounts estimated from QCM data to those estimated from SPR data.....	214
Table 6.5 Comparing the kinetic parameters k_a and k_d obtained by QCM and SPR.....	214

LIST OF FIGURES

Figure 2.1 The principle of SPR.....	42
Figure 2.2 Structural diagram of human IgG.....	43
Figure 2.3 IgG and hexmer peptide ligand HWRGWV binding model from HADDOCK....	43
Figure 3.1 Scheme for the modification of silica surfaces.....	72
Figure 3.2 ToF-SIMS spectra around m/z 45.....	73
Figure 3.3 ToF-SIMS spectra around the peaks from Fmoc group fractions.....	74
Figure 3.4 Peaks for the ions coming from the fraction of Fmoc group in ToF-SIMS positive spectra.....	75
Figure 3.5 Negative cosines of advancing contact angles of buffer drops on APTES and APTES-PEG ₃ -NH ₂ modified silica surfaces.....	76
Figure 3.6 BSA adsorption from 1mg ml ⁻¹ BSA in different buffer solution on bare silica surface, APTES, APTES-PEG ₃ -NH ₂ , acetylated APTES and acetylated APTES-PEG ₃ -NH ₂ modified surfaces.....	77
Figure 3.7 BSA adsorption isotherms on modified silica surfaces APTES-PEG ₃ -NH ₂	78
Figure 3.8 schematic principle of ToF-SIMS.....	79
Figure 3.9 the static SIMS regime.....	80
Figure 3.10 ToF-SIMS spectra around m/z 28.....	82
Figure 4.1 ToF-SIMS spectra of samples of SiO ₂ , APTES, APTES-PEG ₃ -NH-Fmoc and APTES-PEG-NH ₂ and pure peptide HWRGWV within the range of m/z 0~300.....	129
Figure 4.2 Isotherm of hIgG and BSA adsorption on modified surface with and without peptide; the fits correspond to Langmuir adsorption isotherms at the relevant protein concentrations.....	133
Figure 4.3 Wash the adsorbed hIgG and BSA adsorbed on modified silica surface functionalized with peptide ligands by PBS with 1M NaCl.....	134
Figure 4.4 IgG adsorption from cMEM on silica surface functionalized with peptide ligands.....	135
Figure 4.5 Isotherm of hIgG adsorption on modified silica surface functionalized with peptide ligands from PBS buffer and cMEM.....	135
Figure 4.6 Kinetics fitting Langmuir isotherm adsorption model to raw data of hIgG adsorption on surface functionalized with peptide recorded by QCM.....	136
Figure 4.7 The kinetics of protein adsorption on silica surfaces with and without spacer and peptides.....	136
Figure 4.8 Correlation between dissipation and frequency changes of hIgG adsorption from	

1mg ml ⁻¹ solution on modified silica surface of APTES, APTES-PEG3-NH ₂ , APTES-HWRGWV, APTES-AA-HWRGWV and APTES-PEG3-NH-HWRGWV.....	137
Figure 4.9 Correlation between dissipation and frequency changes of hIgG adsorption from solution on modified silica surface of APTES.....	137
Figure 5.1 Phase images and topographic images acquired with tapping-mode AFM (size ~ 5μm ²) of following samples: SAM of HS(CH ₂) ₁₁ EG ₃ OH prepared by immersing in 1 mM thiolate ethanol solution for 24 hrs; SAM of HS(CH ₂) ₁₁ EG ₆ NH ₂ prepared by immersing in 1 mM thiolate ethanol solution for 24hrs; SAM of HS(CH ₂) ₁₁ EG ₆ NH ₂ prepared by immersing in 1 mM thiolate THF solution for 1 day and for 4 days; SAM of HS(CH ₂) ₁₁ EG ₆ NH ₂ prepared by immersing in 1 mM thiolate ethanol with 3% TEA solution for 1 day.....	165
Figure 5.2 High resolution XPS C1s spectra of pure SAMs of EG ₃ OH, EG ₆ NH ₂ and mixture SAM prepared by immersing into 1mM 1:1 mole ratio of EG ₃ OH and EG ₆ NH ₂ thiol solution.....	169
Figure 5.3 Phase contrast tapping-mode AFM images of SAMs prepared using ethanol with 3% TEA as solvent: SAM of HS(CH ₂) ₁₁ EG ₃ OH, SAM of the mixture of HS(CH ₂) ₁₁ EG ₃ OH and HS(CH ₂) ₁₁ EG ₆ NH ₂ with the ratio of 1:3, SAM of the mixture of HS(CH ₂) ₁₁ EG ₃ OH and HS(CH ₂) ₁₁ EG ₆ NH ₂ with the ratio of 3:1 and SAM of HS(CH ₂) ₁₁ EG ₆ NH ₂	169
Figure 5.4 Phase contrast tapping-mode AFM images of SAMs prepared with THF as solvent: SAM of HS(CH ₂) ₁₁ EG ₃ OH, SAM of the mixture of HS(CH ₂) ₁₁ EG ₃ OH and HS(CH ₂) ₁₁ EG ₆ NH ₂ and SAM of HS(CH ₂) ₁₁ EG ₆ NH ₂	170
Figure 6.1 (A) A schematic change of reflected intensity vs. angle curve during protein adsorption process obtained with SPR. (B) A schematic reflected intensity vs. time curve obtained with the SPR under fixed angle mode.....	214
Figure 6.2 The schematic diagram of the bilayer structure of protein adsorption on modified gold surface.....	215
Figure 6.3 The spectrum of narrow scan of sulfur peaks of SAM of HS(CH ₂) ₁₁ (CH ₂ CH ₂ O) ₆ NH ₂ right after preparation, after keeping in DMF overnight, after keeping in solution for deprotection of Fmoc group for 1 hour and after keeping in solution for deprotection of side chains.....	215
Figure 6.4 Structure of hexamer peptide ligand HWRGWV.....	216
Figure 6.5 The spectrum of C1s narrow scan of the SAM of HS(CH ₂) ₁₁ (CH ₂ CH ₂ O) ₆ NH ₂ right after preparation; after peptide immobilization and after deprotection of Fmoc group.....	216
Figure 6.6 The spectrum of N1s narrow scan of the SAM of HS(CH ₂) ₁₁ (CH ₂ CH ₂ O) ₆ NH ₂ right after preparation; after peptide immobilization and after deprotection of Fmoc group.....	217

Figure 6.7 ToF-SIMS spectra of samples SAM of HS(CH ₂) ₁₁ (CH ₂ CH ₂ O) ₆ NH ₂ , SAM with the immobilized peptide before deprotection of Fmoc group, SAM with the immobilized peptide after deprotection of Fmoc group and pure peptide HWRGWV within the range of m/z 0~200.....	218
Figure 6.8 SPR calibration curve obtained with the measurement of SPR response to a series of glycerin aqueous solution with concentration range within 0.3~10% (v/v).....	222
Figure 6.9 Isotherm of hIgG and BSA adsorption from PBS buffer on modified gold with and without peptide obtained by SPR.....	222
Figure 6.10 Comparing of the isotherm of hIgG adsorption from PBS buffer and that from cMEM by SPR.....	223
Figure 6.11 Isotherm of hIgG and BSA adsorption on modified gold with and without peptide obtained by QCM.....	223
Figure 6.12 Kinetics fitting of hIgG adsorption on SPR sensor modified with peptide HWRGWV.....	224
Figure 6.13 Kinetics fitting of hIgG adsorption on QCM sensor modified with peptide HWRGWV.....	225
Figure 6.14 Correlation between dissipation (<i>D5</i>) and frequency changes (<i>F5/5</i>) of hIgG adsorption from 1mg ml ⁻¹ solution on top of SAM of HS(CH ₂) ₁₁ (CH ₂ CH ₂ O) ₆ NH ₂ with and without peptide ligand.....	225
Figure 6.15 The relationship between initial slope of SPR response and hIgG concentrations.....	226
Figure 6.16 The relationship between initial slope of QCM response and hIgG concentrations.....	226
Figure 6.17 Regeneration of peptide functionalized SPR sensor for hIgG detection.....	227

Chapter 1. Introduction

1.1 Motivation

Short peptide ligands are of great interest as replacements for monoclonal or polyclonal antibodies in protein isolation and purification, protein detection, pathogen removal, and many other applications (1). In the last ten years, our group has made significant progress in the identification of ligands with sufficient specificity and affinity to separate proteins specifically from complex media (2-28). These peptide ligands were well characterized to deepen the understanding of the mechanisms of these affinity interactions between peptide ligands and target biomolecules and also to optimize the performance of these peptide ligands for separation or detection purposes. Previously, the kinetics and thermodynamics parameters described the affinity interactions between peptide ligands and targets were obtained by chromatography techniques (2, 6, 8-9, 11, 18-19, 23, 26-28). The thermodynamics parameters were derived from isotherms obtained from batch adsorption experiments with chromatography resins and the adsorption amounts at equilibrium were calculated by mass balance. Complex kinetics models were employed to describe the dynamic adsorption processes occurring within chromatography resins and columns to quantify the intrinsic adsorption rates and desorption rates. These methods provided useful information for the practical characterization of peptide ligands on resins, however it is also of interest to determine the fundamental adsorption and binding mechanisms between peptide ligands and target proteins at well-characterized interfaces.

Recently, biosensors have been applied widely to probe the binding events at solid-liquid interfaces for studies of DNA assembly and hybridization (29), blood plasma coagulation (30), pathogen detection (31), enzyme analysis (32), protein conformation analysis (33-34),

DNA-protein interaction (35) and protein-protein interaction (36). Biosensor techniques can monitor surface events *in situ* and directly measure adsorption amounts on solid surfaces in real time. The other merits of biosensors lie in the fact that the labeling of biomolecules is avoidable; consequently, the experiments are simpler and faster when compared with the traditional techniques such as radioimmunoassays (RIAs) and enzyme-linked immunosorbent assays (ELISAs). Biosensors can be divided into several types according to their transduction mechanisms: thermal, optical, electrochemical, acoustic, or piezoelectric (24). Recently, combining biosensor techniques based on different transduction mechanism have attracted more attention, since different transduction mechanisms can provide different perspectives on adsorption events (29, 34-39). In this research, surface plasmon resonance (SPR) spectroscopy and the quartz crystal microbalance (QCM) were chosen since they can provide complementary information of affinity interactions.

Immunoglobulin G (IgG) is the predominant immunoglobulin in blood and other body fluids (40). Quantification of human IgG (hIgG) concentration in human fluids currently is a common test for the diagnosis of diseases (41-43) and purified hIgG has been widely used to treat patients with primary and secondary immune-deficiencies (40, 44). The hexamer peptide HWRGWV was identified using a radiolabeled target screening technique from a combinatorial linear hexamer peptide library built on chromatography resins for IgG purification and detection. This Fc-binding peptide ligand HWRGWV demonstrates the ability to purify IgG. It can isolate hIgG from mammalian cell culture media containing 10% fetal calf serum (cMEM) with more than 95% of both purity and yield (26). Although the short peptide ligand HWRGWV has exhibited promising applications for IgG separation and

concentration determination, limited information is available on the intrinsic mechanisms of affinity interaction between this short peptide ligand and target protein. In this research, two biosensor techniques, QCM and SPR, were employed to investigate the affinity interaction between peptide ligand HWRGWV immobilized on solid surfaces and hIgG in fluids. In addition, these peptide functionalized sensors could have two potential applications. First, they could result in a new method for IgG detection and concentration quantification. Detection and quantification of IgG concentration are critical for both disease diagnostics (41-43) and for quality control in the biopharmaceutical industry (45-47). Second, these peptide-functionalized biosensors could result in a new platform for immunosensor fabrication. The peptide ligand immobilized on sensor surfaces can capture IgG through its Fc fragment and leave the fraction of the IgG molecule responsible for interaction with its epitope free to react. Currently, protein A and protein G are generally used as the anchor proteins for immunosensor. The Fc-specific ligand, HWRGWV, could be an alternative of these protein ligands for this purpose.

1.2 Goals

The primary goal of this project is to develop new methods for the study of affinity interactions between peptide ligand and biomolecules. QCM and SPR were chosen to monitor the hIgG adsorption process on hexamer peptide ligand HWRGWV functionalized solid surfaces. This hexamer peptide ligand was picked since QCM and SPR sensors functionalized with this ligand could have broad potential applications in quantification of IgG for both clinical diagnostics and manufacturing quality control, as well as in the fabrication of new types of immunosensors.

The hexamer peptide ligand HWRGWV was immobilized on modified silica or gold surfaces. The processes of surface modifications and peptide immobilization were optimized and the resulted surfaces were extensively characterized by multiple techniques. The affinity and specificity of the peptide to human IgG binding was investigated by QCM and SPR. Thermodynamics and kinetics parameters were derived from quantification analyses of QCM and SPR data. Finally, preliminary experiments were performed to test the possibility to determine IgG concentrations in bio-media.

1.3 Overviews of this thesis

This dissertation focuses on the study of the affinity interaction between hexamer peptide ligands HWRGWV and immunoglobulin G (IgG) by QCM and SPR.

Chapter 2 reviews the capacities and the advantages of using biosensor techniques including QCM and SPR for the study of affinity interactions between peptide ligands and target biomolecules. The achievements and possible drawbacks of the previous methods employed in our groups for the characterization of peptide ligands are summarized. The critical issues of the fabrication of biosensor for the study of affinity interaction are examined and the potential applications of the hexamer peptide functionalized biosensor are discussed.

Chapter 3 exhibits a new silica surface modification method to introduce amine group for peptide immobilization and to reduce non-specific binding. The characterizations of the resulting surface by multiple methods indicate that the silica surface was modified as desired.

Chapter 4 presents the study of affinity interactions between the peptide ligand HWRGWV immobilized on silica surfaces and IgG in solution by QCM. The affinity and specificity of the peptide ligand to IgG binding are examined. The thermodynamics and

kinetics parameters of this affinity interaction obtained from QCM data are presented. The effects of the overestimation of adsorption amounts by QCM on the obtained values of parameters are discussed. The role of PEG spacer arm in affinity interaction between HWRGWV and IgG are also analyzed.

Chapter 5 shows a new strategy to modify gold surfaces for the study of affinity interactions between peptide ligands and target biomolecules. The formation conditions of SAMs of HS(CH₂)₁₁(CH₂CH₂O)₆NH₂, HS(CH₂)₁₁(CH₂CH₂O)₃OH and mixtures of these two species are presented. The best conditions for the formation of SAMs are summarized.

Chapter 6 presents an investigation of IgG binding on the peptide ligand HWRGWV immobilized on gold surfaces by the parallel experiments with QCM and SPR. The affinity and specificity to IgG binding are presented. Quantitative thermodynamic and kinetics analyses are performed using this QCM and SPR data. The advantage and disadvantages of QCM and SPR for this application are discussed. Preliminary experiments to test the possibility of rapid measurements of IgG concentrations are presented.

All above results are summarized in Chapter 7 with recommendations for future work.

References:

1. Wang G, Salm JR, Gurgel PV, & Carbonell RG (2005) Small peptide ligands for affinity separations of biological molecules. *Chemical Engineering*, eds Gal'an MA & del Valle EM (John Wiley & Sons, Ltd., New York, NY).
2. Bastek PD & Carbonell RG (1999) Adsorption and purification of alpha-1 proteinase inhibitor using a peptide affinity resin. *Abstracts of Papers of The American Chemical Society* 217:U873-U873.

3. Huang PY & Carbonell RG (1999) Affinity chromatographic screening of soluble combinatorial peptide libraries. *Biotechnology and Bioengineering* 63(6):633-641.
4. Kaufman DB, *et al.* (2002) Affinity purification of fibrinogen using a ligand from a peptide library. *Biotechnology and Bioengineering* 77(3):278-289.
5. Huang PY & Carbonell RG (1995) Affinity purification of proteins using ligands derived from peptide libraries. *Biotechnology and Bioengineering* 47(3):288-297.
6. Huang PY, *et al.* (1996) Affinity purification of von Willebrand factor using ligands derived from peptide libraries. *Bioorganic & Medicinal Chemistry* 4(5):699-708.
7. Yang H, *et al.* (2010) Binding site on human immunoglobulin G for the affinity ligand HWRGWV. *Journal of Molecular Recognition* 23:271-282.
8. Wang GQ & Carbonell RG (2005) Characterization of a peptide affinity support that binds selectively to staphylococcal enterotoxin B. *Journal of Chromatography A* 1078(1-2):98-112.
9. Kaufman DB, Hayes T, Buettner J, Hammond DJ, & Carbonell RG (2000) Chromatographic resolution of tryptophan enantiomers with L-Leu-L-Leu-L-Leu peptide - Effects of mobile phase composition and chromatographic support. *Journal of Chromatography A* 874(1):21-26.
10. Heldt CL, *et al.* (2006) A colorimetric assay for viral agents that produce cytopathic effects. *Journal of Virological Methods* 135(1):56-65.
11. Wang G & Carbonell RG (2006) Design of adsorptive columns for specific pathogen removal: application to staphylococcal enterotoxin B. *Biotechnology Progress* 22:1358-1367.
12. Bastek PD, Land JM, Baumbach GA, Hammond DH, & Carbonell RG (2000) Discovery of alpha-1-proteinase inhibitor binding peptides from the screening of a

- solid phase combinatorial peptide library. *Separation Science and Technology* 35(11):1681-1706.
13. Gurgel PV, Carbonell RG, & Swaisgood HE (2000) Fractionation of whey proteins with a hexapeptide ligand affinity resin. *Bioseparation* 9(6):385-392.
 14. Yang H, Gurgel PV, & Carbonell RG (2005) Hexamer peptide affinity resins that bind the Fc region of human immunoglobulin G. *Journal of Peptide Research* 66:120-137.
 15. Wang G, De J, Schoeniger JS, Roe DC, & Carbonell RG (2004) A hexamer peptide ligand that binds selectively to staphylococcal enterotoxin B: isolation from a solid phase combinatorial library. *Journal of Peptide Research* 64(2):51-64.
 16. Gurgel PV, Carbonell RG, & Swaisgood HE (2001) Identification of peptide ligands generated by combinatorial chemistry that bind alpha-lactalbumin. *Separation Science and Technology* 36(11):2411-2431.
 17. Heldt CL, Gurgel PV, Jaykus LA, & Carbonell RG (2008) Identification of trimeric peptides that bind porcine parvovirus from mixtures containing human blood plasma. *Biotechnology Progress* 24(3):554-560.
 18. Heldt CL, Gurgel PV, Jaykus LA, & Carbonell RG (2009) Influence of Peptide Ligand Surface Density and Ethylene Oxide Spacer Arm on the Capture of Porcine Parvovirus. *Biotechnology Progress* 25(5):1411-1418.
 19. Kaufman DB & Carbonell RG (1999) Interaction of fibrinogen with peptide affinity supports - Resin effects. *Abstracts of Papers of The American Chemical Society* 217:U160-U160.
 20. Bastek PD & Carbonell RG (1999) Investigation of the binding mechanism between a peptide affinity resin and alpha-1 proteinase inhibitor. *Abstracts of Papers of The American Chemical Society* 217:U189-U189.

21. Salm JR, Brown D, Hammond D, & Carbonell RG (2001) Ligands from combinatorial peptide libraries for virus detection and removal. *Abstracts of Papers of the American Chemical Society* 221:U122-U122.
22. Salm JR, Carbonell RG, Brown D, & Hammond D (2002) Ligands from combinatorial peptide libraries for virus removal. *Abstracts of Papers of the American Chemical Society* 224:U217-U217.
23. Wang GQ & Carbonell RG (2003) Modeling of breakthrough curves of staphylococcal enterotoxin B in peptide affinity chromatography. *Abstracts of Papers of the American Chemical Society* 225:U197-U197.
24. de Lucena SL, Carbonell RG, & Santana CC (1999) Peptide affinity chromatography process for adsorption of fibrinogen. *Powder Technology* 101(2):173-177.
25. Bastek PD, Lang JM, Baumbach GA, Hammond DJ, & Carbonell RG (1998) Purification of alpha-1 proteinase inhibitor using ligands from combinatorial peptide libraries. *Abstracts of Papers of the American Chemical Society* 216:U328-U328.
26. Yang H, Gurgel PV, & Carbonell RG (2009) Purification of human immunoglobulin G via Fc-specific small peptide ligand affinity chromatography. *Journal of Chromatography A* 1216.
27. Gregori L, *et al.* (2006) Reduction of transmissible spongiform encephalopathy infectivity from human red blood cells with prion protein affinity ligands. *Transfusion* 46(7):1152-1161.
28. Gurgel PV, Carbonell RG, & Swaisgood HE (2001) Studies of the binding of alpha-lactalbumin to immobilized peptide ligands. *Journal of Agricultural and Food Chemistry* 49(12):5765-5770.
29. Su XD, Wu YJ, & Knoll W (2005) Comparison of surface plasmon resonance spectroscopy and quartz crystal microbalance techniques for studying DNA assembly and hybridization. *Biosensors & Bioelectronics* 21(5):719-726.

30. Vikinge TP, *et al.* (2000) Comparison of surface plasmon resonance and quartz crystal microbalance in the study of whole blood and plasma coagulation. *Biosensors & Bioelectronics* 15(11-12):605-613.
31. Spangler BD, Wilkinson EA, Murphy JT, & Tyler BJ (2001) Comparison of the Spreeta (R) surface plasmon resonance sensor and a quartz crystal microbalance for detection of Escherichia coli heat-labile enterotoxin. *Analytica Chimica Acta* 444(1):149-161.
32. Turon X, Rojas OJ, & Deinhammer RS (2008) Enzymatic kinetics of cellulose hydrolysis: A QCM-D study. *Langmuir* 24(8):3880-3887.
33. Reimhult E, Larsson C, Kasemo B, & Hook F (2004) Simultaneous surface plasmon resonance and quartz crystal microbalance with dissipation monitoring measurements of biomolecular adsorption events involving structural transformations and variations in coupled water. *Analytical Chemistry* 76(24):7211-7220.
34. Zhou C, *et al.* (2004) Human immunoglobulin adsorption investigated by means of quartz crystal microbalance dissipation, atomic force microscopy, surface acoustic wave, and surface plasmon resonance techniques. *Langmuir* 20(14):5870-5878.
35. Su XD, Wu YJ, Robelek R, & Knoll W (2005) Surface plasmon resonance spectroscopy and quartz crystal microbalance study of MutS binding with single Thymine-Guanine mismatched DNA. *Front. Biosci.* 10:268-274.
36. Su XD & Zhang H (2004) Comparison of surface plasmon resonance spectroscopy and quartz crystal microbalance for human IgE quantification. *Sensors and Actuators B-Chemical* 100(3):309-314.
37. Damos FS, Mendes RK, & Kubota LT (2004) Applications of QCM, EIS and SPR in the investigation of surfaces and interfaces for the development of (BIO)sensors. *Quimica Nova* 27(6):970-979.

38. Graneli A, Edvardsson M, & Hook F (2004) DNA-based formation of a supported, three-dimensional lipid vesicle matrix probed by QCM-D and SPR. *ChemPhysChem* 5(5):729-733.
39. Stadler H, Mondon M, & Ziegler C (2003) Protein adsorption on surfaces: dynamic contact-angle (DCA) and quartz-crystal microbalance (QCM) measurements. *Analytical and Bioanalytical Chemistry* 375(1):53-61.
40. Leffell MS, Donnenberg AD, & Rose NR (1997) *Handbook of human immunology* (CRC Press, New York, NY) p 73.
41. Hoek FJ, Noach LA, Rauws EAJ, & Tytgat GNJ (1992) Evaluation of the performance of commercial test kits for detection of helicobacterial-pylori antibodies in serum. *Journal of Clinical Microbiology* 30(6):1525-1528.
42. Korhonen MH, *et al.* (1999) A new method with general diagnostic utility for the calculation of immunoglobulin G avidity. *Clinical and Diagnostic Laboratory Immunology* 6(5):725-728.
43. Groen J, Koraka P, Velzing J, Copra C, & Osterhaus A (2000) Evaluation of six immunoassays for detection of dengue virus-specific immunoglobulin M and G antibodies. *Clinical and Diagnostic Laboratory Immunology* 7(6):867-871.
44. Provan D (2005) *Oxford handbook of clinical and laboratory investigation* (Oxford University Press, Oxford, UK).
45. Middendorf C, *et al.* (1993) On-line immunoanalysis for bioprocess control. *Journal of Biotechnology* 31:395-403.
46. Rosen FS & Seligmann M (1993) *Immunodeficiencies* (Harwood Academic Publishers, Chur, Switzerland).
47. Huse K, Bohme HJ, & Scholz GH (2002) Purification of antibodies by affinity chromatography. *Journal of Biochemical and Biophysical Methods* 51(3):217-231.

Chapter 2. Literature Review

2.1 Short Peptides as Affinity Ligands

2.1.1 Overview

Affinity techniques are among the most efficient methods to purify and detect biomolecules (1). Due to their high specificity, monoclonal antibodies are the most common ligands currently used in affinity techniques. Short peptide ligands with sufficient specificity can have many advantages over antibodies for purification or detection purposes. Short peptides are more stable than monoclonal antibodies because they do not require a specific tertiary structure to maintain their biological activity. The manufacture of short peptides can be scaled-up under good manufacturing practices (GMP) conditions at relatively low cost. The interactions between small peptides and proteins tend to be moderate so that the target protein can be eluted under mild condition without a detrimental influence on protein activity (2).

Short peptides have already been successfully screened and identified from peptide libraries in our group for the purification or detection of S protein (3), von Willebrand factor (4), alpha-1 proteinase inhibitor (5), fibrinogen (6), alpha-lactalbumin (7), staphylococcal enterotoxin B (8), human IgG (9) and porcine parvovirus (10).

Although the peptide ligands identified for the different proteins were screened using the same general methodology, the final results obtained were somewhat variable. Some peptide ligands identified by library screening show high high specificity to their target protein. That is the case for peptide YNFEVL and s-protein (3). Other peptide ligands behave as pseudo-affinity ligands, displaying dissociation constants (K_d) in the range of 10^{-5} to 10^{-8} M with their target proteins. An example of this behavior is the peptide ligand RLRSFY and von

Willebrand factor (vWF) (4). In general, pseudo-affinity peptide ligands are more suitable for the capture or concentration of the target molecule at an early stage in purification, while the more specific peptide ligands can be efficient for purifying the protein in one step, but usually it is placed in the later stages to maximize the efficiency of the affinity column (2).

Generally, ligand-target interactions for short peptide ligands are stronger than the pure ion exchange or pure hydrophobic interactions, since the affinity interaction between the peptide ligands and target biomolecules is the result of the interactions of each amino acid in the peptide sequences with the biomolecules. Any charged amino acid in the peptide ligand tends to form ionic interactions with the target molecule, while the amino acids in the ligand with hydrophobic groups interact with the hydrophobic patches on biomolecules (2). For a specific peptide ligand, the interaction could be ion-interaction dominated or hydrophobic-interaction dominated and, in some cases, the dominant force could change with the solvent conditions. For instance, the interaction between WHWRKR and alpha-lactalbumin at low temperatures is dominated by electrostatic interactions, while, as the temperature increases, hydrophobic interactions become the dominant binding mechanism (11).

2.1.2 Characterization of Peptide Ligands by Kinetics and Thermodynamics Analysis

As mentioned above, peptide ligands with different bio-selectivity to targets biomolecules could play different roles in purification processes. In addition, these affinity interactions between peptide ligands and target biomolecules could have different characteristics. In order to optimize the performance of these peptide ligands for bioseparation or detection, these peptides need to be well characterized. Our research group has made extensive efforts to characterize these peptide ligands by quantification of the thermodynamic and kinetic

parameters of the interaction between peptide ligands on chromatographic resins and target biomolecules under different conditions. It has been found that the affinity of the peptides to target biomolecules can depend on the variation of experimental conditions including peptide density (2-4, 8, 12), pH (4, 11-12), temperature (11, 13), and salt concentrations in the buffer (4).

In previous studies of the adsorption isotherm of target proteins to ligands on porous chromatography resins the adsorbed amounts of target biomolecules under different conditions were determined by mass balance (3, 11-12, 14-16). This is an indirect method of measuring the amount of protein adsorbed, and can generate a significant error when the change of protein concentration due to adsorption is small compared to the unbound protein concentration. The kinetic parameters of affinity binding to peptide ligands on resins were studied by dynamic adsorption experiments carried using high performance liquid chromatography (HPLC). Different models have been employed to describe the solute transport within the chromatography column to get the intrinsic kinetic parameters. A lumped kinetic model was employed for the study of the adsorption kinetics of fibrinogen that binds to the short peptide FLLVPL (13). In this work, columns with varying peptide densities were challenged with a fibrinogen solution at a constant flow rate. The concentration of the exit stream was measured continuously as a function of time. The shapes of the breakthrough curves were modeled using the lumped kinetics model that took into account axial dispersion, interparticle mass transfer and intraparticle diffusion, and the rates of adsorption and desorption of the protein to the surface. All the mass transfer parameters were estimated from correlations or measured directly, and the only remaining parameter in each run was the

adsorption rate constant onto the resin. The rate constant for adsorption was obtained by finding the best fit to the breakthrough curve. The resulting analysis showed that the adsorption rates were indeed rate-limiting and that the rate of adsorption was relatively independent of peptide density. Although the lumped kinetics model threw a light on the understanding of the relationship between adsorption rate and peptide density, it was found that the capacity and association constant derived from the fitting of the experimental breakthrough data with this model was inconsistent with equilibrium experiments (13, 17). A more sophisticated effort using the General Rate Model of chromatography was shown to fit well with experimental results in the analysis of Staphylococcal enterotoxin B (SEB) binding with peptide ligand YYWLHH (15, 18). Generally, the reliability of the final results for the kinetics of adsorption and desorption depend on the accuracy of the transport models and the estimation of the mass transfer parameters.

In summary, the affinity interaction between peptide ligands and biomolecules have been studied by indirect methods, batch adsorption mode and chromatography techniques, which may lead to significant errors under certain situations. New methods that can directly monitor the affinity interactions occurring at liquid-solid interface can lead to more detailed information on the nature and rates of these interactions.

2.2 Study Affinity Interactions by Quartz Crystal Microbalance and Surface Plasmon Resonance

2.2.1 Overview

Biosensors have been playing an increasingly important role in research on biointeractions during recent years (19-20). Compared with traditional detection methods, such as filter binding assays, radioimmunoassays and enzyme-linked immunosorbent assays (ELISAs), biosensors are fast, simple and relatively inexpensive. Biosensor systems can directly monitor the macromolecular interactions happening on solid-liquid interface in real time. In addition, the mass transport processes within these systems are generally simpler than those in a chromatography column; consequently, the interpretation of the dynamic adsorption behavior could be relatively easier.

A biosensor is basically a chemical or mass sensor in which the analytical signal is generated by the bio-affinity elements immobilized or physically adsorbed on a transducer (21-22). During the design of an affinity biosensor, the following aspects need to be carefully taken into consideration: the properties of the affinity recognition elements (ligands), the mechanism of signal transduction, and the method of immobilization. This research focuses on short (hexamer) linear peptide ligands. The mechanism of signal transduction and the method of immobilization are discussed in the following paragraphs.

Biosensors can be divided into several types depending on the different transduction mechanisms: thermal, optical, electrochemical, acoustic, or piezoelectric (23). Currently, there is a trend to combine surface detection techniques based on different transduction mechanism, which provides different perspectives on binding events occurring at interface (24-26). In this research, attention is focused on two kinds of techniques: surface plasmon resonance (SPR) and quartz crystal microbalance with dissipation (QCM-D). The features of QCM and SPR techniques are summarized in Table 2.1. The most important difference

between SPR and QCM methods is that SPR measures the dry mass of biomolecules adsorbed on the surface, while QCM measure the total mass on the surface, including the water and ions associated with the biomass (27-28). In general, SPR is more quantitative than QCM, while the advantage of QCM over SPR is its capability to provide a qualitative measure of the viscoelastic properties of the adsorbed protein layer (24). The combination of these two techniques can provide more reliable and complementary data. The principles and applications of these two techniques are presented in detail in the following sections.

2.2.2 Principle of QCM and Its Applications

QCM sensors consist of a thin slice of a single crystal of quartz sandwiched between two metal electrodes, housed in a sealed package that provides a means of connection to a circuit. An alternating electrical voltage applied to these electrodes causes the quartz to vibrate, or oscillate, at its resonant frequency. This frequency is dependent on the mass of the crystal as well as the mass of any layers confined on the surface of the electrode areas of the crystal. When the electrical field applied to the quartz crystal is turned off, the oscillation of the crystal attenuates as a result of the energy lost during oscillation. The dissipation factor, D , is the sum of all the energy lost in the system per oscillation cycle (29). The dissipation depends on the interaction between the film, the sensor surface and the properties of the adsorbed film. When the film on the electrodes of crystal is slippery or when the film is viscous, more energy will be dissipated by friction during the oscillatory motion induced in the film. As a result, the dissipation factor D provides an indirect measure of the flexibility of the adsorbed film.

The merits of the QCM technique are primarily its simplicity and sensitivity (in the ng cm^{-2} range). Sauerbrey reported a linear relationship between the frequency decrease of an oscillating quartz crystal (Δf) and the bound elastic mass of deposited metal, Δm (30),

$$\Delta f = -\frac{2f_0^2 \Delta m}{(\rho_q \mu_q)^{1/2} A} \quad 2-1$$

where f_0 is the fundamental resonance frequency of the quartz crystal, ρ_q is the specific density of the quartz (2.648 g cm^{-3}), μ_q is the shear wave velocity in quartz ($2.947 \times 10^{11} \text{ g cm}^{-1} \text{ s}^{-2}$ for AT-cut quartz crystals) and A is the measuring area.

The Sauerbrey equation was derived based on two assumptions: (1) the film is rigid (no internal friction in the added mass); (2) the film is coupled perfectly to the oscillatory motion of the quartz crystal (no slip between the film and the crystal electrode).

For rigid, evenly distributed, and sufficiently thin adsorbed layers, the Sauerbrey equation has indeed been shown to provide a good approximation (31-32). However, for soft adsorbed films, this is not the case anymore, due mainly to two potential reasons: the first one is connected with the propagation of the shear acoustic wave in a viscoelastic film. For a sufficiently thin and rigid adsorbed film, the adsorbed layer acts as a “dead” mass on the piezoelectric oscillator. On other hand, for a viscoelastic or thicker film coupled on oscillator, the change of frequency is not directly proportional to change of mass. In other words, the effectively coupled mass depends on how the oscillatory motion of the crystal propagates into and through an adsorbed viscoelastic film (33-34). The second reason of the failure of the Sauerbrey relation is the solvent, which, in most cases, is water. In QCM measurements, water (or any other liquid or solvent molecules) may couple as an additional mass via direct

hydration, viscous drag, or entrapment in cavities in the adsorbed film, which contributes to the overestimation of the mass from the Sauerbrey equation. The typical amount of coupled water in different systems has been shown to add a significant variation and it depends on the nature of the film. The mass-uptake estimations could be 1.5 to 10 times larger than the molar mass (27, 29, 34-37).

Early chemical applications of QCM involved monitoring of mass and film thickness in coating equipment in vacuum and on investigating the adsorption in gas phase (32). In the 1980s, solution-based QCM was developed and it found more applications in mainly two fields: electrochemistry and biotechnology. In the area of biotechnology, QCM has been used to measure protein adsorption kinetics (38), protein conformation analysis (24, 39), antibody-antigen interactions (40-41), nucleotide hybridization (26), nucleotide-protein interactions (42-43), and bacteria (44) and cell adsorption (25). In liquid-phase measurements, the QCM is not a simple mass sensor, but provides valuable information about reactions and conditions at the liquid-solid interface.

2.2.3 Principle of SPR and its application

Surface plasmon resonance is an optical technique that is widely recognized as a valuable tool in the investigation of biomolecular interactions (45). It can monitor the dynamic processes occurring on the surface in real time and provide kinetic and thermodynamic data (46-47).

A surface plasmon is a longitudinal charge wave that propagates along the interface of two media with very different optical densities such as metal and water. The attenuated total reflectance (ATR) configuration developed by Krethmann (as shown in Figure 1) is widely

used in most SPR instruments. A monochromatic, p-polarized light traveling through an optically dense medium (glass) reaches an interface between this medium and an optical medium with lower density (buffer) and then reflects back into the denser medium (Figure 1). Under conditions of total internal reflection, most of the light will be reflected back into the higher-density medium but there is still a small portion of light, the evanescent wave, that penetrates the interface into the less-dense medium a distance of approximately one wavelength (48). The evanescent wave vector can be expressed in the form,

$$K_{ev} = \frac{\omega_0}{c} \eta_g \sin \theta \quad 2-2$$

where, ω_0 is the frequency of incident light, c is the speed of light in a vacuum, η_g is the refractive index of the dense medium, and θ is the angle of incident light. The wave vector corresponding to the surface plasmon is expressed by the formula,

$$K_{sp} = \frac{\omega_0}{c} \eta_g \sqrt{\frac{\epsilon_m \eta_s^2}{\epsilon_m + \eta_s^2}} \quad 2-3$$

where, η_s is the refractive index of the dielectric medium on the top of the sensor surface, and ϵ_m is the dielectric constant of the metal film.

When the incidence angle of the light is chosen in such a way that the magnitude of the evanescent wave is equal to that of the surface plasmon wave vector,

$$K_{ev} = K_{sp} \quad 2-4$$

the evanescent wave of the light can couple with the plasmon in the metal film. In other words, the surface plasmon is resonantly excited. In this situation, the incident light dissipates energy into the metal film. As a result, the intensity of reflected light is reduced

and forms a dip (49). Since K_{ev} is a function of the refractive index of the dielectric medium n_s , n_s can be measured by recording the change of this incident angle satisfying the condition required for surface plasmon resonance.

When binding events occur on the surface, the adsorbed protein molecules replace the buffer solution close to the sensor surface. The difference between the refractive index of the adsorbed protein molecules and that of the buffer solution replaced will be detected by SPR. There is no difference between the water molecules attached on the surface of proteins or entrapped in the adsorbed protein layer and those in buffer solution replaced by the adsorbed protein layer. Consequently, water molecules within the adsorbed protein layer cannot be detected by the SPR. In other word, the mass measured by SPR is “dry mass”.

As an optical technique used for the study of affinity interactions, SPR has been developed in the 1980's (50). After that, SPR has played a significant role in the research of biomolecules and their interactions. In the past decades, SPR has also been increasingly used for detection and identification of chemical and biological substances (45).

2.2.4 Importance of Surface Preparation for Ligand Immobilization

Biomolecules can be immobilized on sensor surfaces by physical adsorption, covalent bonding, crosslinking, entrapment, or encapsulation. Among those methods, adsorption and covalent bonding are the most commonly used (28, 51). Physical adsorption of the biocomponent based on van der Waals attractive forces is the simplest method available and it is feasible for various substrates. However, this method does not provide high surface density of affinity elements, and the adsorbed biomolecules could be lost through changes in pH, ionic strength, or temperature due to adsorption reversibility (51-52). Covalent bonding

to the surface can lead to slight modifications of the biomolecules, but, this approach results in more stable surfaces, and is more reliable and reproducible DNA-based formation of a supported, three-dimensional lipid vesicle matrix probed by QCM-D and SPR (53-55).

For covalent bonding, generally the substrates need to be modified to introduce active groups such as carboxyl, thioacetyl, hydroquinone, or epoxide groups for the immobilization of biomolecules (56-59). Self-assembled monolayers (SAMs) are one of the most convenient methods to modify the sensor surface. A SAM is a molecular assembly obtained by immersion of an appropriate substrate into a solution of a surfactant in organic solvent (60). This simple process makes SAMs technologically attractive for the functionalization of sensor surfaces with active groups.

There are several types of SAMs and among them two kinds, organosilicon on hydroxylated surfaces, and alkanethiols and dialkyl disulfides on gold and other noble metals, are the most common methods for biomolecule immobilization (60-61). Due to their simplicity and versatility, the SAMs of alkanethiols on gold have been the most studied SAMs.

The structure of these SAMs is now well established (62). Sulfur compounds have a strong affinity for transition metal surfaces (63). For an alkanethiols with an alkyl chain longer than 10 carbon atoms, it is possible to obtain very ordered layers, with few defects, depending mostly on the irregularity of the gold surface (31, 62, 64-65). The terminal functional groups of o-substituted alkane thiols dominate the properties of the interfaces between the SAMs and the contacting liquids and these groups offer great versatility to covalently immobilize biological molecules, such as peptides or proteins on sensor surfaces.

Chemisorption of alkanethiols as well as of dialkyl disulfides on clean gold gives indistinguishable monolayers. The rates of formation of SAMs from dialkyl disulfides or alkanethiols are also indistinguishable, but the rates of replacement of molecules from SAMs by thiols are much faster than by disulfides (60).

SAMs of alkylchlorosilanes, alkylalkoxysilanes, and alkylaminosilanes require hydroxylated surfaces as substrates, such as silicon oxide, aluminum oxide, quartz, glass, mica, and zinc selenide, for their formations. The driving force for this self-assembly is the formation of polysiloxane, which is connected to surface silanol groups (-SiOH) via Si-O-Si bonds (61). The control of the quality of the SAMs of silanes is generally harder than that of alkanethiols. The formation of silane SAMs is sensitive to water. While incomplete monolayers are formed in the absence of moisture on substrate, the excess water results in facile polymerization in solution and polysiloxane deposition of the surface (60). The advantage of SAMs of silane over those of alkanethiols is their relatively higher stability (61).

Besides the introduction of active groups for immobilization of biomolecules, there are other two objectives of surface modification. First, adding a spacer arm on top of a substrate is desirable to enhance the availability of the ligands on the surface of the modified layer. Spacer arms have been widely used in affinity chromatography or membranes for bioseparations. They can play a significant role in the affinity interaction between ligands on solid surfaces and biomolecules in solution, especially for small ligands, and this effect could be even more critical when the active site of the target molecule is located in a pocket (1, 66). A good spacer arm should have just enough length to facilitate the formation of ligand and

target biomolecule complex. If no spacer arm, or too short a spacer arm is used, it might be hard to form the complex of ligand and target molecule due to steric hindrance; if it is too long the density of ligand could be low and nonspecific binding to spacer arm could become predominant over the affinity interaction (66). The other objective of surface modification is to minimize the background noise from the nonspecific binding of proteins and other species in the bulk solution. Poly (ethylene glycol) (PEG) is well-established as one of the primary components in nonfouling film chemistry. The resistance of PEG coated surfaces to nonspecific binding is dependent on the molecular weight of the PEG and the resulting packing density of the PEG chains (67). In addition, PEG is also a good candidate spacer arm, since PEG brushes have a high flexibility in biological media. Consequently, materials including PEG composite have been widely applied to modify surface for bio-application (68-72).

2.3 Potential Applications of Fc-specific Hexamer Peptide Functionalized

Biosensor

2.3.1 Fc-specific Peptide Ligand for IgG Purification

Antibodies, also known as immunoglobulins (Ig), are glycoproteins produced by white blood cells, each having a special antigen-binding pocket that is sensitive to specific parts of an antigen protein. The human immunoglobulins account for approximately 20% of all proteins in human plasma, and can be divided into five classes or isotypes: IgG, IgA, IgM, IgD, and IgE. Among them, IgG is the most abundant class of Igs in the body, constituting

approximately 75% of the total immunoglobulins at an average concentration of 12 mg/ml in adult blood (73).

As shown in Figure 2.1, IgG has a Y-shaped structure with the molecular weights of the heavy (H) and light (L) chains being 50 and 25 KDa, respectively. Although the general structures of IgGs are very similar, a small region at the tip of the protein is extremely variable, allowing millions of IgGs with slightly different tip structures, or antigen binding sites, to exist. As shown in Figure 2.1, the "V" label indicates a variable region where the amino acid composition varies with the response antigens, while the "C" label denotes a constant region where the amino acid composition is relatively invariant for IgGs. Starting from the amino terminus, the L chains include the VL and CL domains while the H chains encompass the VH, CH1, hinge, CH2, and CH3 regions. The V regions of both heavy and light chains are responsible for antigen binding by forming a pocket with six loops. The C region is engaged in a variety of effector functions (74).

IgG and its fragments have found a wide array of applications as pharmaceutical compounds, in addition to their common usage in the purification and localization of proteins. Conventionally, IgG preparations have been produced exclusively by precipitation techniques, preferably involving cold ethanol fractionation. In recent years, however, chromatographic steps have been introduced into the downstream of the ethanol fractionation steps (75). Ion-exchange chromatography, hydrophobic interaction chromatography, size-exclusion chromatography, and affinity chromatography have all been involved in IgG capture and purification and, among them, affinity chromatography allows the possibility of obtaining several fold purification with high recovery in fewer steps (76).

Staphylococcus aureus Protein A and *Streptococcus* Protein G are the most common affinity ligands for IgG purifications and detections (76-77). However, the drawbacks associated with these two protein ligands, including high cost and low stability, have given rise to the searching for alternative affinity ligands for antibody purification (76, 78). Special attention has been paid to the use of small ligands for affinity purification of antibodies due to their advantages of being more stable (no three-dimensional structure), less immunogenic, and less expensive than large protein ligands. Some synthetic small ligands have been extensively studied for IgG purification and detection, such as the hydrophobic charge induced ligand MEP (4-mercapto ethyl pyridine) (79), the Protein A mimetic peptide Kaptiv-GY based on the sequence (RTY)₄K₂KG (TG19318) (80) and a synthetic ligand MAbSorbant A2P derived from a triazine derivative ligand 22/8 (81). However none of these ligands that bind to antibodies behaved like Protein A in their binding specificity to the Fc fragment. The ability to bind through the Fc fragment is an important function since it allows the ligand to be used as a universal ligand for whole antibodies and Fc-fusion proteins, potentially diminishing the time required to develop separation processes for new antibodies.

Three hexamer peptide ligands, HWRGWV, HFRRHL, and HYFKFD, identified by our group, were the first reported short peptide ligands that were able to mimic the binding specificity of Protein A to the Fc fragment of human IgG (hIgG) (9). The performance of the peptide HWRGWV for the purification of hIgG in complex fluids has been extensively studied and characterized. An HWRGWV resin with a peptide density of 0.08 meq g⁻¹ of dry resin was able to purify hIgG from mammalian cell culture media containing 10% fetal calf serum (cMEM) with both purity and yield as high as 95%, comparable to Protein A and A2P

agarose gels (12). The ligand also demonstrated its ability to isolate hIgG from Cohn II+III paste and yields of 82% and purities of 73% were obtained in one step. Bound IgG can be eluted under milder conditions than with Protein A, with the target molecule being released from the resin at pH 4, in contrast to the typical pH 3.0 elution using Protein A. The ligand was found to bind to IgG from different organisms, including bovine, murine, goat, and rabbit IgGs. The peptide also displayed affinity to different subclasses of IgG, such as HIgG1, HIgG2, HIgG3, and HIgG4.

2.3.2 Potential Application for IgG Concentration Quantification

Quantification of immunoglobulin concentrations in serum is one of the basic tools commonly used for investigating abnormalities relating to the immune system and exposure to infectious disease in humans and domestic species (73, 82). Besides serum, other body fluids, including urine, saliva, milk and especially colostrums are all possible samples that can be subjected to immunoglobulin quantification assays (73). Classical measurements of hIgG involve techniques such as fluorescence immunoassays, radioimmunoassays (RIA) and enzyme-linked immunosorbent assays (ELISA). However, they are time-consuming and need labeling of biomolecules. For clinical diagnostics purposes, ELISA-based assays are only employed for the measurement of antibody production against defined pathogens or antigens for the investigation of suspected immunodeficiency (82). There are three types of assays, (immunodiffusion, nephelometric, and turbimetric) commonly used by clinical immunology laboratories to quantify human IgG, IgA, IgM, IgE and the kappa and lambda light chains of Igs (73). The principle of these assays is similar, with highly avid antibody reagents added to the sample containing immunoglobulins to form immune complexes, which are subsequently

detected visually or by light-scattering techniques such as immunodiffusion, nephelometry, or turbimetry. A variety of immunological reagents are used in clinical assays for the quantification of human immunoglobulins. In the early years, polyclonal antibodies were extensively used and more recently, well documented murine monoclonal antibodies have become available. They are highly specific for human immunoglobulin and especially useful in quantifying the amount of human IgG and IgA subclasses, where maximal specificity is a requirement (73).

Besides diagnostic applications, the quantification of immunoglobulin is also important for antibody production and dairy production. Several online immuno-monitoring systems have been successfully developed for the measurement of hIgG based on turbidimetric assays (83) and fluorescence measurements (84).

Biosensors have attracted wide-spread attention in the field of immunoglobulin quantification in recent years for many reasons such as simple instrumentation, fast operation, and high sensitivity and selectivity. Meanwhile, several biosensors have been developed for measurement of hIgG, including piezoelectric (85) and piezomagnetic biosensors (86), surface plasmon resonance biosensors (87-88) and electrochemical biosensors such as amperometric biosensors (89) and potentiometric biosensors (90). The majority of hIgG detection methodologies employed biosensor techniques are based on the protein A or protein G sensing platform. However, in spite of its high selectivity, protein A has some drawbacks such as its high cost, relatively low stability and the difficulty to immobilize it in the proper orientation (91). As mentioned early, the hexamer peptide ligand HWRGWV has a similar binding capability as protein A, and as a small ligand, the

immobilization of HWRGWV in the right orientation is much easier. This ligand is a good candidate to replace protein A for the production of a biosensors for immunoglobulin quantification.

2.3.3 IgG Oriented Immobilization and Potential Application in Immunosensor Fabrication

As mentioned earlier, the peptide ligand HWRGWV was found to bind the Fc fragment of IgG, which is the conserved part of the molecule. The binding site was, however, different from that for Protein A and Protein G attachment (91). According to mass spectrometry data, the hexamer peptide ligand HWRGWV binds to the pFc portion of hIgG. Figure 2.3 shows the result of a docking calculation using the HADDOCK (High Ambiguity Driven Docking) program indicating that HWRGWV binds to the Ser383-Asn389 (SNGQPEN) motif on the Fc fragment of hIgG. The binding of the loop to HWRGWV is specific, involving several forces of hydrogen bonding, hydrophobic, and possibly electrostatic interactions (92). Since the binding site is at the base of the Fc fragment, it is possible that when HWRGWV binds to hIgG it may orient the antibody at the interface in such a way that the variable region for antigen binding, the Fab fragments, will be more accessible to binding antigen in solution.

Orientation of IgG is critical for its applications for immunoassays and immunosensors. For immunoassay or immunosensor applications, the antibodies need to be immobilized onto a solid surface. The simplest method is a non-covalent adsorption of antibodies on surfaces. However, many studies over the past few years have proven that these types of procedures generally denature the majority of adsorbed antibodies (93-95). Alternatively, proteins can be covalently coupled to chemically activated surfaces through the reaction of lysine side chains

on the protein surface. IgGs can be directly coupled to amine-reactive surfaces (41, 96) or they can be biotinylated using NHS-activated biotin and then immobilized onto streptavidin (SA)-coated surfaces (95). Covalent immobilization could reduce the chances of denaturation, but the random attachment can cause the loss of binding activity of IgGs to antigens due to the following reasons. First, the antigen-binding site could be modified during the chemical modification of IgG. Second, the steric hindrance from the substrate and adjacently immobilized antibodies reduce the availability of immobilized IgG to antigens. Third, since there are multiple binding sites on the protein surface, IgG could be immobilized by multiple covalent bonds which could increase the chance of denaturation. For these reasons, antibodies are sometimes specifically immobilized onto surfaces such that the antigen-binding site is oriented away from the surface itself. Specific orientation can be accomplished by using an intermediate protein that binds to the Fc region of antibodies (97-99). The intermediate protein can be protein A or protein G to capture and orient IgG on solid surface. This type of immobilization strategy can result in a significantly higher fraction of active antibodies. As mentioned earlier, the short peptide HWRGWV has similar IgG binding behavior as protein A, while has several advantages over these protein ligands. Consequently, it could be an alternative to replace protein A and protein G for the application of immunoassay and immunosensors.

References:

1. Mohr P & Pommerening K (1986) *Affinity chromatography: practical and theoretical aspects* (CRC Press, New York).

2. Wang G, Salm JR, Gurgel PV, & Carbonell RG (2005) Small peptide ligands for affinity separations of biological molecules. *Chemical Engineering*, eds Gal'an MA & del Valle EM (John Wiley & Sons, Ltd., New York, NY).
3. Huang PY & Carbonell RG (1995) Affinity purification of proteins using ligands derived from peptide libraries. *Biotechnology and Bioengineering* 47(3):288-297.
4. Huang PY, *et al.* (1996) Affinity purification of von Willebrand factor using ligands derived from peptide libraries. *Bioorganic & Medicinal Chemistry* 4(5):699-708.
5. Bastek PD, Lang JM, Baumbach GA, Hammond DJ, & Carbonell RG (1998) Purification of alpha-1 proteinase inhibitor using ligands from combinatorial peptide libraries. *Abstracts Of Papers Of The American Chemical Society* 216:U328-U328.
6. de Lucena SL, Carbonell RG, & Santana CC (1999) Peptide affinity chromatography process for adsorption of fibrinogen. *Powder Technology* 101(2):173-177.
7. Gurgel PV, Carbonell RG, & Swaisgood HE (2000) Fractionation of whey proteins with a hexapeptide ligand affinity resin. *Bioseparation* 9(6):385-392.
8. Wang G, De J, Schoeniger JS, Roe DC, & Carbonell RG (2004) A hexamer peptide ligand that binds selectively to staphylococcal enterotoxin B: isolation from a solid phase combinatorial library. *Journal Of Peptide Research* 64(2):51-64.
9. Yang H, Gurgel PV, & Carbonell RG (2005) Hexamer peptide affinity resins that bind the Fc region of human immunoglobulin G. *Journal of Peptide Research* 66:120-137.
10. Heldt CL, Gurgel PV, Jaykus LA, & Carbonell RG (2008) Identification of trimeric peptides that bind porcine parvovirus from mixtures containing human blood plasma. *Biotechnology Progress* 24(3):554-560.
11. Gurgel PV, Carbonell RG, & Swaisgood HE (2001) Studies of the binding of alpha-lactalbumin to immobilized peptide ligands. *Journal of Agricultural and Food Chemistry* 49(12):5765-5770.

12. Yang H, Gurgel PV, & Carbonell RG (2009) Purification of human immunoglobulin G via Fc-specific small peptide ligand affinity chromatography. *Journal of Chromatography A* 1216.
13. Kaufman DB, *et al.* (2002) Affinity purification of fibrinogen using a ligand from a peptide library. *Biotechnology and Bioengineering* 77(3):278-289.
14. Kaufman DB & Carbonell RG (1999) Interaction of fibrinogen with peptide affinity supports - Resin effects. *Abstracts of Papers of The American Chemical Society* 217:U160-U160.
15. Wang GQ & Carbonell RG (2005) Characterization of a peptide affinity support that binds selectively to staphylococcal enterotoxin B. *Journal of Chromatography A* 1078(1-2):98-112.
16. Bastek PD & Carbonell RG (1999) Investigation of the binding mechanism between a peptide affinity resin and alpha-1 proteinase inhibitor. *Abstracts of Papers of The American Chemical Society* 217:U189-U189.
17. Kaufman DB, Hayes T, Buettner J, Hammond DJ, & Carbonell RG (2000) Chromatographic resolution of tryptophan enantiomers with L-Leu-L-Leu-L-Leu peptide - Effects of mobile phase composition and chromatographic support. *Journal of Chromatography A* 874(1):21-26.
18. Wang G & Carbonell RG (2006) Design of adsorptive columns for specific pathogen removal: application to staphylococcal enterotoxin B. *Biotechnology Progress* 22:1358-1367.
19. Baird CL & Myszka DG (2001) Current and emerging commercial optical biosensors. *Journal of Molecular Recognition* 14(5):261-268.
20. Collings AF & Caruso F (1997) Biosensors: recent advances. *Reports on Progress in Physics* 60(11):1397-1445.
21. Byfield MP & Abuknesha RA (1994) Biochemical aspects of biosensors. *Biosensors & Bioelectronics* 9(4-5):373-400.

22. Rogers KR & Mulchandani A (1998) *Affinity biosensors: techniques and protocols* (Humana Press Inc., Totowa, NJ) pp 1-4.
23. Lippa PB, Sokoll LJ, & Chan DW (2001) Immunosensors - principles and applications to clinical chemistry. *Clinica Chimica Acta* 314(1-2):1-26.
24. Zhou C, *et al.* (2004) Human immunoglobulin adsorption investigated by means of quartz crystal microbalance dissipation, atomic force microscopy, surface acoustic wave, and surface plasmon resonance techniques. *Langmuir* 20(14):5870-5878.
25. Viking TP, *et al.* (2000) Comparison of surface plasmon resonance and quartz crystal microbalance in the study of whole blood and plasma coagulation. *Biosensors & Bioelectronics* 15(11-12):605-613.
26. Su XD, Wu YJ, & Knoll W (2005) Comparison of surface plasmon resonance spectroscopy and quartz crystal microbalance techniques for studying DNA assembly and hybridization. *Biosensors & Bioelectronics* 21(5):719-726.
27. Hook F, *et al.* (2001) Variations in coupled water, viscoelastic properties, and film thickness of a Mefp-1 protein film during adsorption and cross-linking: A quartz crystal microbalance with dissipation monitoring, ellipsometry, and surface plasmon resonance study. *Analytical Chemistry* 73(24):5796-5804.
28. Damos FS, Mendes RK, & Kubota LT (2004) Applications of QCM, EIS and SPR in the investigation of surfaces and interfaces for the development of (BIO)sensors. *Quimica Nova* 27(6):970-979.
29. Hook F, *et al.* (2002) A comparative study of protein adsorption on titanium oxide surfaces using in situ ellipsometry, optical waveguide lightmode spectroscopy, and quartz crystal microbalance/dissipation. *Colloids And Surfaces B-Biointerfaces* 24(2):155-170.
30. Marx KA (2003) Quartz crystal microbalance: A useful tool for studying thin polymer films and complex biomolecular systems at the solution-surface interface. *Biomacromolecules* 4(5):1099-1120.

31. Strong L & Whitesides GM (1988) Structures of self-assembled monolayer films of organosulfur compounds adsorbed on gold single-crystals - electron-diffraction studies. *Langmuir* 4(3):546-558.
32. O'Sullivan CK & Guilbault GG (1999) Commercial quartz crystal microbalances - theory and applications. *Biosensors & Bioelectronics* 14(8-9):663-670.
33. Johannsmann D, Mathauer K, Wegner G, & Knoll W (1992) Viscoelastic properties of thin films probed with quartz crystal resonator. *Physical Review B* 46(12):7808-7815.
34. Hook F, Rodahl M, Brzezinski P, & Kasemo B (1998) Measurements using the quartz crystal microbalance technique of ferritin monolayers on methyl-thiolated gold: Dependence of energy dissipation and saturation coverage on salt concentration. *Journal of Colloid and Interface Science* 208(1):63-67.
35. Su XD, Chew FT, & Li SFY (2000) Design and application of piezoelectric quartz crystal-based immunoassay. *Analytical Sciences* 16(2):107-114.
36. Choi KH, *et al.* (2003) Investigation of protein adsorption with simultaneous measurements of atomic force microscope and quartz crystal microbalance. *Journal of Vacuum Science & Technology B* 21(4):1433-1436.
37. Stadler H, Mondon M, & Ziegler C (2003) Protein adsorption on surfaces: dynamic contact-angle (DCA) and quartz-crystal microbalance (QCM) measurements. *Analytical and Bioanalytical Chemistry* 375(1):53-61.
38. Su XD & Zhang H (2004) Comparison of surface plasmon resonance spectroscopy and quartz crystal microbalance for human IgE quantification. *Sensors and Actuators B-Chemical* 100(3):309-314.
39. Reimhult E, Larsson C, Kasemo B, & Hook F (2004) Simultaneous surface plasmon resonance and quartz crystal microbalance with dissipation monitoring measurements of biomolecular adsorption events involving structural transformations and variations in coupled water. *Analytical Chemistry* 76(24):7211-7220.

40. Carrigan SD, Scott G, & Tabrizian M (2005) Real-time QCM-D immunoassay through oriented antibody immobilization using cross-linked hydrogel biointerfaces. *Langmuir* 21(13):5966-5973.
41. Caruso F, Rodda E, & Furlong DN (1996) Orientational aspects of antibody immobilization and immunological activity on quartz crystal microbalance electrodes. *Journal of Colloid and Interface Science* 178(1):104-115.
42. Graneli A, Edvardsson M, & Hook F (2004) DNA-based formation of a supported, three-dimensional lipid vesicle matrix probed by QCM-D and SPR. *ChemPhysChem* 5(5):729-733.
43. Niikura K, Nagata K, & Okahata Y (1996) Quantitative detection of protein binding onto DNA by using a quartz-crystal microbalance. *Chemistry Letters* (10):863-864.
44. Poitras C & Tufenkji N (2009) A QCM-D-based biosensor for E. coli O157:H7 highlighting the relevance of the dissipation slope as a transduction signal. *Biosensors and Bioelectronics* 24:2137–2142.
45. Homola J, Yee SS, & Gauglitz G (1999) Surface plasmon resonance sensors: review. *Sensors and Actuators B-Chemical* 54(1-2):3-15.
46. Fivash M, Towler EM, & Fisher RJ (1998) BIAcore for macromolecular interaction. *Current Opinion in Biotechnology* 9(1):97-101.
47. McDonnell JM (2001) Surface plasmon resonance: towards an understanding of the mechanisms of biological molecular recognition. *Current Opinion in Chemical Biology* 5(5):572-577.
48. Rich RL & Myszka DG (2000) Advances in surface plasmon resonance biosensor analysis. *Current Opinion in Biotechnology* 11(1):54-61.
49. Green RJ, *et al.* (2000) Surface plasmon resonance analysis of dynamic biological interactions with biomaterials. *Biomaterials* 21(18):1823-1835.

50. Liedberg B, Nylander C, & Lundstrom I (1983) Surface plasmon resonance for gas detection and biosensing. *Sensors and Actuators B* 4:299-304.
51. Williams RA & Blanch HW (1994) Covalent Immobilization Of Protein Monolayers For Biosensor Applications. *Biosensors & Bioelectronics* 9(2):159-167.
52. Mello LD & Kubota LT (2002) Review of the use of biosensors as analytical tools in the food and drink industries. *Food Chemistry* 77(2):237-256.
53. Oh SJ, Hong BJ, Choi KY, & Park JW (2006) Surface modification for DNA and protein microarrays. *Omics-A Journal of Integrative Biology* 10(3):327-343.
54. Bilitewski U (2006) Protein-sensing assay formats and devices. *Analytica Chimica Acta* 568(1-2):232-247.
55. Tomizaki KY, Usui K, & Mihara H (2005) Protein-detecting microarrays: Current accomplishments and requirements. *ChemBiochem* 6(5):783-799.
56. Gnauck M, *et al.* (2007) Carboxy-terminated oligo(ethylene glycol)-alkane phosphate: Synthesis and self-assembly on titanium oxide surfaces. *Langmuir* 23(2):377-381.
57. Houseman BT, Huh JH, Kron SJ, & Mrksich M (2002) Peptide chips for the quantitative evaluation of protein kinase activity. *Nature Biotechnology* 20(3):270-274.
58. Nyquist RM, *et al.* (2000) Characterization of self-assembled monolayers for biosensor applications. *Langmuir* 16(4):1793-1800.
59. Xia N, Hu YH, Grainger DW, & Castner DG (2002) Functionalized poly(ethylene glycol)-grafted polysiloxane monolayers for control of protein binding. *Langmuir* 18(8):3255-3262.
60. Ulman A (1996) Formation and structure of self-assembled monolayers. *Chemical Reviews* 96(4):1533-1554.

61. Wink T, vanZuilen SJ, Bult A, & vanBennekom WP (1997) Self-assembled monolayers for biosensors. *Analyst* 122(4):R43-R50.
62. Bain CD & Whitesides GM (1988) Molecular-level control over surface order in self-assembled monolayer films of thiols on gold. *Science* 240(4848):62-63.
63. Sellers H, Ulman A, Shnidman Y, & Eilers JE (1993) Structure and binding of alkylthiolates on gold and silver Surface: implications for self-assembly. *Journal of American Chemistry Society* 115:9389.
64. Bain CD & Whitesides GM (1988) Correlations Between Wettability And Structure In Monolayers Of Alkanethiols Adsorbed On Gold. *Journal of the American Chemical Society* 110(11):3665-3666.
65. Bain CD, *et al.* (1989) Formation of monolayer films by the spontaneous assembly of organic thiols from solution onto gold. *Journal of the American Chemical Society* 111(1):321-335.
66. Hage DS (2006) *Handbook of affinity chromatography* (CRC Press, Boca Raton, FL) pp 557, 539.
67. Prime KL & Whitesides GM (1993) Adsorption of proteins onto surfaces containing end-attached oligo(ethylene oxide) - a model system using self-assembled monolayers. *Journal of the American Chemical Society* 115(23):10714-10721.
68. Matsushima A, Kodera Y, Hiroto M, Nishimura H, & Inada Y (1996) Bioconjugates of proteins and polyethylene glycol: Potent tools in biotechnological processes. *Journal of Molecular Catalysis B-Enzymatic* 2(1):1-17.
69. Cha TW, Boiadjiev V, Lozano J, Yang H, & Zhu XY (2002) Immobilization of oligonucleotides on poly(ethylene glycol) brush-coated Si surfaces. *Analytical Biochemistry* 311(1):27-32.
70. Kwon Y, Han ZZ, Karatan E, Mrksich M, & Kay BK (2004) Antibody arrays prepared by cutinase-mediated immobilization on self-assembled monolayers. *Analytical Chemistry* 76(19):5713-5720.

71. Martin Y & Vermette P (2006) Low-fouling amine-terminated poly(ethylene glycol) thin layers and effect of immobilization conditions on their mechanical and physicochemical properties. *Macromolecules* 39(23):8083-8091.
72. Ajikumar PK, *et al.* (2007) Carboxyl-terminated dendrimer-coated bioactive interface for protein microarray: High-sensitivity detection of antigen in complex biological samples. *Langmuir* 23(10):5670-5677.
73. Leffell MS, Donnenberg AD, & Rose NR (1997) *Handbook of human immunology* (CRC Press, New York, NY) p 73.
74. Nezlin R (1998) *The Immunoglobulins: structure and function* (Academic Press, New York, USA) pp 36-37.
75. Curling JM (1980) *Methods of plasma protein fractionation.* (Academic Press, London, UK) pp 96-98.
76. Huse K, Bohme HJ, & Scholz GH (2002) Purification of antibodies by affinity chromatography. *Journal of Biochemical and Biophysical Methods* 51(3):217-231.
77. Roque ACA, Lowe CR, & Taipa MA (2004) Antibodies and genetically engineered related molecules: Production and purification. *Biotechnology Progress* 20(3):639-654.
78. Low D, O'Leary R, & Pujar NS (2007) Future of antibody purification. *Journal of Chromatography B-Analytical Technologies in the Biomedical and Life Sciences* 848(1):48-63.
79. Boschetti E (2001) The use of thiophilic chromatography for antibody purification: a review. . *Journal of Biochemical and Biophysical Methods* 49:361-389.
80. Verdoliva A, Pannone F, Rossi M, Catello S, & V. M (2002) Affinity purification of polyclonal antibodies using a new all-D synthetic peptide ligand: comparison with protein A and protein G. . *Journal of Immunological Methods* 271: (1-2):77-88.

81. Newcombe AR, *et al.* (2005) Optimised affinity purification of polyclonal antibodies from hyper immunised ovine serum using a synthetic Protein A adsorbent, MAbsorbento (R) A2P. *Journal of Chromatography B. Biomedical Science* 814(Apl. (2)):209-215.
82. Provan D (2005) *Oxford handbook of clinical and laboratory investigation* (Oxford University Press, Oxford, UK).
83. Middendorf C, *et al.* (1993) On-line immunoanalysis for bioprocess control. *Journal of Biotechnology* 31:395-403.
84. Reif OW, Lausch R, Scheper T, & Freitag R (1994) Fluorescein isothiocyanate-labeled protein G as an affinity ligand in affinity/immunocapillary electrophoresis with fluorescence detection. *Analytical Chemistry* 66:4027-4033. .
85. Chen H, *et al.* (2007) A novel piezoelectric immunoagglutination assay technique with antibody-modified liposome. *Biosensors & Bioelectronics* 22(993-999).
86. Ogi H, Motohisa K, Matsumoto T, Mizugaki T, & Hirao M (2006) Wireless electrodeless piezomagnetic biosensor with an isolated nickel oscillator. *Biosensors & Bioelectronics* 21:2001-2005.
87. Labib M, Hedstrom M, Amin M, & Mattiasson B (2009) A multipurpose capacitive biosensor for assay and quality control of human immunoglobulin G. *Biotechnology and Bioengineering* 104(2):312-320.
88. Mytych DT, La S, Barger T, Ferbas J, & Swanson SJ (2009) The development and validation of a sensitive, dual-flow cell, SPR-based biosensor immunoassay for the detection, semi-quantitation, and characterization of antibodies to darbepoetin alfa and epoetin alfa in human serum. *Journal of Pharmaceutical and Biomedical Analysis* 49(2):415-426.
89. Bian C, Xia S, Xu Y, Chen S, & Cui Z (2005) A micro amperometric immunosensor based on two electrochemical layers for immobilizing antibody. *IEEE Sensors* 2001:416-419.
90. Li J & Gao H (2008) A renewable potentiometric immunosensor based on Fe₃O₄ nanoparticles immobilized anti-IgG. *Electroanalysis* 8:881-887.

91. Denizli A & Arica Y (2000) Protein A immobilized microporous polyhydroxyethyl methacrylate affinity membranes for selective sorption of human-immunoglobulin G from human plasma. *Journal of Biomaterial Science, Polymer Edition* 11:367-382.
92. Yang H, *et al.* (2010) Binding site on human immunoglobulin G for the affinity ligand HWRGWV. *Journal of Molecular Recognition* 23:271-282.
93. Rao SV, Anderson KW, & Bachas LG (1998) Oriented immobilization of proteins. *Mikrochimica Acta* 128(3-4):127-143.
94. Turkova J (1999) Oriented immobilization of biologically active proteins as a tool for revealing protein interactions and function. *Journal of Chromatography B* 722(1-2):11-31.
95. Peluso P, *et al.* (2003) Optimizing antibody immobilization strategies for the construction of protein microarrays. *Analytical Biochemistry* 312(2):113-124.
96. Lu B, Xie JM, Lu CL, Wu CG, & Wei Y (1995) Oriented immobilization of Fab' fragments on silica surfaces. *Analytical Chemistry* 67(1):83-87.
97. Bae YM, Oh BK, Lee W, Lee WH, & Choi JW (2005) Study on orientation of immunoglobulin G on protein G layer. *Biosensors & Bioelectronics* 21(1):103-110.
98. Brogan KL & Schoenfish MH (2005) Influence of antibody immobilization strategy on molecular recognition force microscopy measurements. *Langmuir* 21(7):3054-3060.
99. Starodub NF, Pirogova LV, Demchenko A, & Nabok AV (2005) Antibody immobilisation on the metal and silicon surfaces. The use of self-assembled layers and specific receptors. *Bioelectrochemistry* 66(1-2):111-115.

Table 2.1 Comparison of QCM and SPR

	QCM	SPR
Measurement	Total mass	Dry mass
Response range	Å - μm	Å - 300 nm
Intrinsic sensitivity*	1Hz ~ 17.7 ng cm ⁻²	1 millidegree ~ 0.64 ng cm ⁻²
Environmental effect	Sensitive	Less sensitive
Applicability	Any coating with a viscosity and viscoelasticity contrast with the surrounding medium	Any coating with an optical contrast with the surrounding medium
Other functions	QCM damping is reflective of the viscoelasticity of a coating	
Limitation	Liquid phase frequency response is complicated for thin film thickness measurements	Refractive index of the coating must be known if a simple measurement is to provide the thickness and mass

* The intrinsic sensitivities of QCM and SPR depend on the instrument fabrication and the value provided here is for the devices used in this study: QCM-D apparatus (model E4, Q-Sense AB, Göthenburg, Sweden) and SPR-Navi device (KSV, Instruments OY, Helsinki, Finland).

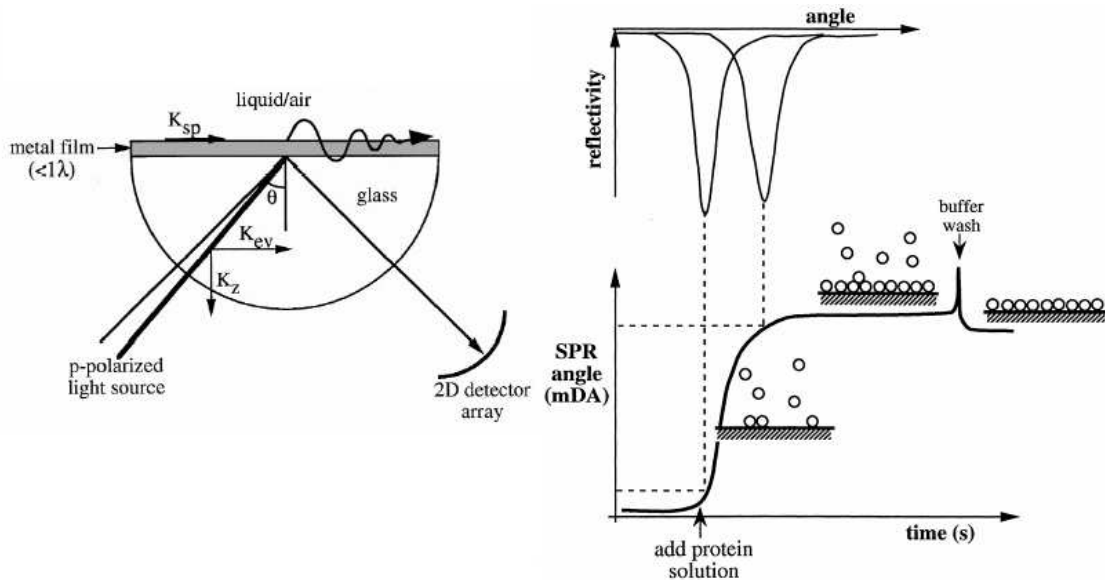


Figure 2.1 The principle of SPR

Chapter 2. Literature Review

2.1 Short Peptides as Affinity Ligands

2.1.1 Overview

Affinity techniques are among the most efficient methods to purify and detect biomolecules (1). Due to their high specificity, monoclonal antibodies are the most common ligands currently used in affinity techniques. Short peptide ligands with sufficient specificity can have many advantages over antibodies for purification or detection purposes. Short peptides are more stable than monoclonal antibodies because they do not require a specific tertiary structure to maintain their biological activity. The manufacture of short peptides can be scaled-up under good manufacturing practices (GMP) conditions at relatively low cost. The interactions between small peptides and proteins tend to be moderate so that the target protein can be eluted under mild condition without a detrimental influence on protein activity (2).

Short peptides have already been successfully screened and identified from peptide libraries in our group for the purification or detection of S protein (3), von Willebrand factor (4), alpha-1 proteinase inhibitor (5), fibrinogen (6), alpha-lactalbumin (7), staphylococcal enterotoxin B (8), human IgG (9) and porcine parvovirus (10).

Although the peptide ligands identified for the different proteins were screened using the same general methodology, the final results obtained were somewhat variable. Some peptide ligands identified by library screening show high high specificity to their target protein. That is the case for peptide YNFEVL and s-protein (3). Other peptide ligands behave as pseudo-affinity ligands, displaying dissociation constants (K_d) in the range of 10^{-5} to 10^{-8} M with their target proteins. An example of this behavior is the peptide ligand RLRSFY and von

Willebrand factor (vWF) (4). In general, pseudo-affinity peptide ligands are more suitable for the capture or concentration of the target molecule at an early stage in purification, while the more specific peptide ligands can be efficient for purifying the protein in one step, but usually it is placed in the later stages to maximize the efficiency of the affinity column (2).

Generally, ligand-target interactions for short peptide ligands are stronger than the pure ion exchange or pure hydrophobic interactions, since the affinity interaction between the peptide ligands and target biomolecules is the result of the interactions of each amino acid in the peptide sequences with the biomolecules. Any charged amino acid in the peptide ligand tends to form ionic interactions with the target molecule, while the amino acids in the ligand with hydrophobic groups interact with the hydrophobic patches on biomolecules (2). For a specific peptide ligand, the interaction could be ion-interaction dominated or hydrophobic-interaction dominated and, in some cases, the dominant force could change with the solvent conditions. For instance, the interaction between WHWRKR and alpha-lactalbumin at low temperatures is dominated by electrostatic interactions, while, as the temperature increases, hydrophobic interactions become the dominant binding mechanism (11).

2.1.2 Characterization of Peptide Ligands by Kinetics and Thermodynamics Analysis

As mentioned above, peptide ligands with different bio-selectivity to targets biomolecules could play different roles in purification processes. In addition, these affinity interactions between peptide ligands and target biomolecules could have different characteristics. In order to optimize the performance of these peptide ligands for bioseparation or detection, these peptides need to be well characterized. Our research group has made extensive efforts to characterize these peptide ligands by quantification of the thermodynamic and kinetic

parameters of the interaction between peptide ligands on chromatographic resins and target biomolecules under different conditions. It has been found that the affinity of the peptides to target biomolecules can depend on the variation of experimental conditions including peptide density (2-4, 8, 12), pH (4, 11-12), temperature (11, 13), and salt concentrations in the buffer (4).

In previous studies of the adsorption isotherm of target proteins to ligands on porous chromatography resins the adsorbed amounts of target biomolecules under different conditions were determined by mass balance (3, 11-12, 14-16). This is an indirect method of measuring the amount of protein adsorbed, and can generate a significant error when the change of protein concentration due to adsorption is small compared to the unbound protein concentration. The kinetic parameters of affinity binding to peptide ligands on resins were studied by dynamic adsorption experiments carried using high performance liquid chromatography (HPLC). Different models have been employed to describe the solute transport within the chromatography column to get the intrinsic kinetic parameters. A lumped kinetic model was employed for the study of the adsorption kinetics of fibrinogen that binds to the short peptide FLLVPL (13). In this work, columns with varying peptide densities were challenged with a fibrinogen solution at a constant flow rate. The concentration of the exit stream was measured continuously as a function of time. The shapes of the breakthrough curves were modeled using the lumped kinetics model that took into account axial dispersion, interparticle mass transfer and intraparticle diffusion, and the rates of adsorption and desorption of the protein to the surface. All the mass transfer parameters were estimated from correlations or measured directly, and the only remaining parameter in each run was the

adsorption rate constant onto the resin. The rate constant for adsorption was obtained by finding the best fit to the breakthrough curve. The resulting analysis showed that the adsorption rates were indeed rate-limiting and that the rate of adsorption was relatively independent of peptide density. Although the lumped kinetics model threw a light on the understanding of the relationship between adsorption rate and peptide density, it was found that the capacity and association constant derived from the fitting of the experimental breakthrough data with this model was inconsistent with equilibrium experiments (13, 17). A more sophisticated effort using the General Rate Model of chromatography was shown to fit well with experimental results in the analysis of Staphylococcal enterotoxin B (SEB) binding with peptide ligand YYWLHH (15, 18). Generally, the reliability of the final results for the kinetics of adsorption and desorption depend on the accuracy of the transport models and the estimation of the mass transfer parameters.

In summary, the affinity interaction between peptide ligands and biomolecules have been studied by indirect methods, batch adsorption mode and chromatography techniques, which may lead to significant errors under certain situations. New methods that can directly monitor the affinity interactions occurring at liquid-solid interface can lead to more detailed information on the nature and rates of these interactions.

2.2 Study Affinity Interactions by Quartz Crystal Microbalance and Surface Plasmon Resonance

2.2.1 Overview

Biosensors have been playing an increasingly important role in research on biointeractions during recent years (19-20). Compared with traditional detection methods, such as filter binding assays, radioimmunoassays and enzyme-linked immunosorbent assays (ELISAs), biosensors are fast, simple and relatively inexpensive. Biosensor systems can directly monitor the macromolecular interactions happening on solid-liquid interface in real time. In addition, the mass transport processes within these systems are generally simpler than those in a chromatography column; consequently, the interpretation of the dynamic adsorption behavior could be relatively easier.

A biosensor is basically a chemical or mass sensor in which the analytical signal is generated by the bio-affinity elements immobilized or physically adsorbed on a transducer (21-22). During the design of an affinity biosensor, the following aspects need to be carefully taken into consideration: the properties of the affinity recognition elements (ligands), the mechanism of signal transduction, and the method of immobilization. This research focuses on short (hexamer) linear peptide ligands. The mechanism of signal transduction and the method of immobilization are discussed in the following paragraphs.

Biosensors can be divided into several types depending on the different transduction mechanisms: thermal, optical, electrochemical, acoustic, or piezoelectric (23). Currently, there is a trend to combine surface detection techniques based on different transduction mechanism, which provides different perspectives on binding events occurring at interface (24-26). In this research, attention is focused on two kinds of techniques: surface plasmon resonance (SPR) and quartz crystal microbalance with dissipation (QCM-D). The features of QCM and SPR techniques are summarized in Table 2.1. The most important difference

between SPR and QCM methods is that SPR measures the dry mass of biomolecules adsorbed on the surface, while QCM measure the total mass on the surface, including the water and ions associated with the biomass (27-28). In general, SPR is more quantitative than QCM, while the advantage of QCM over SPR is its capability to provide a qualitative measure of the viscoelastic properties of the adsorbed protein layer (24). The combination of these two techniques can provide more reliable and complementary data. The principles and applications of these two techniques are presented in detail in the following sections.

2.2.2 Principle of QCM and Its Applications

QCM sensors consist of a thin slice of a single crystal of quartz sandwiched between two metal electrodes, housed in a sealed package that provides a means of connection to a circuit. An alternating electrical voltage applied to these electrodes causes the quartz to vibrate, or oscillate, at its resonant frequency. This frequency is dependent on the mass of the crystal as well as the mass of any layers confined on the surface of the electrode areas of the crystal. When the electrical field applied to the quartz crystal is turned off, the oscillation of the crystal attenuates as a result of the energy lost during oscillation. The dissipation factor, D , is the sum of all the energy lost in the system per oscillation cycle (29). The dissipation depends on the interaction between the film, the sensor surface and the properties of the adsorbed film. When the film on the electrodes of crystal is slippery or when the film is viscous, more energy will be dissipated by friction during the oscillatory motion induced in the film. As a result, the dissipation factor D provides an indirect measure of the flexibility of the adsorbed film.

The merits of the QCM technique are primarily its simplicity and sensitivity (in the ng cm^{-2} range). Sauerbrey reported a linear relationship between the frequency decrease of an oscillating quartz crystal (Δf) and the bound elastic mass of deposited metal, Δm (30),

$$\Delta f = -\frac{2f_0^2 \Delta m}{(\rho_q \mu_q)^{1/2} A} \quad 2-1$$

where f_0 is the fundamental resonance frequency of the quartz crystal, ρ_q is the specific density of the quartz (2.648 g cm^{-3}), μ_q is the shear wave velocity in quartz ($2.947 \times 10^{11} \text{ g cm}^{-1} \text{ s}^{-2}$ for AT-cut quartz crystals) and A is the measuring area.

The Sauerbrey equation was derived based on two assumptions: (1) the film is rigid (no internal friction in the added mass); (2) the film is coupled perfectly to the oscillatory motion of the quartz crystal (no slip between the film and the crystal electrode).

For rigid, evenly distributed, and sufficiently thin adsorbed layers, the Sauerbrey equation has indeed been shown to provide a good approximation (31-32). However, for soft adsorbed films, this is not the case anymore, due mainly to two potential reasons: the first one is connected with the propagation of the shear acoustic wave in a viscoelastic film. For a sufficiently thin and rigid adsorbed film, the adsorbed layer acts as a “dead” mass on the piezoelectric oscillator. On other hand, for a viscoelastic or thicker film coupled on oscillator, the change of frequency is not directly proportional to change of mass. In other words, the effectively coupled mass depends on how the oscillatory motion of the crystal propagates into and through an adsorbed viscoelastic film (33-34). The second reason of the failure of the Sauerbrey relation is the solvent, which, in most cases, is water. In QCM measurements, water (or any other liquid or solvent molecules) may couple as an additional mass via direct

hydration, viscous drag, or entrapment in cavities in the adsorbed film, which contributes to the overestimation of the mass from the Sauerbrey equation. The typical amount of coupled water in different systems has been shown to add a significant variation and it depends on the nature of the film. The mass-uptake estimations could be 1.5 to 10 times larger than the molar mass (27, 29, 34-37).

Early chemical applications of QCM involved monitoring of mass and film thickness in coating equipment in vacuum and on investigating the adsorption in gas phase (32). In the 1980s, solution-based QCM was developed and it found more applications in mainly two fields: electrochemistry and biotechnology. In the area of biotechnology, QCM has been used to measure protein adsorption kinetics (38), protein conformation analysis (24, 39), antibody-antigen interactions (40-41), nucleotide hybridization (26), nucleotide-protein interactions (42-43), and bacteria (44) and cell adsorption (25). In liquid-phase measurements, the QCM is not a simple mass sensor, but provides valuable information about reactions and conditions at the liquid-solid interface.

2.2.3 Principle of SPR and its application

Surface plasmon resonance is an optical technique that is widely recognized as a valuable tool in the investigation of biomolecular interactions (45). It can monitor the dynamic processes occurring on the surface in real time and provide kinetic and thermodynamic data (46-47).

A surface plasmon is a longitudinal charge wave that propagates along the interface of two media with very different optical densities such as metal and water. The attenuated total reflectance (ATR) configuration developed by Krethmann (as shown in Figure 1) is widely

used in most SPR instruments. A monochromatic, p-polarized light traveling through an optically dense medium (glass) reaches an interface between this medium and an optical medium with lower density (buffer) and then reflects back into the denser medium (Figure 1). Under conditions of total internal reflection, most of the light will be reflected back into the higher-density medium but there is still a small portion of light, the evanescent wave, that penetrates the interface into the less-dense medium a distance of approximately one wavelength (48). The evanescent wave vector can be expressed in the form,

$$K_{ev} = \frac{\omega_0}{c} \eta_g \sin \theta \quad 2-2$$

where, ω_0 is the frequency of incident light, c is the speed of light in a vacuum, η_g is the refractive index of the dense medium, and θ is the angle of incident light. The wave vector corresponding to the surface plasmon is expressed by the formula,

$$K_{sp} = \frac{\omega_0}{c} \eta_g \sqrt{\frac{\epsilon_m \eta_s^2}{\epsilon_m + \eta_s^2}} \quad 2-3$$

where, η_s is the refractive index of the dielectric medium on the top of the sensor surface, and ϵ_m is the dielectric constant of the metal film.

When the incidence angle of the light is chosen in such a way that the magnitude of the evanescent wave is equal to that of the surface plasmon wave vector,

$$K_{ev} = K_{sp} \quad 2-4$$

the evanescent wave of the light can couple with the plasmon in the metal film. In other words, the surface plasmon is resonantly excited. In this situation, the incident light dissipates energy into the metal film. As a result, the intensity of reflected light is reduced

and forms a dip (49). Since K_{ev} is a function of the refractive index of the dielectric medium n_s , n_s can be measured by recording the change of this incident angle satisfying the condition required for surface plasmon resonance.

When binding events occur on the surface, the adsorbed protein molecules replace the buffer solution close to the sensor surface. The difference between the refractive index of the adsorbed protein molecules and that of the buffer solution replaced will be detected by SPR. There is no difference between the water molecules attached on the surface of proteins or entrapped in the adsorbed protein layer and those in buffer solution replaced by the adsorbed protein layer. Consequently, water molecules within the adsorbed protein layer cannot be detected by the SPR. In other word, the mass measured by SPR is “dry mass”.

As an optical technique used for the study of affinity interactions, SPR has been developed in the 1980's (50). After that, SPR has played a significant role in the research of biomolecules and their interactions. In the past decades, SPR has also been increasingly used for detection and identification of chemical and biological substances (45).

2.2.4 Importance of Surface Preparation for Ligand Immobilization

Biomolecules can be immobilized on sensor surfaces by physical adsorption, covalent bonding, crosslinking, entrapment, or encapsulation. Among those methods, adsorption and covalent bonding are the most commonly used (28, 51). Physical adsorption of the biocomponent based on van der Waals attractive forces is the simplest method available and it is feasible for various substrates. However, this method does not provide high surface density of affinity elements, and the adsorbed biomolecules could be lost through changes in pH, ionic strength, or temperature due to adsorption reversibility (51-52). Covalent bonding

to the surface can lead to slight modifications of the biomolecules, but, this approach results in more stable surfaces, and is more reliable and reproducible DNA-based formation of a supported, three-dimensional lipid vesicle matrix probed by QCM-D and SPR (53-55).

For covalent bonding, generally the substrates need to be modified to introduce active groups such as carboxyl, thioacetyl, hydroquinone, or epoxide groups for the immobilization of biomolecules (56-59). Self-assembled monolayers (SAMs) are one of the most convenient methods to modify the sensor surface. A SAM is a molecular assembly obtained by immersion of an appropriate substrate into a solution of a surfactant in organic solvent (60). This simple process makes SAMs technologically attractive for the functionalization of sensor surfaces with active groups.

There are several types of SAMs and among them two kinds, organosilicon on hydroxylated surfaces, and alkanethiols and dialkyl disulfides on gold and other noble metals, are the most common methods for biomolecule immobilization (60-61). Due to their simplicity and versatility, the SAMs of alkanethiols on gold have been the most studied SAMs.

The structure of these SAMs is now well established (62). Sulfur compounds have a strong affinity for transition metal surfaces (63). For an alkanethiols with an alkyl chain longer than 10 carbon atoms, it is possible to obtain very ordered layers, with few defects, depending mostly on the irregularity of the gold surface (31, 62, 64-65). The terminal functional groups of o-substituted alkane thiols dominate the properties of the interfaces between the SAMs and the contacting liquids and these groups offer great versatility to covalently immobilize biological molecules, such as peptides or proteins on sensor surfaces.

Chemisorption of alkanethiols as well as of dialkyl disulfides on clean gold gives indistinguishable monolayers. The rates of formation of SAMs from dialkyl disulfides or alkanethiols are also indistinguishable, but the rates of replacement of molecules from SAMs by thiols are much faster than by disulfides (60).

SAMs of alkylchlorosilanes, alkylalkoxysilanes, and alkylaminosilanes require hydroxylated surfaces as substrates, such as silicon oxide, aluminum oxide, quartz, glass, mica, and zinc selenide, for their formations. The driving force for this self-assembly is the formation of polysiloxane, which is connected to surface silanol groups (-SiOH) via Si-O-Si bonds (61). The control of the quality of the SAMs of silanes is generally harder than that of alkanethiols. The formation of silane SAMs is sensitive to water. While incomplete monolayers are formed in the absence of moisture on substrate, the excess water results in facile polymerization in solution and polysiloxane deposition of the surface (60). The advantage of SAMs of silane over those of alkanethiols is their relatively higher stability (61).

Besides the introduction of active groups for immobilization of biomolecules, there are other two objectives of surface modification. First, adding a spacer arm on top of a substrate is desirable to enhance the availability of the ligands on the surface of the modified layer. Spacer arms have been widely used in affinity chromatography or membranes for bioseparations. They can play a significant role in the affinity interaction between ligands on solid surfaces and biomolecules in solution, especially for small ligands, and this effect could be even more critical when the active site of the target molecule is located in a pocket (1, 66). A good spacer arm should have just enough length to facilitate the formation of ligand and

target biomolecule complex. If no spacer arm, or too short a spacer arm is used, it might be hard to form the complex of ligand and target molecule due to steric hindrance; if it is too long the density of ligand could be low and nonspecific binding to spacer arm could become predominant over the affinity interaction (66). The other objective of surface modification is to minimize the background noise from the nonspecific binding of proteins and other species in the bulk solution. Poly (ethylene glycol) (PEG) is well-established as one of the primary components in nonfouling film chemistry. The resistance of PEG coated surfaces to nonspecific binding is dependent on the molecular weight of the PEG and the resulting packing density of the PEG chains (67). In addition, PEG is also a good candidate spacer arm, since PEG brushes have a high flexibility in biological media. Consequently, materials including PEG composite have been widely applied to modify surface for bio-application (68-72).

2.3 Potential Applications of Fc-specific Hexamer Peptide Functionalized

Biosensor

2.3.1 Fc-specific Peptide Ligand for IgG Purification

Antibodies, also known as immunoglobulins (Ig), are glycoproteins produced by white blood cells, each having a special antigen-binding pocket that is sensitive to specific parts of an antigen protein. The human immunoglobulins account for approximately 20% of all proteins in human plasma, and can be divided into five classes or isotypes: IgG, IgA, IgM, IgD, and IgE. Among them, IgG is the most abundant class of Igs in the body, constituting

approximately 75% of the total immunoglobulins at an average concentration of 12 mg/ml in adult blood (73).

As shown in Figure 2.1, IgG has a Y-shaped structure with the molecular weights of the heavy (H) and light (L) chains being 50 and 25 KDa, respectively. Although the general structures of IgGs are very similar, a small region at the tip of the protein is extremely variable, allowing millions of IgGs with slightly different tip structures, or antigen binding sites, to exist. As shown in Figure 2.1, the "V" label indicates a variable region where the amino acid composition varies with the response antigens, while the "C" label denotes a constant region where the amino acid composition is relatively invariant for IgGs. Starting from the amino terminus, the L chains include the VL and CL domains while the H chains encompass the VH, CH1, hinge, CH2, and CH3 regions. The V regions of both heavy and light chains are responsible for antigen binding by forming a pocket with six loops. The C region is engaged in a variety of effector functions (74).

IgG and its fragments have found a wide array of applications as pharmaceutical compounds, in addition to their common usage in the purification and localization of proteins. Conventionally, IgG preparations have been produced exclusively by precipitation techniques, preferably involving cold ethanol fractionation. In recent years, however, chromatographic steps have been introduced into the downstream of the ethanol fractionation steps (75). Ion-exchange chromatography, hydrophobic interaction chromatography, size-exclusion chromatography, and affinity chromatography have all been involved in IgG capture and purification and, among them, affinity chromatography allows the possibility of obtaining several fold purification with high recovery in fewer steps (76).

Staphylococcus aureus Protein A and *Streptococcus* Protein G are the most common affinity ligands for IgG purifications and detections (76-77). However, the drawbacks associated with these two protein ligands, including high cost and low stability, have given rise to the searching for alternative affinity ligands for antibody purification (76, 78). Special attention has been paid to the use of small ligands for affinity purification of antibodies due to their advantages of being more stable (no three-dimensional structure), less immunogenic, and less expensive than large protein ligands. Some synthetic small ligands have been extensively studied for IgG purification and detection, such as the hydrophobic charge induced ligand MEP (4-mercapto ethyl pyridine) (79), the Protein A mimetic peptide Kaptiv-GY based on the sequence (RTY)₄K₂KG (TG19318) (80) and a synthetic ligand MAbSorbant A2P derived from a triazine derivative ligand 22/8 (81). However none of these ligands that bind to antibodies behaved like Protein A in their binding specificity to the Fc fragment. The ability to bind through the Fc fragment is an important function since it allows the ligand to be used as a universal ligand for whole antibodies and Fc-fusion proteins, potentially diminishing the time required to develop separation processes for new antibodies.

Three hexamer peptide ligands, HWRGWV, HFRRHL, and HYFKFD, identified by our group, were the first reported short peptide ligands that were able to mimic the binding specificity of Protein A to the Fc fragment of human IgG (hIgG) (9). The performance of the peptide HWRGWV for the purification of hIgG in complex fluids has been extensively studied and characterized. An HWRGWV resin with a peptide density of 0.08 meq g⁻¹ of dry resin was able to purify hIgG from mammalian cell culture media containing 10% fetal calf serum (cMEM) with both purity and yield as high as 95%, comparable to Protein A and A2P

agarose gels (12). The ligand also demonstrated its ability to isolate hIgG from Cohn II+III paste and yields of 82% and purities of 73% were obtained in one step. Bound IgG can be eluted under milder conditions than with Protein A, with the target molecule being released from the resin at pH 4, in contrast to the typical pH 3.0 elution using Protein A. The ligand was found to bind to IgG from different organisms, including bovine, murine, goat, and rabbit IgGs. The peptide also displayed affinity to different subclasses of IgG, such as HIgG1, HIgG2, HIgG3, and HIgG4.

2.3.2 Potential Application for IgG Concentration Quantification

Quantification of immunoglobulin concentrations in serum is one of the basic tools commonly used for investigating abnormalities relating to the immune system and exposure to infectious disease in humans and domestic species (73, 82). Besides serum, other body fluids, including urine, saliva, milk and especially colostrums are all possible samples that can be subjected to immunoglobulin quantification assays (73). Classical measurements of hIgG involve techniques such as fluorescence immunoassays, radioimmunoassays (RIA) and enzyme-linked immunosorbent assays (ELISA). However, they are time-consuming and need labeling of biomolecules. For clinical diagnostics purposes, ELISA-based assays are only employed for the measurement of antibody production against defined pathogens or antigens for the investigation of suspected immunodeficiency (82). There are three types of assays, (immunodiffusion, nephelometric, and turbimetric) commonly used by clinical immunology laboratories to quantify human IgG, IgA, IgM, IgE and the kappa and lambda light chains of Igs (73). The principle of these assays is similar, with highly avid antibody reagents added to the sample containing immunoglobulins to form immune complexes, which are subsequently

detected visually or by light-scattering techniques such as immunodiffusion, nephelometry, or turbimetry. A variety of immunological reagents are used in clinical assays for the quantification of human immunoglobulins. In the early years, polyclonal antibodies were extensively used and more recently, well documented murine monoclonal antibodies have become available. They are highly specific for human immunoglobulin and especially useful in quantifying the amount of human IgG and IgA subclasses, where maximal specificity is a requirement (73).

Besides diagnostic applications, the quantification of immunoglobulin is also important for antibody production and dairy production. Several online immuno-monitoring systems have been successfully developed for the measurement of hIgG based on turbidimetric assays (83) and fluorescence measurements (84).

Biosensors have attracted wide-spread attention in the field of immunoglobulin quantification in recent years for many reasons such as simple instrumentation, fast operation, and high sensitivity and selectivity. Meanwhile, several biosensors have been developed for measurement of hIgG, including piezoelectric (85) and piezomagnetic biosensors (86), surface plasmon resonance biosensors (87-88) and electrochemical biosensors such as amperometric biosensors (89) and potentiometric biosensors (90). The majority of hIgG detection methodologies employed biosensor techniques are based on the protein A or protein G sensing platform. However, in spite of its high selectivity, protein A has some drawbacks such as its high cost, relatively low stability and the difficulty to immobilize it in the proper orientation (91). As mentioned early, the hexamer peptide ligand HWRGWV has a similar binding capability as protein A, and as a small ligand, the

immobilization of HWRGWV in the right orientation is much easier. This ligand is a good candidate to replace protein A for the production of a biosensors for immunoglobulin quantification.

2.3.3 IgG Oriented Immobilization and Potential Application in Immunosensor Fabrication

As mentioned earlier, the peptide ligand HWRGWV was found to bind the Fc fragment of IgG, which is the conserved part of the molecule. The binding site was, however, different from that for Protein A and Protein G attachment (91). According to mass spectrometry data, the hexamer peptide ligand HWRGWV binds to the pFc portion of hIgG. Figure 2.3 shows the result of a docking calculation using the HADDOCK (High Ambiguity Driven Docking) program indicating that HWRGWV binds to the Ser383-Asn389 (SNGQPEN) motif on the Fc fragment of hIgG. The binding of the loop to HWRGWV is specific, involving several forces of hydrogen bonding, hydrophobic, and possibly electrostatic interactions (92). Since the binding site is at the base of the Fc fragment, it is possible that when HWRGWV binds to hIgG it may orient the antibody at the interface in such a way that the variable region for antigen binding, the Fab fragments, will be more accessible to binding antigen in solution.

Orientation of IgG is critical for its applications for immunoassays and immunosensors. For immunoassay or immunosensor applications, the antibodies need to be immobilized onto a solid surface. The simplest method is a non-covalent adsorption of antibodies on surfaces. However, many studies over the past few years have proven that these types of procedures generally denature the majority of adsorbed antibodies (93-95). Alternatively, proteins can be covalently coupled to chemically activated surfaces through the reaction of lysine side chains

on the protein surface. IgGs can be directly coupled to amine-reactive surfaces (41, 96) or they can be biotinylated using NHS-activated biotin and then immobilized onto streptavidin (SA)-coated surfaces (95). Covalent immobilization could reduce the chances of denaturation, but the random attachment can cause the loss of binding activity of IgGs to antigens due to the following reasons. First, the antigen-binding site could be modified during the chemical modification of IgG. Second, the steric hindrance from the substrate and adjacently immobilized antibodies reduce the availability of immobilized IgG to antigens. Third, since there are multiple binding sites on the protein surface, IgG could be immobilized by multiple covalent bonds which could increase the chance of denaturation. For these reasons, antibodies are sometimes specifically immobilized onto surfaces such that the antigen-binding site is oriented away from the surface itself. Specific orientation can be accomplished by using an intermediate protein that binds to the Fc region of antibodies (97-99). The intermediate protein can be protein A or protein G to capture and orient IgG on solid surface. This type of immobilization strategy can result in a significantly higher fraction of active antibodies. As mentioned earlier, the short peptide HWRGWV has similar IgG binding behavior as protein A, while has several advantages over these protein ligands. Consequently, it could be an alternative to replace protein A and protein G for the application of immunoassay and immunosensors.

References:

1. Mohr P & Pommerening K (1986) *Affinity chromatography: practical and theoretical aspects* (CRC Press, New York).

2. Wang G, Salm JR, Gurgel PV, & Carbonell RG (2005) Small peptide ligands for affinity separations of biological molecules. *Chemical Engineering*, eds Gal'an MA & del Valle EM (John Wiley & Sons, Ltd., New York, NY).
3. Huang PY & Carbonell RG (1995) Affinity purification of proteins using ligands derived from peptide libraries. *Biotechnology and Bioengineering* 47(3):288-297.
4. Huang PY, *et al.* (1996) Affinity purification of von Willebrand factor using ligands derived from peptide libraries. *Bioorganic & Medicinal Chemistry* 4(5):699-708.
5. Bastek PD, Lang JM, Baumbach GA, Hammond DJ, & Carbonell RG (1998) Purification of alpha-1 proteinase inhibitor using ligands from combinatorial peptide libraries. *Abstracts Of Papers Of The American Chemical Society* 216:U328-U328.
6. de Lucena SL, Carbonell RG, & Santana CC (1999) Peptide affinity chromatography process for adsorption of fibrinogen. *Powder Technology* 101(2):173-177.
7. Gurgel PV, Carbonell RG, & Swaisgood HE (2000) Fractionation of whey proteins with a hexapeptide ligand affinity resin. *Bioseparation* 9(6):385-392.
8. Wang G, De J, Schoeniger JS, Roe DC, & Carbonell RG (2004) A hexamer peptide ligand that binds selectively to staphylococcal enterotoxin B: isolation from a solid phase combinatorial library. *Journal Of Peptide Research* 64(2):51-64.
9. Yang H, Gurgel PV, & Carbonell RG (2005) Hexamer peptide affinity resins that bind the Fc region of human immunoglobulin G. *Journal of Peptide Research* 66:120-137.
10. Heldt CL, Gurgel PV, Jaykus LA, & Carbonell RG (2008) Identification of trimeric peptides that bind porcine parvovirus from mixtures containing human blood plasma. *Biotechnology Progress* 24(3):554-560.
11. Gurgel PV, Carbonell RG, & Swaisgood HE (2001) Studies of the binding of alpha-lactalbumin to immobilized peptide ligands. *Journal of Agricultural and Food Chemistry* 49(12):5765-5770.

12. Yang H, Gurgel PV, & Carbonell RG (2009) Purification of human immunoglobulin G via Fc-specific small peptide ligand affinity chromatography. *Journal of Chromatography A* 1216.
13. Kaufman DB, *et al.* (2002) Affinity purification of fibrinogen using a ligand from a peptide library. *Biotechnology and Bioengineering* 77(3):278-289.
14. Kaufman DB & Carbonell RG (1999) Interaction of fibrinogen with peptide affinity supports - Resin effects. *Abstracts of Papers of The American Chemical Society* 217:U160-U160.
15. Wang GQ & Carbonell RG (2005) Characterization of a peptide affinity support that binds selectively to staphylococcal enterotoxin B. *Journal of Chromatography A* 1078(1-2):98-112.
16. Bastek PD & Carbonell RG (1999) Investigation of the binding mechanism between a peptide affinity resin and alpha-1 proteinase inhibitor. *Abstracts of Papers of The American Chemical Society* 217:U189-U189.
17. Kaufman DB, Hayes T, Buettner J, Hammond DJ, & Carbonell RG (2000) Chromatographic resolution of tryptophan enantiomers with L-Leu-L-Leu-L-Leu peptide - Effects of mobile phase composition and chromatographic support. *Journal of Chromatography A* 874(1):21-26.
18. Wang G & Carbonell RG (2006) Design of adsorptive columns for specific pathogen removal: application to staphylococcal enterotoxin B. *Biotechnology Progress* 22:1358-1367.
19. Baird CL & Myszka DG (2001) Current and emerging commercial optical biosensors. *Journal of Molecular Recognition* 14(5):261-268.
20. Collings AF & Caruso F (1997) Biosensors: recent advances. *Reports on Progress in Physics* 60(11):1397-1445.
21. Byfield MP & Abuknesha RA (1994) Biochemical aspects of biosensors. *Biosensors & Bioelectronics* 9(4-5):373-400.

22. Rogers KR & Mulchandani A (1998) *Affinity biosensors: techniques and protocols* (Humana Press Inc., Totowa, NJ) pp 1-4.
23. Lippa PB, Sokoll LJ, & Chan DW (2001) Immunosensors - principles and applications to clinical chemistry. *Clinica Chimica Acta* 314(1-2):1-26.
24. Zhou C, *et al.* (2004) Human immunoglobulin adsorption investigated by means of quartz crystal microbalance dissipation, atomic force microscopy, surface acoustic wave, and surface plasmon resonance techniques. *Langmuir* 20(14):5870-5878.
25. Viking TP, *et al.* (2000) Comparison of surface plasmon resonance and quartz crystal microbalance in the study of whole blood and plasma coagulation. *Biosensors & Bioelectronics* 15(11-12):605-613.
26. Su XD, Wu YJ, & Knoll W (2005) Comparison of surface plasmon resonance spectroscopy and quartz crystal microbalance techniques for studying DNA assembly and hybridization. *Biosensors & Bioelectronics* 21(5):719-726.
27. Hook F, *et al.* (2001) Variations in coupled water, viscoelastic properties, and film thickness of a Mefp-1 protein film during adsorption and cross-linking: A quartz crystal microbalance with dissipation monitoring, ellipsometry, and surface plasmon resonance study. *Analytical Chemistry* 73(24):5796-5804.
28. Damos FS, Mendes RK, & Kubota LT (2004) Applications of QCM, EIS and SPR in the investigation of surfaces and interfaces for the development of (BIO)sensors. *Quimica Nova* 27(6):970-979.
29. Hook F, *et al.* (2002) A comparative study of protein adsorption on titanium oxide surfaces using in situ ellipsometry, optical waveguide lightmode spectroscopy, and quartz crystal microbalance/dissipation. *Colloids And Surfaces B-Biointerfaces* 24(2):155-170.
30. Marx KA (2003) Quartz crystal microbalance: A useful tool for studying thin polymer films and complex biomolecular systems at the solution-surface interface. *Biomacromolecules* 4(5):1099-1120.

31. Strong L & Whitesides GM (1988) Structures of self-assembled monolayer films of organosulfur compounds adsorbed on gold single-crystals - electron-diffraction studies. *Langmuir* 4(3):546-558.
32. O'Sullivan CK & Guilbault GG (1999) Commercial quartz crystal microbalances - theory and applications. *Biosensors & Bioelectronics* 14(8-9):663-670.
33. Johannsmann D, Mathauer K, Wegner G, & Knoll W (1992) Viscoelastic properties of thin films probed with quartz crystal resonator. *Physical Review B* 46(12):7808-7815.
34. Hook F, Rodahl M, Brzezinski P, & Kasemo B (1998) Measurements using the quartz crystal microbalance technique of ferritin monolayers on methyl-thiolated gold: Dependence of energy dissipation and saturation coverage on salt concentration. *Journal of Colloid and Interface Science* 208(1):63-67.
35. Su XD, Chew FT, & Li SFY (2000) Design and application of piezoelectric quartz crystal-based immunoassay. *Analytical Sciences* 16(2):107-114.
36. Choi KH, *et al.* (2003) Investigation of protein adsorption with simultaneous measurements of atomic force microscope and quartz crystal microbalance. *Journal of Vacuum Science & Technology B* 21(4):1433-1436.
37. Stadler H, Mondon M, & Ziegler C (2003) Protein adsorption on surfaces: dynamic contact-angle (DCA) and quartz-crystal microbalance (QCM) measurements. *Analytical and Bioanalytical Chemistry* 375(1):53-61.
38. Su XD & Zhang H (2004) Comparison of surface plasmon resonance spectroscopy and quartz crystal microbalance for human IgE quantification. *Sensors and Actuators B-Chemical* 100(3):309-314.
39. Reimhult E, Larsson C, Kasemo B, & Hook F (2004) Simultaneous surface plasmon resonance and quartz crystal microbalance with dissipation monitoring measurements of biomolecular adsorption events involving structural transformations and variations in coupled water. *Analytical Chemistry* 76(24):7211-7220.

40. Carrigan SD, Scott G, & Tabrizian M (2005) Real-time QCM-D immunoassay through oriented antibody immobilization using cross-linked hydrogel biointerfaces. *Langmuir* 21(13):5966-5973.
41. Caruso F, Rodda E, & Furlong DN (1996) Orientational aspects of antibody immobilization and immunological activity on quartz crystal microbalance electrodes. *Journal of Colloid and Interface Science* 178(1):104-115.
42. Graneli A, Edvardsson M, & Hook F (2004) DNA-based formation of a supported, three-dimensional lipid vesicle matrix probed by QCM-D and SPR. *ChemPhysChem* 5(5):729-733.
43. Niikura K, Nagata K, & Okahata Y (1996) Quantitative detection of protein binding onto DNA by using a quartz-crystal microbalance. *Chemistry Letters* (10):863-864.
44. Poitras C & Tufenkji N (2009) A QCM-D-based biosensor for *E. coli* O157:H7 highlighting the relevance of the dissipation slope as a transduction signal. *Biosensors and Bioelectronics* 24:2137–2142.
45. Homola J, Yee SS, & Gauglitz G (1999) Surface plasmon resonance sensors: review. *Sensors and Actuators B-Chemical* 54(1-2):3-15.
46. Fivash M, Towler EM, & Fisher RJ (1998) BIAcore for macromolecular interaction. *Current Opinion in Biotechnology* 9(1):97-101.
47. McDonnell JM (2001) Surface plasmon resonance: towards an understanding of the mechanisms of biological molecular recognition. *Current Opinion in Chemical Biology* 5(5):572-577.
48. Rich RL & Myszka DG (2000) Advances in surface plasmon resonance biosensor analysis. *Current Opinion in Biotechnology* 11(1):54-61.
49. Green RJ, *et al.* (2000) Surface plasmon resonance analysis of dynamic biological interactions with biomaterials. *Biomaterials* 21(18):1823-1835.

50. Liedberg B, Nylander C, & Lundstrom I (1983) Surface plasmon resonance for gas detection and biosensing. *Sensors and Actuators B* 4:299-304.
51. Williams RA & Blanch HW (1994) Covalent Immobilization Of Protein Monolayers For Biosensor Applications. *Biosensors & Bioelectronics* 9(2):159-167.
52. Mello LD & Kubota LT (2002) Review of the use of biosensors as analytical tools in the food and drink industries. *Food Chemistry* 77(2):237-256.
53. Oh SJ, Hong BJ, Choi KY, & Park JW (2006) Surface modification for DNA and protein microarrays. *Omics-A Journal of Integrative Biology* 10(3):327-343.
54. Bilitewski U (2006) Protein-sensing assay formats and devices. *Analytica Chimica Acta* 568(1-2):232-247.
55. Tomizaki KY, Usui K, & Mihara H (2005) Protein-detecting microarrays: Current accomplishments and requirements. *ChemBiochem* 6(5):783-799.
56. Gnauck M, *et al.* (2007) Carboxy-terminated oligo(ethylene glycol)-alkane phosphate: Synthesis and self-assembly on titanium oxide surfaces. *Langmuir* 23(2):377-381.
57. Houseman BT, Huh JH, Kron SJ, & Mrksich M (2002) Peptide chips for the quantitative evaluation of protein kinase activity. *Nature Biotechnology* 20(3):270-274.
58. Nyquist RM, *et al.* (2000) Characterization of self-assembled monolayers for biosensor applications. *Langmuir* 16(4):1793-1800.
59. Xia N, Hu YH, Grainger DW, & Castner DG (2002) Functionalized poly(ethylene glycol)-grafted polysiloxane monolayers for control of protein binding. *Langmuir* 18(8):3255-3262.
60. Ulman A (1996) Formation and structure of self-assembled monolayers. *Chemical Reviews* 96(4):1533-1554.

61. Wink T, vanZuilen SJ, Bult A, & vanBennekom WP (1997) Self-assembled monolayers for biosensors. *Analyst* 122(4):R43-R50.
62. Bain CD & Whitesides GM (1988) Molecular-level control over surface order in self-assembled monolayer films of thiols on gold. *Science* 240(4848):62-63.
63. Sellers H, Ulman A, Shnidman Y, & Eilers JE (1993) Structure and binding of alkylthiolates on gold and silver Surface: implications for self-assembly. *Journal of American Chemistry Society* 115:9389.
64. Bain CD & Whitesides GM (1988) Correlations Between Wettability And Structure In Monolayers Of Alkanethiols Adsorbed On Gold. *Journal of the American Chemical Society* 110(11):3665-3666.
65. Bain CD, *et al.* (1989) Formation of monolayer films by the spontaneous assembly of organic thiols from solution onto gold. *Journal of the American Chemical Society* 111(1):321-335.
66. Hage DS (2006) *Handbook of affinity chromatography* (CRC Press, Boca Raton, FL) pp 557, 539.
67. Prime KL & Whitesides GM (1993) Adsorption of proteins onto surfaces containing end-attached oligo(ethylene oxide) - a model system using self-assembled monolayers. *Journal of the American Chemical Society* 115(23):10714-10721.
68. Matsushima A, Kodera Y, Hiroto M, Nishimura H, & Inada Y (1996) Bioconjugates of proteins and polyethylene glycol: Potent tools in biotechnological processes. *Journal of Molecular Catalysis B-Enzymatic* 2(1):1-17.
69. Cha TW, Boiadjiev V, Lozano J, Yang H, & Zhu XY (2002) Immobilization of oligonucleotides on poly(ethylene glycol) brush-coated Si surfaces. *Analytical Biochemistry* 311(1):27-32.
70. Kwon Y, Han ZZ, Karatan E, Mrksich M, & Kay BK (2004) Antibody arrays prepared by cutinase-mediated immobilization on self-assembled monolayers. *Analytical Chemistry* 76(19):5713-5720.

71. Martin Y & Vermette P (2006) Low-fouling amine-terminated poly(ethylene glycol) thin layers and effect of immobilization conditions on their mechanical and physicochemical properties. *Macromolecules* 39(23):8083-8091.
72. Ajikumar PK, *et al.* (2007) Carboxyl-terminated dendrimer-coated bioactive interface for protein microarray: High-sensitivity detection of antigen in complex biological samples. *Langmuir* 23(10):5670-5677.
73. Leffell MS, Donnenberg AD, & Rose NR (1997) *Handbook of human immunology* (CRC Press, New York, NY) p 73.
74. Nezlin R (1998) *The Immunoglobulins: structure and function* (Academic Press, New York, USA) pp 36-37.
75. Curling JM (1980) *Methods of plasma protein fractionation*. (Academic Press, London, UK) pp 96-98.
76. Huse K, Bohme HJ, & Scholz GH (2002) Purification of antibodies by affinity chromatography. *Journal of Biochemical and Biophysical Methods* 51(3):217-231.
77. Roque ACA, Lowe CR, & Taipa MA (2004) Antibodies and genetically engineered related molecules: Production and purification. *Biotechnology Progress* 20(3):639-654.
78. Low D, O'Leary R, & Pujar NS (2007) Future of antibody purification. *Journal of Chromatography B-Analytical Technologies in the Biomedical and Life Sciences* 848(1):48-63.
79. Boschetti E (2001) The use of thiophilic chromatography for antibody purification: a review. . *Journal of Biochemical and Biophysical Methods* 49:361-389.
80. Verdoliva A, Pannone F, Rossi M, Catello S, & V. M (2002) Affinity purification of polyclonal antibodies using a new all-D synthetic peptide ligand: comparison with protein A and protein G. . *Journal of Immunological Methods* 271: (1-2):77-88.

81. Newcombe AR, *et al.* (2005) Optimised affinity purification of polyclonal antibodies from hyper immunised ovine serum using a synthetic Protein A adsorbent, MAbsorbento (R) A2P. *Journal of Chromatography B. Biomedical Science* 814(Appl. (2)):209-215.
82. Provan D (2005) *Oxford handbook of clinical and laboratory investigation* (Oxford University Press, Oxford, UK).
83. Middendorf C, *et al.* (1993) On-line immunoanalysis for bioprocess control. *Journal of Biotechnology* 31:395-403.
84. Reif OW, Lausch R, Scheper T, & Freitag R (1994) Fluorescein isothiocyanate-labeled protein G as an affinity ligand in affinity/immunocapillary electrophoresis with fluorescence detection. *Analytical Chemistry* 66:4027-4033. .
85. Chen H, *et al.* (2007) A novel piezoelectric immunoagglutination assay technique with antibody-modified liposome. *Biosensors & Bioelectronics* 22(993-999).
86. Ogi H, Motohisa K, Matsumoto T, Mizugaki T, & Hirao M (2006) Wireless electrodeless piezomagnetic biosensor with an isolated nickel oscillator. *Biosensors & Bioelectronics* 21:2001-2005.
87. Labib M, Hedstrom M, Amin M, & Mattiasson B (2009) A multipurpose capacitive biosensor for assay and quality control of human immunoglobulin G. *Biotechnology and Bioengineering* 104(2):312-320.
88. Mytych DT, La S, Barger T, Ferbas J, & Swanson SJ (2009) The development and validation of a sensitive, dual-flow cell, SPR-based biosensor immunoassay for the detection, semi-quantitation, and characterization of antibodies to darbepoetin alfa and epoetin alfa in human serum. *Journal of Pharmaceutical and Biomedical Analysis* 49(2):415-426.
89. Bian C, Xia S, Xu Y, Chen S, & Cui Z (2005) A micro amperometric immunosensor based on two electrochemical layers for immobilizing antibody. *IEEE Sensors* 2001:416-419.
90. Li J & Gao H (2008) A renewable potentiometric immunosensor based on Fe₃O₄ nanoparticles immobilized anti-IgG. *Electroanalysis* 8:881-887.

91. Denizli A & Arica Y (2000) Protein A immobilized microporous polyhydroxyethyl methacrylate affinity membranes for selective sorption of human-immunoglobulin G from human plasma. *Journal of Biomaterial Science, Polymer Edition* 11:367-382.
92. Yang H, *et al.* (2010) Binding site on human immunoglobulin G for the affinity ligand HWRGWV. *Journal of Molecular Recognition* 23:271-282.
93. Rao SV, Anderson KW, & Bachas LG (1998) Oriented immobilization of proteins. *Mikrochimica Acta* 128(3-4):127-143.
94. Turkova J (1999) Oriented immobilization of biologically active proteins as a tool for revealing protein interactions and function. *Journal of Chromatography B* 722(1-2):11-31.
95. Peluso P, *et al.* (2003) Optimizing antibody immobilization strategies for the construction of protein microarrays. *Analytical Biochemistry* 312(2):113-124.
96. Lu B, Xie JM, Lu CL, Wu CG, & Wei Y (1995) Oriented immobilization of Fab' fragments on silica surfaces. *Analytical Chemistry* 67(1):83-87.
97. Bae YM, Oh BK, Lee W, Lee WH, & Choi JW (2005) Study on orientation of immunoglobulin G on protein G layer. *Biosensors & Bioelectronics* 21(1):103-110.
98. Brogan KL & Schoenfisch MH (2005) Influence of antibody immobilization strategy on molecular recognition force microscopy measurements. *Langmuir* 21(7):3054-3060.
99. Starodub NF, Pirogova LV, Demchenko A, & Nabok AV (2005) Antibody immobilisation on the metal and silicon surfaces. The use of self-assembled layers and specific receptors. *Bioelectrochemistry* 66(1-2):111-115.

Table 2.1 Comparison of QCM and SPR

	QCM	SPR
Measurement	Total mass	Dry mass
Response range	Å - μm	Å - 300 nm
Intrinsic sensitivity*	1Hz ~ 17.7 ng cm ⁻²	1 millidegree ~ 0.64 ng cm ⁻²
Environmental effect	Sensitive	Less sensitive
Applicability	Any coating with a viscosity and viscoelasticity contrast with the surrounding medium	Any coating with an optical contrast with the surrounding medium
Other functions	QCM damping is reflective of the viscoelasticity of a coating	
Limitation	Liquid phase frequency response is complicated for thin film thickness measurements	Refractive index of the coating must be known if a simple measurement is to provide the thickness and mass

* The intrinsic sensitivities of QCM and SPR depend on the instrument fabrication and the value provided here is for the devices used in this study: QCM-D apparatus (model E4, Q-Sense AB, Göthenburg, Sweden) and SPR-Navi device (KSV, Instruments OY, Helsinki, Finland).

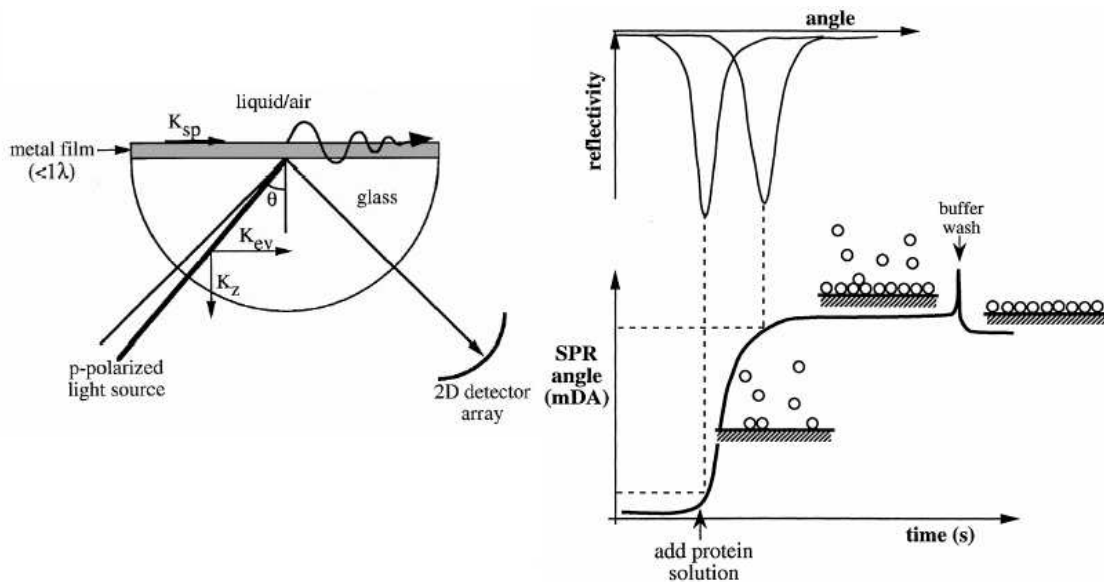


Figure 2.1 The principle of SPR

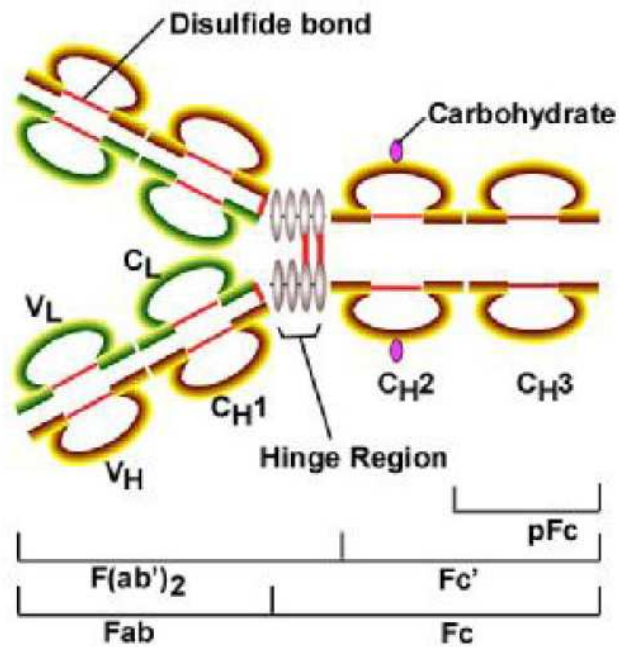


Figure 2.2 Structural diagram of human IgG1
 Green line: light chain; brown line: heavy chain.
 Each “C” like structure denotes one of the IgG domains. The enzymatic fragments Fab, Fc, F(ab')₂, Fc' and pFc are indicated below the diagram.

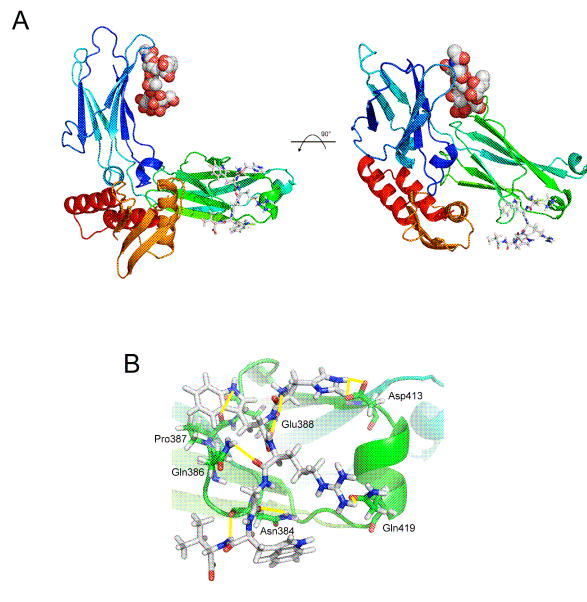


Figure 2.3 IgG and hexamer peptide ligand HWRGWV binding model from HADDOCK

**Chapter 3. Modification of Silica Surfaces for Bioanalytical Applications
via Self-Assembly and Covalent Attachment of Amine-Terminated PEG
Chains**

Abstract

Flat silica surfaces were modified by the addition of short polyethylene glycol chains at high density, and terminated by the addition of primary amine functional groups. This kind of construct can be used to immobilize biomolecules, allowing for its use in fundamental studies of surface interactions between immobilized biomolecules and their targets.

A self-assembling monolayer (SAM) of 3-amino-propyl triethoxy silane (APTES) was formed on the silica surface as an initial anchor layer, then short chains of polyethylene glycol with Fmoc-protected amine groups at one end and carboxyl groups at the other end were coupled to the silane SAM to reduce nonspecific binding. The amine groups at the end were liberated by Fmoc deprotection, to make them available for immobilization of biomolecules. The estimated surface chain density from ellipsometric thickness measurement of PEG chains and amine groups is $2.74 \text{ chains nm}^{-2}$. The modified surfaces were characterized by time of flight-secondary ion mass spectroscopy (ToF-SIMS). The presence of peaks from the Fmoc group in the spectra of the sample before deprotection provides direct evidence of successful immobilization. The $\text{pK}_{1/2}$ of the amine group on the surface, determined by contact angle titration, is around 7, a value that is much lower than that of its free analogue in solution.

The amount of protein adsorption on the modified quartz surface was determined by quartz crystal microbalance (QCM) measurements. Although there is some nonspecific protein adsorption on the modified surfaces with the PEG layer terminated by amines, the adsorption amount is much lower than that on bare silica surfaces and on the silica surfaces modified only with APTES. The protein adsorption results on the surface with free amine

groups are dependent on the pH and they are consistent with isoelectric point measurements by contact angle titration.

3.1 Introduction

Bioactive surfaces have numerous potential applications, including affinity bioseparations, diagnostics and biosensors, proteomics, biochips and bioreactors. Biomolecules can be immobilized on the substrate by physical adsorption, covalent bonding, crosslinking, entrapment, or encapsulation. Among those methods, adsorption and covalent bonding are the most commonly used. Physical adsorption of the biocomponent based on van der Waals attractive forces is the simplest method available and it is feasible for various substrates. However, this method does not provide high surface density of affinity elements, and the adsorbed biomolecules could be lost through changes in pH, ionic strength, or temperature due to adsorption reversibility (1-2).

Covalent bonding to the surface can lead to slight modifications of the biomolecules, but, this approach results in more stable surfaces, and is more reliable and reproducible (1, 3-5). For covalent bonding, generally the substrates need to be modified to introduce active groups, such as carboxyl, thioacetyl, hydroquinone, or epoxide groups for the immobilization of biomolecules (6-9). In addition, adding a spacer arm on top of substrate is desirable to enhance the availability of the ligands on surface and to reduce nonspecific binding of proteins and other species from the bulk solution. Polyethylene glycol (PEG) is a good candidate spacer arm, since PEG brushes have a high flexibility in biological media, and can help minimize nonspecific protein binding and cell adhesion on surfaces (2, 10-12). The resistance of PEG coated surfaces to nonspecific binding is related to the molecular weight of

the PEG and the resulting packing density of the PEG chains (13). High chain densities on a surface can be achieved by various methods, including alkanethiol-based self-assembling monolayers (SAM) on gold surfaces. Whitesides and colleagues (13-15) studied alkanethiols with various functional groups including oligo(ethylene glycol) and demonstrated that SAMs containing this compound resist the adsorption of proteins. Mrksich and colleagues (13-15) successfully applied these kinds of oligo(ethylene-glycol)-coated surfaces to the immobilization of proteins and peptides on sensors. One potential limitation of a thiol SAM is its tendency to be slowly oxidized after prolonged exposure to air and light (16-17) or to buffer for days or weeks. In addition, the formation of thiol SAMs is only viable for noble metal substrates.

Beside SAMs on gold surfaces, other approaches have been taken for the modification of substrates for high chain density of PEG chains with functional groups. Jaehne and co-workers (6) modified titanium oxide surfaces with carboxy-terminated oligo(ethylene glycol)-alkane phosphate but the resulting density of PEG chains of 2.03 molecules nm^{-2} was not as high as expected. Zhu and colleagues functionalized Cl-terminated silicon surfaces with high-density PEG chain ends with hydroxyl groups for the immobilization of oligonucleotides (18). These surfaces are not very stable under strong acidic or basic conditions, but the problem was resolved by using multiple-arm PEGs in the study of the immobilization of poly histidine-tagged proteins by the affinity interaction with Cu^{2+} ions chelating with iminodiacetic acid groups at the end of PEG arms (19). Several arms of multiple-arm PEGs reacted with the Si-Cl surfaces, enhancing the stability of the PEG layer on the surface.

In this study we focused on the formation of high density of PEG chain coatings with amine groups as functional groups for immobilization onto silica surface. Our main interest here was to obtain amine-terminated chains on the surface for the immobilization of small peptide ligands through their carboxyl groups. As far as we are aware, the only prior work in this area is that of Howorka and colleagues (20) who modified glass surfaces with PEG chains ending with amine groups for the fabrication of DNA oligonucleotide microarrays. In their work, they grafted high density PEG-diamine (MW 2000) on SAMs of 3-glycidoxypropyl trimethoxysilane (20). In this approach, both ends of the PEG-diamine can react with the SAM on the surface, thus reducing the number of terminal amines potentially available for attachment of biomolecules. To reduce this effect, a large excess of the diamine is necessary during the coupling reaction.

Our interest is to study the affinity interaction of high density peptides immobilized on the surface through their carboxyl terminals with target proteins in complex biological media. To this end, this paper describes the modification of quartz silica surfaces via the formation of a self-assembling monolayer of APTES, followed by reaction with a PEG compound with Fmoc protection on the amino end and a free carboxyl end that was used to react with the free amine on the APTES. We used a smaller molecular weight PEG than that used by Howorka and colleagues in an effort to obtain a higher chain density. In addition, the carboxyl-amine reaction with the Fmoc-protected PEG helped to ensure the availability of the free amine at the end of the PEG after the deprotection of the Fmoc. This paper presents a detailed analysis of the surface properties of this PEG-modified quartz via ellipsometry to estimate the chain density, contact angle titration to measure the $pK_{1/2}$ of the surface amino

groups, ToF-SIMS to verify that the surface modification steps have successfully gone to completion, and nonspecific protein binding studies of the modified surface with free amines to verify that the protein adsorption is dependent on electrostatic interactions with the amine groups as expected. This paper will lay the groundwork for additional studies involving the attachment of peptides to these surfaces through their carboxyl termini.

3.2 Materials and Methods

3.2.1 Materials

Anhydrous toluene (99.8%), γ -amino-propyl triethoxy silane (APTES) (99%), N,N-dimethylformamide (DMF, ACS reagent, $\geq 99.8\%$), piperidine (biotech grade, $\geq 99.5\%$), bovine serum albumin (BSA, $\geq 98\%$), ethanol (200 proof, absolute, for molecular biology), phosphate buffered saline (PBS pH 7.4, monobasic sodium phosphate, dibasic sodium phosphate, sodium chloride 0.138M, potassium chloride 0.0027M) were obtained from Sigma-Aldrich (St. Louis, MO) and used as received unless specified otherwise. Fmoc-11-amino-3,6,9-trioxaundecanoic acid (Fmoc-mini-PEG-3TM) was obtained from Peptides International, Inc. (Louisville, KY). Ethyl-3-(3-dimethylaminopropyl) carbodiimide hydrochloride (EDC) and N-hydroxysuccinimide (NHS) were obtained from Pierce (Rockford, IL). Nitrogen gas, purity 99.99%, was obtained from National Welders Supply, Inc (Raleigh, NC). Deionized water (DI water, resistivity $> 16 \text{ M}\Omega\cdot\text{cm}$) and Milli-Q water (resistivity $> 18 \text{ M}\Omega\cdot\text{cm}$) were obtained by using the Millipore water purification system (Billerica, MA). Buffer solutions used for contact-angle titration measurements were 0.01 M in concentration and were prepared using Milli-Q water and the following reagents: pH 1~2,

hydrochloric acid/potassium chloride; pH 3~5, acetic acid/sodium acetate; pH 6~8 monobasic sodium phosphate/dibasic sodium phosphate; pH 9~10 sodium carbonate/sodium bicarbonate; pH 11~12, dibasic sodium phosphate/sodium hydroxide. All the reagents used to prepare the buffer solutions were obtained from Sigma-Aldrich (St. Louis, MO).

The buffers used for QCM experiment were the buffer prepared the same methods mentioned above with the addition of sodium chloride and potassium chloride to a final concentration of 0.138 M and 0.0027 M respectively.

3.2.2 Preparation of Substrates

Single-side polished silicon wafers with [100] orientation (Wafer World Inc., West Palm Beach, FL) were cut into small pieces (~1 to 3 cm²), followed by removal of debris using pressurized air. Silica-coated QCM sensors were obtained from Q-sense Inc. (Glen Burnie, MD). The silica wafer slides and silica-coated QCM sensors were placed into an ultraviolet/ozone (UVO) cleaner (Model 42, Suprasil lamp, Jelight Co., Irvine, CA) for 20 minutes. The lamp used was comprised of low-pressure quartz-mercury, with UV radiation peaks at 184 and 254 nm, which can produce mono- and di-atomic oxygen. Atomic oxygen cleans any hydrocarbon impurities present on the sample surface by oxidation, producing gaseous CO and CO₂. In addition, atomic oxygen can increase the density of –OH groups on the silica surface which is the attachment point for silane molecules (21).

3.2.3 Surface Modification

The cleaned surface of the silica wafer slides or QCM sensor were modified using the approach illustrated in Figure 3.1. The first step was to form a self-assembled monolayer of APTES on the silica surface. The cleaned substrates were immersed into 1 wt% APTES

solution in anhydrous toluene at 60°C for 5 minutes. The samples were then rinsed with toluene at least 5 times and sonicated in toluene for 5 minutes. After that, the samples were rinsed sequentially with toluene, acetone, ethanol and DI water, then dried by nitrogen stream. The silanization method was adopted from Petri and his colleague's work (22).

The second step was to couple the carboxyl termini of the Fmoc-mini-PEG-3TM to the primary amines on the SAM of APTES, using EDC and NHS as coupling agents (23). Fmoc-mini-PEG-3TM, EDC and NHS were dissolved in a mixture of 0.1M 2-(N-morpholino) ethanesulfonic acid hemisodium salt (MES, pH 4.7, Sigma, St. Louis, MO, prepared using Milli-Q water) and 200 proof ethanol in the ratio of 1:1 to final concentrations of 5, 2.5 and 3.75 mg ml⁻¹ respectively. The samples with APTES layers were placed in this solution right after drying and were kept immersed at room temperature overnight (~16 hours) with gentle shaking. Samples were then removed from the solution, rinsed with ethanol, followed by rinsing with DI water. The physically adsorbed Fmoc-mini-PEG-3TM remaining on the surfaces was removed by sonication at 40 Hz (Branson ultrasonic cleaner, Model 2510, Branson Ultrasonics Corporation, Danbury, CT) in a 1:1 mixture of DI water and ethanol at room temperature for 5 minutes in ethanol. The samples were rinsed with ethanol and DI water at least 5 times, and then dried with nitrogen flow.

Step 3 was to de-protect the amine group at the amino terminus of Fmoc-mini-PEG-3TM. The Fmoc groups were removed by keeping the samples in 50% (v/v) piperidine solution in DMF for 1 hour (24). Samples were then rinsed with DMF at least 5 times, further cleaned by sonication at 40Hz in DMF for 5 minutes, and rinsed again with DMF 5 times. In some experiments the amine groups were acetylated by immersing in a mixture of 10% (v/v) acetic

anhydride in acetone and 0.5M sodium acetate aqueous solution, at a ratio of 1:10 at room temperature for 2 hours. The surfaces were then rinsed with DI water and further washed with an ultrasonic bath again by sonication at 40Hz in DI water at room temperature for 5 minutes. Samples were dried with a nitrogen stream and kept in vacuum before any further characterization experiments.

For convenience, in this paper the surface samples obtained after each step will be referred to as APTES (after formation of the SAMs), APTES-PEG₃-NH-Fmoc (after attachment of the Fmoc-protected PEG), and APTES-PEG₃-NH₂ (after deprotection of the amine).

3.2.4 Ellipsometric Film-Thickness Measurements

The thicknesses of the surface films on the silica surface after each step were estimated with a Rudolph/Auto EL Ellipsometer equipped with a He-Ne Laser ($\lambda=632.8$ nm) with fixed incidence angle of 70.0° (New Jersey, USA), using the refractive indices of Si, SiO₂ and APTES as 3.838, 1.462, and 1.424 respectively (22). For the PEG layer, it was assumed that its refractive index was similar to that of APTES. The data presented are the averages of at least 5 points with an error of ± 2 Å.

The grafted surface density (σ , chain nm⁻²) can be estimated from the thickness measurement using

$$\sigma = \frac{N_A d \rho_0 \times 10^{-22}}{M_w} \quad 3-1$$

where N_A is Avogadro's number; d (Å) is the measured film thickness, M_w (g mole⁻¹) is the molecular weight of the chain, and ρ_0 (g cm⁻³) is the density of the layer (25). Since the actual densities of the immobilized layers are unknown and they depend on the surface chain

densities, the bulk density of APTES (0.946 g cm^{-3}) and PEG layer (1.08 g cm^{-3} , value provided by supplier) were used. The grafted surface density calculated by this equation is only a rough estimation due to the difference between the density of layer immobilized on surface and that of bulk material.

3.2.5 Contact-Angle Measurements and Contact-Angle Titrations

Contact angle measurements were performed using a Ramé-Hart contact angle goniometer (model 100-00, Ramé-Hart, NJ, USA) equipped with a CCD camera and analyzed with Ramé-Hart software under ambient conditions. The advancing contact angle of DI water (pH 6.8) or aqueous buffer solutions with different pH values on modified silica surfaces were measured. The buffers used for this experiment were described in 2.1. Before the acquisition of contact angle data, the samples were immersed for 30 minutes into the buffer solution that was to be used for measurement. After removal from the solution, the sample was briefly rinsed with DI water, dried with a nitrogen stream and then mounted in the goniometer. The advancing contact angles were read by dropping $4 \mu\text{l}$ of probing buffer solution onto the surface. Each data point reported represents an average of five measurements on the same sample, with an error smaller than $\pm 1.5^\circ$.

3.2.6 Time of Flight Secondary Ion Mass Spectroscopy (ToF-SIMS)

The ToF-SIMS measurements were performed on a PHI TRIFT I mass spectrometer (Model 2100, Kanagawa, Japan). In order to detect chemical components within only 2~3 nm deep from the top of the surface, static model was chosen. The experiment was operated at a pressure below 1×10^{-8} Torr (1 Torr = 133Pa). A Ga^+ source operating at 15keV and giving a dc ion beam current of $1 \mu\text{A}$ was used. Charge compensation was accomplished with a pulsed

low energy electron flood gun. The estimated raster area was about $80 \times 80 \mu\text{m}$. The total primary ion dose was maintained below 10^{13} ions cm^{-2} . The mass resolution obtained under these operating conditions was $m/\Delta m > 5000$ at $m/z = 28$, Δm is the smallest mass difference that can be resolved between two species. Δm is about 0.056 amu in this study, which is high enough to resolve some important peaks like $\text{C}_2\text{H}_5\text{O}^+$ (m/z 45.03) from SiOH^+ (m/z 44.98). Spectra for positive and negative ions were acquired within 5 minutes. The mass scales of the positive and negative ion ToF-SIMS spectra were calibrated to the CH_3^+ , C_2H_3^+ , Si^+ and CH^- , CN^- , and Si^- peaks respectively, before further analysis.

The pure Fmoc-mini-PEG-3TM obtained from Peptides International Inc. without any treatment was used as positive control for this experiment. Fmoc-mini-PEG-3TM is gel at room temperature and it was spread into a thin film directly with a clean pipette tip on silica wafer surface cleaned by UVO with the method described in section 3.2.2. In addition, there are three samples obtained after each modification step, APTES, APTES-PEG₃-NH-Fmoc, and APTES-PEG₃-NH₂. Both positive and negative spectra were collected from each sample and positive control.

3.2.7 Quartz Crystal Microbalance (QCM)

A commercial QCM-D apparatus (model E4, Q-Sense AB, Gothenburg, Sweden) was used to measure the changes in the resonance frequency (ΔF) and in the energy dissipation (ΔD) due to the protein adsorption process.

The QCM crystal (diameter 14 mm, 5 MHz) was excited to oscillation in the thickness-shear mode at its fundamental resonance frequency and odd overtones ($n = 3, 5, 7, 9, 11, 13$)

by applying a RF voltage across the electrodes on both sides of crystal. The voltage applied to the oscillating crystal was automatically switched on and off, and the crystal decays as an exponentially damped sinusoidal function,

$$q(t) = A_0 \exp\left(-\frac{t}{\tau}\right) \sin(\omega t + \varphi) \quad 3-2$$

where q is the amplitude of oscillation, t is time, τ is the relaxation time, φ is the phase constant and ω is the oscillation frequency, from which the resonance frequency and the energy dissipation can be calculated by the following two equations (26-27):

$$D = \frac{2}{\omega\tau} \quad 3-3$$

$$F = \frac{\omega}{2\pi} \quad 3-4$$

The Q-sense software numerically fits the amplitude and gives out the value of F and D .

Classically, the Sauerbrey relationship (28) has been used for quantitative determination of mass deposited on the crystal surface,

$$\Delta f = -\frac{2f_0^2 \Delta m}{n(\rho_q \mu_q)^{1/2} A} = \frac{1}{nC} \frac{\Delta m}{A} \quad 3-5$$

where f_0 is the fundamental resonance frequency of the quartz crystal, ρ_q is the specific bulk density of the quartz (2.648 g cm^{-3}), μ_q is the shear wave velocity in quartz ($2.947 \times 10^{11} \text{ g cm}^{-1} \text{ s}^{-2}$ for AT-cut quartz crystals), A is the measuring area, and n is the number of the overtone (26, 29). For the sensor used in this work, C is equal to $17.7 \text{ ng cm}^{-2} \text{ Hz}^{-1}$, according the information provided by the instrument company.

The measurements were done in small cells, designed to provide a rapid, non-perturbing exchange of the liquid over one side of the QCM-D sensor. The temperature of the QCM-D

chamber and liquid inside were controlled at 25 ± 0.1 °C. All solutions were passed through a Corning 0.22 μm polyethersulfone (Sigma-Aldrich, St. Louis, MO) filter and degassed by sonication at room temperature before use.

Since there is some variation between the results recorded by different overtones, in this studies the average of the frequency changes of overtone 3, 5, 7, 9, 11 was used and the error bar indicates the difference between overtones.

The bovine serum albumin (BSA) adsorption amount on silica surface before and after modification was measured. The BSA was dissolved into PBS buffer for pH 6.0, 7.4, 8.0 and acetate buffer of pH 4.0 to a final concentration of 0.05~10 mg ml^{-1} .

The QCM-D apparatus (model E4) has four chambers and each chamber is connected to the pump by tubing. First, the buffer was continually pumped at the flow rate of $100 \mu\text{l min}^{-1}$ through each chamber to get a stable baseline (indicated by a variation of frequencies of less than 0.5 Hz for 30 minutes). The pump was then stopped and the flow was switched to the protein solution with known bulk concentration. The pump was re-started and kept at a flow rate of $100 \mu\text{l min}^{-1}$. The adsorption was monitored until the change of frequencies was less than 1 Hz for 30 minutes.

3.3 Results and Discussion

3.3.1 Modification of silica surface

As mentioned earlier, the modification of the silica surface was achieved through a 3-step process: first, the monolayer of APTES was formed spontaneously during the contact of the silane solution with the silica substrate, then Fmoc-mini-PEG-3TM was coupled to it, and

finally the Fmoc group at the end was removed, exposing the amine functional group. After each step, the thickness of the formed layer and the contact angle were measured and the results are summarized in Table 3.1. Under the experimental conditions described in section 3.2.2, the thickness of the APTES monolayer was about 8 Å, which is close to the theoretical thickness of APTES monolayer of 7 Å (30) and values reported in the literature (22).

Coupling of the Fmoc-mini-PEG-3TM increased the thickness by 14 Å and removing the 9-fluorenylmethyloxycarbonyl (Fmoc) protecting group reduced the thickness of PEG layer to 8 Å. Assuming that the bond length of C-C is 1.52 Å, the C-O bond length is 1.52 Å, and the C-N bond length is 1.45 Å (31), the full length of stretched the mini-PEG without the Fmoc group should be about 17.6 Å. The thickness obtained was lower than half of the full stretch length calculated. This may suggest that the density of the mini-PEG layer obtained is not very high so that there is enough room for the mini-PEG chains to be in an extended conformation.

According to Equation 3-1, the estimated chain density of APTES is 3.86 chain nm⁻² and that of the PEG chain is 2.74 chain nm⁻². This indicates that about 70 percent of the amine groups of APTES on the surface reacted with Fmoc-mini-PEG-3TM. The density of PEG chain obtained in this study was significantly higher than that obtained by Howorka and colleagues (1.14 chain nm⁻², estimated by Equation 3-1 from the ellipsometry measurement of 3.5 nm) (20).

The contact angle of DI water on APTES monolayer was about 53° which is within the range of 42° ~ 68° reported in the literature (22, 32). After coupling PEG layer to the surface, the contact angle dropped due to an increase in hydrophilicity (12, 33-35). The average

contact angle measured after PEG attachment was only 23°. There was not too much change of contact angle after deprotection. It seems from these results that the relatively hydrophobic Fmoc group must have been buried inside the film, thus exposing the hydrophilic groups of PEG to the aqueous phase. Since the density of the PEG chain is not very high, it is possible for the hydrophobic ends to be hidden inside the film surface.

3.3.2 Characterization of the Modified Silica Surfaces by ToF-SIMS

The modified surfaces were subjected to ToF-SIMS analysis to confirm the success of each step of modification. Fmoc-mini-PEG-3TM directly spread on silica wafer surface was included as positive control, in addition to the three samples obtained after each step, APTES, APTES-PEG₃-NH-Fmoc, and APTES-PEG₃-NH₂. Both positive and negative ion spectra were collected for each sample, and the main peaks identified are summarized in Table 3.2.

For the sample comprised of an APTES SAM layer (column b in Table 3.2), the main peaks found in the wide scan negative ion SIMS were H⁻, CN⁻, O⁻, OH⁻, C⁻, CH⁻, and C₂⁻. Among those, the CN⁻ peak at m/z 26 is the characteristic peak, indicating a successful deposition of APTES (36). Peaks relative to O⁻ and OH⁻ could be from the silane bond, silica substrate, and also physical adsorption of water on top of the APTES layer (36). In the positive ion spectrum of APTES, the signals around m/z 28 are the strongest. It is an asymmetric peak (as shown in Appendix 3-1) with contributions from Si⁺ (m/z 27.99) and CH₂N⁺ (m/z 28.02) (37). Other important peaks are from the ions C₂H₃⁺, CH₃N⁺, CH₄N⁺, C₂H₅⁺, C₃H₅⁺, C₃H₇⁺, C₂H₄N⁺ and C₃H₇N⁺.

For the samples of APTES-PEG₃-NH-Fmoc and APTES-PEG₃-NH₂ (columns c and d in Table 3.2, respectively), it was expected to observe the characteristic peak for poly(ethylene

glycol) around m/z 45, which corresponds to the secondary ion of $C_2H_5O^+$ (38-39). However, since the PEG sample only has three repeat units of ethylene glycol, the intensity of this peak should not be very strong. In addition around $m/z = 45$, there are other peaks from $SiOH^+$ (37). Fortunately the resolution of ToF-SIMS used in this work was high enough to distinguish these two peaks from each other. As shown in Figure 3.2, the peak of $SiOH^+$ is at m/z 44.98 in the APTES sample (Figure 3.2b), while the peak for $C_2H_5O^+$ is at m/z 44.03 in the spectrum of the control Fmoc-mini-PEG-3TM directly spread on the silica wafer surface (Figure 3.2a). Since the thickness of the mini-PEG layer linked to the APTES film is only about 2 nm, both of these peaks were detected in the spectra of APTES-PEG₃-NH-Fmoc and APTES-PEG₃-NH₂ modified silica wafer. Due to the difference of thickness, the peak of $SiOH^+$ in the spectrum of APTES-PEG₃-NH-Fmoc is relatively weaker than that of APTES-PEG₃-NH₂.

Comparing columns b, c and d in Table 3.2, there are several differences in the peaks that are significant. First, there is a series of peaks at m/z 165, 178, 179, 180 found only in the spectrum of the sample of APTES-PEG₃-NH-Fmoc, but with almost no count within these ranges in the sample with only APTES self assembled layer and very low counts for APTES-PEG₃-NH₂ (as shown in Figure 3.3). These peaks were identified as potentially coming from Fmoc groups in this positive spectrum (40-42) and the structure of these four peaks are specified in Figure 3.4. There is also one peak at 165 in the negative spectrum of this positive control sample from Fmoc (40-42) and again this peak only appeared in the spectrum of the sample of APTES-PEG₃-NH-Fmoc. These results are direct evidence of the presence of PEG₃-NH₂-Fmoc layer and the successful removal of the Fmoc by deprotection.

The other interesting results are the yield of peaks of NH_3^+ and NH_4^+ . The yield of these two peaks could be interpreted as an indication of the degree of protonation of the primary amine groups present (43-44). The normalized intensities of these two peaks are higher for APTES-PEG₃-NH₂ compared to those of APTES, which indicates that the amine groups at the end of APTES are more difficult to protonate than those at the end of APTES-PEG₃-NH₂. In summary, the ToF-SIMS results provide ample evidence that the chemistry is effectively creating the type of surface anticipated in Figure 3.1, with the creation of the APTES layer first, followed by the attachment of the Fmoc-protected PEG, and ultimately the exposure of the amino group at the end of the PEG layer upon deprotection.

3.3.3 Determination of the pKa of Amine Groups on Surface by Contact Angle

Titration

The dissociation constants of surface acidic or basic groups often differ from the free analogs in solution. Several factors contribute to these differences, including the low dielectric permittivity region close to the acidic and basic groups, a reduction of the degrees of freedom caused by immobilization, and excess electrostatic free energy of supporting surface and change in the dielectric constant of the solution in the vicinity of a charged surface (45). The contact angle titration method is widely used as a simple approach to determine the pK value of functional groups on surfaces (46-47). The “non-reactive spreading” protocol proposed by Creager and his colleagues was used in this work (46).

The contact angle results obtained for aqueous buffer solutions at different pH values on silica surfaces with an APTES monolayer only and a sample containing a PEG layer on top of the APTES layer are illustrated in Figure 3.5. It can be seen from the results that the $\text{pK}_{1/2}$

of the amine groups on APTES monolayer is about 6.2. It is in the middle range of two values identified in the literature, and used as reference, 7.4 (48-49) and 4.3 (50) and both of them were obtained using the contact angle titration by other groups. The wide range of $pK_{1/2}$ values obtained from these different studies may be caused by differences in the substrate cleaning process, silanization conditions and/or pre-treatments before surface titration. For the APTES-PEG₃-NH₂ modified surface, contact angle data points begin at pH 4, because the contact angles of the buffer with pH below that were too small to be measured. The $pK_{1/2}$ of amino groups on the surface with APTES-PEG₃-NH₂ is about 7. It is slightly higher than that of amino groups of APTES monolayer. One possible reason for this difference is that the amine groups at the end of PEG chain have more freedom comparing with the amino groups at the end of APTES which may the amine groups are relatively easy to be protonated.

3.3.4 Measurement of Nonspecific Protein Adsorption by QCM

The QCM sensors with silica surfaces were modified in the same way used in the modification of silica wafers. The adsorption of pure BSA on the modified silica surfaces was monitored by QCM-D E4 in parallel until the frequency change was lower than 1 Hz for at least 30 minutes. Typically, it took 3~8 hours for each sample to reach full equilibrium.

The isoelectric point of BSA is 4.7 (51) and the $pK_{1/2}$ of the amine group on the APTES and the APTES-PEG-NH₂ measured by contact angle titration is around 7. In order to study the effect of pH on the adsorption of BSA by the QCM surface, four buffer pH values were selected: pH 4, which is below both the pI of BSA and $pK_{1/2}$ of the amine group; pH 6.0, which is between these two, and 7.4 and 8, above both. The amount of adsorption from 1 mg ml⁻¹ BSA in phosphate-buffered saline (pH 6.0, pH 7.4 or pH 8.0) or acetate buffered saline

(pH 4.0) onto the modified silica surfaces were measured and compared with the bare silica surface and the surface modified only by APTES. In order to exclude the effects of the charge-to-charge interactions on the adsorption, the amine groups on a sample with APTES surface and a sample with APTES-PEG₃-NH₂ were acetylated by acetic anhydride, and were included as controls. The results are summarized in Figure 3.6. Generally, the frequency change caused by protein adsorption on the surface with mini-PEG layer (Figure 3.6, column c) was about 50~60 percent of that on the bare silica surface (Figure 3.6, column a) and the surface with only APTES layer (Figure 3.6, column b) at all buffer conditions. In addition, the surface with amine groups (column b and c) adsorbed more protein than their corresponding acetylated surfaces (Figure 3.6, columns d and e). The surfaces with free amine groups (Figure 3.6, columns b and c) adsorbed the most BSA from 1 mg ml⁻¹ BSA solution at pH 6.0 and least at pH 8.0, while the dependence of adsorption amount on acetylated samples (Figure 3.6, columns d and e) on pH seems to be relatively weak. Charge-to-charge interactions appear to play an important role in the BSA adsorption by surfaces with free amine groups at all buffer conditions, especially, at pH 6.0, when the charge on surface and net charge on BSA are opposite.

For the APTES-PEG₃-NH₂ sample, the isotherms for BSA adsorption at different pH values were also obtained and shown in Figure 3.7. The protein adsorption amounts provided here were converted from the frequency change caused by protein binding at equilibrium by using the Sauerbrey relationship (Equation 3-5). The isotherm adsorption data were fitted to a Langmuir model and the obtained maximum capacity (Q_m) and dissociation constant (K_d) values at different pH levels are listed in Table 3.3. The results in Table 3.3

clearly indicate the effect of pH on the adsorption. The K_d value at pH 6.0 is significantly smaller, indicating that the electrostatic interactions between the opposite charges on the protein and the surface are playing a major role in the adsorption process. Also showed in Table 3.3, the maximum capacity Q_m is much larger than that for a full monolayer of BSA on surface which should be around 2 mg m^{-2} (52). The adsorption amount measured by QCM is probably overestimated as a result of using the oversimplified Sauerbrey model (53) or due to the presence of water molecules associated with protein adsorbed on the surface (54).

3.4 Conclusions

A new method is presented to modify silica surfaces with PEG chains terminated with amine groups. The density of PEG chain and amine group obtained is approximately $2.74 \text{ chain nm}^{-2}$. In other words, the average distance between two chains is about 6 \AA . ToF-SIMS results provided direct evidence that the silica surface was modified as we expected. According to the contact angle titration and ToF-SIMS experiment results, the amine group at the end of PEG chains has higher activity than that at the end of APTES.

It was also shown that PEG chains as short as three repeat units can significantly reduce BSA adsorption on the surface. The adsorption of BSA on the modified surface with PEG termination with free amine groups depends on pH of the solution since the adsorption process is controlled to a great degree by charge-charge interactions.

These well-characterized surfaces will be used in future studies to attach small affinity peptide ligands through their carboxyl terminus in order to characterize the specific interactions of proteins with these small biological ligands.

Reference:

1. Damos FS, Mendes RK, & Kubota LT (2004) Applications of QCM, EIS and SPR in the investigation of surfaces and interfaces for the development of (BIO)sensors. *Quimica Nova* 27(6):970-979.
2. Williams RA & Blanch HW (1994) Covalent immobilization of protein monolayers for biosensor applications. *Biosensors & Bioelectronics* 9(2):159-167.
3. Oh SJ, Hong BJ, Choi KY, & Park JW (2006) Surface modification for DNA and protein microarrays. *Omics-A Journal of Integrative Biology* 10(3):327-343.
4. Mello LD & Kubota LT (2002) Review of the use of biosensors as analytical tools in the food and drink industries. *Food Chemistry* 77(2):237-256.
5. Bilitewski U (2006) Protein-sensing assay formats and devices. *Analytica Chimica Acta* 568(1-2):232-247.
6. Gnauck M, *et al.* (2007) Carboxy-terminated oligo(ethylene glycol)-alkane phosphate: Synthesis and self-assembly on titanium oxide surfaces. *Langmuir* 23(2):377-381.
7. Houseman BT, Huh JH, Kron SJ, & Mrksich M (2002) Peptide chips for the quantitative evaluation of protein kinase activity. *Nature Biotechnology* 20(3):270-274.
8. Nyquist RM, *et al.* (2000) Characterization of self-assembled monolayers for biosensor applications. *Langmuir* 16(4):1793-1800.
9. Xia N, Hu YH, Grainger DW, & Castner DG (2002) Functionalized poly(ethylene glycol)-grafted polysiloxane monolayers for control of protein binding. *Langmuir* 18(8):3255-3262.
10. Wink T, vanZuilen SJ, Bult A, & vanBennekom WP (1997) Self-assembled monolayers for biosensors. *Analyst* 122(4):R43-R50.

11. Chaki NK & Vijayamohanan K (2002) Self-assembled monolayers as a tunable platform for biosensor applications. *Biosensors & Bioelectronics* 17(1-2):1-12.
12. Tokumitsu S, *et al.* (2002) Grafting of alkanethiol-terminated poly(ethylene glycol) on gold. *Langmuir* 18(23):8862-8870.
13. Prime KL & Whitesides GM (1993) Adsorption of proteins onto surfaces containing end-attached oligo(ethylene oxide) - a model system using self-assembled monolayers. *Journal of the American Chemical Society* 115(23):10714-10721.
14. Prime KL & Whitesides GM (1991) Self-assembled organic monolayers - model systems for studying adsorption of proteins at surfaces. *Science* 252(5009):1164-1167.
15. Palegrosdemange C, Simon ES, Prime KL, & Whitesides GM (1991) Formation of self-assembled monolayers by chemisorption of derivatives of oligo(ethylene glycol) of structure HS(CH₂)₁₁(OCH₂CH₂)meta-OH on gold. *Journal of the American Chemical Society* 113(1):12-20.
16. Flynn NT, Tran TNT, Cima MJ, & Langer R (2003) Long-term stability of self-assembled monolayers in biological media. *Langmuir* 19(26):10909-10915.
17. Valiokas R, Ostblom M, Svedhem S, Svensson SCT, & Liedberg B (2002) Thermal stability of self-assembled monolayers: Influence of lateral hydrogen bonding. *Journal Of Physical Chemistry B* 106(40):10401-10409.
18. Cha TW, Boiadjiev V, Lozano J, Yang H, & Zhu XY (2002) Immobilization of oligonucleotides on poly(ethylene glycol) brush-coated Si surfaces. *Analytical Biochemistry* 311(1):27-32.
19. Cha T, Guo A, Jun Y, Pei DQ, & Zhu XY (2004) Immobilization of oriented protein molecules on poly(ethylene glycol)-coated Si(111). *Proteomics* 4(7):1965-1976.
20. Schlapak R, *et al.* (2006) Glass surfaces grafted with high-density poly(ethylene glycol) as substrates for DNA oligonucleotide microarrays. *Langmuir* 22(1):277-285.

21. Efimenko K, Novick B, Carbonell RG, DeSimone JM, & Genzer J (2002) Formation of self-assembled monolayers of semifluorinated and hydrocarbon chlorosilane precursors on silica surfaces from liquid carbon dioxide. *Langmuir* 18(16):6170-6179.
22. Petri DFS, Wenz G, Schunk P, & Schimmel T (1999) An improved method for the assembly of amino-terminated monolayers on SiO₂ and the vapor deposition of gold layers. *Langmuir* 15(13):4520-4523.
23. Staros JV, Wright RW, & Swingle DM (1986) Enhancement by N-hydroxysufosuccinimide of water-soluble carbodimide-mediated coupling reactions. *Analytical Biochemistry* 156(1):220-222.
24. Carpino LA, Chao HG, Beyermann M, & Bienert M (1991) ((9-Fluorenylmethyl)oxy)carbonyl amino-acid chlorides in solid-phase peptide synthesis. *Journal of Organic Chemistry* 56(8):2635-2642.
25. P.A. C (1983) The adsorption of prothrombin to phosphatidylserine multilayers quantitated by ellipsometry. *Journal of Biological Chemistry* 258(4):2426-2431.
26. Rodahl M, Hook F, & Kasemo B (1996) QCM operation in liquids: An explanation of measured variations in frequency and Q factor with liquid conductivity. *Analytical Chemistry* 68(13):2219-2227.
27. Rodahl M, *et al.* (1997) Simultaneous frequency and dissipation factor QCM measurements of biomolecular adsorption and cell adhesion. *Faraday Discussions*:229-246.
28. Sauerbrey G (1959) Verwendung Von Schwingquarzen Zur Wagung Dunner Schichten Und Zur Mikrowagung. *Zeitschrift Fur Physik* 155(2):206-222.
29. Sauerbrey G (1959) Verwendung von schwingquarzen zur wagung dunner schichten und zur mikrowagung. (Translated from English) *Zeitschrift Fur Physik* 155(2):206-222 (in English).
30. Vandenberg ET, *et al.* (1991) Structure of 3-aminopropyl triethoxy silane on silicon-oxide. *Journal of Colloid And Interface Science* 147(1):103-118.

31. Lide DL (2003) *CRC Handbook of Chemistry and Physics* (CRC Press, Boca Raton, FL.) 84th Ed.
32. Kowalczyk D, Slomkowski S, Chehimi MM, & Delamar M (1996) Adsorption of aminopropyltriethoxy silane on quartz: an XPS and contact angle measurements study. *International Journal of Adhesion and adhesives* 16:227-232.
33. Zhu XY, *et al.* (2001) Grafting of high-density poly(ethylene glycol) monolayers on Si(111). *Langmuir* 17(25):7798-7803.
34. Andruzzi L, *et al.* (2005) Oligo(ethylene glycol) containing polymer brushes as bioselective surfaces. *Langmuir* 21(6):2495-2504.
35. Jo S & Park K (2000) Surface modification using silanated poly(ethylene glycol)s. *Biomaterials* 21(6):605-616.
36. Allen GC, Sorbello F, Altavilla C, Castorina A, & Ciliberto E (2005) Macro-, micro- and nano-investigations on 3-aminopropyltrimethoxysilane self-assembly-monolayers. *Thin Solid Films* 483(1-2):306-311.
37. Vanooij WJ & Sabata A (1993) Characterization Of Films Of Organofunctional Silanes By Tof-Sims .2. Films Of Gamma-Aps, Aeaps And Fps On Cold-Rolled Steel And Cold-Rolled Zinc Substrates. *Surface And Interface Analysis* 20(5):475-484.
38. Newman J, Carloson B, Michael R, Moulder J, & Hohlt T (1991) Static SIMS handbook of polymer analysis. *Perkin-Elmer Corporation*.
39. Norrman K, Papra A, Kamounah FS, Gadegaard N, & Larsen NB (2002) Quantification of grafted poly(ethylene glycol)-silanes on silicon by time-of-flight secondary ion mass spectrometry. *Journal Of Mass Spectrometry* 37(7):699-708.
40. Drouot C, *et al.* (1996) Step-by-step control by time-of-flight secondary ion mass spectrometry of a peptide synthesis carried out on polymer beads. *Rapid Communications In Mass Spectrometry* 10(12):1509-1511.

41. Drouot C, *et al.* (1997) ToF-SIMS analysis of polymer bound fmoc-protected peptides. *Tetrahedron Letters* 38(14):2455-2458.
42. Enjalbal C, *et al.* (1999) Monitoring and quantification on solid support of a by-product formation during peptide synthesis by ToF-SIMS. *Tetrahedron Letters* 40(34):6217-6220.
43. Vanooij WJ & Sabata A (1991) Characterization of films of organofunctional silanes by ToF-SIMS And XPS .1. films of N-[2-(vinylbenzylamino)-ethyl]-3-aminopropyltri-methoxysilane on zinc and gamma-aminopropyltriethoxysilane on steel substrates. *Journal of Adhesion Science and Technology* 5(10):843-863.
44. Vanooij WJ & Sabata A (1992) Characterization of polymer surfaces and polymer metal interfaces by static secondary ion mass-spectrometry. *Surface and Interface Analysis* 19(1-12):101-113.
45. Zhmud BV & Golub AA (1994) Protolytic equilibria of ligands immobilized at rigid matrix surfaces - a theoretical study. *Journal of Colloid and Interface Science* 167(1):186-192.
46. Creager SE & Clarke J (1994) Contact-angle titrations of mixed omega-mercaptoalkanoic acid alkanethiol monolayers on gold - reactive vs nonreactive spreading, and chain-length effects on surface pk(a) values. *Langmuir* 10(10):3675-3683.
47. Bain CD & Whitesides GM (1989) A study by contact-angle of the acid-base behavior of monolayers containing omega-mercaptocarboxylic acids adsorbed on gold - an example of reactive spreading. *Langmuir* 5(6):1370-1378.
48. Zhang H, He HX, Mu T, & Liu ZF (1998) Force titration of amino group-terminated self-assembled monolayers of 4-aminothiophenol on gold using chemical force microscopy. *Thin Solid Films* 329:778-780.
49. Zhang H, He HX, Wang J, Mu T, & Liu ZF (1998) Force titration of amino group-terminated self-assembled monolayers using chemical force microscopy. *Applied Physics A-Materials Science & Processing* 66:S269-S271.

50. Vezenov DV, Noy A, Rozsnyai LF, & Lieber CM (1997) Force titrations and ionization state sensitive imaging of functional groups in aqueous solutions by chemical force microscopy. *Journal Of The American Chemical Society* 119(8):2006-2015.
51. Dawson RMC, Elliott DC, Elliott WH, & Jones KM eds (1986) *Data for Biochemical Research* (Oxford Univ. Press, , Oxford, UK), 3rd Ed.
52. Giacomelli CE & Norde W (2001) The adsorption-desorption cycle. reversibility of the BSA-silica system. *Journal of Colloid and Interface Science* 233(2):234-240.
53. Stadler H, Mondon M, & Ziegler C (2003) Protein adsorption on surfaces: dynamic contact-angle (DCA) and quartz-crystal microbalance (QCM) measurements. *Analytical And Bioanalytical Chemistry* 375(1):53-61.
54. Zhou C, *et al.* (2004) Human immunoglobulin adsorption investigated by means of quartz crystal microbalance dissipation, atomic force microscopy, surface acoustic wave, and surface plasmon resonance techniques. *Langmuir* 20(14):5870-5878.
55. Eexell U (2003) Surface characterization using ToF-SIMS, AES and XPS of silane films and organic coating deposited on metals substrates., *Ph.D thesis*.
56. Raghavan D, VanLandingham M, Gu X, & Nguyen T (2000) Characterization of heterogeneous regions in polymer systems using tapping mode and force mode atomic force microscopy. *Langmuir* 16(24):9448-9459.

Table 3.1 Thickness and contact angle measurements of modified silica surface

Sample	APTES	APTES-PEG ₃ -NH-Fmoc	APTES-PEG ₃ -NH ₂
Average thickness (Å)	8±1	22±1	16±1
Average contact angle (°)	53±1	23±1	23±1

Table 3.2 Positive and negative ion detection mode SIMS peaks of modified silica surfaces: (a) Fmoc-mini-PEG-3TM directly spread on silica wafer surface, (b) APTES, (c) APTES-PEG3-NH-Fmoc and (d) APTES-PEG3-NH2 modified silica wafer

Peaks (m/z)	Ion	Normalized intensity*			
		a	b	c	d
14	CH ₂ ⁺ , N ⁺	0.91	0.78	0.65	0.71
17	NH ₃ ⁺	0.01	0.09	0.15	0.5
18	NH ₄ ⁺	0.03	0.19	0.19	1.28
28	Si ⁺ , CH ₂ N ⁺	1.29	40.4	15.8	25.6
29	CH ₃ N ⁺ , C ₂ H ₅ ⁺	2.32	19.4	10.5	17.3
30	CH ₄ N ⁺	0.35	3.82	3.88	5.47
42	C ₂ H ₄ N ⁺	0.61	2.82	3.51	2.14
43	C ₃ H ₇ ⁺ , C ₂ H ₃ O ⁺	2.68	3.16	3.3	4.44
44	CON ⁺ , C ₂ H ₆ N ⁺	1.22	1.02	5.91	3.51
45	SiOH ⁺ /C ₂ H ₅ O ⁺	2.73	3.87	2.54	3.02
57	C ₃ H ₇ N ⁺ , C ₃ H ₅ O ⁺	1.65	1.2	1.97	2.62
58	C ₃ H ₈ N ⁺ , C ₃ H ₆ O ⁺ , C ₂ H ₄ ON ⁺	0.2	0.21	7.32	6.25
165	C ₁₂ H ₈ CH ⁺	3.48	0.01	0.23	0.02
178	C ₁₄ H ₉ ⁺	12.1	0.01	0.3	0.02
179	C ₁₄ H ₁₀ ⁺	14.7	0	0.23	0.02
180	C ₁₄ H ₁₁ ⁺	2.77	0	0.04	0.01
-1	H ⁻	44.0	24.0	30.9	32.5
-12	C ⁻	3.94	1.21	2	1.66
-13	CH ⁻	8.48	4.17	5.68	4.86
-16	O ⁻	13.4	29.4	26.0	24.8
-17	OH ⁻	6.76	16.9	13.4	13.0
-24	C ₂ ⁻	1.35	0.82	0.63	0.54
-26	CN ⁻	0.55	2.33	2.3	1.09
-27	Si ⁻	0.06	0.71	0.33	0.34
-28	SiH ⁻	0.07	0.66	0.32	0.34
-165	C ₁₂ H ₉ ⁻	0.13	0	0.02	0

*Peak areas divided by the total positive or negative ion yield in percentage

Table 3.3 Apparent dissociation constant and maximum capacity of the BSA adsorption on modified silica surface APTES-PEG₃-NH₂

pH	Dissociation constant $K_d, \mu\text{M}$	Binding capacity $Q_m, \text{mg m}^{-2}$
4	26.3	6.73
6	7.49	7.02
7.4	16.5	6.97
8	25.3	6.18

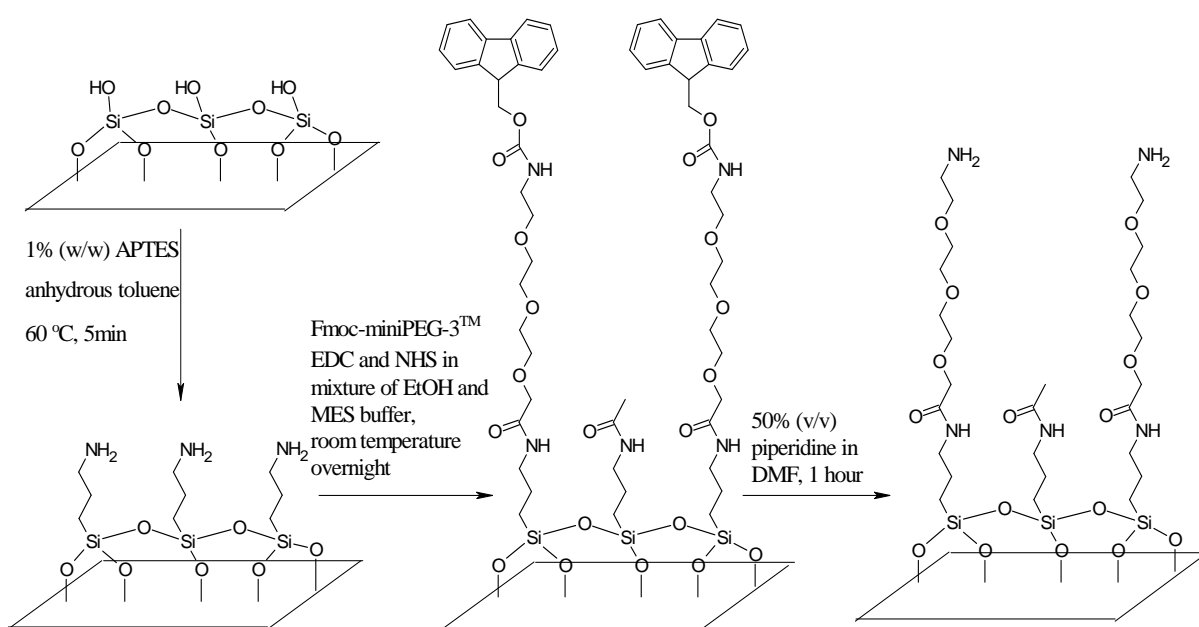


Figure 3.1 Scheme for the modification of silica surfaces

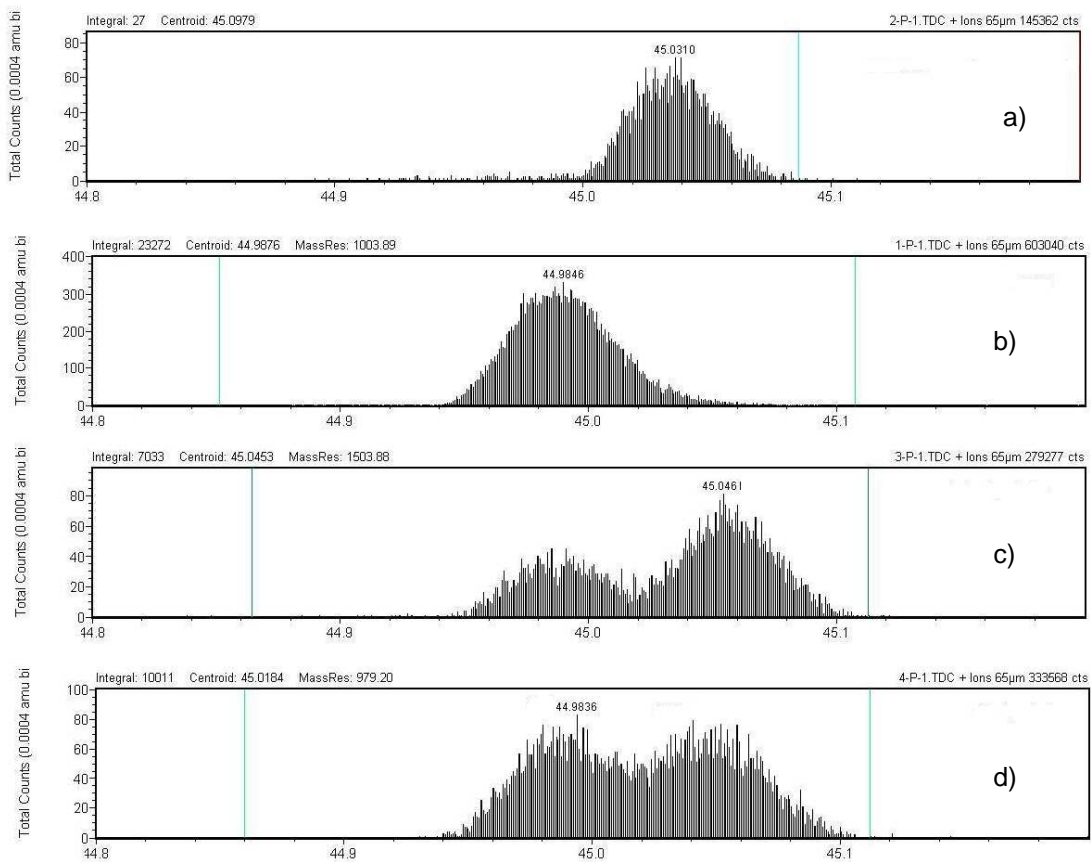


Figure 3.2 ToF-SIMS spectra around m/z 45 (a) Fmoc-mini-PEG-3TM directly spread on silica wafer surfaces, (b) APTES (c) APTES-PEG₃-NH-Fmoc (d) APTES-PEG₃-NH₂ modified silica wafer

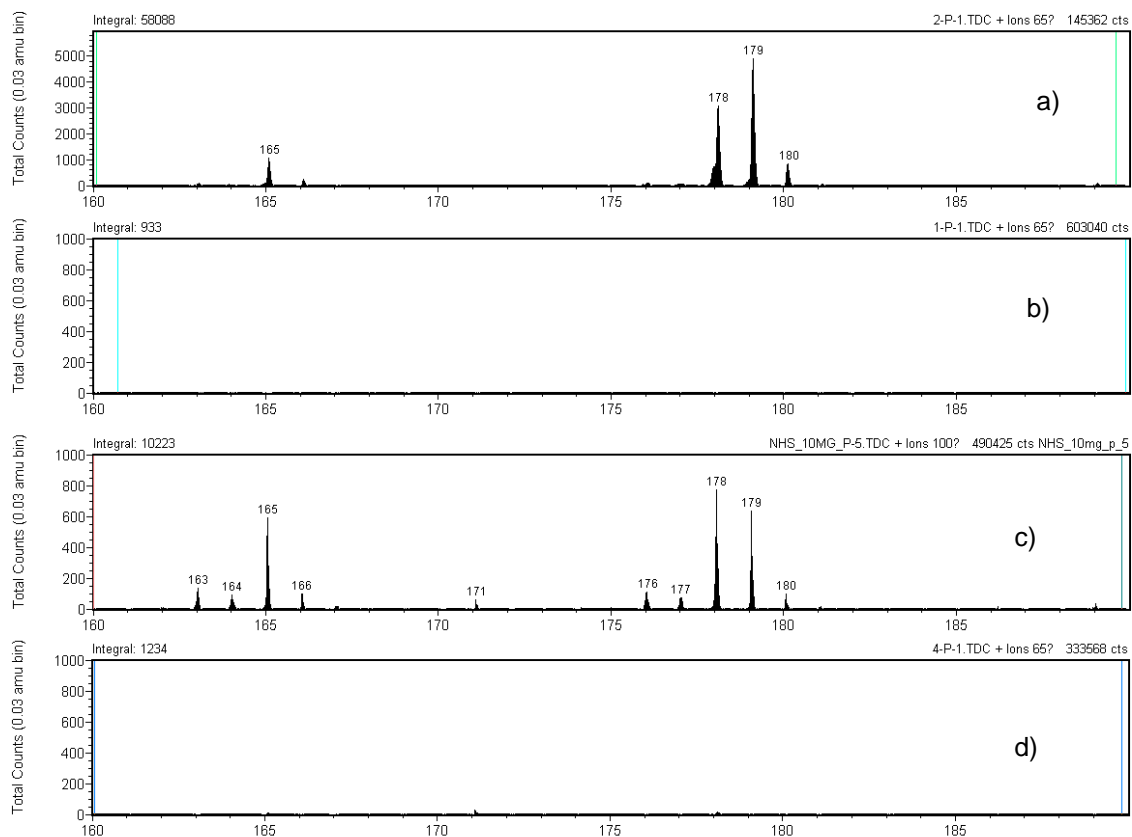


Figure 3.3 ToF-SIMS spectra around the peaks from Fmoc group fractions: (a) Fmoc-mini-PEG-3TM directly spread on silica wafer surfaces, (b) APTES, (c) APTES-PEG₃-NH-Fmoc and (d) APTES-PEG₃-NH₂ modified silica wafer

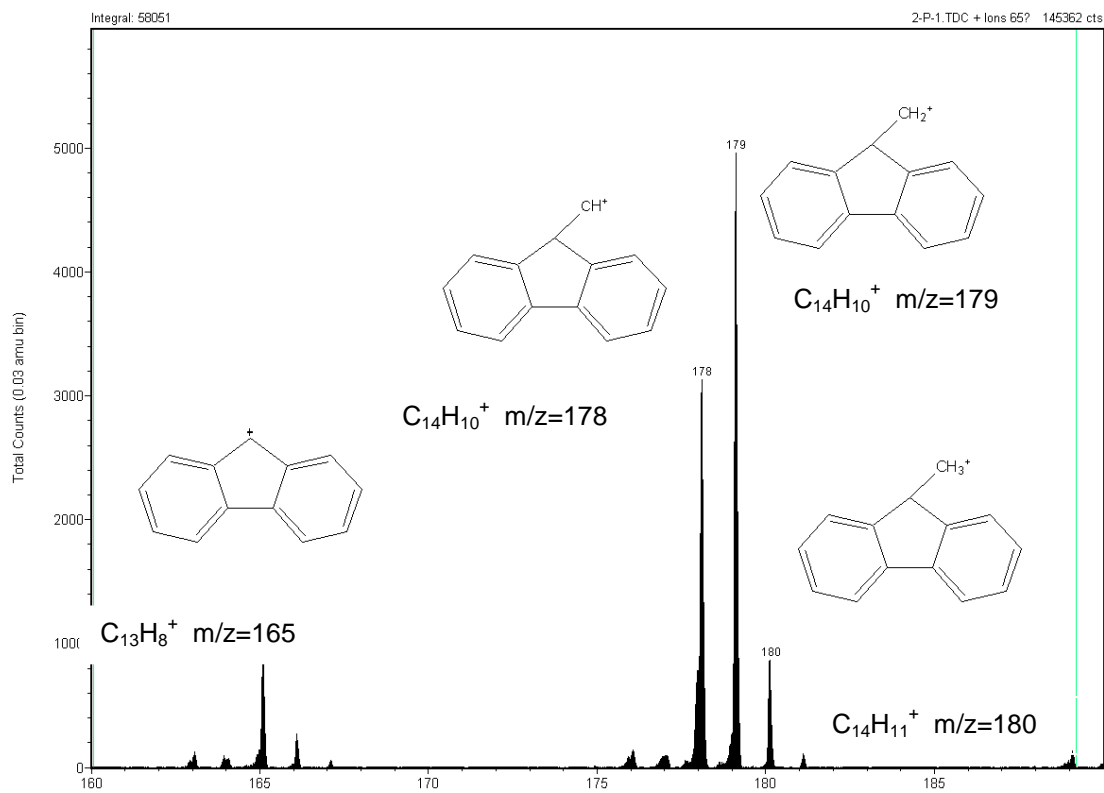


Figure 3.4 Peaks for the ions coming from the fraction of Fmoc group in ToF-SIMS positive spectra

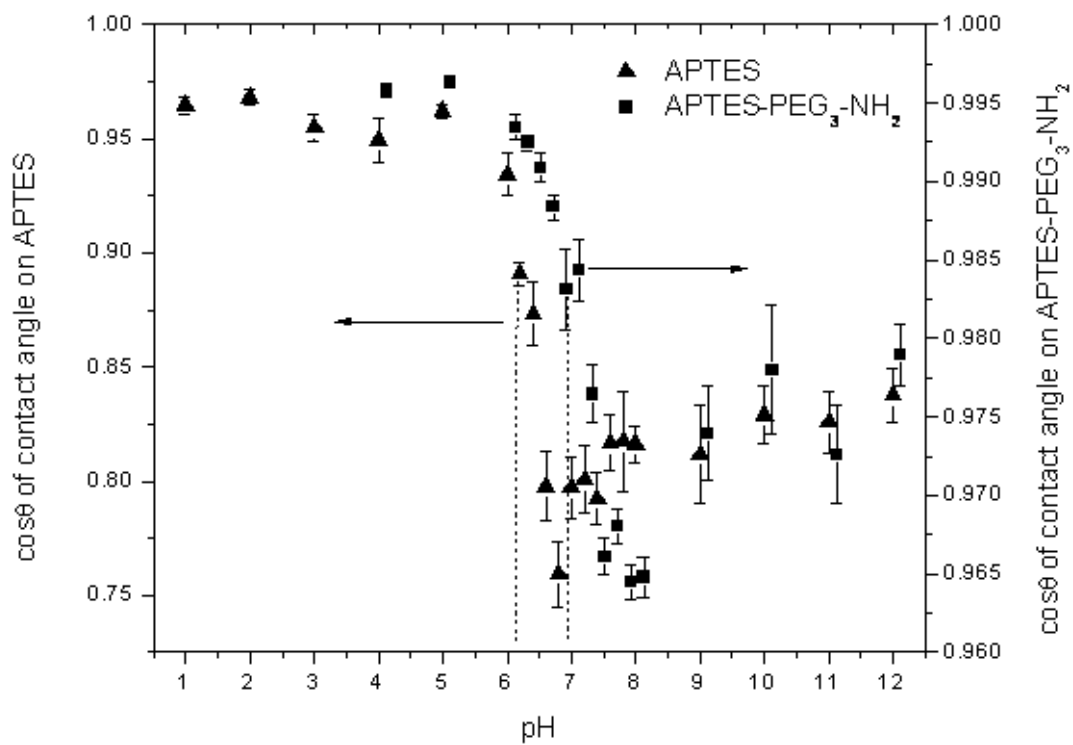


Figure 3.5 Negative consines of advancing contact angles of buffer drops on APTES (triangle) and APTES-PEG₃-NH₂ (square) modified silica surfaces

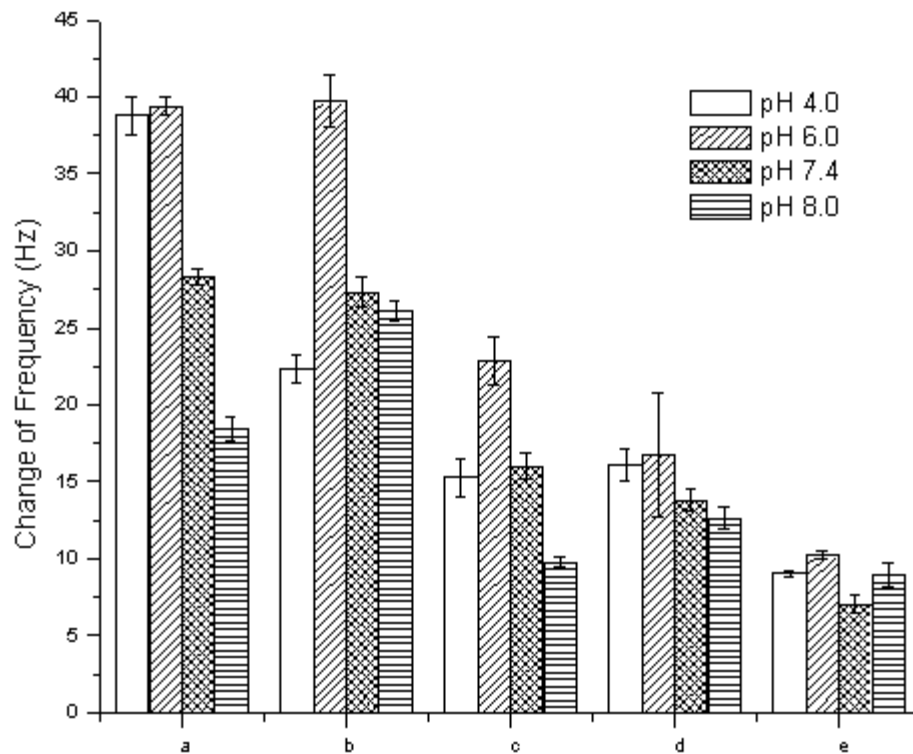


Figure 3.6 BSA adsorption from 1 mg ml^{-1} BSA in different buffer solution on (a) bare silica surface, (b) APTES, (c) APTES-PEG₃-NH₂, (d) acetylated APTES and (e) acetylated APTES-PEG₃-NH₂ modified surfaces

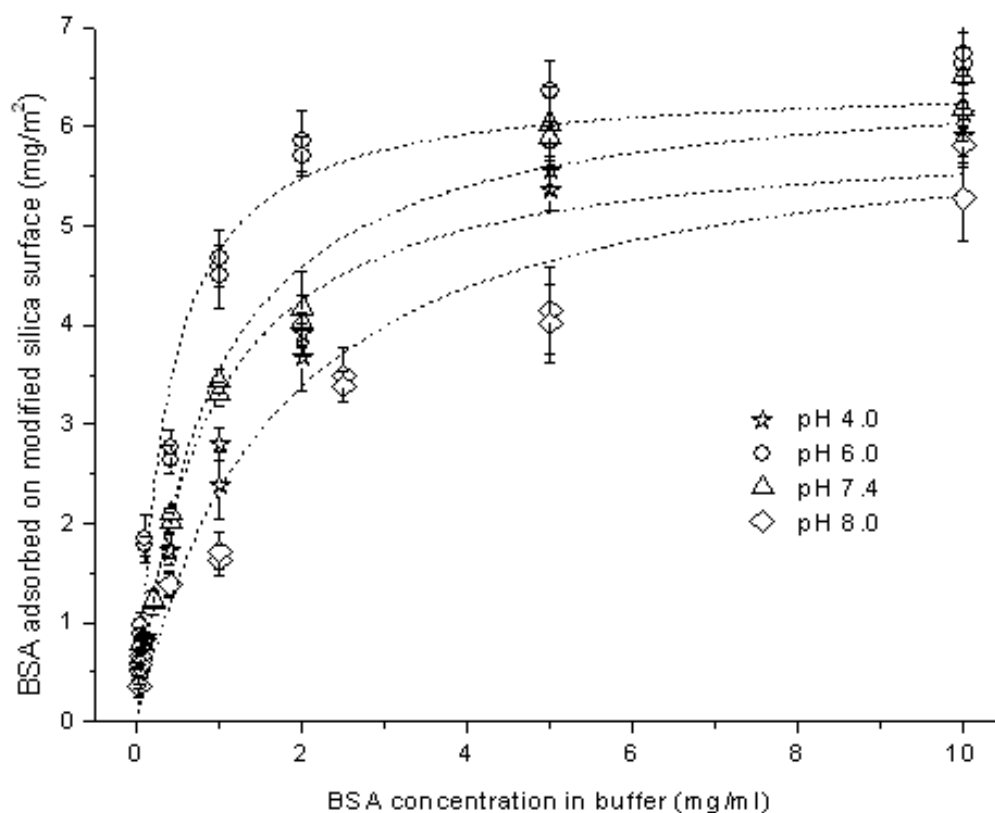


Figure 3.7 The isotherms of BSA adsorption on modified silica surfaces APTES-PEG₃-NH₂ from PBS buffer (pH6.0, 7.4 and 8.0) and from acetate buffer (pH 4,0). The dash lines were the fitting lines to Langmuir equation

Appendix 3-1. Principle of ToF-SIMS

TOF-SIMS is a powerful tool for obtaining information on the chemical composition of surfaces (37, 55). The general principle of TOF-SIMS is shown in Figure 3.8.

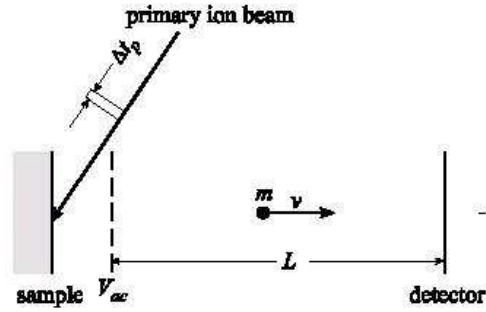


Figure 3.8 schematic principle of ToF-SIMS

The area to be analyzed was bombarded by pulses of primary ions with a duration time Δt_p , which is as short as possible, in ultra-high vacuum condition. During the bombardment, sample material is sputtered from the surface. The majority of this sputtered material is in the form of neutral atoms and molecules; however, a very small percentage of the sputtered material is emitted as either positively or negatively charged ions. All the “secondary” ions generated by a same pulse were accelerated by a constant voltage V_{ac} over a very short distance. The accelerated ions with virtually same kinetic energy E_{kin} simultaneously enter the field free flight path of length L . The mass to the charge ratio could be measured according to the following equations (55):

$$E_{kin} = zV_{ac} = \frac{mv^2}{2} \quad 3-6$$

$$t = \frac{L}{v} = L \sqrt{\frac{m}{2zV_{ac}}} \quad 3-7$$

$$\frac{m}{z} = \frac{2V_{ac}t^2}{L^2}$$

3-8

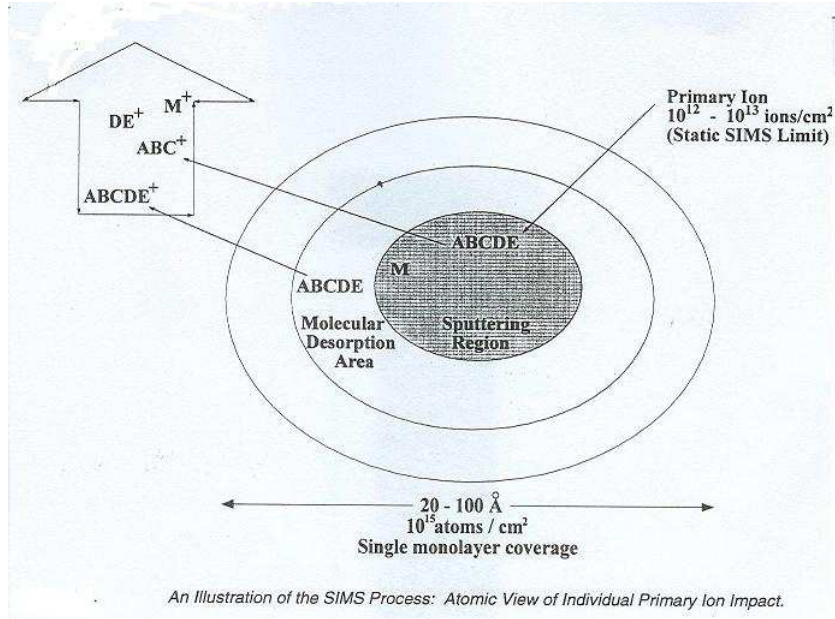


Figure 3.9 the static SIMS regime
(From the operator's guide of TOF-SIMS of Phi physical electronics. Inc.)

The regime bombarded by primary ion is known as the “static” SIMS regime, within which the number of primary ions impacting the surface per unit area is so lower that each successive primary ion strike a virgin area of the surface. The static regime does not end abruptly (as shown in Figure 3.9), but generally it is referred to the area where the density of primary ion is within the range of $10^{12} \sim 10^{13}$ primary ions cm^{-2} . The “static” SIMS can detect the signal within 2~3 nm on the surface (56).

ToF-SIMS is a technique based on mass spectrometry, which is determined that it is not a quantitative technique. The fundamental reason for mass spectrometry not being quantitative in principle is the different response factors associated with different species. This related

property termed the secondary ion yield, which is the number of secondary ions detected relative to the number of primary ions used. The secondary ion yield is affected by many factors, ionization probability, element type, chemical structure, etc. Furthermore, there is no unique signal. The smaller the ions the less specific they are, i.e. they can be formed via various reaction channels and originated from different part of surface (39).

Appendix 3-2. ToF-SIMS spectra around m/z 28

As shown in Figure 3.10 a, the most strongest peaks in the spectrum of APTES was a asymmetric peaks from the contributions of Si^+ (m/z 27.99) and CH_2N^+ (m/z 28.02) (37). It was clear that the signal from Si^+ was so strong that it was hard to distinguish the signal of CH_2N^+ from that of Si^+ . For the positive control (Fmoc-mini-PEG-3TM gel spread on silica wafer surface), there was an obvious peak from CH_2N^+ (m/z 28.02) and there was weak signal of Si^+ from the silica wafer below the Fmoc-mini-PEG-3TM gel (Figure 3.10 b). Two partially overlapped peaks of Si^+ (m/z 27.99) and CH_2N^+ (m/z 28.02) appeared in the spectra of APTES-PEG₃-NH-Fmoc and APTES-PEG₃-NH₂ (Figure 3.10 c and d). The intensity from Si^+ was much weak comparing with that in the spectra of APTES due to the attenuation effects. In addition, the signal from Si^+ was became relatively stronger after removing of Fmoc group which reduced the thickness of organic layer on silica surface and also the attenuation effect. All in all, the changes of the relatively signals of Si^+ and CH_2N^+ were explainable by the modification process.

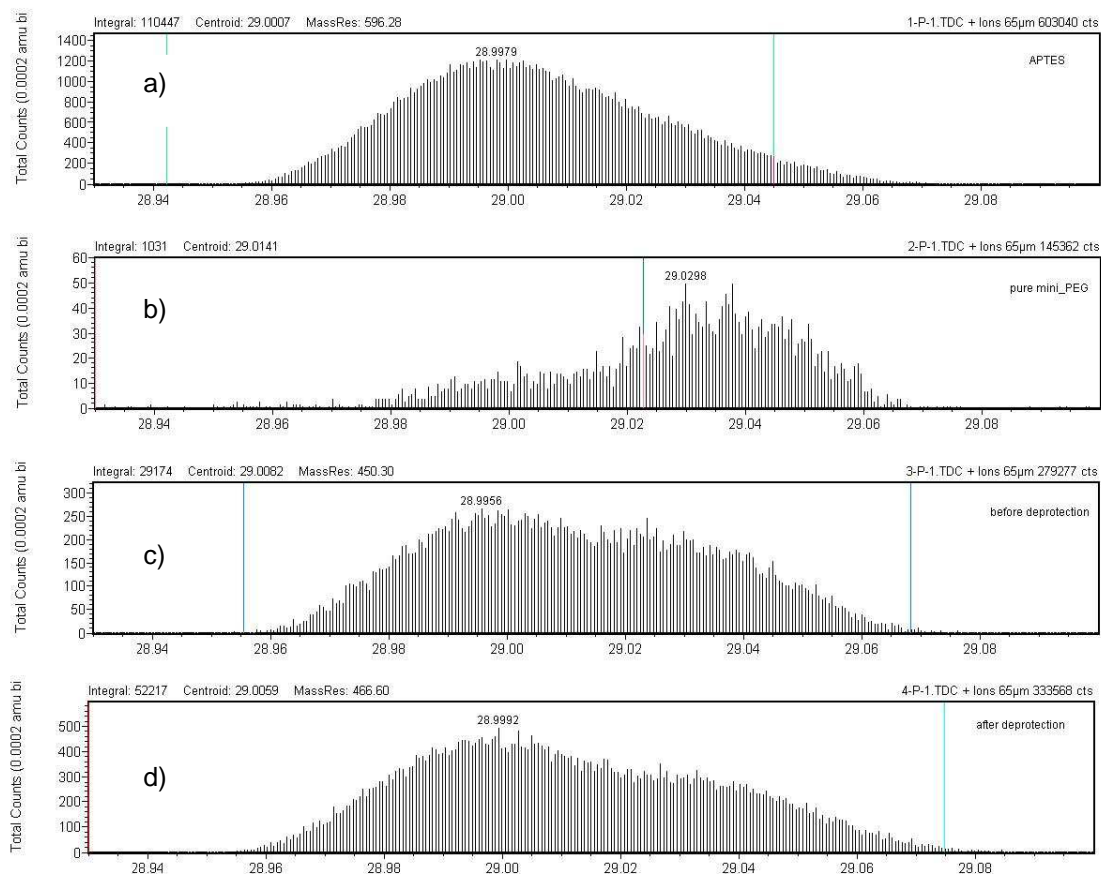


Figure 3.10 ToF-SIMS spectra around m/z 28 (a) Fmoc-mini-PEG-3TM directly spread on silica wafer surfaces, (b) APTES (c) APTES-PEG₃-NH-Fmoc (d) APTES-PEG₃-NH₂ modified silica wafer

**Chapter 4: Study of the Affinity Interaction between Hexamer Peptide
HWRGWV Immobilized on Modified Silica Surface and Human
Immunoglobulin G by Quartz Crystal Microbalance**

Abstract

The hexamer peptide ligand HWRGWV binds specifically to the Fc fragment of immunoglobulin G (IgG). The affinity interaction between the human immunoglobulin G (hIgG) and this short peptide ligand immobilized on a flat surface was studied by quartz crystal microbalance (QCM) in real time. The QCM sensor with a native silicon oxide surface film was modified to allow for peptide immobilization. A self-assembling monolayer of 3-amino-propyl triethoxy silane was formed on the surface as an initial anchor layer. Short chains of poly(ethylene glycol) (PEG) with Fmoc-protected amino groups at one end and carboxyl groups at the other end were then coupled through the carboxyl terminal to the amino groups on the silane. The short PEG chains worked as spacer arms to reduce nonspecific binding to the substrate. The amino groups at the end of the ethylene glycol chains were deprotected, and Fmoc-protected HWRGWV was immobilized through its carboxyl terminal to these amines. The modified surfaces were characterized by ellipsometry and time of flight-secondary ion mass spectroscopy (ToF-SIMS). The immobilization of peptide was optimized, and the highest peptide surface density reached was $0.88 \text{ chains nm}^{-2}$, which is high enough to ensure that every hIgG molecule adsorbed on the surface interacts with more than one peptide ligand on surface. The spectrum of ToF-SIMS demonstrated the presence of the peptide after immobilization with a series of characteristic peaks from amino acids and fragments of the peptide HWRGWV. Both thermodynamic and kinetic parameters of affinity interaction were obtained by analysis of QCM results. The maximum binding capacity was found to be 4.6 mg m^{-2} , which corresponds to a monolayer of hIgG and is close to that obtained from batch experiments with chromatography resin under similar conditions.

The value of dissociation constant obtained in the present study was lower than that obtained from with chromatography resin, probably due to the overestimation of protein binding by QCM. It was found that a PEG spacer arm enhanced the accessibility of the peptide to protein target at high concentrations.

4.1 Introduction

Immunoglobulins (Ig), or antibodies, act as protective agents against pathogens trying to invade an organism. They form an important class of proteins present in blood, saliva and other body fluids. Human immunoglobulins can be divided into five isotypes: IgG, IgA, IgM, IgD and IgE. Among them, IgG is the most abundant class of immunoglobulins, constituting about 75% of the total Ig in adult blood. Immunoglobulins have found a wide range of applications in fields such as immunotherapy, diagnostics and histology (1). Usually, IgG is isolated from pooled blood plasma or produced in hybridoma cell culture. Affinity ligands such as *Staphylococcus aureus* Protein A and *Streptococcus* Protein G are widely used as affinity ligands for IgG separation and the determination of IgG concentrations (2). However, as protein ligands, protein A and protein G have several disadvantages such as high cost, variable binding specificity to different monoclonal antibodies, low stability under washing, cleaning and regeneration conditions, high immunogenicity upon leakage from the resin, and requires product elution at pH 3 which tends to denature antibodies (2). The drawbacks associated with these two proteins have given rise to searching for alternative affinity ligands.

Our group has found several small peptide ligands that bind hIgG through its Fc portion, with potential applicability to antibody purification and detection. The hexamer peptide ligand HWRGWV was screened from a one-bead-one-peptide combinatorial library

synthesized on chromatography resins (3). A chromatography resin with HWRGWV can purify human IgG (hIgG) from complete minimal essential medium (cMEM) with purities and yields as high as 95%, which are comparable to what is obtained with Protein A as affinity ligand (4). HWRGWV offers several potential advantages over Protein A, such as it can be produced at relatively low costs under good manufacturing practices (GMP) conditions, it is chemically robust, less immunogenic, and allows product elution at pH 4 (3, 5).

Although the short peptide ligand HWRGWV has exhibited promising applications for IgG separation and concentration determination, limited information is available on the intrinsic mechanisms of affinity interaction between this short peptide ligand and target protein. Previously, our group has obtained the thermodynamic parameters of affinity interactions between target biomolecules and peptide-functionalized chromatography resins by using batch experiments to determine isotherms, and the adsorption amounts were calculated from mass balance (5-10). This indirect method to measure adsorption can generate a significant error when the change of protein concentration due to adsorption is small compared to the absolute protein concentration. The kinetic parameters of the affinity binding to peptide ligands on resins were studied by dynamic adsorption experiments carried on high performance liquid chromatography (HPLC). Different models were employed to describe the solute transport within the chromatography column to get the intrinsic kinetic parameters. A lumped kinetic model was employed for the study of the adsorption kinetics of fibrinogen that binds to the short peptide FLLVPL. However, the capacity and association constant derived from the fitting of the experimental breakthrough data with this model was

inconsistent with equilibrium experiments (11-12). A more sophisticated model involving theoretical plate estimations and General Rate Model was shown to fit well with experimental results in the analysis of Staphylococcal enterotoxin B (SEB) binding with peptide ligand YYWLHH (9, 13).

Generally, the reliability of the final results for the kinetic rate of adsorption and desorption highly rely on the accuracy of the transport models and the estimation of the mass transfer parameters. Surface detection methods like quartz crystal microbalance (QCM), which monitor the adsorption step on a surface *in situ*, can provide more direct measurement of adsorption amount in real time and enhanced insights on the role of ligand display on binding.

QCM is a well established technique for monitoring solute adsorption to surfaces in the gas phase (14) as well as liquid phases (15). It also has found applications in studies of affinity reactions and pathogen detection in real time (16-22). In this work, we utilize this technique to determine the thermodynamic and kinetic parameters of the affinity interactions between hIgG in solution and immobilized HWRGWV on a flat silica surface. If the peptide immobilized on a QCM sensor has similar high affinity and specificity for IgG adsorption as on a chromatography resin, it could lead to a novel method for IgG concentration determination but also provide a new platform for the development of immunosensors. Because the ligand binds to the Fc fragment of IgG, the results of this study could also lead to a new method to orient the IgG molecules on sensor surfaces. This orientation effect has been found to be important in maintaining high affinity activity of immobilized IgG for immunosensor applications (23-29).

In order to investigate the interaction between ligand and protein the QCM sensor needs to be functionalized by attaching the peptide ligand. The immobilized ligand density can affect the interactions between the peptide ligands and the target biomolecule. For affinity interactions of some small proteins with peptide ligands, such as s-protein to the peptide sequence YNFEVL and SEB to peptide ligand YYWLHH, the binding is monovalent and highly specific. In these cases the binding capacity increases with increasing ligand density, while the association constant remains constant at low ligand density and decreases at high ligand density due to steric effects (8-9). Thus there is an optimal density at which the peptide ligands have high capacity and minimal steric hindrance. For the specific adsorption between ligands and larger molecules, such as von Willebrand Factor (vWF) with small peptide ligand Ac-RVRSFYK on a resin surface, the binding is attributed to multivalent interactions and increasing the ligand density typically increases both the binding capacity and the association constant (30). The peptide density can also affect the selectivity of ligand, for instance, two trimeric peptide ligands, WRW and KYY, both exhibit higher selectivity to porcine parvovirus (PPV) from solutions containing 7.5% human blood plasma at low peptide density (31). For the specific case of IgG adsorption, it was found that maintaining the right ligand density of peptide is crucial to ensure high purity and yield for hIgG purification, since increases in ligand density from 0.8 to 11 chains nm^{-2} (0.04 to 0.55 meq g^{-1}) increased binding capacity to hIgG but also increased non-specific binding of competitive proteins. A peptide density of 1.6 chains nm^{-2} (0.08 meq g^{-1}) exhibited both appropriate binding capacity and specificity (5). In Chapter 3, we discussed in detail the optimization of the silica surface modification process to introduce a high density of primary amino groups

on the silica surface for peptide immobilization. Here the peptide immobilization process was optimized and the best conditions obtained were used for the study of affinity interactions by QCM. QCM recorded the binding processes of hIgG on modified silica surfaces and provided both the data required for kinetics and thermodynamics analyses.

4.2 Materials and Methods

4.2.1 Materials

The following chemicals were obtained from Sigma-Aldrich (St. Louis, MO): Anhydrous toluene (99.8%), γ -amino-propyltriethoxysilane (99%), N,N-dimethylformamide (DMF, ACS reagent, 99.8%), anhydrous N,N-dimethylformamide (DMF), dichloromethane (DCM, ACS reagent, 99.5%), ethanol (200 proof, absolute, for molecular biology), methanol (ACS reagent, 99.5%), piperidine (biotech grade, $\geq 99.5\%$), diisopropylethylamine (DIPEA), hydroxybenzotriazole (HOBt), trifluoroacetic acid (TFA, ACS reagent, $\geq 98\%$), anisole ($\geq 99\%$), triisopropyl silane (TIPS, ACS reagent, $\geq 99\%$), N,N'-diisopropylcarbodiimide (DIC, $\geq 99.5\%$), bromo-tris-pyrrolidino-phosphonium hexafluorophosphate (PyBrOP, $\geq 95\%$), acetic anhydride (ACS reagent, $\geq 98.0\%$), sodium acetate (ACS reagent, $\geq 99.0\%$), bovine serum albumin (BSA, $\geq 98\%$) and phosphate buffered saline (pH 7.4, monobasic sodium phosphate, dibasic sodium phosphate, sodium chloride 0.138M, potassium chloride 0.0027M). Ethyl-3-(3-dimethylaminopropyl) carbodiimide hydrochloride (EDC) and N-hydroxysuccinimide (NHS) were obtained from Pierce (Rockford, IL). 2-(1H-benzotriazole-1-yl)-1,1,3,3-tetramethyluronium tetrafluoroborate (TBTU) was obtained from Calbiochem-Novabiochem Corp (San Diego, CA). Human immunoglobulin (hIgG purity 97%) was

obtained from Equitech-Bio, Inc. (Kerrville, TX). Nitrogen gas, purity 99.99%, was obtained from National Welders Supply, Inc. (Raleigh, NC). Deionized water (resistivity > 16 M Ω ·cm) and Milli-Q water (resistivity > 18 M Ω ·cm) were obtained by using a Millipore water purification system (Billerica, MA). Fmoc-11-amino-3,6,9-trioxaundecanoic acid (Fmoc-mini-PEG-3TM) was obtained from Peptides International, Inc. (Louisville, KY). Peptides Fmoc-His-Trp-Arg-Gly-Trp-Val-OH, Fmoc-His(Trt)-Trp(Boc)-Arg(Pbf)-Gly-Trp(Boc)-Val-OH, and Fmoc-His(Trt)-Trp(Boc)-Arg(Pbf)-Gly-Trp(Boc)-Val-Ala-Ala-OH were custom synthesized using Fmoc chemistry by Peptides International, Inc. (Louisville, KY). All the chemicals and proteins were used as received.

4.2.2 Surface Modification

PEG chains with amino terminal groups were introduced on the surface of the silica to allow peptide immobilization. The modification details were described in Chapter 3. In short, the silica surface was first modified by 3-amino propyl triethoxy silane (APTES) to form a self-assembled monolayer. Functionalized PEG chains with a carboxyl group at one end and an Fmoc-protected amine group at other end were immobilized on top of the APTES layer, followed by the de-protection of the amine groups at end of the PEG chains, generating the site for the immobilization of peptide ligands. The modification was proven to be as described by characterization by ellipsometry and ToF-SIMS.

4.2.3 Peptide Immobilization and Protection Group Deprotection

The hexamer peptide ligand HWRGWV was immobilized on the modified surface through a coupling reaction between the carboxyl group at the C terminal of the peptide and

amine groups on the sensor surface using coupling reagents. The results using several kinds of coupling reagents were compared, including two kinds of carbodiimide, DIC and EDC, one aminium-based reagent (TBTU) and one phosphonium-based reagent PyBrOP. Besides coupling reagent type, the effects of peptide and coupling reagent concentrations on reaction were studied by the combination of two peptide concentration levels and two coupling reagents concentration levels. For each kind of coupling reagent, two different peptide concentrations were used, 1 and 10 mg ml⁻¹. The coupling reagent concentration was chosen depending on the molar concentration of peptide; for a peptide concentration of 1 mg ml⁻¹, the coupling reagent used was either equal or 10 times the molar concentration of peptide; and for a peptide concentration of 10 mg ml⁻¹ the coupling reagent concentration was either equal or 2.5 times of the molar concentration of peptide. DMF was used as solvent for all the experiments.

In order to test the effect of steric hindrance of amino acid side chains of the C terminal amino acid on peptide immobilization density, two amino acids, Fmoc-Alanine-OH and Fmoc-Valine-OH, were immobilized on the modified silica surface.

The details of the immobilization process are as follows: peptides Fmoc-His-Trp-Arg-Gly-Trp-Val-OH, Fmoc-His(Trt)-Trp(Boc)-Arg(Pbf)-Gly-Trp(Boc)-Val-OH, Fmoc-His(Trt)-Trp(Boc)-Arg(Pbf)-Gly-Trp(Boc)-Val-Ala-Ala-OH, and amino acids Fmoc-Alanine-OH and Fmoc-Valine-OH were dissolved to a final concentration of 1 or 10 mg ml⁻¹. Anhydrous DMF was used as solvent for all experiments unless stated otherwise. For the experiment using TBTU as coupling reagent, 1, 2.5 or 10 equivalents of TBTU and HOBT based on the molar concentration of peptide and 2 equivalents of DIPEA to TBTU were added to the

peptide solutions. When using EDC as coupling reagent, 1, 2.5 or 10 equivalents of EDC to the molar concentration of peptide and 2.5 equivalents of NHS to DEC were added to the peptide solution. Ethanol or DMF were used as solvents. For the experiment using PyBrOP as coupling reagent, 1, 2.5 or 10 equivalents of PyBrOP and HOBt were added into the peptide solution, which was then cooled to 0°C using an ice bath. Three equivalents of DIPEA were added to the cooled solution and mixed on ice bath for 1 minute. Modified silica surfaces with SAMs of APTES or APTES with PEG chains were put into 5 ml of one of the above solutions in a glass Petri dish. The dish was gently shaken overnight (16 hours) at room temperature, followed by rinsing the surface 5 times with 5 ml of DMF, and put into a glass vial with 20 ml of DMF, and sonicated for 5 min. The materials were then rinsed again with 5 ml of DMF 3 times and dried with nitrogen flow.

The Fmoc groups at N-terminal ends were de-protected by incubation in 50% piperidine in DMF for one hour. After that the samples were rinsed with 5 ml of DMF 5 times, sonicated in 5 ml of DMF for 5 minutes, rinsed again with 5 ml of DMF 3 times and dried with nitrogen flow.

The side chain protection groups were deprotected by incubating in 5 ml of a mixture containing TFA, anisole, purified water, and TIPS in the volume ratio of 88:5:5:2 for 2 hours. After that, the surfaces were washed with 5 ml of DCM, DMF, methanol, DI water and 10% ethanol. This wash sequence was repeated 2 more times in this order. The sensors were then placed into 5 ml of 10% acetic acid for 5 minutes to remove CO₂ adduct from Trp. Finally, the sensors were rinsed with water and dried with nitrogen gas.

4.2.4 Film-Thickness Measurements by Ellipsometry

The thicknesses of the films on the silica surfaces were determined with a Rudolph/Auto EL Ellipsometer equipped with a He-Ne Laser ($\lambda=632.8$ nm) with fixed incidence angle of 70.0° (New Jersey, USA), using the refractive indices of Si, SiO₂ and APTES as 3.838-0.018i, 1.462, and 1.424 respectively (32). For the PEG layer and peptide layer, it was assumed that their refractive indexes were similar to that of APTES. The data presented is the average of at least 5 points with error less than $\pm 2 \text{ \AA}$.

The grafting density (σ , chain nm⁻²) can be estimated from the thickness measurement using the expression,

$$\sigma = \frac{N_A d \rho_0 \times 10^{-22}}{M_w} \quad 4-1$$

where N_A is Avogadro's number; d (\AA) is the film thickness measurement, M_w (g mole^{-1}) is the molecular weight of the chain, and ρ_0 (g cm^{-3}) is the density. It is assumed that ρ_0 is 0.946 g cm^{-3} of the APTES layer, 1.08 g cm^{-3} for PEG films and 1 g cm^{-3} for peptide layer (values provided by the respective suppliers).

4.2.5 Time of Flight Secondary Ion Mass Spectroscopy (ToF-SIMS)

ToF-SIMS analysis of the samples was performed using an ION-TOF SIMS 5 instrument (ION-TOF GmbH, Münster, Germany). Operational parameters used were the same as those described in Chapter 3.

The spectrum of the peptide HWRGWV (powder) was used as positive control. The pure peptide powder sample was attached on a clean silica wafer with a stick tape made with polydimethylsiloxane. The peptide in powder form was evenly spread on the tape and pressured tightly, and then the loose powder was blown away using nitrogen gas before

loading on the sample holder. After each step of surface modification, one sample was collected. There were six samples in total for each silica wafer analyzed (unless stated otherwise): pure peptide (HWRGWV, positive control), bare silica surface (SiO_2), silica surface with APTES (APTES), APTES with immobilized Fmoc-mini-PEG-3TM on silica surface before deprotection (APTES-PEG₃-NH-Fmoc), APTES with immobilized Fmoc-mini-PEG-3TM on silica surface after deprotection (APTES-PEG₃-NH₂) and peptide immobilized on top of APTES-PEG-NH₂ (APTES-PEG₃-NH-HWRGWV-Fmoc). Both positive and negative ions spectra were acquired for each sample. The ToF-SIMS spectra were collected right after the preparation of the samples. The mass scales of the positive and negative ion ToF-SIMS spectra were calibrated to the CH_3^+ , C_2H_3^+ , C_2H_5^+ and CH^- , C_2H_2^- , CN^- peaks respectively, before further analysis.

4.2.6 Quartz Crystal Microbalance (QCM) Experiments and Data Analysis

A commercial QCM-D apparatus (model E4, Q-Sense AB, Göthenburg, Sweden) was used to measure the changes in the resonance frequency (ΔF) and in the energy dissipation (ΔD) due to the protein adsorption process. The adsorption of hIgG or BSA on modified silica surfaces from PBS buffer or complex complete minimum essential medium (cMEM) containing 10% fetal calf serum was recorded until the adsorption reached equilibrium (change of frequencies was less than 1 Hz for 30 min). The protein concentrations used were within the range of 0.005 ~ 5 mg ml⁻¹. All the experiments were performed at least in duplicate. The operation of the QCM is the same as that described in Chapter 3. In short, stable baselines were obtained with the flow of PBS buffer, and then protein solutions were introduced to the QCM chamber to replace buffer solutions. The adsorption process was

monitored until equilibrium was reached (the changes of frequency were less than 1 Hz for 30 minutes). The frequencies at equilibrium were used to plot the isotherm to obtain thermodynamic parameters. The recorded frequency changes as a function of time were used to do the kinetics analysis described below in section 4.2.6.2. The ΔF data were converted to the amount of adsorbed protein by using the Sauerbrey equation (33),

$$\Delta F_n = \frac{1}{nC} \frac{\Delta m}{A} \quad 4-2$$

where $\Delta m/A$ is the mass adsorbed per surface area, ΔF_n is the frequency change of overtone n and the mass sensitivity constant, C , is equal to $17.7 \text{ ng cm}^{-1} \text{ Hz}^{-1}$ (value from instrument provider).

Along with the change of resonance frequency, ΔF_n the change of dissipation, ΔD_n was recorded as a function of time. Then, ΔD_n was analyzed by plotting the dissipation (ΔD_n) against the resonance frequency ($\Delta F_n/n$), which eliminated time as an explicit parameter. The slope of the plot of ΔD vs. $\Delta F_n/n$, labelled with the term K , is a measure of the energy dissipation per unit mass added to the surface during the adsorption process. A more rigid and compact mass is expected to yield a small K value and *vice versa* (34). For studies related to adsorbed proteins, generally, significant changes in K value might be due to conformation changes in the protein (15, 35-38).

4.2.6.1 Protein Adsorption Isotherm Curve and Langmuir Model Fitting

The isotherms were obtained by plotting the measured adsorbed protein per area of surface at equilibrium obtained by QCM against the protein concentration at equilibrium with

the surface. The isotherm curves were fitted to the Langmuir equation by nonlinear least-squares regression,

$$Q = \frac{Q_{\max} \times C_b}{K_d + C_b} \quad 4-3$$

where Q ($mg\ m^{-2}$) is the adsorbed protein at equilibrium with a protein solution with a concentration of C_b (M), K_d (M) is the dissociation constant and Q_{\max} ($mg\ m^{-2}$) is the maximum adsorption capacity. By fitting the QCM isotherm curves into this equation the values of K_d and Q_{\max} can be obtained.

4.2.6.2 Kinetics Analysis

The convective mass transport step and the intrinsic adsorption step occurring at the fluid-solid interface in the QCM can be described by the following two ordinary differential equations,

$$\frac{dq}{dt} = k_m (C_b - C_s) \quad 4-4$$

$$\frac{dq}{dt} = k_a C_s (Q_{\max} - q) - k_d q \quad 4-5$$

Here q ($mg\ m^{-2}$) is the surface concentration of the adsorbed protein at time t (s); Q_{\max} is the maximum adsorption amount obtained from the isotherm study, k_a ($m^3\ mol^{-1}\ s^{-1}$) and k_d (s^{-1}) are respectively the adsorption and desorption rate constants. C_b (M) is the protein concentration in bulk solution and C_s ($mol\ m^{-2}$) is the concentration in the fluid adjacent to the sensor surface. The transfer coefficient k_m was estimated from the mass transfer Sherwood number, Sh ($k_m d_H / D$), according to the following correlation (39),

$$Sh = 1.07(Re \cdot Sc \cdot d / d_H)^{1/3} \quad 4-6$$

In this expression, Re ($\rho v d_H / \mu$) is the Reynolds number, and Sc ($\mu / \rho D$) is the Schmidt number. This equation is valid for the mass transfer in a mini-channel (hydraulic diameter in the range of 0.2~3 mm) at low Reynolds numbers ($Re < 250$) (39). For the QCM E4 system, d , the inside diameter, is 14 mm and d_H , the hydraulic diameter of the chamber is 0.44 mm. Under the conditions in this study, the viscosity μ and the density ρ were about 1 mPa·s and 1 kg l⁻¹ respectively; the average velocity was about 4.6×10^{-4} m s⁻¹, and the Reynolds number has a value of 0.2. Equation 4-6 is valid for this research. The diffusion constant of IgG, D is 3.7×10^{-11} m² s⁻¹ (40). The estimated transfer coefficient k_m from Sherwood number was 1.1×10^{-7} m s⁻¹.

A MATLAB (The MathWorks, Inc., Natick, MA) code was written to solve these two coupled ordinary differential equations for the quantities q and C_s using the built-in function *ode23s* in MATLAB. The nonlinear least squares regression function *lsqcurvefit* was used to fit the dynamic response data of the QCM to estimate the association rate, k_a . The dissociation rate k_d value was calculated by the relationship of $K_d = k_d / k_a$, while the dissociation constant, K_d was obtained from the isotherm fit described in section 4.2.6.1. The dynamic experiments were done under a continuous feed of solvent at a fixed feed bulk concentration C_b . As a result, the bulk IgG concentration in the chamber was considered to be constant.

4.2.6.3 Effect of Spacer Arm on the Affinity Interaction

Spacer arms are widely used in affinity chromatography to reduce steric hindrance. In this study peptide can be directly immobilized on top of APTES or at the end of spacer arm, PEG chain. For the peptide with two additional alanines at C terminal end, these two alanines also

worked as spacer arm. The QCM equilibrium measurement of ΔF and ΔD for IgG adsorption on different surfaces, including APTES, APTES-PEG₃-NH₂, APTES-HWRGWV, APTES-AA-HWRGWV and APTES-PEG₃-NH-HWRGWV, were compared to investigate the role of spacer arm in the affinity interaction of hIgG with immobilized short peptide ligand.

4.3 Results and Discussion

4.3.1 Grafting of Peptide on Modified Silica Surface

In order to covalently immobilize the peptide ligand on the surfaces, the silica substrate had to be modified to introduce amine groups for immobilization of the peptide ligand and short PEG spacer arms to enhance the accessibility of peptide ligand to protein binding and also reduce nonspecific binding to the substrate. The estimated density from thickness measurement of PEG chains and the amine groups is about 2.74 chains nm⁻². The details of the modification and characterization of the silica surface have been discussed in Chapter 3.

The peptide Fmoc-HWRGWV-OH was immobilized on the modified silica surface by a coupling reaction between the carboxyl groups of the peptide and the amine groups on the surface. The efficiency of the peptide immobilization relies on both the activity and amount of the amine group on the surface and the carboxyl group at the peptide end in solution. In addition, the presence of side protection groups on the amino acid residues and the presence of different amino acids on the C terminal can have an effect on the coupling efficiency. In Chapter 3 all the efforts on improving amine group density on silica surface were discussed and the optimized surface modification condition was used in this study. Here the effect of peptide concentration, coupling reagent, and variations of peptide structure were investigated.

4.3.1.1 Effect of Peptide Concentration, Coupling Reagent Types and Concentration

For a peptide coupling reaction, typically, the carboxylic acid moiety needs to be activated by a suitable peptide coupling reagent to ensure high yield (41). Besides yield, the other important issue of coupling reaction is racemization (41-42), which can occur at the C-terminal amino acid residue in the course of a coupling reaction due to the ionization of the α -hydrogen and the formation of an oxazolone intermediate. An appropriate racemization-suppressing agent needs to be added to suppress the undesired racemization and other side reactions, and thus minimize the loss of the optical integrity at the chiral center (41-42). In this study, the catalytic capability of four kinds of coupling reagents: DIC, EDC, TBTU and PyBrOP were compared. Carbodiimides, as the lowest cost coupling reagents with high activity, have been widely used both in industry and research laboratories (43). The shortcomings of using carbodiimides are the tendency to racemization and low yields due to the formation of the poorly active N-acylurea (43). For this kind of coupling reagents, adding additives such as hydroxybenzotriazole (HOBt) or Cl-HOBt can reduce racemization of the protected amino acid and avoid the formation of other less reactive derivatives (43). The other two kinds of commonly used coupling reagents are phosphonium and aminium salts. The structures of two kinds of coupling reagents both incorporate an equivalent of HOBt. With the presence of a tertiary base such as N,N-diisopropylethylamine (DIEA), they can form the corresponding active species oxybenzotriazole (OBt) esters. Adding an extra equivalent of HOBt can accelerate the coupling process (41).

Hydroxybenzotriazole (HOBt) was used as additive for all conditions to reduce racemization and to further raise the reaction conversion. The thicknesses before and after

peptide immobilization were measured by ellipsometry and this thickness difference was used to estimate the peptide density using Eq. 4-1. In this part of the work, the peptide with only a single protecting group for the amine group at the N-terminal (Fmoc-HWRGWV-OH) was used.

As shown in Table 4.1, among these four kinds of coupling reagents, DIC had the worst performance, as the thickness of the peptide layer obtained after the immobilization step was less than 5 Å, for all peptide concentrations and peptide/coupling reagent ratios tested. Due to the poor performance, DIC was excluded from further studies. EDC combined with NHS as coupling reagent and ethanol as a solvent was proven to be an efficient method to immobilize high-density short poly(ethylene glycol) spacer arms on top of an APTES monolayer on silica surface (more details in Chapter 3). It was also chosen for peptide immobilization. The solubility of peptide in ethanol is low (less than 5 mg ml⁻¹), so DMF was used instead in this study. As shown in Table 4.1, with EDC and NHS as coupling reagent, the immobilization density increased with increases of peptide and coupling reagent concentration. When TBTU or PyBrOP were used as the coupling reagents, peptide density was also correlated positively with peptide and coupling reagent concentrations, but the dependence on peptide concentration was much weaker than that using EDC and NHS as coupling reagent. The highest surface density, 0.88 chain nm⁻², was obtained with TBTU as a coupling reagent. To conclude, TBTU was found to be the best for this reaction. With TBTU, relatively high peptide density could be achieved at relatively low peptide concentration (1 mg ml⁻¹) and coupling reagent concentrations (same molar concentration as peptide). These conditions were used for all the following experiments. Considering the price difference between the

peptide and coupling reagents, a low peptide concentration (1 mg ml^{-1}) and a high coupling reagent concentrations (10 times molar concentration of peptide) were used. Under these conditions the peptide density obtained was about $0.8 \text{ chain nm}^{-2}$, which is very close to the density using high peptide concentration ($0.88 \text{ chain nm}^{-2}$).

4.3.1.2 Effect of Peptide Structure

Besides coupling reagents, the structure of the peptide itself could significantly affect the activity of the carboxyl group at C terminal. Protecting groups on the residue can result in steric hindrance effects that reduce coupling efficiency to the surface and changes in amino acid structure at the C terminal can alter the reactivity of the carboxyl group to the surface. It was found that the density of immobilized Fmoc-valine-OH ($1.35 \text{ chain nm}^{-2}$ on APTES and $1.54 \text{ chain nm}^{-2}$ on APTES-PEG₃-NH₂) is only about half of that of Fmoc-alanine-OH ($2.46 \text{ chain nm}^{-2}$ on APTES and $2.95 \text{ chain nm}^{-2}$ on APTES-PEG₃-NH₂). As a result, it was decided to do one fully-protected sample with two additional alanines at the C-terminal [His(Trt)-Trp(Boc)-Arg(Pbf)-Gly-Trp(Boc)-Val-Ala-Ala-OH], that act as a spacer to enhance the immobilization density of peptide. Three kinds of peptides were compared: peptide without side-chain protecting-groups Fmoc-His-Trp-Arg-Gly-Trp-Val-OH; and two versions of side-chain protected peptides, without and with the carboxy-terminal alanine residues Fmoc-His(Trt)-Trp(Boc)-Arg(Pbf)-Gly-Trp(Boc)-Val-OH, and Fmoc-His(Trt)-Trp(Boc)-Arg(Pbf)-Gly-Trp(Boc)-Val-Ala-Ala-OH.

Protection of the side chains is a commonly used strategy in peptide synthesis to avoid undesirable side reactions (44). For instance, as a strongly nucleophilic group, the tri-functional guanidine side chain group of Arg in HWRGWV could react with the α -carboxyl

group at the C-terminal in the same peptide molecule to form a ring structure or self-polymerize by the same reaction with the α -carboxyl group at C-terminal on other peptide molecules (45). These side reactions could affect the ability of the α -carboxyl group at C-terminal to react with amine groups on the surface for immobilization in our work. In this study, the surface density of the immobilized peptides with and without side chain protection was compared. As shown in Table 4.2, the resulting surface density decreased slightly with the protection of side chains for the immobilization on APTES-PEG₃-NH₂, while it was almost doubled by the protection of side chain for the immobilization on the surface of APTES layer. It is apparent that protecting side chains enhance the activity of the carboxyl group on the peptide by reducing the probability of undesirable side reactions. However, the side chain protection groups also made the peptide molecule more hydrophobic. The fully protected peptide is less compatible with a hydrophilic surface as the APTES-PEG₃-NH₂ (contact angle of distilled water ~ 25 degrees), which is lower than that of APTES surface (contact angle of distilled water ~ 53 degrees). As a result of these two effects, the peptide density using side protecting groups increased only on the more hydrophobic APTES surface.

As mentioned above, the activity of the carboxyl group at the C-end of the peptide could be enhanced if hindrance can be reduced by the addition of two alanines at the C-terminal end of the peptide. As shown in Table 4.3, the surface density of the peptide with two alanines at the C terminal immobilized on APTES surface is 1.22 chain nm⁻², which is much higher than that without two alanines. On the other hand, there is almost no difference in surface density for the immobilization on APTES-PEG₃-NH₂ between the peptide with and without two alanines at the C terminal. This could be explained by the fact that the amine

group at the end of APTES has less flexibility than that at the end of PEG chains. Consequently, reducing the steric hindrance by adding alanines had a more obvious effect on the immobilization on APTES surface than that on APTES-PEG₃-NH₂.

In summary, the effects of protecting the side chains on the peptide and adding two alanines at the C-terminal on peptide immobilization density depended on the presence of a spacer arm on the surface, which changed both the exposure of the amine groups and also the hydrophilicity of the surface. The immobilization density of Fmoc-His-Trp-Arg-Gly-Trp-Val-OH on the surface without spacer arms was only about half of that on the surface with spacer arms. But the immobilization density on the surface with spacer arms cannot be further enhanced by both side chain protection and adding two alanine as those for surface without spacer arm. In the experiments to analyze IgG-peptide interactions, only Fmoc-His-Trp-Arg-Gly-Trp-Val-OH was used for the immobilization on the surface of APTES-PEG₃-NH₂ and the peptide density was 0.80 chain nm⁻² which is half of the best peptide density for resin, 1.6 chain nm⁻² (5).

4.3.2 Characterization of the Modified Surfaces with ToF-SIMS

ToF-SIMS is proven to be highly efficient in the determination of elemental and molecular composition characterization of various kinds of solid surfaces, including peptides synthesized on solid supports (46-49). ToF-SIMS can provide high mass range, high mass resolution and high surface sensitivity spectra with low surface damage (50). Here, ToF-SIMS was chosen to confirm the success of each step in surface modification instead of fast atom bombardment (FAB) or matrix assisted laser desorption ionization (MALDI) mass spectrometry because it does not need any prior solubilization process. The samples in our

work have very small surface area, and cleaving, collecting and solubilizing the immobilized peptide can be very challenging.

Both positive and negative ion mass spectra were collected for the samples after each modification step. In total, six samples were analyzed: SiO₂, APTES, APTES-PEG₃-NH-Fmoc, APTES-PEG₃-NH₂ and APTES-PEG₃-NH-HWRGWV-Fmoc, and HWRGWV as a positive control. The main peaks from peptide were identified in the both positive and negative ion mass spectra of the positive control, and were then compared to the intensity of these peaks in the spectra of the five intermediate and final samples. These characteristic surface peaks should only appear with significant intensity in the spectra of APTES-PEG₃-NH-HWRGWV-Fmoc.

In the positive spectrum of the positive HWRGWV control, shown in Figure 4.1 (1-3f), a series of characteristic peaks from the amino acid side chains or the amino acids backbone of the peptide were identified (51-52), including m/z 43, 59, 73, 100, 112 for Arg, m/z 81, 82, 110 for His, m/z 130, 159, 170 for Trp, m/z 41 for Gly and m/z 43, 100 for Val. This spectrum also shows the characteristic peaks associated with the N-terminal Fmoc protecting group (m/z 165, 178, 179, 180) (48-49). There are several relatively strong peaks observed that correspond to fragments of the peptide: Gly-Trp ($\text{CH}_3\text{-CO-NH}^+=\text{CH-CH}_2\text{-C}_8\text{H}_6\text{N}$, m/z 202), His-Trp ($\text{C}_3\text{H}_4\text{N-C}_2\text{H}_4\text{-CO-NH}^+=\text{CH-CH}_2\text{-C}_8\text{H}_6\text{N}$, m/z 281). The peaks from other relatively large fragments such as His-Trp-Arg ($\text{C}_3\text{H}_4\text{N-C}_2\text{H}_4\text{-CO-NH=C(CH}_2\text{-C}_8\text{H}_6\text{N)-CO-NH}_2\text{-(C}_2\text{H}_2\text{)}_4\text{-CH}_5\text{N}_3^+$ (m/z 494) and whole peptide (m/z 1002, 1061), were also found in the spectrum of the positive control, but the signal-to-noise ratio for these peaks was relatively weak (the result was not shown here). All these peptide peaks identified in the

positive spectra were used as reference peaks in the analysis of the spectra of samples collected after each step of silica surface modification and peptide immobilization.

The spectrum of APTES-PEG₃-NH-HWRGWV-Fmoc was compared with the other four spectra of reference samples, as shown in Figure 4.1 (1-3a, 1-3b, 1-3c and 1-3d, collected before peptide immobilization). Generally, the overall peak patterns and intensities of APTES-PEG₃-NH-HWRGWV-Fmoc are significantly different from the spectra without peptide. The intensity of Si⁺ at m/z 28 had diminished; all the peaks from the single amino acids present in the ligand (Arg, His, Trp, Gly, Val) and the peaks of fragment Gly-Trp and His-Trp, His-Trp-Arg were only found in the spectrum of APTES-PEG₃-NH-HWRGWV but not in those of other four samples. The peaks from the Fmoc group appeared only in the spectra of APTES-PEG₃-NH-Fmoc and APTES-PEG₃-NH-HWRGWV-Fmoc. However, the peaks from large fragments and whole peptide were not found in the spectra of APTES-PEG₃-NH-HWRGWV-Fmoc. The peptide immobilized on solid surface tends to be broken into smaller pieces by primary ion pulse of ToF-SIMS (more detail of ionization of sample by ToF-SIMS included in Appendix 3-1), comparing with the free peptide in state of powder.

Generally, the negative ion spectra were far less intense than the corresponding positive ion spectra, and they are not shown here. The peak of CN⁻ (m/z 26) is one of the characteristic peaks for molecules with amine groups (53-56) and it was observed in the spectra of all samples except SiO₂. Consistent with our expectation, the peak of OCN⁻ (m/z 42) from the peptide backbone was observed with significant intensity in the spectra of HWRGWV and APTES-PEG₃-NH-HWRGWV-Fmoc but was much weaker in the spectra of other samples. One important peak in the negative spectra is from Fmoc groups (m/z 165)

(48). This peak was observed only in the spectra of APTES-PEG₃-NH-Fmoc, APTES-PEG₃-NH-HWRGWV-Fmoc (the amine group at N-terminal was protected by Fmoc group before deprotection step) and peptide powder. In summary, ToF-SIMS spectra provided direct evidence peptide was successfully immobilized on silica surface.

4.3.3 Study of the Affinity Interaction between Peptide Ligand and hIgG by QCM

Hexamer peptide HWRGWV on solid chromatography resin surface was proven to be able to specifically bind to hIgG (3). In this study, this peptide was immobilized on modified flat silica surface as described above. It was first necessary to determine whether or not the affinity to hIgG was maintained after immobilization on a surface that is quite different from a chromatography resin with a peptide density of 0.80 chains nm⁻². To do so, the role of the presence immobilized peptide on the isotherm curve of hIgG adsorption from PBS buffer was investigated. In addition, the adsorption behavior of hIgG was compared to that of another protein, bovine serum albumin (BSA) to check whether or not the immobilized peptide adsorption to hIgG is specific. BSA was chosen since it should only have nonspecific interactions with HWRGWV. As a highly hydrophobic protein, and since albumin is the contaminant in highest concentration in plasma and in some cell culture media, it makes a good model for comparison. The Langmuir equation was fit to the isotherm curves obtained (as shown in Figure 4.2) as described in section 4.2.6.1. The dissociation constants (K_d) and maximum binding capabilities (Q_m) obtained from Langmuir fits were summarized in Table 4.3.

The results in Figure 4.2 show that the amount of hIgG adsorbed on the surface with peptide is significantly higher than that on the surface without peptide for each hIgG

concentration within the range of 0.005 to 5 mg ml⁻¹. The maximum binding capacity for IgG binding is significantly higher in the presence of peptide as opposed to surfaces without HWRGWV (as shown in Table 4.3). The dissociation constant of hIgG adsorption on surface with peptide is two orders of magnitudes smaller than that of hIgG adsorption on surface without peptide. These results indicate that the adsorption of hIgG on the surface with peptide is dominated by the affinity interaction between peptide ligand and hIgG instead of the nonspecific binding to the substrate.

In comparison to IgG adsorption behavior, the adsorption of BSA shows weaker dependence on the presence of peptide. Instead of increasing, the absolute adsorption amount decreased by a factor of 2 in the presence of peptide on the surface (as shown in Figure 4.2). The dissociation constant for adsorption of BSA on the surface with and without peptide are very similar. It is also evident that BSA was retained on the surface with HWRGWV ligands predominantly by electrostatic interactions since the majority of BSA was eluted with 1M salt (as shown in Figure 4.3), while the hIgG adsorbed on this surface remained adsorbed almost after washing with high salt concentration buffer.

In order to further confirm the specificity of immobilized peptide to hIgG adsorption, the isotherm of hIgG adsorption from cMEM that had been spiked with hIgG was obtained and compared with the isotherm observed from PBS buffer. The total amounts of hIgG adsorbed from cMEM-containing hIgG at different concentrations were measured by QCM. In order to remove nonspecifically bound albumin, the most common protein contaminant in cMEM, the hIgG sample injection was followed by an injection of PBS buffer with 1M NaCl. As shown in Figure 4.4, about half amount of adsorption from cMEM could be removed from the

surface with 1M NaCl, while most of adsorption from cMEM with IgG couldn't wash away. The cMEM with 10% fetal bovine serum solution contains about 2 mg ml⁻¹ BSA (57). As shown in Figure 4.4, before the wash step with high salt concentration buffer, the change of frequencies by adsorption is about 12 Hz (corresponding to 2.1 mg m⁻² protein on surface), which is close to the adsorption amount from 2mg ml⁻¹ BSA solution in PBS buffer. The difference was that most of the adsorption of BSA from PBS from buffer could be removed from the surface by a buffer containing 1N NaCl, while for the cMEM experiment only half the amount was removable under the same conditions. After the wash step, the adsorption amount from cMEM was about 1 mg m⁻² which was about 9% of the maximum capacity (11 mg m⁻²) of hIgG adsorption from cMEM. In order to minimize the effects of cMEM, the adsorption amounts after wash step were used to plot the isotherm. As shown in Figure 4.5, with an increase of hIgG concentration in cMEM, the adsorption amount increased significantly, which is in the same trend as that from buffer solution, except that the absolute adsorption amount at each hIgG concentration from cMEM is lower than that from buffer. This difference may be caused by the competition between hIgG and the albumin in cMEM during the binding step. The K_d of the adsorption from cMEM is 0.46 μ M, which is very close to that obtained from buffer solution, 0.43 μ M. To conclude, the affinity of the protein adsorption is does not seem to be significantly affected by the complex media.

In order to compare the affinity interaction occurring on the flat silica surface with that on resin surfaces the amounts of protein adsorbed to each material need to be quantified. The Sauerbrey relationship is widely used to quantify adsorption amounts from QCM responses, but it should be used with caution. The Sauerbrey equation is only valid for uniform,

ultrathin, rigid films with material properties indistinguishable from those of the crystal resonator QCM (15, 58-60).

It has been reported that QCM tends to overestimate the adsorbed amount of proteins for several reasons. First, the frequency changes recorded by QCM include are the result of adsorption of proteins and also water bound on protein molecules or entrapped inside the adsorbed layers (35-37). Second, the Sauerbrey relationship, excludes the contribution of the viscoelasticity of adsorbed layer on frequencies changes, and can skew the estimated adsorption amounts (20, 35, 38, 61-67). Although the estimation of the adsorption amount from QCM by the Sauerbrey equation may not be a perfect method for quantification analysis, it is a straightforward way to obtain an approximate estimate of kinetic and thermodynamic parameters. The maximum binding capacity obtained in the present study was 14 mg m^{-2} , with the knowledge that QCM tends to overestimate the adsorption amount. Based on the known hydrodynamic dimensions of hIgG ($235 \times 44 \times 44 \text{ \AA}$), closely packed “end on” and “side-on” monolayers of unperturbed hIgG molecules would give surface concentrations of 13 and 2.4 mg m^{-2} , respectively (1). Since it is unlikely that all of the hIgG molecules on the surface are in an “end on” configuration, it is worthwhile exploring potential correction factors that could be applied to the maximum binding capacity measured in this study.

In Zhou’s work (38) on hIgG adsorption on a hydrophobilized gold surface, the overestimation of mass adsorption by QCM was quantified by comparison to adsorption measurements using surface plasmon resonance (SPR) and love mode surface acoustic wave (SAW) techniques. SPR measures only the amount of adsorbed protein (“dry mass”), while

QCM and SAW, acoustic wave devices, measure the combined mass uptake coming from both adsorbed protein and entrapped water (“wet mass”). In addition, SAW signal is not as sensitive to viscoelastic effects as that of QCM (68). Zhou’s work suggests that the “wet mass” is overestimated by QCM by 1.2 to 1.6 times if the Sauerbrey relationship is used to calculate the amount of protein adsorbed. It was also claimed that the overestimation was mainly from viscoelastic effects and that water content contributed less than 10% of the weight adsorbed (38). However in other references, it has been pointed out that the effect of neglecting the viscoelastic effects by using the Sauerbrey equation led to an underestimation of the amount adsorbed in comparison with that attained from fitting into the more complicated Voigt-Kelvin model (35, 37, 69). Furthermore, for thin protein layers such as those formed by IgG adsorption on hydrophilic TiO₂ surfaces, this difference was found to be in the range of 10% (37, 69). The other contribution verified consistently by all references is that of water molecules embedded inside or associated on top of adsorbed protein layers (35-38, 70-76). In Vörös’ study (37) on IgG adsorption on a TiO₂ surface, the “wet mass” measured by QCM is about 3 times of the “dry mass” measured by optical waveguide light mode spectroscopy (OWLS). Since the frequency and dissipation changes observed in our system (as shown in Figure 4.8) caused by hIgG adsorption at equilibrium at high protein concentration (1~5 mg ml⁻¹) are very close to those reported by Vörös (ΔF : 56 ~ 68 Hz (reconstructed from the adsorption amount data: 10 - 12 mg m⁻²), ΔD : 2 ~ 2.5 x10⁻⁶) (37), it is reasonable to assume that the QCM-derived mass in our system is also about 3 times of that of “dry mass” at equilibrium at high concentrations. If this assumption is correct, then the maximum binding capacity of hIgG in our system should be adjusted to 4.6 mg m⁻²,

which is a capacity comparable to that determined for a chromatographic resin with same peptide density, 4.3 mg m^{-2} obtained under same adsorption conditions (5). This suggests that a monolayer of hIgG with different conformations was formed on the surface when in equilibrium at saturation concentrations.

The value of K_d of hIgG adsorption on silica surface functionalized by peptide ligand obtained from QCM experiments is in the order of 10^{-7} M , which is one order of magnitude smaller than that value for the same ligand immobilized onto polymethacrylate-based chromatography resins (in the order of 10^{-6} M) (5). The effect of overestimation of QCM on the measurement of K_d is not straightforward. It depends on the relationship between the ratio of QCM-derived mass to “dry mass” and the amount of protein adsorption at various concentrations. There is no clear way of making such corrections, other than to make measurements on a different device (SPR for example) in which the amount of water adsorption does not affect the resulting signals.

4.3.4 Kinetics Analysis of QCM Data

The kinetic parameters, namely the adsorption rate constant k_a and the desorption rate constant k_d , were estimated by using nonlinear least squares regression fitting of the dynamic measurements of protein adsorption as a function of time, described in section 4.2.6.2. The raw adsorption rate data and fitted curves at various protein concentrations are shown in Figure 4.6 and the k_a and k_d values are summarized in Table 4.4.

The values of the rate constants depend on the measurements of K_d and Q_{max} (the original Q_{max} value) as well as the estimate of the mass transfer coefficient ($1.1 \times 10^{-7} \text{ m s}^{-1}$) described in section 4.2.6.2. Because of the uncertainty in these parameters, it is not a surprise that this

model did not seem to represent the raw data perfectly (as shown in Figure 4.6). It is clear from the results in Table 4.4 that the values of k_a are dependent on protein concentration. Intrinsic rate constants should be independent on protein concentration, and this point to a potential problem with estimated values of the dissociation constant and the binding capacity. As shown in Figure 4.6, the calculated protein concentration near the sensor surface (C_s) was noticeably lower than that in bulk solution, C_b . The difference was more obvious at low protein concentrations and at the initial stage of adsorption. These results indicate that the transport of the protein from bulk to surface limited the adsorption rate and it was necessary to include the mass transport equation into the kinetic model. As shown in Table 4.5, neglect of the existence of transport limitation (transfer coefficient k_m approaching infinity) led to an underestimation of the intrinsic association and dissociation rate constants by about 1 time for all experiments. In addition, in order to test the sensitivity of the estimated kinetics parameters on the value of the mass transfer coefficient k_m , another correlation found in literature were used to estimate the Sherwood number (77)

$$Sh = 1.58(\text{Re} \cdot Sc \cdot d / d_H)^{1/3} \quad 4-7$$

This empirical equation was derived from the experiments for laminar flow in narrow channels (gaps 0.2~0.5 mm), which also has similar geometry as the QCM chamber (gap: 0.26 mm) in this study. In addition, as mentioned in section 4.2.6.2, under the experimental condition in this study, the Reynolds number of the flow in QCM chamber was in the laminar regime. The k_m calculated with this equation has a value of $1.6 \times 10^{-7} \text{ m s}^{-1}$. As shown in Table 4.5, there was almost no change in the estimation of association rates if transfer coefficient increased from 1.1×10^{-7} to $1.6 \times 10^{-7} \text{ m s}^{-1}$.

The estimation of association rates is not sensitivity to the value of transfer coefficient in this study.

4.3.5 The Effects of PEG Spacer Arm on the Affinity Interaction between Peptide Ligand and IgG

Spacer arms are widely used in affinity chromatography or membranes for bioseparations to enhance the accessibility of ligands. These spacer arms can significantly affect the protein-ligand interactions, especially for small ligands, and this effect could be even more critical when the active site of the target molecule is located in a pocket (2, 78). A good spacer arm should have just enough length to facilitate the formation of ligand and target biomolecule complex. If no spacer or too short a spacer arm is used, it might be hard to form the complex of ligand and target molecule due to steric hindrance; if it is too long, the density of ligand could be low and nonspecific binding to the spacer arm could become predominant over the affinity interaction (2). In the work of Heldt et al., it was found that extension of the ligand using a PEG spacer of 4 repeat units enhanced the binding of porcine parvovirus (PPV) to peptide ligand WRW on a resin (31). In this study, the silica surface was functionalized first with an amine group associated with APTES and then a spacer arm consisting of a short PEG chain with 3 repeat units was attached. The peptide can be immobilized directly on top of the APTES or through the spacer arm. In 4.3.2 the impact of spacer on peptide immobilization density were discussed. In this section we describe the effect of spacer arm on binding. The modified silica surfaces with or without peptide ligand and spacer arm were challenged with 1mg ml^{-1} protein solutions and the adsorption processes were compared.

As shown in Figure 4.7, the IgG equilibrium adsorption amount on APTES-HWRGWV surface is about 4 times of that on the APTES surface alone. In addition, the adsorption amount of hIgG on APTES-HWRGWV is about 10-fold of that of BSA at similar protein concentration. All in all, the affinity of peptide ligand immobilized on APTES for hIgG adsorption was very similar to that immobilized on APTES-PEG₃-NH₂. The spacer arm does not seem to be critical to maintain the affinity of the peptide ligand immobilized on silica surface. As mentioned before, the value of spacer arm is more obvious when the binding site is hard to reach. It may hint that the binding site resides on the IgG molecule surface or at least not in deep pocket. This deduction conformed to the study of binding sites by the mass spectrometry and docking simulation done in our group (79). Compared to the adsorption process on the surface with spacer arm (APTES-PEG₃-NH-HWRGWV), the adsorption process on surface without peptide is faster (as shown in Figure 4.7). It is apparent that the spacer arm provides additional degrees of freedom and conformation and that this can reduce the rate of adsorption while at the same time not having a strong influence on the binding capacity.

This is a phenomenon that is not often considered when spacer arms are being used in affinity applications. It was also found that the IgG adsorption rate increased by adding two alanines between the peptide and APTES (APTES-AA-HWRGWV, as shown in Figure 4.7). These two alanines as a short spacer arm reduce potential steric hindrance, while the length of two alanines is much less than that of PEG₃ and hence there was less chance that the HWRGWV could interact with the substrate. Consequently the association between peptide and hIgG was higher than that on top of APTES.

4.3.6 Dissipation Analysis

The analysis of energy dissipation provides additional information about the influence of spacer arm in the affinity interaction between immobilized peptide and target protein. The measurement of ΔD relates the viscoelastic property of adsorbed layer. Generally, compact and rigid adsorbed layers lead to relatively smaller changes in dissipation comparing with that from loosely packing adsorbents (34, 80-81). A convenient way of presenting the data of dissipation is to display the quantity K which equates to the derivate of dissipation change respective to absolute value of frequency change (the slope of ΔD versus $-\Delta F$ curve). The K value is a measure of the energy dissipation per unit mass added to the surface (34). As shown in Figure 4.8, the dissipation of $\Delta D5$ versus $-\Delta F5/5$ was plotted characterizing the viscoelastic nature of the hIgG layers adsorbed at the solid/liquid interface. Here $\Delta D5$ is the change of dissipation and $\Delta F5/5$ is the change of frequency normalized by number of overtone, which were recorded simultaneously by QCM at overtone 5th.

For the case of protein adsorption directly on surface of APTES it is clear that the slope of the dissipation-frequency change curves increased from 9×10^{-8} to $3 \times 10^{-8} \text{ Hz}^{-1}$ at a $-\Delta F5/5$ of 19 Hz. This evident switch is associated with a relatively large conformation change (15, 35-38). As shown in Figure 4.9, this phenomenon was only observed when IgG concentration was high (1 and 5 mg/ml). With increase of IgG surface density, the adsorbed IgG could change from “side-on” to “end-on” conformation to allow more protein to adsorb on surface (28). IgG adsorbed on surface with “end-on” conformation has less association with the surface than that bound on surface with “side-on” conformation, and consequently leads to relatively large dissipation change.

For the adsorption on the other four surfaces (APTES-PEG₃-NH₂, APTES-HWRGWV, APTES-AA-HWRGWV and APTES-PEG₃-NH-HWRGWV) the plots of ΔD vs. ΔF are almost straight lines with small deviation. These results indicated that no significant conformation change happened on these surfaces. For the adsorption on APTES-PEG₃-NH-HWRGWV, the slope slightly decreased with frequency in the full range of data. This may be the result of lost of water molecules associated with protein or PEG layers with increasing packing density. The data of APTES-HWRGWV and APTES-AA-HWRGWV had the same trend; at low frequencies, the slope decreases slightly with increasing frequency, which is same result observed on the surface of APTES-PEG₃-NH-HWRGWV. At higher frequencies (45~50 Hz) the slope switched to higher value, but the changes of slopes is less significant compared with that on the APTES surface. When the adsorbed protein on surface became crowded, for part of protein, the conformation may change for “side-on” to “end-on”. The frequency at which the conformation change happened for the IgG adsorption on the surface with peptide (45~50 Hz) was much higher than that of IgG adsorption on APTES surface (19~22 Hz). This discrepancy could be caused by the difference in water amount in adsorbed protein layer. The protein adsorbed on surface with peptide ligand could have more water molecules embedded inside, since amide bond or peptide side chain tends to bound solvent by H-binding. For the same protein surface density, the change of frequencies recorded by QCM could be different.

4.4 Conclusions

HWRGWV was successfully immobilized on a silica surface with a surface density about 0.8 chain nm⁻²; in other words, the average distance between two peptide chains was about 1

nm. It was high enough to ensure that every hIgG molecule (235×44×44Å) adsorbed on the surface could interact with more than one peptide at the interface. The silica surface functionalized by peptide was characterized by ToF-SIMS. The presence of peaks from Fmoc groups and peptide itself provided direct evidence that the peptide was immobilized on the surface at the proper orientation through the carboxyl terminus.

High affinity and specificity of HWRGWV to hIgG binding was maintained after immobilization on the solid surface as evidenced by the adsorption isotherms of hIgG from both buffer and cMEM, compared to that of BSA adsorption. Both the equilibrium thermodynamic and kinetics parameters were obtained by analysis of QCM data. The PEG spacer arm is not necessary to keep the affinity to hIgG binding.

References:

1. Leffell MS, Donnenberg AD, & Rose NR (1997) *Handbook of human immunology* (CRC Press, New York, NY) p 73.
2. Hage DS (2006) *Handbook of affinity chromatography* (CRC Press, Boca Raton, FL) pp 557, 539.
3. Yang H, Gurgel PV, & Carbonell RG (2005) Hexamer peptide affinity resins that bind the Fc region of human immunoglobulin G. *Journal of Peptide Research* 66:120-137.
4. Yang HO, Gurgel PV, & Carbonell RG (2009) Purification of human immunoglobulin G via Fc-specific small peptide ligand affinity chromatography. *Journal of Chromatography A* 1216(6):910-918.
5. Yang H, Gurgel PV, & Carbonell RG (2009) Purification of human immunoglobulin G via Fc-specific small peptide ligand affinity chromatography. *Journal of Chromatography A* 1216.

6. Gurgel PV, Carbonell RG, & Swaisgood HE (2001) Studies of the binding of alpha-lactalbumin to immobilized peptide ligands. *Journal of Agricultural and Food Chemistry* 49(12):5765-5770.
7. Kaufman DB & Carbonell RG (1999) Interaction of fibrinogen with peptide affinity supports - Resin effects. *Abstracts of Papers of The American Chemical Society* 217:U160-U160.
8. Huang PY & Carbonell RG (1995) Affinity purification of proteins using ligands derived from peptide libraries. *Biotechnology and Bioengineering* 47(3):288-297.
9. Wang GQ & Carbonell RG (2005) Characterization of a peptide affinity support that binds selectively to staphylococcal enterotoxin B. *Journal of Chromatography A* 1078(1-2):98-112.
10. Bastek PD & Carbonell RG (1999) Investigation of the binding mechanism between a peptide affinity resin and alpha-1 proteinase inhibitor. *Abstracts of Papers of The American Chemical Society* 217:U189-U189.
11. Kaufman DB, Hayes T, Buettner J, Hammond DJ, & Carbonell RG (2000) Chromatographic resolution of tryptophan enantiomers with L-Leu-L-Leu-L-Leu peptide - Effects of mobile phase composition and chromatographic support. *Journal of Chromatography A* 874(1):21-26.
12. Kaufman DB, *et al.* (2002) Affinity purification of fibrinogen using a ligand from a peptide library. *Biotechnology and Bioengineering* 77(3):278-289.
13. Wang G & Carbonell RG (2006) Design of adsorptive columns for specific pathogen removal: application to staphylococcal enterotoxin B. *Biotechnology Progress* 22:1358-1367.
14. O'Sullivan CK & Guilbault GG (1999) Commercial quartz crystal microbalances - theory and applications. *Biosensors & Bioelectronics* 14(8-9):663-670.
15. Rodahl M, Hook F, Krozer A, Brzezinski P, & Kasemo B (1995) Quartz-crystal microbalance setup for frequency and Q-factor measurements In gaseous and liquid environments. *Review of Scientific Instruments* 66(7):3924-3930.

16. Hong SR, Choi SJ, Do Jeong H, & Hong S (2009) Development of QCM biosensor to detect a marine derived pathogenic bacteria *Edwardsiella tarda* using a novel immobilisation method. *Biosensors & Bioelectronics* 24(6):1635-1640.
17. Carrigan SD, Scott G, & Tabrizian M (2005) Real-time QCM-D immunoassay through oriented antibody immobilization using cross-linked hydrogel biointerfaces. *Langmuir* 21(13):5966-5973.
18. Gerdon AE, Wright DW, & Cliffl DE (2005) Quartz crystal microbalance detection of glutathione-protected nanoclusters using antibody recognition. *Analytical Chemistry* 77(1):304-310.
19. Medina MB (2005) A biosensor method for a competitive immunoassay detection of *staphylococcal enterotoxin B* (SEB) in milk. *Journal of Rapid Methods and Automation in Microbiology* 13(1):37-55.
20. Reimhult E, Larsson C, Kasemo B, & Hook F (2004) Simultaneous surface plasmon resonance and quartz crystal microbalance with dissipation monitoring measurements of biomolecular adsorption events involving structural transformations and variations in coupled water. *Analytical Chemistry* 76(24):7211-7220.
21. Damos FS, Mendes RK, & Kubota LT (2004) Applications of QCM, EIS and SPR in the investigation of surfaces and interfaces for the development of (BIO)sensors. *Quimica Nova* 27(6):970-979.
22. Patel PD (2002) (Bio)sensors for measurement of analytes implicated in food safety: a review. *Trac-Trends in Analytical Chemistry* 21(2):96-115.
23. Lu B (1995) Oriented immobilization of Fab' fragment on silica surfaces. *Analytical Chemistry* 67(1):83-97.
24. Kwon Y, Han ZZ, Karatan E, Mrksich M, & Kay BK (2004) Antibody arrays prepared by cutinase-mediated immobilization on self-assembled monolayers. *Analytical Chemistry* 76(19):5713-5720.
25. Bae YM, Oh BK, Lee W, Lee WH, & Choi JW (2005) Study on orientation of immunoglobulin G on protein G layer. *Biosensors & Bioelectronics* 21(1):103-110.

26. Starodub NF, Pirogova LV, Demchenko A, & Nabok AV (2005) Antibody immobilisation on the metal and silicon surfaces. The use of self-assembled layers and specific receptors. *Bioelectrochemistry* 66(1-2):111-115.
27. Lu B, Xie JM, Lu CL, Wu CG, & Wei Y (1995) Oriented immobilization of Fab' fragments on silica surfaces. *Analytical Chemistry* 67(1):83-87.
28. Buijs J, Lichtenbelt JWT, Norde W, & Lyklema J (1995) Adsorption of monoclonal IgGs and their F(ab')(2) fragments on polymeric surfaces. *Colloids and Surfaces B-Biointerfaces* 5(1-2):11-23.
29. Caruso F, Rodda E, & Furlong DN (1996) Orientational aspects of antibody immobilization and immunological activity on quartz crystal microbalance electrodes. *Journal of Colloid and Interface Science* 178(1):104-115.
30. Huang PY, *et al.* (1996) Affinity purification of von Willebrand factor using ligands derived from peptide libraries. *Bioorganic & Medicinal Chemistry* 4(5):699-708.
31. Heldt CL, Gurgel PV, Jaykus LA, & Carbonell RG (2009) Influence of Peptide Ligand Surface Density and Ethylene Oxide Spacer Arm on the Capture of Porcine Parvovirus. *Biotechnology Progress* 25(5):1411-1418.
32. Petri DFS, Wenz G, Schunk P, & Schimmel T (1999) An improved method for the assembly of amino-terminated monolayers on SiO₂ and the vapor deposition of gold layers. *Langmuir* 15(13):4520-4523.
33. Sauerbrey G (1959) Verwendung von schwingquarzen zur wagung dunner schichten und zur mikrowagung. *Zeitschrift Fur Physik* 155(2):206-222.
34. Rodahl M, *et al.* (1997) Simultaneous frequency and dissipation factor QCM measurements of biomolecular adsorption and cell adhesion. *Faraday Discussions*:229-246.
35. Hook F, *et al.* (2001) Variations in coupled water, viscoelastic properties, and film thickness of a Mefp-1 protein film during adsorption and cross-linking: A quartz crystal microbalance with dissipation monitoring, ellipsometry, and surface plasmon resonance study. *Analytical Chemistry* 73(24):5796-5804.

36. Su XD & Zhang H (2004) Comparison of surface plasmon resonance spectroscopy and quartz crystal microbalance for human IgE quantification. *Sensors and Actuators B-Chemical* 100(3):309-314.
37. Voros J (2004) The density and refractive index of adsorbing protein layers. *Biophysical Journal* 87(1):553-561.
38. Zhou C, *et al.* (2004) Human immunoglobulin adsorption investigated by means of quartz crystal microbalance dissipation, atomic force microscopy, surface acoustic wave, and surface plasmon resonance techniques. *Langmuir* 20(14):5870-5878.
39. Wilk J (2009) Experimental investigation of convective mass/heat transfer in short minichannel at low Reynolds numbers. *Experimental Thermal and Fluid Science* 33(2):267-272.
40. Torstein J, Jens F, & Einar R (1998) Photon correlation spectroscopy of human IgG. *Journal of Protein Chemistry* 7(2):165-171.
41. Albericio F & Carpino LA (1997) Coupling reagents and activation. *Solid-Phase Peptide Synthesis, Methods in Enzymology*, Vol 289, pp 104-126.
42. Han SY & Kim YA (2004) Recent development of peptide coupling reagents in organic synthesis. *Tetrahedron* 60(11):2447-2467.
43. Marder O & Albericio F (2003) Industrial application of coupling reagents in peptides. *Chimica Oggi-Chemistry Today* 21(6):35-40.
44. Pennington MW & Dunn BM (1994) *Peptide synthesis protocols* (Humana Press Inc., Totowa, New Jersey) pp 3--33.
45. Bechinger B, *et al.* (1999) Peptide structural analysis by solid-state NMR spectroscopy. *Biopolymers* 51(3):174-190.
46. Maux D, Enjalbal C, Martinez J, & Aubagnac JL (2001) Static secondary ion mass spectrometry to monitor solid-phase peptide synthesis. *Journal of the American Society for Mass Spectrometry* 12(10):1099-1105.

47. Drouot C, *et al.* (1996) Step-by-step control by time-of-flight secondary ion mass spectrometry of a peptide synthesis carried out on polymer beads. *Rapid Communications in Mass Spectrometry* 10(12):1509-1511.
48. Enjalbal C, Martinez J, Subra G, Combarieu R, & Aubagnac JL (1998) Time-of-flight secondary ion mass spectrometry of Fmoc amino acids linked to solid supports through ionic interactions. *Rapid Communications in Mass Spectrometry* 12(22):1715-1720.
49. Drouot C, *et al.* (1997) ToF-SIMS analysis of polymer bound fmoc-protected peptides. *Tetrahedron Letters* 38(14):2455-2458.
50. Belu AM, Graham DJ, & Castner DG (2003) Time-of-flight secondary ion mass spectrometry: techniques and applications for the characterization of biomaterial surfaces. *Biomaterials* 24(21):3635-3653.
51. Mantus DS, Ratner BD, Carlson BA, & Moulder JF (1993) Static secondary ion mass spectrometry of adsorbed proteins. *Analytical Chemistry* 65(10):1431-1438.
52. Wagner MS, Tyler BJ, & Castner DG (2002) Interpretation of static time-of-flight secondary ion mass spectra of adsorbed protein films by multivariate pattern recognition. *Analytical Chemistry* 74(8):1824-1835.
53. Vanooij WJ & Sabata A (1991) Characterization of films of organofunctional silanes by ToF-SIMS And XPS .1. films of N-[2-(vinylbenzylamino)-ethyl]-3-aminopropyltri-methoxysilane on zinc and gamma-aminopropyltriethoxysilane on steel substrates. *Journal of Adhesion Science and Technology* 5(10):843-863.
54. Graf N, *et al.* (2008) Optimization of cleaning and aminosilanzation protocols for Si wafer to be used as platforms for biochip microarrays by surface analysis (XPS, ToF-SIMS and NEXAFS spectroscopy). *Surface And Interface Analysis* 40:180-183.
55. Poulin S, Durrieu MC, Polizu S, & Yahia LH (2006) Bioactive molecules for biomimetic materials: Identification of RGD peptide sequences by TOF-S-SIMS analysis. *Applied Surface Science* 252(19):6738-6741.

56. Makohliso SA, *et al.* (1999) Surface characterization of a biochip prototype for cell-based biosensor applications. *Langmuir* 15(8):2940-2946.
57. Giles S & Czuprynski C (2003) Novel role for albumin in innate immunity: serum albumin inhibits the growth of blastomyces dermatitidis yeast form in vitro *Infection and Immunity* 71(11):6648–6652. .
58. Kanazawa KK & Gordon JG (1985) The Oscillation frequency of a quartz resonator in contact with a liquid *Analytica Chimica Acta* 175:99-105.
59. Johannsmann D, Mathauer K, Wegner G, & Knoll W (1992) Viscoelastic properties of thin films probed with quartz crystal resonator. *Physical Review B* 46(12):7808-7815.
60. Kosslinger C, *et al.* (1992) A quartz crystal biosensor for measurement in liquids. *Biosensors & Bioelectronics* 7(6):397-404.
61. Marx KA (2003) Quartz crystal microbalance: A useful tool for studying thin polymer films and complex biomolecular systems at the solution-surface interface. *Biomacromolecules* 4(5):1099-1120.
62. Patel AR & Frank CW (2006) Quantitative analysis of tethered vesicle assemblies by quartz crystal microbalance with dissipation monitoring: Binding dynamics and bound water content. *Langmuir* 22(18):7587-7599.
63. Limson J, Odunuga OO, Green H, Hook F, & Blatch GL (2004) The use of a quartz crystal microbalance with dissipation for the measurement of protein-protein interactions: a qualitative and quantitative analysis of the interactions between molecular chaperones. *South African Journal of Science* 100(11-12):678-682.
64. Niikura K, Nagata K, & Okahata Y (1996) Quantitative detection of protein binding onto DNA by using a quartz-crystal microbalance. *Chemistry Letters* (10):863-864.
65. Vikinge TP, *et al.* (2000) Comparison of surface plasmon resonance and quartz crystal microbalance in the study of whole blood and plasma coagulation. *Biosensors & Bioelectronics* 15(11-12):605-613.

66. Hook F, Rodahl M, Brzezinski P, & Kasemo B (1998) Measurements using the quartz crystal microbalance technique of ferritin monolayers on methyl-thiolated gold: Dependence of energy dissipation and saturation coverage on salt concentration. *Journal of Colloid and Interface Science* 208(1):63-67.
67. Stadler H, Mondon M, & Ziegler C (2003) Protein adsorption on surfaces: dynamic contact-angle (DCA) and quartz-crystal microbalance (QCM) measurements. *Analytical and Bioanalytical Chemistry* 375(1):53-61.
68. Friedt JM, Francis L, Choi KH, Frederix F, & Campitelli A (2003) Combined atomic force microscope and acoustic wave devices: application to electrodeposition. *J. Vac. Sci. Technol. A* 21(4):1500-1505.
69. Hook F, *et al.* (2002) A comparative study of protein adsorption on titanium oxide surfaces using in situ ellipsometry, optical waveguide lightmode spectroscopy, and quartz crystal microbalance/dissipation. *Colloids and Surfaces B-Biointerfaces* 24(2):155-170.
70. Spangler BD, Wilkinson EA, Murphy JT, & Tyler BJ (2001) Comparison of the Spreeta (R) surface plasmon resonance sensor and a quartz crystal microbalance for detection of Escherichia coli heat-labile enterotoxin. *Analytica Chimica Acta* 444(1):149-161.
71. Bailey LE, Kambhampati D, Kanazawa KK, Knoll W, & Frank CW (2002) Using surface plasmon resonance and the quartz crystal microbalance to monitor in situ the interfacial behavior of thin organic films. *Langmuir* 18(2):479-489.
72. Su XD, Wu YJ, & Knoll W (2005) Comparison of surface plasmon resonance spectroscopy and quartz crystal microbalance techniques for studying DNA assembly and hybridization. *Biosensors & Bioelectronics* 21(5):719-726.
73. Tamerler C, Oren EE, Duman M, Venkatasubramanian E, & Sarikaya M (2006) Adsorption kinetics of an engineered gold binding peptide by surface plasmon resonance spectroscopy and a quartz crystal microbalance. *Langmuir* 22(18):7712-7718.

74. Teichroeb JH, Forrest JA, Jones LW, Chan J, & Dalton K (2008) Quartz crystal microbalance study of protein adsorption kinetics on poly(2-hydroxyethyl methacrylate). *Journal of Colloid and Interface Science* 325(1):157-164.
75. Fang JJ, Wang P, Du XB, & Zhu DM (2009) Detailed analysis of quartz crystal microbalance and surface plasmon resonance spectroscopy in probing molecular adsorption onto solid-liquid interfaces. *Journal of Physical Chemistry C* 113(36):16121-16127.
76. Messina GML, Satriano C, & Marletta G (2009) A multitechnique study of preferential protein adsorption on hydrophobic and hydrophilic plasma-modified polymer surfaces. *Colloids and Surfaces B-Biointerfaces* 70(1):76-83.
77. Acosta RE, Muller RH, & Tobias CW (1985) Transport process in narrow (capillary) channels. *AIChE Journal* 31(3):473-482.
78. Gunter Z & Sherma J (1973) *CRC handbook of chromatography: general data and principles* (CRC Press, Inc., Boca Raton, Florida) p 89.
79. Yang H, *et al.* (2010) Binding site on human immunoglobulin G for the affinity ligand HWRGWV. *Journal of Molecular Recognition* 23:271-282.
80. Hook F, Rodahl M, Kasemo B, & Brzezinski P (1998) Structural changes in hemoglobin during adsorption to solid surfaces: Effects of pH, ionic strength, and ligand binding. *Proceedings of the National Academy of Sciences of the United States of America* 95(21):12271-12276.
81. Rodahl M, Hook F, & Kasemo B (1996) QCM operation in liquids: An explanation of measured variations in frequency and Q factor with liquid conductivity. *Analytical Chemistry* 68(13):2219-2227.

Table 4.1 Effect of coupling reagent and peptide concentrations on peptide immobilization density

Coupling Reagent	Concentration of peptide, mg ml ⁻¹	Molar ratio of coupling reagent to peptide	Thickness of peptide layer, Å	Surface density, chain nm ⁻²
DIC+HOBt	1	1:10	3±0.5	0.16
	10	1:2.5	5±0.8	0.27
EDC+NHS+HOBt	1	1:1	6±1.1	0.33
		1:10	7±0.7	0.41
	10	1:1	11±1.2	0.62
		1:2.5	13±1.3	0.73
TBTU+HOBt	1	1:1	13±1.4	0.77
		1:10	14±1.0	0.81
	10	1:1	15±1.1	0.86
		1:2.5	15±0.9	0.88
PyBrOP+HOBt	1	1:1	11±1.2	0.63
		1:10	10±1.2	0.59
	10	1:1	12±1.1	0.72
		1:2.5	13±1.2	0.75

Table 4.2 Effect of side-chain protection on peptide density

Peptide	Immobilization peptide on APTES-PEG3-NH ₂		Immobilization peptide on APTES	
	Thickness, Å	Surface density, chain nm ⁻²	Thickness, Å	Surface density, chain nm ⁻²
Fmoc-His-Trp-Arg-Gly-Trp-Val-OH	14	0.81	7	0.38
Fmoc-His(Trt)-Trp(Boc)-Arg(Pbf)-Gly-Trp(Boc)-Val-OH	22	0.76	25	0.86
Fmoc-His(Trt)-Trp(Boc)-Arg(Pbf)-Gly-Trp(Boc)-Val-Ala-Ala-OH	20	0.71	38	1.22

Table 4.3 Apparent dissociation constant and maximum binding capacity of the BSA and hIgG adsorption on modified silica surface APTES-PEG₃-NH₂ and APTES-PEG₃-NH-HWRGWV-NH₂

Surface	Protein	K_d , μM	Q_m , mg m ⁻²	R^2
APTES-PEG ₃ -NH ₂	hIgG	14.1	4.6	0.87
	BSA	16.5	6.97	0.953
APTES-PEG ₃ -NH-HWRGWV-NH ₂	hIgG	0.43	14	0.986
	BSA	20.5	3.38	0.913

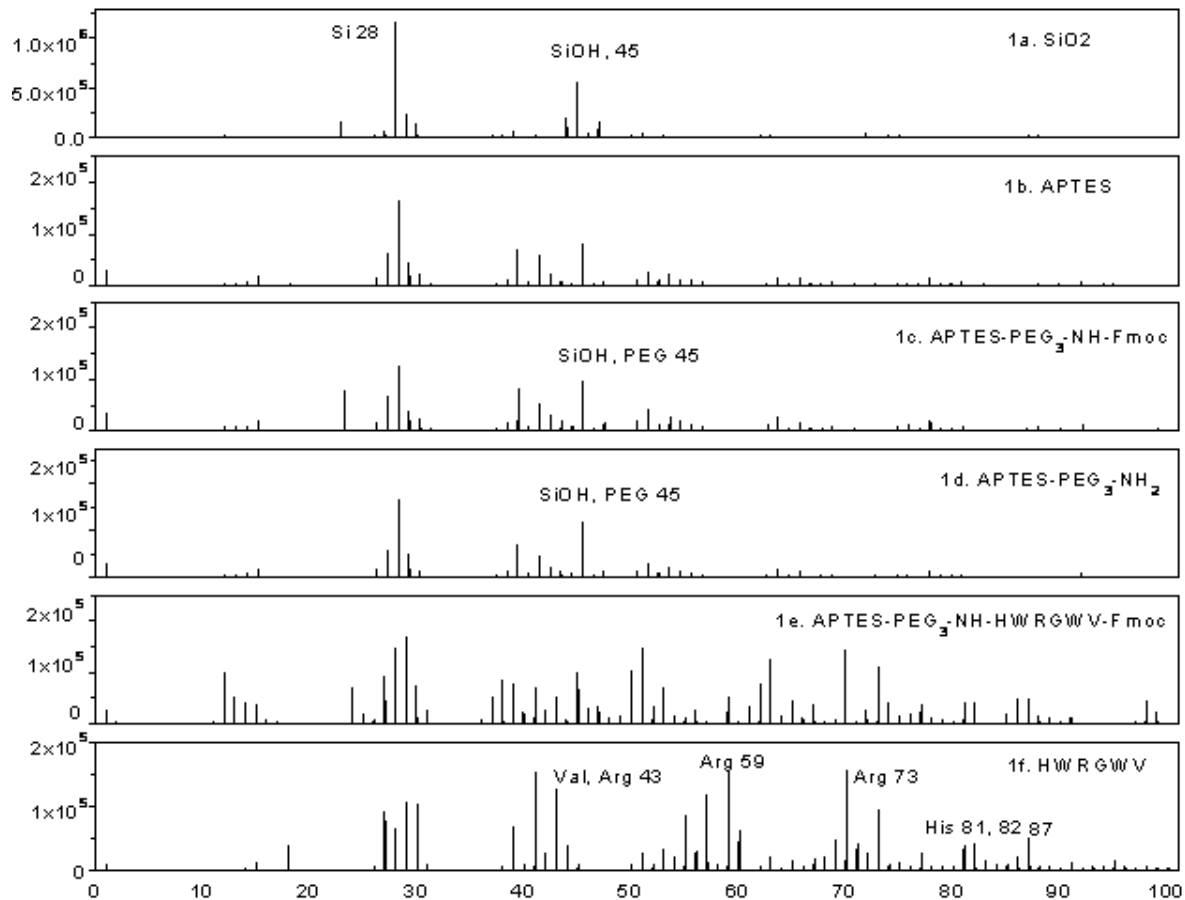
Table 4.4 Association rates and dissociation rates of hIgG adsorption on silica surface functionalized with peptide ligands

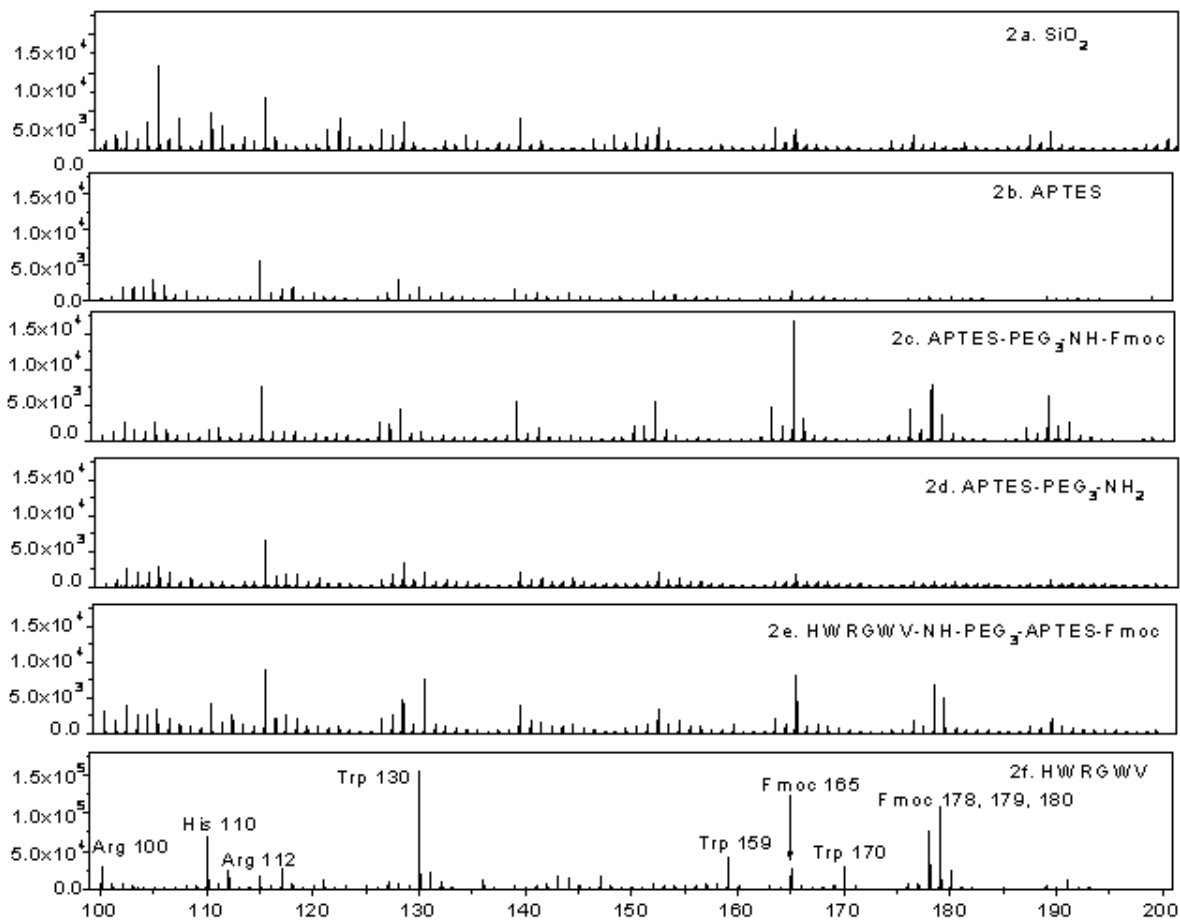
IgG Concentration (mg ml ⁻¹)	k_a (m ³ mol ⁻¹ s ⁻¹)	k_d (s ⁻¹) × 10 ³
0.04	0.70	3.01
0.10	0.36	1.55
0.20	0.31	1.33
1.00	0.16	0.69
5.00	0.11	0.47

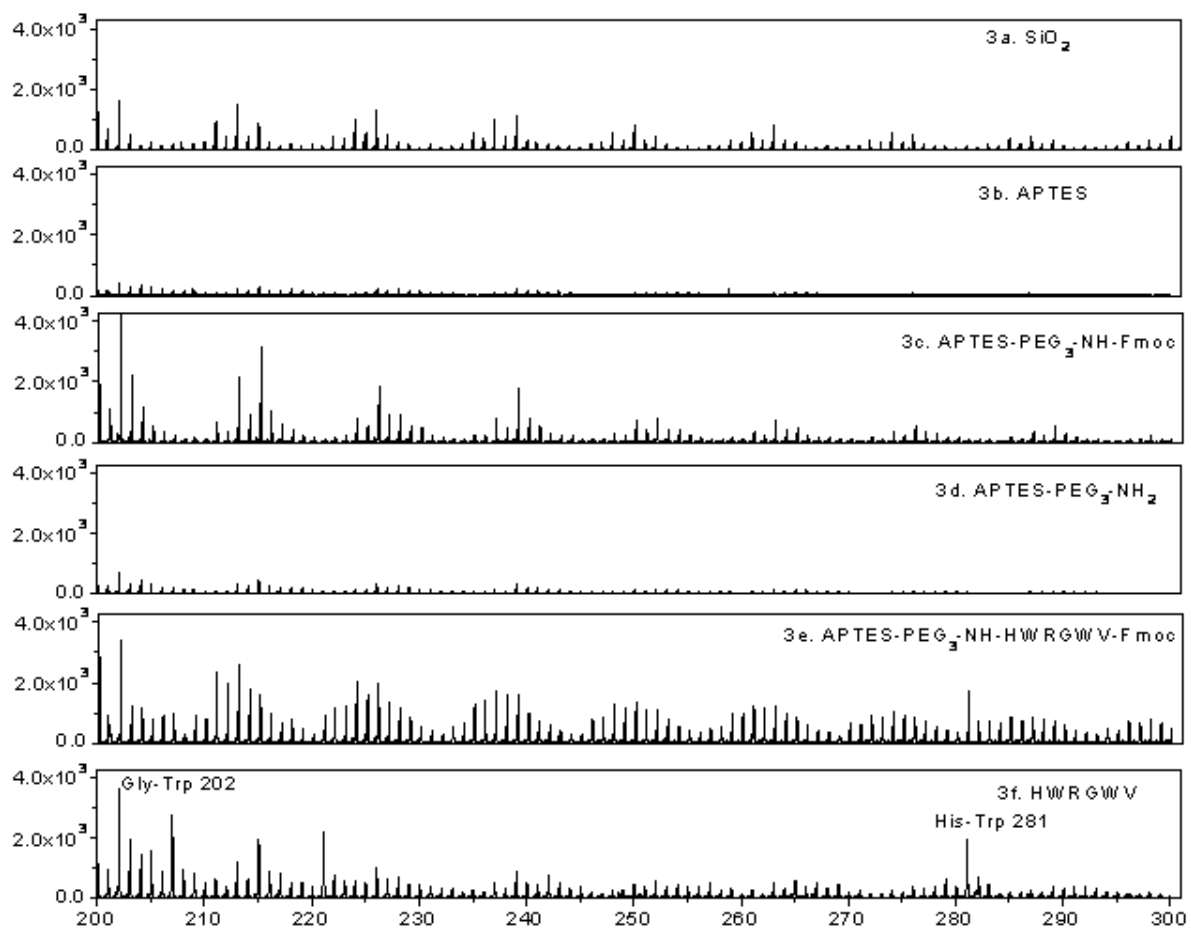
Table 4.5 Dependence of the estimated association rates on the transfer coefficient k_m value

IgG Concentration (mg ml ⁻¹)	k_a (m ³ mol ⁻¹ s ⁻¹)		
	$k_m = 1.1 \times 10^{-7}$ m s ⁻¹	$k_m = 1.6 \times 10^{-7}$ m s ⁻¹	$k_m \rightarrow \infty$
0.04	0.70	0.69	0.39
0.10	0.36	0.36	0.17
0.20	0.31	0.31	0.15
1.00	0.16	0.16	0.09
5.00	0.11	0.11	0.05

Figure 4.1 ToF-SIMS spectra of samples SiO₂ (a), APTES (b), APTES-PEG₃-NH-Fmoc(c) and APTES-PEG-NH₂(d) and pure peptide HWRGWV (e) within the range of m/z 0~100 (1a~1f), 100~200 (2a~2f), 200~300 (3a~3f)







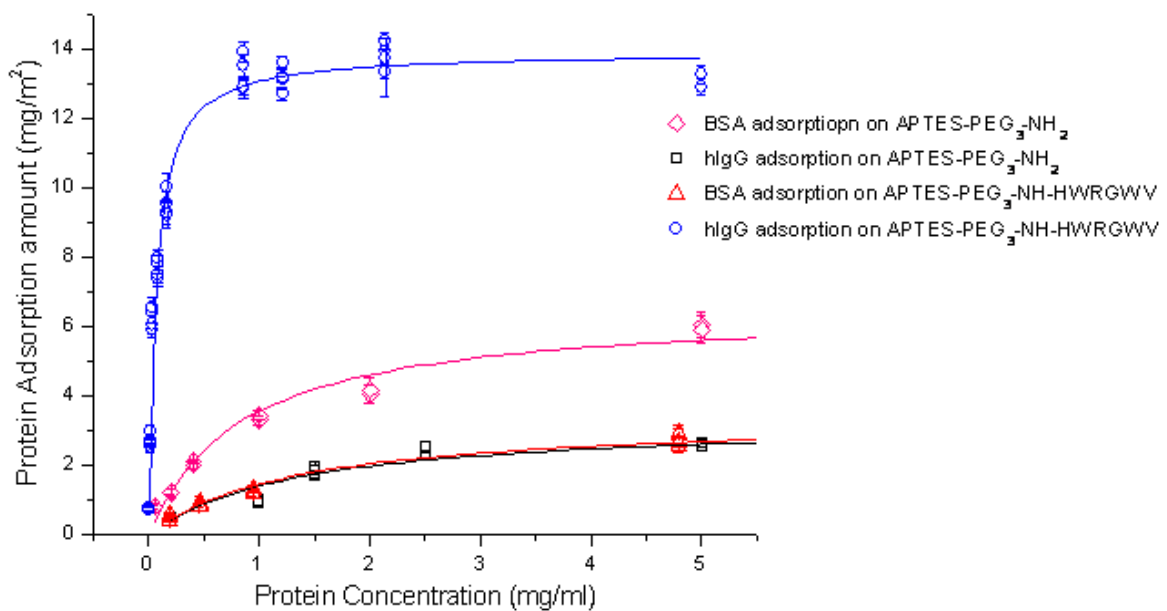


Figure 4.2 Isotherm of hIgG and BSA adsorption on modified surface with and without peptide; the fits correspond to Langmuir adsorption isotherms at the relevant protein concentrations

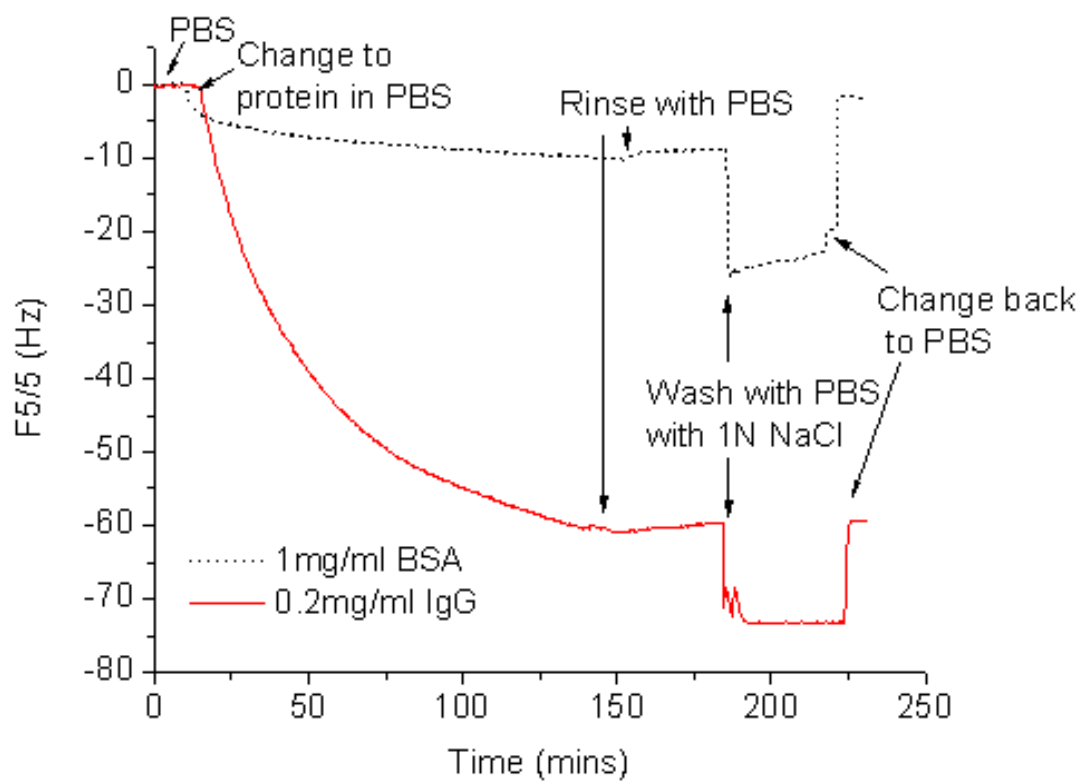


Figure 4.3 Wash the adsorbed hIgG and BSA adsorbed on modified silica surface functionalized with peptide ligands by PBS with 1M NaCl

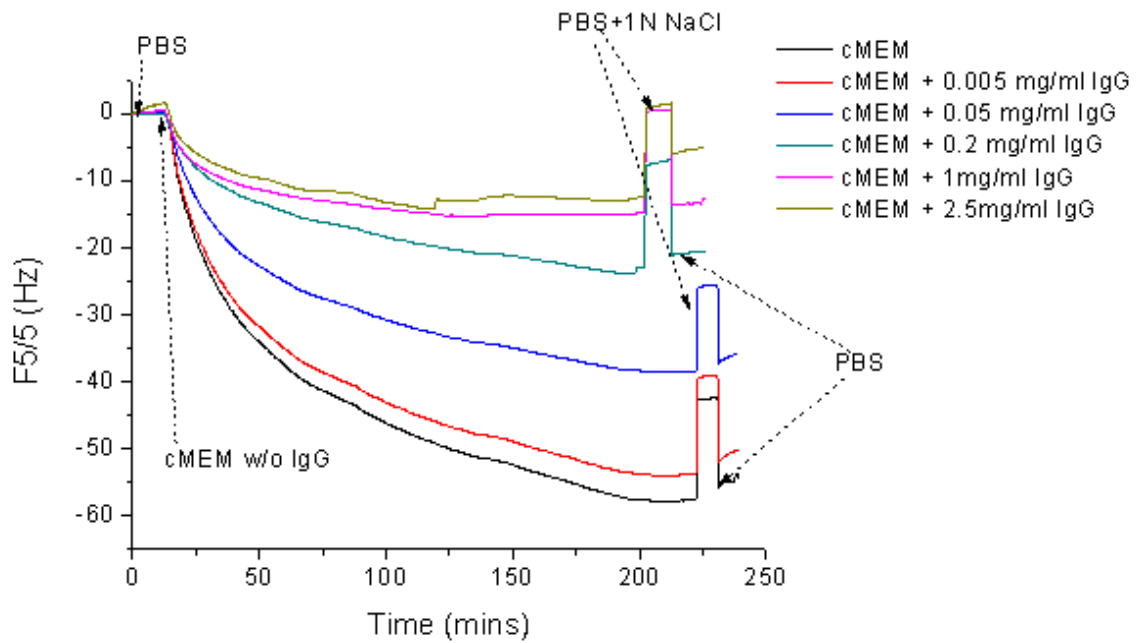


Figure 4.4 IgG adsorption from cMEM on silica surface functionalized with peptide ligands

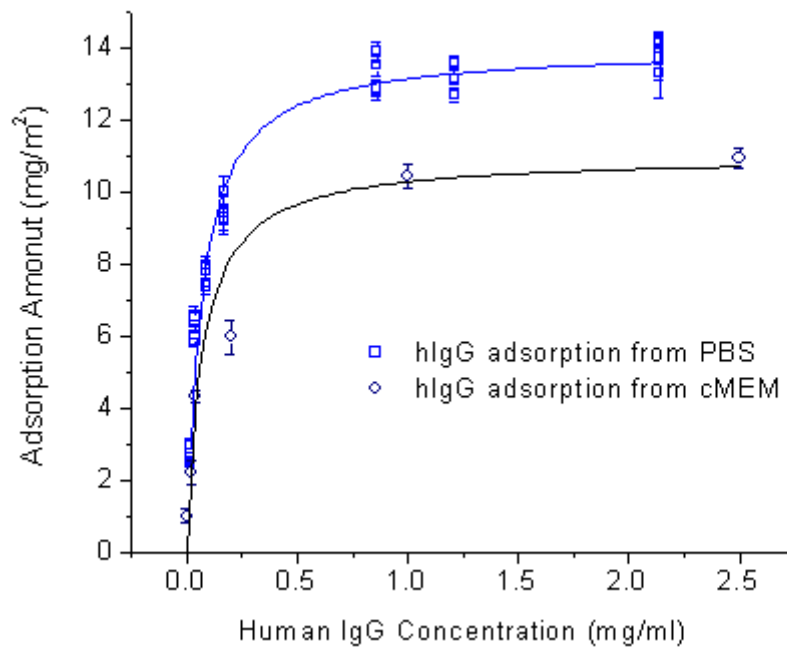


Figure 4.5 Isotherm of hIgG adsorption on modified silica surface functionalized with peptide ligands from PBS buffer and cMEM

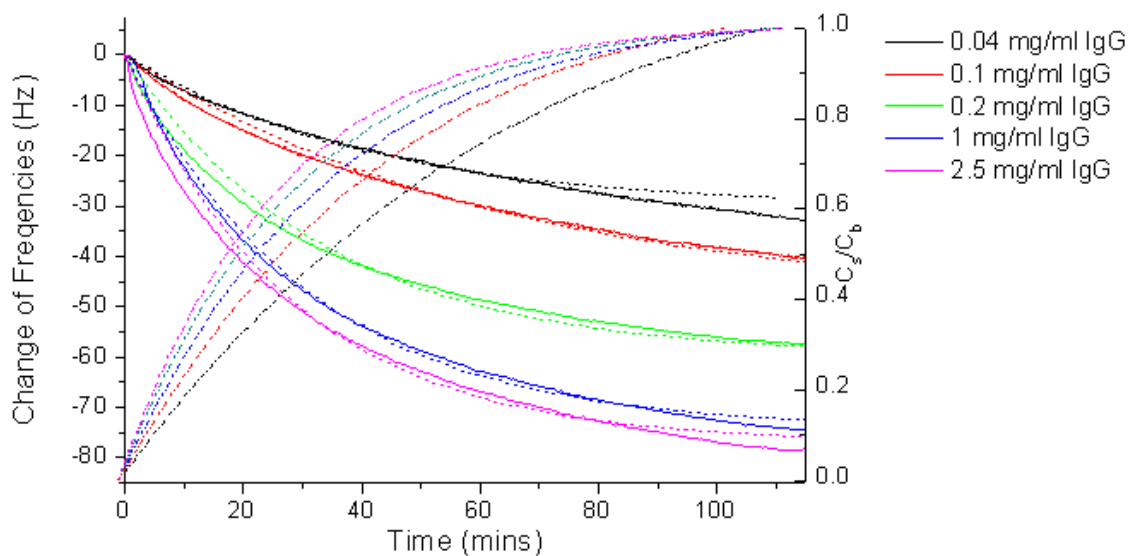


Figure 4.6 Kinetics fitting Langmuir isotherm adsorption model to raw data of hIgG adsorption on surface functionalized with peptide recorded by QCM. QCM experiment data (solid line), fitting result (dot line) and modeling of the normalized protein concentration close to sensor surface (C_s/C_b)

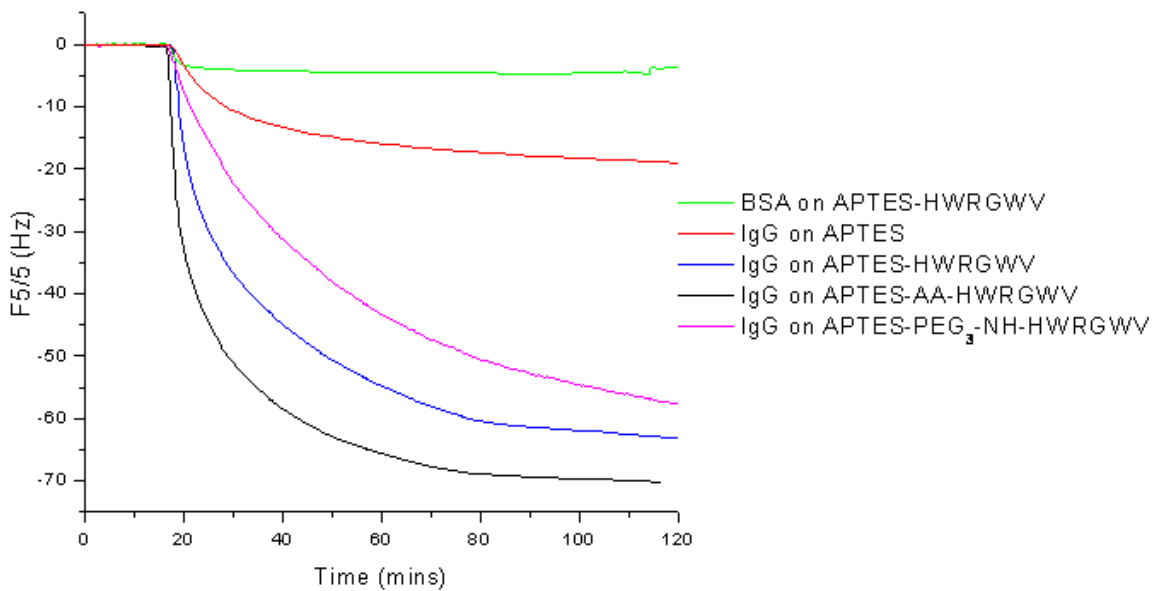


Figure 4.7 The kinetics of protein adsorption on silica surfaces with and without spacer and peptides. The frequency changes recorded by QCM for hIgG or BSA adsorption with concentration of 1 mg ml^{-1} on modified silica surface of APTES, APTES-HWRGWV, APTES-AA-HWRGWV and APTES-PEG₃-HWRGWV

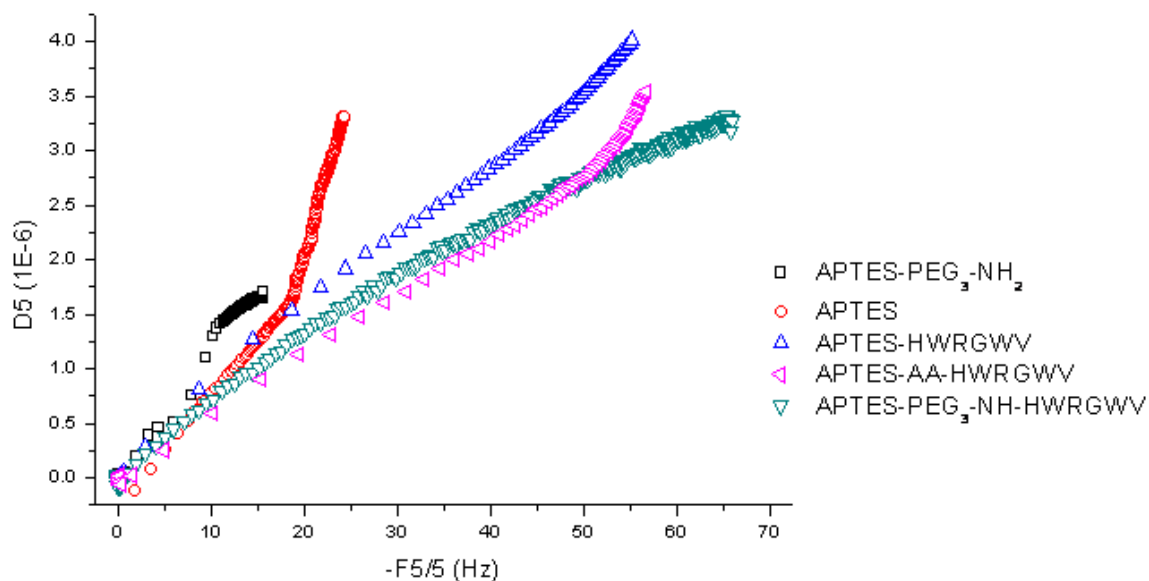


Figure 4.8 Correlation between dissipation and frequency changes of hIgG adsorption from 1mg ml^{-1} solution on modified silica surface of APTES, APTES-PEG₃-NH₂, APTES-HWRGWV, APTES-AA-HWRGWV and APTES-PEG₃-NH-HWRGWV

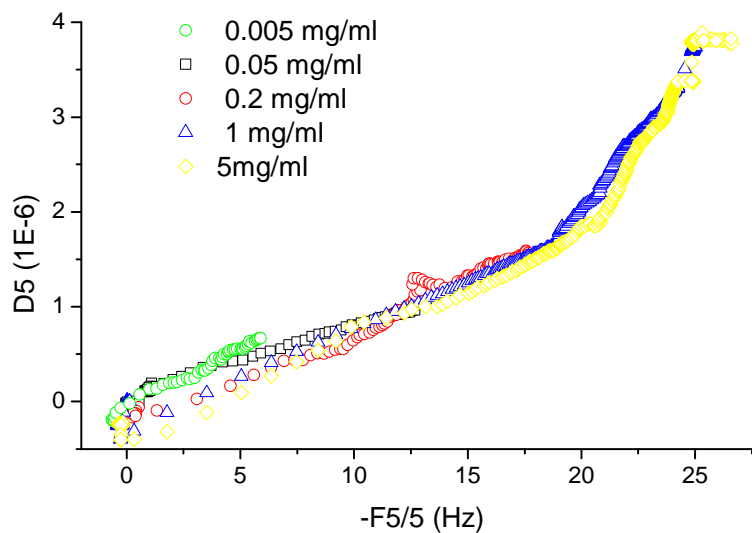


Figure 4.9 Correlation between dissipation and frequency changes of hIgG adsorption from solution on modified silica surface of APTES

**Chapter 5. Formation and Characterization of Self-Assembled Monolayers
of Thiolate Containing Oligo(ethylene glycol) Terminated with Amine
Groups on Gold**

Abstract

Self-assembled monolayers (SAMs) of oligo(ethylene glycol)-terminated alkanethiols can resist the adsorption of proteins. A two-component SAM using $\text{HS}(\text{CH}_2)_{11}(\text{CH}_2\text{CH}_2\text{O})_6\text{NH}_2$ and $\text{HS}(\text{CH}_2)_{11}(\text{CH}_2\text{CH}_2\text{O})_3\text{OH}$ could be an excellent candidate as an anchor layer for the immobilization of ligands in the study of protein-ligand binding events on surfaces with lower background resulting from non-specific protein binding. Mixed SAMs are formed by the co-adsorption of thiols. Consequently, the composition of the SAM and surface properties depend on the concentration of thiol in solution and preparation conditions such as the solvent and adsorption time. In this work, the dependence of the surface properties of pure SAMs of $\text{HS}(\text{CH}_2)_{11}(\text{CH}_2\text{CH}_2\text{O})_6\text{NH}_2$ and $\text{HS}(\text{CH}_2)_{11}(\text{CH}_2\text{CH}_2\text{O})_3\text{OH}$ on thiol binding conditions was studied. Both contact angle measurement and chemical force microscopy (CFM) results indicated that the SAM formed by immersion into 1 mM thiol solution in ethanol with 3% of TEA as solvent for 1 day was more uniform than that formed in ethanol or THF for the same formation time.

The best formation condition for a SAM of $\text{HS}(\text{CH}_2)_{11}(\text{CH}_2\text{CH}_2\text{O})_6\text{NH}_2$ was used to produce a two-component SAM on a gold surface. The mixed SAM was subjected to characterization by X-ray photoelectron spectroscopy (XPS) and CFM. The XPS results indicated the dependence of surface compositions on thiol solution formulations. However, quantification of the amine group density on the surfaces analyzed by XPS spectra or radiolabeling methods did not yield useful results. Analysis of the CFM results showed that no phase separation happened for the two-component SAM of $\text{HS}(\text{CH}_2)_{11}(\text{CH}_2\text{CH}_2\text{O})_6\text{NH}_2$ and $\text{HS}(\text{CH}_2)_{11}(\text{CH}_2\text{CH}_2\text{O})_3\text{OH}$.

5.1 Introduction

In Chapter 3, the modification of silica surfaces to introduce high-density poly ethylene glycol chains and amino groups for the immobilization of ligands was discussed in detail. These materials also show low non-specific protein binding, making them suitable materials for specific binding and detection of specific proteins. As discussed earlier (Section 3.1), a high surface density of PEG chains could provide a surface with low non-specific binding, while a high density of the terminal amino groups, which are the attachment points for the specific ligands, would allow for a better control of the final ligand density, and an optimization of target binding, as ligand density is a critical parameter for affinity chromatography using short peptide ligands. In this chapter, we discuss a strategy to modify a gold surface for similar purposes.

Although self-assembled monolayers (SAM) of alkanethiols have some disadvantages, including instability over long term use and the limitation of use only with noble metal substrates (1-2), they are still attractive due to their simple formation process and well-organized structure (3-8). Whitesides and colleagues (9-11) studied alkanethiols with various functional groups including oligo(ethylene glycol) and demonstrated that SAMs containing this compound resist the adsorption of proteins. They demonstrated that the resistance to the adsorption of proteins increased with the length of the oligo(ethylene oxide) chain and also the mole fraction of the thiolate containing PEG in mixed SAMs (10). SAMs containing PEG chains and functional groups have already been applied for the immobilizations of biomolecules for various applications. SAMs formed from oligo(ethylene glycol)-terminated thiols with a reactive carboxyl end group have been reported to couple peptides for cell

adhesion studies (12-14), and to immobilize proteins for enzyme kinetics studies (15-16), as well as for studies on affinity interactions. (17). There is a very limited number of references on SAMs formed from oligo(ethylene glycol)-terminated thiols ending with amine groups. Mrksich and colleagues reported the use of a SAM containing EG₃NH₂ for coupling a phosphonate ligand onto a gold surface (18). In that work, the phosphonate ligand was first coupled to a disulfide with a structure given by HO-EG₃-(CH₂)₉-S-S-(CH₂)₉-EG₃-NH₂, followed by mixing with a symmetrical EG₃ disulfide (HO-EG₃-(CH₂)₉-S-S-(CH₂)₉-EG₃-OH) and the final phosphonate ligand density obtained was 1%. The ligand density of 1% was high enough for the study for the interaction between phosphonate ligand and cutinase, but it is not sufficient enough for the purpose of this study. As mentioned in Chapter 3, high peptide density is critical for the affinity interaction between short peptide ligands and target biomolecules. In addition, in this study the peptide ligand is small in size in comparison with the target protein (hIgG) and consequently, a short spacer arm was desired to enhance the availability of ligand exposure.

Therefore, we pursued a new strategy to modify gold surfaces by SAMs with the following two kinds of thiols: HS(CH₂)₁₁(CH₂CH₂O)₆NH₂ (in short, EG₆NH₂) and HS(CH₂)₁₁(CH₂CH₂O)₃OH (in short, EG₃OH). The mixture of the EG₆NH₂ and EG₃OH was used to adjust the amine group density on the surface and the difference in chain length between these two thiols could work as spacer arm. The formation conditions of the SAMs of pure EG₆NH₂, EG₃OH, or mixture of these two, were studied and the modified gold surface was characterized by contact angle measurement, X-ray spectroscopy (XPS) and chemical force microscopy (CFM).

5.2 Materials and Methods

5.2.1 Material

Ethanol (200 proof, absolute, for molecular biology), Tetrahydrofuran (THF, ACS reagent 99.5%), triethylene amine (TEA, ACS reagent 99%) and cyanoborohydride (NaCNBH_3 , ACS reagent 99%), were obtained from Sigma-Aldrich (St. Louis, MO). Deionized water (resistivity $> 16 \text{ M}\Omega\cdot\text{cm}$) and Milli-Q water (resistivity $> 18 \text{ M}\Omega\cdot\text{cm}$) were obtained by using a Millipore water purification system (Billerica, MA). Alkanethiols of structures of $\text{HS}(\text{CH}_2)_{11}(\text{CH}_2\text{CH}_2\text{O})_6\text{NH}_2$ and $\text{HS}(\text{CH}_2)_{11}(\text{CH}_2\text{CH}_2\text{O})_3\text{OH}$ were obtained from Prochimia Surfaces, Ltd. (Gdańsk, Poland). $[^{14}\text{C}]$ -formaldehyde (H^{14}CHO , 55 mCi/mmol, 0.1 mCi/ml) was obtained from American Radiolabeled Chemicals Inc. (St. Louis, MO). Nitrogen gas, purity 99.99%, was obtained from National Welders Supply, Inc. (Raleigh, NC). All the reagents were used as received.

5.2.2 Formation of SAMs

A glass slide coated with 100 nm of gold (dimension: $25 \times 6.25 \times 1 \text{ mm}$, EMF Corporation, Ithaca, NY) was cleaned with an ultraviolet/ozone (UVO) cleaner (Model 42, Suprasil lamp, Jelight Co., Irvine, CA) for 20 minutes. The glass slide was quickly immersed and kept in ethanol to prevent contamination from air and a nitrogen stream was used to dry the slide before use. The cleaned glass slide was modified by immersing into thiol solution of $\text{HS}(\text{CH}_2)_{11}(\text{CH}_2\text{CH}_2\text{O})_6\text{NH}_2$, or $\text{HS}(\text{CH}_2)_{11}(\text{CH}_2\text{CH}_2\text{O})_3\text{OH}$ or the mixture of these two, with a total thiol concentration of 1mM for all experiments in this study. One of following solvents were used: pure 200-proof ethanol, ethanol with 3% (v/v) tri-ethylene amine (TEA)

or THF. After immersing the glass slide in the thiol solution for 1 to 4 days, the slide was removed from the solution and rinsed 5 times with 5 ml of ethanol and sonicated for 5 minutes in ethanol, followed by rinsing three times with 5 ml of ethanol, and finally drying with nitrogen.

5.2.3 Contact Angle Measurement

Contact angle measurements were performed under ambient conditions using a Ramé-Hart contact angle goniometer (model 100-00, Ramé-Hart, NJ, USA) equipped with a CCD camera and analyzed with Ramé-Hart software. The advancing contact angle of DI water (pH 6.8) was measured by dropping 4 μl of DI water onto the modified gold surface and then the receding contact angle was measured by withdrawal of 2 μl DI water from the surface with a syringe. Each data point reported represents an average of five measurements on the same sample, with an error smaller than $\pm 1.5^\circ$.

5.2.4 Chemical Force Microscopy (CFM) Experiments

All CFM images were acquired with a scanning probe microscope (SPM, mode JSPM-5200, JEOL, Inc., Tokyo, Japan) under vacuum ($\sim 10^{-6}$ Torr). The SPM was operated in tapping mode using an AFM probe tip terminated with diamine molecules (product no. CT.AU.NH₃, provided by Novascan Technologies, Inc., Iowa, USA). The resonance frequency of the tip was 300 kHz, and the spring constant was 40 N m⁻¹. The dimension of the cantilever was 125 \times 40 \times 4 μm . Tip geometry was pyramidal and its height was 14 μm , with a radius of less than 10 nm. For the tip used in this study the lateral resolution was on the order of 10 nm (information provided by the vendor). Both phase and topography images were recorded at the same time.

5.2.5 X-ray Spectroscopy (XPS) Experiments

The XPS measurements were performed on a Perkin-Elmer Physical Electronics Industries Model 5400 ESCA system (Perkin-Elmer, Inc., Physical Electronics Division, Eden Prairie, MN) with a concentric hemispherical analyzer. The photoelectrons were excited by Mg Ka X-rays at 400 W of power. The system was operated under 10^{-8} - 10^{-9} Torr of pressure. The take-off angle, which is defined as the angle between the collection axis of the photoelectron analyzer and the sample plane, was 70° . The diameter of the analyzed spots was about 0.6 mm. For the survey scans for carbon, the signal for the binding energy (BE) within the range of 0 to 1200 eV were recorded; pass energy was set as 100 eV, with an energy step of 1.0 eV and the dwell time of 100 ms. High resolution spectra were recorded at 200 eV pass energy with a energy step of 0.1 eV and dwell time of 1.2 s. For survey spectra, the average of 3 scans was recorded for all samples. For the high resolution spectra of C 1s the average of 5 scans were recorded.

All peaks were calibrated with a reference of Au4f at 84.0 eV in the survey scans and C-C component at 285 eV for the high resolution scans. The data were analyzed and fitted using the CasaXPS software suite (Casa Systems Inc. Andover, MA) to measure the relative amount of elements or components. The results presented in this study are the averages of three measurements obtained on different positions of the same sample.

5.2.6 Measurement of Amine Group Density by Radiolabeling Method

The gold slides were modified by the SAM of EG₆NH₂ by the same method described in section 5.2.2 and then put into a 5-ml glass vial (Fisher Scientific, Inc., Pittsburgh, PA) with 4 ml of PBS buffer (pH7.4). The gold slide has a surface area of 1.56 cm² (25 × 6.25 mm)

and the theoretical density of EG₆NH₂ was assumed to be the same as that of SAM of HS(CH₂)₁₁(CH₂CH₂O)₆OH, which is 2.14 molecule nm⁻² (19). Therefore, the theoretical amount of amine group in a well-packed SAM of EG₆NH₂ on one slide was 1.22 nmole. Based on the calculated amount of amine groups, 1, 2, 5 or 10 equivalents of radiolabeled formaldehyde (H¹⁴CHO) were added to a vial with one piece of gold slide. Then NaCNBH₃ was added at 10 molar excess of the amount of H¹⁴CHO. The vial was gently shaken at room temperature for 4 hours, followed by removal of the slide from the solution, and rinsing 10 times with 5 ml of DI water. The level of radioactivity in the slide was counted using a Packard 1500 Tri-Carb Liquid Scintillation Analyzer (Meridan, CT) using CytoScint ES scintillation liquid from ICN (Mesa, CA). The amount of radioactivity corresponds to the number of amines acetylated with the radiolabeled formaldehyde.

5.3 Results and Discussion

5.3.1 Formation of pure SAMs of EG₆NH₂ and EG₃OH

The formation of a SAM includes at least three steps: physical adsorption of thiol on the surface, conversion of the physical adsorption to chemical adsorption, and the rearrangement and organization of the molecules to form compact structures that minimize the Gibbs free energy of adsorption (20). Kinetic studies of alkanethiol adsorption onto Au(111) surfaces have shown that at relatively dilute solutions the two initial steps are well described by diffusion-controlled Langmuir adsorption and the adsorption rate showed strong dependence on thiol concentration (8). When the thiol concentration was as high as 1 mM, the first two steps finished within a few minutes, while it required over 100 minutes at 1 μM

concentration (21). The last step is similar to a crystallization process, where alkyl chains get out of the disordered state and into unit cells, thus forming a two-dimensional crystal. The kinetics of the last step is related to chain disorder such as gauche defects, the different components of chain-chain interaction including van der Waals, dipole-dipole, charge-charge forces and the exchange rates between thiolate on surface and thiol in solution or surface mobility of chains. The last step is a relatively slow step when compared with the initial steps, and it could take up to several days (3).

In order to avoid the diffusional transport limitation, a thiol concentration of 1 mM was used for all the experiments in this study. Two SAM-formation times of 1 day or 4 days were used and compared. Ethanol was the typical solvent for the formation of SAM containing PEG (10-11, 13, 19, 22-23) and it was also chosen for this study. Jiang and his colleagues reported that SAMs of thiol containing amine groups tended to form bilayers on a gold surface when ethanol was used as a solvent (24). They suggested adding 3% (v/v) TEA into ethanol to break the H bonding between the bilayer components and to suppress the ionization of NH_2 groups which also prevented the formation of compact SAMs due to strong electrostatic repulsion in closely packed SAMs on surface. In this study, the effect of adding 3% (v/v) TEA in the ethanol solution on the formation of SAM of EG_6NH_2 was investigated. In addition, one polar aprotic solvent, THF was also used to compare with ethanol (a polar protic solvent) to study the effect of solvent on the formation of SAMs of EG_6NH_2 . THF was chosen because by comparing the Hansen solubility parameter (HSP) values of ethanol and THF, it was possible to predict the status of the dissolved thiols in the solvent. A comparison of the HSP values of ethanol and THF is presented in Table 5.1(25). In summary, the

dispersion bonds inside of these two solvent are close, the polar bonds in ethanol are stronger than those in THF, and the H-bonds in ethanol are much stronger than those in THF (26). According to the comparison of these two solvents, it is reasonable to predict that there is less interaction between solvent molecules with PEG (-CH₂CH₂O-) chains in THF than that in ethanol due to the difference in H-bonds. In addition, the incompatibility between the hydrophobic chain -(CH₂)₁₁- and THF is less than that in ethanol, due to the difference in polar bonds. The summation of these two effects could lead to a relatively higher chance for the thiol of EG₆NH₂ or EG₃OH to form micelles in ethanol than in THF with the hydrophobic chains in the core and the PEG chains exposed to ethanol. For these reasons, THF was also chosen and compared to the common used solution ethanol for the formation of SAM of EG₆NH₂ and EG₃OH, since it could be better than ethanol to disperse thiol molecules in solvent for SAM formation.

All in all, three solvents were used and compared: ethanol, ethanol with 3% TEA and THF. The thiol concentration was 1 mM for all experiments and the SAM was formed by immersing in the thiol solution for 1 day or 4 days.

SAMs formed under different conditions were subjected to characterization by contact angle measurements and CFM.

5.3.1.1 Contact Angle Measurement

Measurement of contact angles is one of the most rapid and convenient methods of characterizing surfaces (27). The equilibrium contact angle θ_Y between a liquid and a solid surface is given by the Young equation,

$$\cos \theta_Y = (\gamma_{SV} - \gamma_{SL}) / \gamma_{LV} \quad 5-1$$

where γ_{SV} , γ_{SL} and γ_{LV} are the interfacial tensions between solid/vapor, solid/liquid and liquid/vapor, respectively (28). The Young equation assumes a perfectly flat and homogenous surface but, in practice, solid surfaces are not ideal. Surface roughness and heterogeneity cause a deviation in the equilibrium contact angle from that predicted by Young's equation (27, 29-31). Instead of one equilibrium state, a drop will assume a wide spectrum of contact angles between the advancing contact angle θ_a (highest) and receding contact angle θ_r (lowest) and the difference between advancing contact angle and receding contact angle is referred to as contact angle hysteresis (32). Although the contributions to contact angle hysteresis are not fully understood, it seems that the major causes of contact angle hysteresis are surface roughness and surface heterogeneity (27, 33-34).

In this study advancing and receding contact angles were measured and the hystereses were calculated for SAMs formed under different conditions. All these results are listed in Table 5.2.

For SAM of EG₃OH, the advancing contact angle was around 29~33 deg and receding contact angle was around 17~24 deg. Considering the variation within one sample, which is on the order of ± 1.5 deg, the variations in advancing contact angles of SAMs of EG₃OH prepared under different conditions (± 2 deg) were insignificant. Comparing with the measurements of advancing contact angles, the variations in receding contact angles were relatively large and this variation also led to differences in hysteresis values. As shown in Table 5.2, the hysteresis of the SAM of EG₃OH prepared in THF is smaller than that prepared in ethanol, and adding TEA didn't affect the hysteresis significantly. This result was consistent as our prediction based on the difference in the properties of the solvents. The thiol

functional groups should disperse better in THF than in ethanol, and this in turn can benefit the formation of well-organized SAMs. The motivation of adding TEA was to suppress H-bonding and charge-to-charge interactions between amine groups, which do not exist in EG₃OH. Here the results indicated that the TEA did not significantly affect the interaction between the thiol groups of EG₃OH. In addition, the contact angle measurements of SAMs of EG₃OH prepared in ethanol obtained in this study were close to those of the SAMs of HS(CH₂)₁₁(CH₂CH₂O)_nOH (n=2, 4) prepared under same conditions reported in literature (10).

As shown in Table 5.2, the hydrophobicity of SAMs of EG₃OH varied significantly with formation conditions. For SAMs of EG₆NH₂, the advancing contact angle was around 63 degrees and the hysteresis of the SAMs formed in ethanol were the largest compared to those SAMs obtained in other solvents. The extension of the formation time to 4 days did not significantly change the contact angles and hysteresis. Adding 3% of TEA into to ethanol greatly reduced the contact angles and hysteresis and there was no obvious dependence on time. The contact angle and hysteresis of DI water on the SAM formed in THF for 1 day was smaller than that formed in ethanol but larger than that formed in ethanol with 3% TEA. After lengthening the formation time to 4 days, the contact angle was close to that of a SAM formed in ethanol with 3% TEA. It was found that the advancing and receding contact angles measurements were larger when hysteresis was larger. In other words, the surface was relatively hydrophobic when the surface was less uniform. From these results one could infer that under these conditions a bilayer was formed in ethanol, which led to the exposure of hydrophobic chains on the surface and the bilayer was not uniform even after immersion for

4 days. The wetting properties of the SAMs formed in THF for 4 days were similar to those of the SAMs formed in ethanol with 3% TEA for 1 day.

5.3.1.2 CFM Characterization

As discussed earlier, the wetting properties of the SAMs of EG₆NH₂ were strongly dependent on preparation conditions. CFM was used in an effort to understand the possible reasons for these differences.

Atomic force microscopy (AFM) is a powerful tool for determining the topology of surfaces. Recently, the development of different AFM operation modes allows it to probe different structural and property details of samples, including friction, and lateral chemical surface composition (35).

The AFM operated under tapping mode can simultaneously provide topography imaging and phase imaging (35-36). The interpretation of topography image is straightforward, while the formation of phase images is relatively complex. The phase shifts recorded arise from the difference of phase angles between the cantilever oscillation and its response, and are related to tip-sample interactions determined by energy dissipation from adhesion/repulsion, energy hysteresis and viscoelasticity. Consequently, phase imaging reflects differences in chemical properties on surfaces (36). More details about AFM principles and operation modes are included in Appendix 5-1. The uses of tips modified by covalent linking of organic monolayers that terminate in well-defined functional groups can enhance the force between the tips and surface and consequently, the chemical sensitivity. This ability to discriminate between chemically distinct functional groups has led to naming this variation of AFM as chemical force microscopy (CFM) (37-38).

In this study, an AFM tip functionalized with diamine groups was chosen, since it has relatively stronger repulsion force with an NH_2 group than OH and $-\text{CH}_2-$ groups on the surface (39). When this tip approached an area with NH_2 groups, the relatively strong repulsion force between the tip and the surface leads to a relatively large phase shift.

According to the contact angle measurements, the formation of SAMs of EG_3OH did not depend on solvent or immersion time. Therefore, only the SAMs formed by immersing in ethanol for 24 hours (in short, $\text{EG}_3\text{OH-EtOH}$) were included in this study. The SAM of EG_6NH_2 formed with ethanol or ethanol with 3% TEA as solvent did not show a time dependence, and consequently only SAMs of EG_6NH_2 formed in ethanol and ethanol with 3% TEA for 1 day (in short, $\text{EG}_6\text{NH}_2\text{-EtOH}$ and $\text{EG}_6\text{NH}_2\text{-EtOH TEA}$, respectively) were included in this study. The other two samples consisted of SAMs of EG_6NH_2 formed in THF for 1 day and 4 days (in short, $\text{EG}_6\text{NH}_2\text{-THF-1 day}$ and $\text{EG}_6\text{NH}_2\text{-THF-4 days}$ respectively). The phase images and topography images of these five samples were collected and summarized in Figure 5.1 (A-F).

As shown in Figure 5.1, the roughness of the topographic images of the SAMs of EG_6NH_2 prepared under different conditions (Figures 5.1 2B, 3B, 4B and 5B) and those of $\text{EG}_3\text{OH-EtOH}$ were similar (Figure 5.1 1B). The only noticeable difference is that the roughness for the SAM of EG_6NH_2 is about double the value of those of the other four surfaces.

However, the phase images for these five samples were quite different. In general, the variation of phase shifts in the phase image of $\text{EG}_3\text{OH-EtOH}$, as shown in Figure 5.1 1A, at less than 5 degrees, was much smaller than that of SAMs of EG_6NH_2 formed under different conditions, at around 15 degrees (Figures 5.1 2A, 3A, 4A and 5A). The relative surface areas

of bright and dark regions in the phase images of SAMs of EG₆NH₂ formed under different conditions are quite different. For EG₆NH₂-EtOH (Figure 5.1 2A) the bright regions are in the form of circles with diameters in the range of 1 to 15 nm and these spots are evenly distributed on the surface. For EG₆NH₂-EtOH TEA, as shown in Figure 5.1 5A, the surface was filled with bright regions separated by dark lines of thickness 1-3 nm. For the EG₆NH₂-THF-1 day, as shown in Figure 5.1 3A, the bright regions were continuous and filled with dark regions with diameters in the range of 1 to 10 nm. The phase image of EG₆NH₂-THF-4 days (Figure 5.1 4A) was similar to that of EG₆NH₂-EtOH TEA (Figure 5.1 5A).

The quantitative interpretation of the phase shifts is complicated (40), but some interpretation is possible by comparing the phase images obtained under different conditions. The bright regions should correspond to the areas of the surface containing amine groups, so that, with the lengthening of immersion time from 1 day to 4 day, the SAM of EG₆NH₂ formed in THF became more and more organized (indicated by the reduction in contact angle hysteresis) and consequently, more and more amine groups were exposed on top of the surface (compare Figure 5.1 3A with 5.1 4A). Without adding TEA, the SAM formed in ethanol resulted in a highly heterogeneous surface, as demonstrated by both AFM phase images and the large contact angle hysteresis measurement. With the present of TEA, the SAM of EG₆NH₂ formed in ethanol is as uniformed as that form in THF for 4 days.

In summary, THF was a better solvent than ethanol, but it needed a relatively long time to form high quality SAMs; ethanol with 3% TEA was the best solvent for the formation of SAMs of EG₆NH₂. Unless indicated otherwise, for all the following experiments, ethanol

with 3% TEA was chosen as the solvent for the formation of mixed EG₆NH₂ and EG₃OH and 1 day was chosen as formation time.

5.3.2 Formation of mixed SAMs of EG₆NH₂ and EG₃OH

As mentioned in section 5.1, mixing of EG₆NH₂ and EG₃OH at different ratios was proposed to adjust the surface density of amine groups. However, the ratio of the fractions of the two components in a mixed monolayer is not always the same as that in solution but reflects the relative solubility of the components in solution and interactions between the functional groups in the monolayers (41). Consequently, a method to quantify amine group density on the surface was needed.

Besides the amine group density, the other important issue for the application of biomolecules is the distribution of activity groups. An even distribution and mixture of the species on a molecular level are desirable for immobilization of biomolecules to reduce steric hindrance and increase coupling efficiency. It has been reported that phase separation could happen in the nanometer scale in SAMs of n-alkanethiols on gold (42-43). In this study, an effort was made to quantify the amine group density on the surface and to probe the possibility of phase separation in mixed SAMs.

5.3.2.1 Amine Group Density Quantification by Radiolabeling Method

Radiolabeling amino groups with [¹⁴C]-Formaldehyde in the presence of NaBH₃CN is a widely used procedure to label free primary amino groups in proteins (44). The primary amine reacts first with formaldehyde to form a Schiff base, which is then reduced by NaBH₃CN to the secondary amine. Although the secondary amine can again react and form

the tertiary amine, the stoichiometry of $[\text{NH}_2]/[\text{HCHO}]$ can be fairly well controlled to 1 under appropriate reaction conditions. This reaction was also used to measure the amine groups of silane on flat Ti surfaces by reaction with ^{14}C formaldehyde at 20°C for 4 h (45). It was assumed that the small formaldehyde molecule can diffuse into the film of silane and react with all the primary amine groups (49).

The same reaction conditions were used to radiolabel the amine group of SAMs of EG_6NH_2 for the measurement of amine group density. The measured amine group density was compared with the calculated chain density of EG_6NH_2 , assuming the structure of SAM of EG_6NH_2 is the same as that of $\text{HS}(\text{CH}_2)_{11}(\text{CH}_2\text{CH}_2\text{O})_6\text{OH}$, which is $2.14 \text{ molecule nm}^{-2}$ (19). As shown in Table 5.3, radioactivity counts depended on the amount of ^{14}C -formaldehyde added. The radioactivity counts ceased to increase when the ^{14}C -Formaldehyde concentration was in a 5x molar excess to amino groups. The maximum measured amine group density was approximately 22% of the theoretical maximum limit. This difference may be caused by the erroneous expectation of 100 percent conversion, or perhaps it is due to the assumption that the surface structure EG_6NH_2 is the same as $\text{HS}(\text{CH}_2)_{11}(\text{CH}_2\text{CH}_2\text{O})_6\text{OH}$. Generally, SAMs of thiolates are much more well-organized than those of silanes (3), which could make the diffusion of formaldehyde and the reaction with amine group difficult. Since it was hard to reach 100 percent conversion, the radiolabeling method was not feasible for the quantification of amine group on top of SAM of thiolate.

5.3.2.2 Characterization of Mixed SAM and Amine Group Density Quantification by

XPS

Besides a radiolabeling method, an attempt was made to use XPS to quantify the amine group density on the surface. Both survey scan and narrow scans were performed.

Survey scans probed for the elements C, O and N in the SAMs, while the signal of sulfur was too weak to be detected for most of the samples. The peak areas were used to estimate the relative abundance of these elements in SAMs. The results were normalized based on C amount and summarized in Table 5.4. As shown in Table 5.4, the relative abundance of nitrogen was higher for the mixed SAMs formed with higher fraction of EG₆NH₂ in solution, while the relative abundance of oxygen did not show any dependence on the formulation of the thiol solution. Theoretically, the relative abundance of oxygen should also increase with increases in the mole fraction of EG₆NH₂ in solution, but since the difference in relative abundance of oxygen between EG₆NH₂ and EG₃OH is small (as shown in Table 5.4), and oxygen and carbon are both common elements in contamination from air, it was not a surprise that the experimental measurement of oxygen only showed random deviations. The nitrogen results were explainable considering the difference of the theoretical ratios of EG₆NH₂ and EG₃OH (as shown in Table 5.4). Although the experimental result was consistent with our expectation, the survey scan was still not a suitable method to quantify the amine group density on the surface because the measured fractions of both SAMs of EG₆NH₂ and EG₃OH were biased from the theoretical calculation due to attenuation effects. For well organized SAMs, the fragments of -(CH₂)₁₁- are at the bottom of the layer and subjected to additional attenuation effects compared with the elements arising from the fragmentation of EG₆NH₂ (O and N). Consequently, experimental measurements deviated from the theoretical ratios. This made the relationship between survey scan measurements

and the real amine group amounts difficult. Also, the signal of nitrogen was not strong, and a small measurement variation could lead to a significant error in the estimation of amine group amount.

As shown in Figure 5.2, the narrow scan of the C with high resolution showed a split peak for the sample of SAMs of EG₃OH, EG₆NH₂ and their mixtures prepared in a solution with a 1:1 molar ratio of EG₃OH to EG₆NH₂. The split peaks were fitted with several components: C-C (285 eV), C-O (286.6 eV), and C-N (286.1 eV) (46) and the relative surface areas of different components were calculated by software and summarized in Table 5.5. As shown in Table 5.5, as the ratio of EG₆NH₂ to EG₃OH in the thiol solution increased, the fraction of C-O component increased, indicating that the fraction of EG₆NH₂ thiolate on the surface increased. However, the ratio of C-N seems to be fairly random. As shown in Figure 5.2, the C-N peak lies between two strong peaks from C-C and C-O, which already overlapped to some extent. Therefore, a small error in the fitting line could lead to a significant deviation of the estimated C-N component amount from its true value.

Although the fitting to the C spectra from the surface indicated that there is an increase in the fraction of EG₆NH₂ on the surface resulting from an increase in the mole fraction of this component in solution, further quantification of the chain density from these spectra, which also involved the attenuation effect, is complicated (47).

Up to this point there is no reliable method to quantify the amine group density on surface formed from mixed SAMs.

5.3.2.3 Study the Amine Group Distribution in Mixed SAMs by CFM

According to the CFM results of the pure SAMs presented in section 5.3.1.2, the phase imaging was more sensitive to chemical heterogeneity than to topography imaging. Therefore, only the phase image results of the mixed SAM are presented here.

As shown in Figure 5.3, there was no obvious difference seen in the phase images of mixed SAMs formed from various thiol solutions (molar ratio of EG₃OH : EG₆NH₂ = 1:0, 3:1, 1:3 and 0:1) in ethanol with 3% of TEA as solvent in both scan sizes of 500nm² and 5μm². All the phase images of the mixed SAMs were similar to that of pure SAMs of EG₆NH₂. However, as shown in Figure 5.4, for the case of mixed SAMs formed in THF for 1 day, phase separation in order of nanometers was observed and the area with amine groups in mixed SAM (formed from the thiol solution of EG₃OH and EG₆NH₂ in ratio of 1:1) was smaller than that of pure SAM of EG₆NH₂. It means that, CFM method employed in this study has the capability to detect phase separation in the scale above the lateral resolution of AFM (~10 nm). As shown by XPS spectra, it is apparent that the surface composition changed with increasing ratio of EG₆NH₂ to EG₃OH for the mixed SAMs formed in ethanol with 3% TEA. In other word, the amine group surface density was increased with the increasing of the ratio of EG₆NH₂ to EG₃OH in thiol solution, while CFM didn't detect any change. The only possible explanation for these results is that the amine groups were evenly distributed in the mixed SAMs of EG₃OH and EG₆NH₂ formed with ethanol with 3% TEA as solvent. No phase separation was found within the lateral resolution (in the order of 10 nm) analysis method used in this study.

5.4 Conclusions

The formation conditions of pure SAMs of EG₆NH₂ were studied, and ethanol with 3% of TEA was found to be the best solvent for this application. Both contact angle measurement and CFM results indicated that the SAM formed by immersing into 1 mM thiol solution with ethanol with 3% of TEA as solvent for 1 day was more uniform than that formed in ethanol or THF for the same formation time.

The mixed SAMs of EG₆NH₂ and EG₃OH were formed under the best conditions for the formation of pure SAM. Attempts were made to quantify the amine group density on the surface by radiolabeling amine groups with [¹⁴C]-formaldehyde, analyzing the XPS survey and narrow scans results. None of these methods were suitable for the quantization of amine group density. The CFM scan result indicated that no phase separation in the scale of 10 nm for the mixed SAM formed in the ethanol with 3% of TEA.

Reference:

1. Valiokas R, Ostblom M, Svedhem S, Svensson SCT, & Liedberg B (2002) Thermal stability of self-assembled monolayers: Influence of lateral hydrogen bonding. *Journal of Physical Chemistry B* 106(40):10401-10409.
2. Flynn NT, Tran TNT, Cima MJ, & Langer R (2003) Long-term stability of self-assembled monolayers in biological media. *Langmuir* 19(26):10909-10915.
3. Ulman A (1996) Formation and structure of self-assembled monolayers. *Chemical Reviews* 96(4):1533-1554.
4. Navarro M, Benetti EM, Zapotoczny S, Planell JA, & Vancso GJ (2008) Buried, covalently attached RGD peptide motifs in poly(methacrylic acid) brush layers: The effect of brush structure on cell adhesion. *Langmuir* 24(19):10996-11002.

5. Wang P, Hadjar O, Gassman PL, & Laskin J (2008) Reactive landing of peptide ions on self-assembled monolayer surfaces: an alternative approach for covalent immobilization of peptides on surfaces. *Physical Chemistry Chemical Physics* 10(11):1512-1522.
6. Chaki NK & Vijayamohanan K (2002) Self-assembled monolayers as a tunable platform for biosensor applications. *Biosensors & Bioelectronics* 17(1-2):1-12.
7. Wink T, vanZuilen SJ, Bult A, & vanBennekom WP (1997) Self-assembled monolayers for biosensors. *Analyst* 122(4):R43-R50.
8. Schreiber F (2000) Structure and growth of self-assembling monolayers. *Progress in Surface Science* 65(5-8):151-256.
9. Prime KL & Whitesides GM (1991) Self-assembled organic monolayers - model systems for studying adsorption of proteins at surfaces. *Science* 252(5009):1164-1167.
10. Prime KL & Whitesides GM (1993) Adsorption of proteins onto surfaces containing end-attached oligo(ethylene oxide) - a model system using self-assembled monolayers. *Journal of the American Chemical Society* 115(23):10714-10721.
11. Palegrosdemange C, Simon ES, Prime KL, & Whitesides GM (1991) Formation of self-assembled monolayers by chemisorption of derivatives of oligo(ethylene glycol) of structure HS(CH₂)₁₁(OCH₂CH₂)_nmeta-OH on gold. *Journal of the American Chemical Society* 113(1):12-20.
12. Houseman BT & Mrksich M (2001) The microenvironment of immobilized Arg-Gly-Asp peptides is an important determinant of cell adhesion. *Biomaterials* 22(9):943-955.
13. Roberts C, *et al.* (1998) Using mixed self-assembled monolayers presenting RGD and (EG)₃OH groups to characterize long-term attachment of bovine capillary endothelial cells to surfaces. *Journal of the American Chemical Society* 120:6548-6555.
14. Murphy WL, Mercurius KO, Koide S, & Mrksich M (2004) Substrates for cell adhesion prepared via active site-directed immobilization of a protein domain. *Langmuir* 20(4):1026-1030.

15. Houseman BT, Huh JH, Kron SJ, & Mrksich M (2002) Peptide chips for the quantitative evaluation of protein kinase activity. *Nature Biotechnology* 20(3):270-274.
16. Nayak S, Yeo WS, & Mrksich M (2007) Determination of kinetic parameters for interfacial enzymatic reactions on self-assembled monolayers. *Langmuir* 23(10):5578-5583.
17. Ho M, *et al.* (2007) Protein resistant self-assembled monolayers on gold with latent aldehyde functions. *Langmuir* 23:5571-5577.
18. Hodneland CD, Lee YS, Min DH, & Mrksich M (2002) Selective immobilization of proteins to self-assembled monolayers presenting active site-directed capture ligands. *Proceedings of the National Academy of Sciences of the United States of America* 99(8):5048-5052.
19. Wang RLC, Kreuzer HJ, & Grunze M (1997) Molecular conformation and solvation of oligo(ethylene glycol)-terminated self-assembled monolayers and their resistance to protein adsorption. *Journal of Physical Chemistry B* 101(47):9767-9773.
20. Folkers JP, Laibinis PE, Whitesides GM, & Deutch J (1994) Phase-behavior of 2-component self-assembled monolayers of alkanethiolates on gold. *Journal of Physical Chemistry* 98(2):563-571.
21. Bain CD, *et al.* (1989) Formation of monolayer films by the spontaneous assembly of organic thiols from solution onto gold. *Journal of the American Chemical Society* 111(1):321-335.
22. Yang ZH, Galloway JA, & Yu HU (1999) Protein interactions with poly(ethylene glycol) self-assembled monolayers on glass substrates: Diffusion and adsorption. *Langmuir* 15(24):8405-8411.
23. Vanderah DJ, Valincius G, & Meuse CW (2002) Self-assembled monolayers of methyl 1-thiahexa(ethylene oxide) for the inhibition of protein adsorption. *Langmuir* 18(12):4674-4680.

24. Wang H, Chen S, Li L, & Jiang YY (2005) Improved method for the preparation of carboxylic acid and amine terminated self-assembled monolayers of alkanethiolates. *Langmuir* 21(7):2633-2636.
25. Hansen CM (2007) *Hansen solubility parameters: A use's handbook* (CRC Press, Boca Raton, FL) p 324.
26. Lide DL (2003) *CRC Handbook of Chemistry and Physics* (CRC Press, Boca Raton, FL.) 84th Ed.
27. Kwok DY & Neumann AW (1999) Contact angle measurement and contact angle interpretation. *Advances In Colloid And Interface Science* 81(3):167-249.
28. Young T (1805) An essay on the cohesion of fluids. *Philosophical Transactions of the Royal Society* 95(65-87).
29. Wenzel RN (1949) Surface roughness and contact angle *Journal of Physical and Colloid Chemistry* 53(9):1466-1467.
30. Cassie ABD & Baxter S (1944) Wettability of porous surfaces. *Trans. Faraday Soc.* 40:0546-0550.
31. Cassie ABD (1948) Contact angles. *Discussions of the Faraday Society* 3:11-16.
32. Johnson RE & Dettre RH (1964) Contact angle hysteresis .3. study of an idealized heterogeneous surface. *Journal of Physical Chemistry* 68(7):1744-1754.
33. Extrand CW & Kumagai Y (1997) An experimental study of contact angle hysteresis. *Journal of Colloid and Interface Science* 191(2):378-383.
34. Johnson RE & Dettre RH (1964) Contact angle hysteresis III study of an idealized heterogenous surface. *Journal of Physical Chemistry* 68(7):1744-1750.
35. Garcia R & Perez R (2002) Dynamic atomic force microscopy methods. *Surface Science Reports* 47:197-301.

36. Jandt K (2001) Atomic force microscopy of biomaterial surfaces and interfaces. *Surface Science* 491:303-332.
37. Noy A, Sanders CH, Vezenov DV, Wong SS, & Lieber CM (1998) Chemically-sensitive imaging in tapping mode by chemical force microscopy: Relationship between phase lag and adhesion. *Langmuir* 14(7):1508-1511.
38. Noy A, Vezenov DV, & Lieber CM (1997) Chemical force microscopy. *Annual Review of Material Science* 27:381-421.
39. Vegte EWVD & Hadziioannou G (1997) Scanning force microscopy with chemical specificity: an extensive study of chemically specific tip-surface interactions and the chemical imaging of surface functional groups. *Langmuir* 13:4357-4368.
40. Garcia R & Perez R (2002) Dynamic atomic force microscopy methods. *Surface Science Reports* 47(6-8):197-301.
41. Bain CD, Evall J, & Whitesides GM (1989) Formation of monolayers by the coadsorption of thiols on gold - variation in the head group, tail group, and solvent. *Journal of the American Chemical Society* 111(18):7155-7164.
42. Stranickyk SJ, *et al.* (1996) Nanometer-scale phase separation in mixed composition self-assembled monolayers. *Nanotechnology* (7):438-442.
43. Hobara D, Ota M, Imabayashi SI, Niki K, & Kakiuchi T (1998) Phase separation of binary self-assembled thiol monolayers composed of 1-hexadecanethiol and 3-mercaptopropionic acid on Au(111) studied by scanning tunneling microscopy and cyclic voltammetry. *Journal of Electroanalytical Chemistry* 444:113-119.
44. Seligman SJ (1993) Radiolabeling of synthetic peptides by acetylation of the N-terminal amino group. *Analytical Biochemistry* 211(2):324-325.
45. Xiao SJ, Textor M, Spencer ND, & Sigrist H (1998) Covalent attachment of cell-adhesive, (Arg-Gly-Asp)-containing peptides to titanium surfaces. *Langmuir* 14(19):5507-5516.

46. Ishida T, *et al.* (1998) High resolution x-ray photoelectron spectroscopy measurements of octadecanethiol self-assembled monolayers on Au(111). *Langmuir* 14(8):2092-2096.
47. Jablonski A (2009) Quantification of surface-sensitive electron spectroscopies. *Surface Science* 603(10-12):1342-1352.
48. Giessibl FJ (2003) Advances in atomic force microscopy. *Reviews of Modern Physics* 75(3):949-983.

Table 5.1 Hansen solubility parameter (HSP) values of THF and ethanol

	δD , Dispersion	δP , Polar	δH , Hydrogen bonding
THF	16.8	5.7	8
Ethanol	15.8	8.8	19.4

Table 5.2 Advancing and receding contact angle measurements and contact angle hysteresis of the SAM formed under different conditions, mean value (standard deviation)

Solvent	SAM of HS(CH ₂) ₁₁ EG ₆ NH ₂			SAM of HS(CH ₂) ₁₁ EG ₃ OH		
	θ_a , deg	θ_r , deg	hysteresis, deg	θ_a , deg	θ_r , deg	hysteresis, deg
Ethanol	63(1.5)	44 (2.1)	19	32 (1.1)	22(2.0)	10
Ethanol 4 days	65 (1.9)	46 (2.3)	19	31 (1.3)	19 (1.9)	12
Ethanol with 3% TEA	37 (1.1)	27(1.2)	10	29 (1.7)	17 (1.5)	12
Ethanol with 3% TEA, 4day	36 (1.1)	28 (1.4)	9	30 (1.8)	19 (2.0)	11
THF 1 day	57 (1.2)	45(2.3)	12	33 (1.1)	24(1.5)	9
THF 4 day	37 (1.2)	27 (1.7)	10	32 (1.3)	24 (1.4)	8

Table 5.3 Radioactivity of SAM of EG₆NH₂ radiolabeled by H¹⁴CHO

H ¹⁴ CHO : theoretical amount of amine group of SAM	Radioactivity counts, dpm (standard deviation)	Measured amine group amount: calculated amount
1x	24081 (41)	0.16
2x	26789 (101)	0.18
5x	33440 (72)	0.22
10x	33498 (110)	0.22

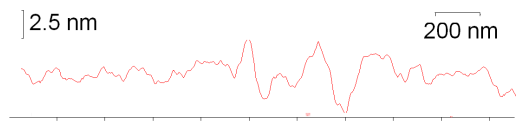
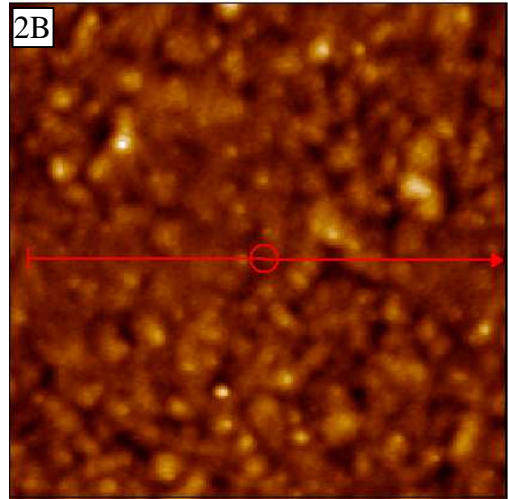
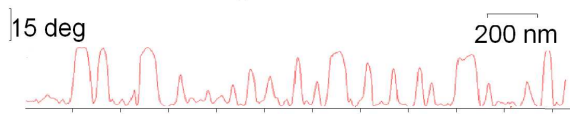
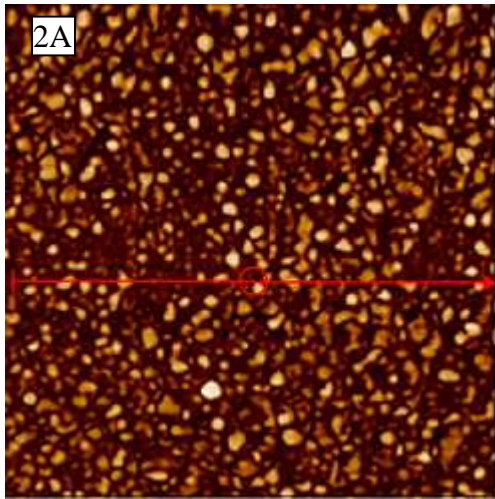
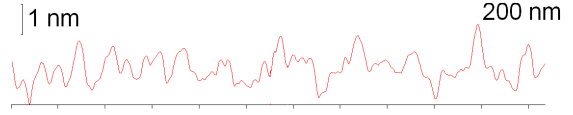
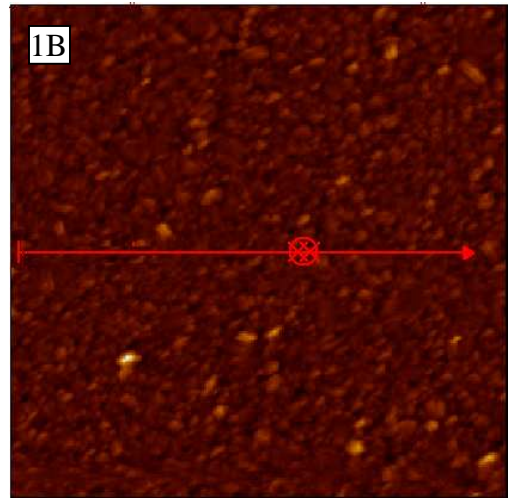
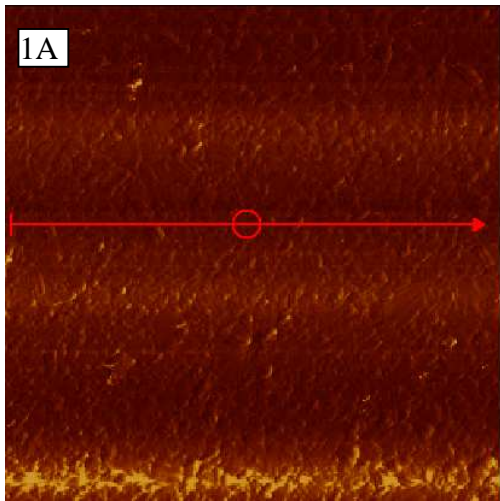
Table 5.4 The relative abundance of C, N and O estimated from the peak areas obtained from survey scan

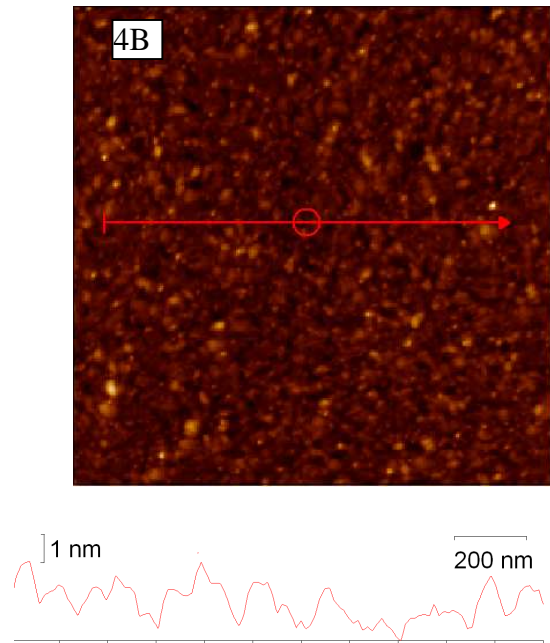
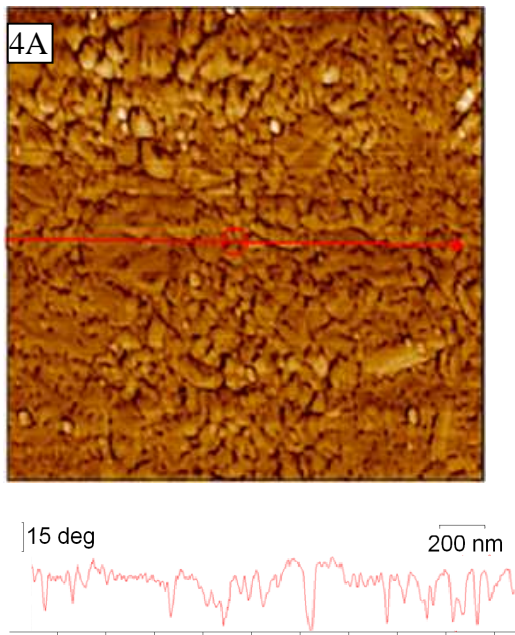
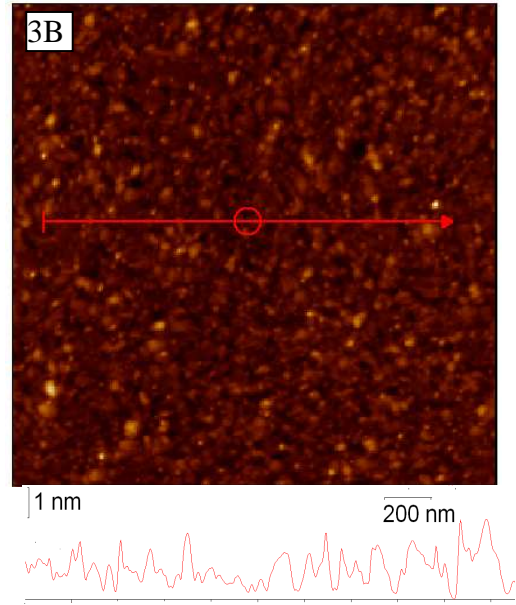
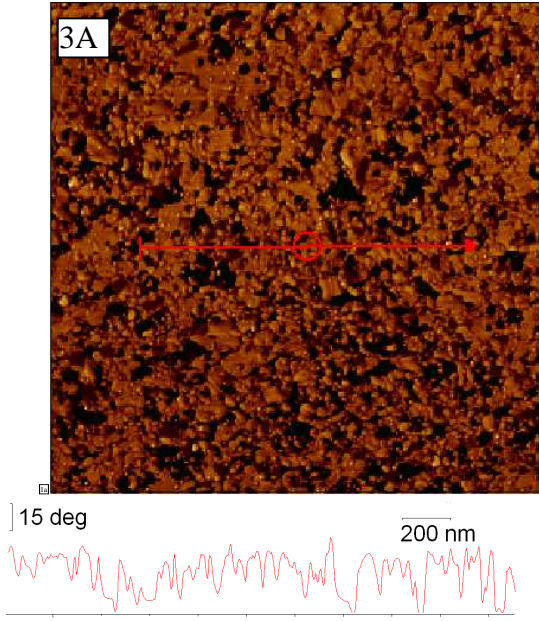
ratio of EG ₆ NH ₂ :EG ₃ OH in thiol solution	C	N	O
1:0	1	0.06	0.34
3:1	1	0.05	0.34
1:1	1	0.02	0.32
1:3	1	0	0.33
0:1	1	0	0.31
Theoretical ratio of EG ₆ NH ₂	1	0.04	0.26
Theoretical ratio of EG ₃ OH	1	0	0.24

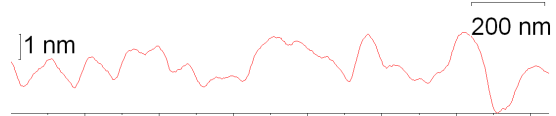
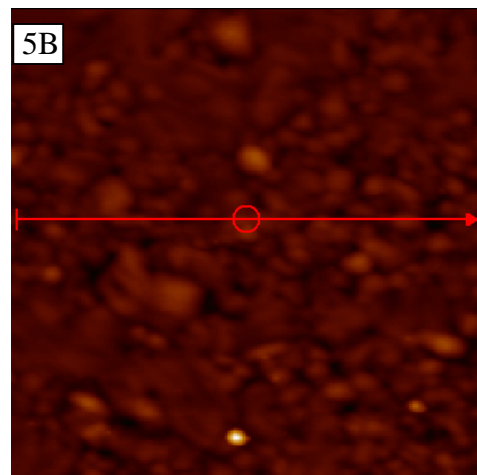
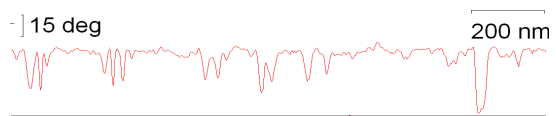
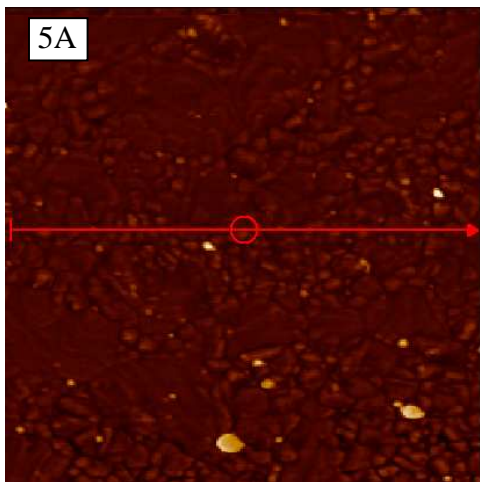
Table 5.5 The relative abundance of difference carbon components estimated by fitting in the spectra of 1Cs narrow scan

EG ₆ NH ₂ :EG ₃ OH in thiol solution	C-C	C-O	C-N
1:0	1	1.26	0.07
3:1	1	1.20	0.07
1:1	1	0.95	0.13
1:3	1	0.72	0.04
0:1	1	0.68	0

Figure 5.1 Phase images (A) and topographic images (B) acquired with tapping-mode AFM (size $\sim 5\mu\text{m}^2$) of following samples: SAM of $\text{HS}(\text{CH}_2)_{11}\text{EG}_3\text{OH}$ prepared by immersing in 1 mM thiolate ethanol solution for 24 hrs (1A, 1B); SAM of $\text{HS}(\text{CH}_2)_{11}\text{EG}_6\text{NH}_2$ prepared by immersing in 1 mM thiolate ethanol solution for 24hrs (2A, 2B); SAM of $\text{HS}(\text{CH}_2)_{11}\text{EG}_6\text{NH}_2$ prepared by immersing in 1 mM thiolate THF solution for 1 day (3A, 3B) and for 4 days (4A, 4B); SAM of $\text{HS}(\text{CH}_2)_{11}\text{EG}_6\text{NH}_2$ prepared by immersing in 1 mM thiolate ethanol with 3% TEA solution for 1 day (5A, 5B) The cross sectional profiles correspond to the line traversing each image.







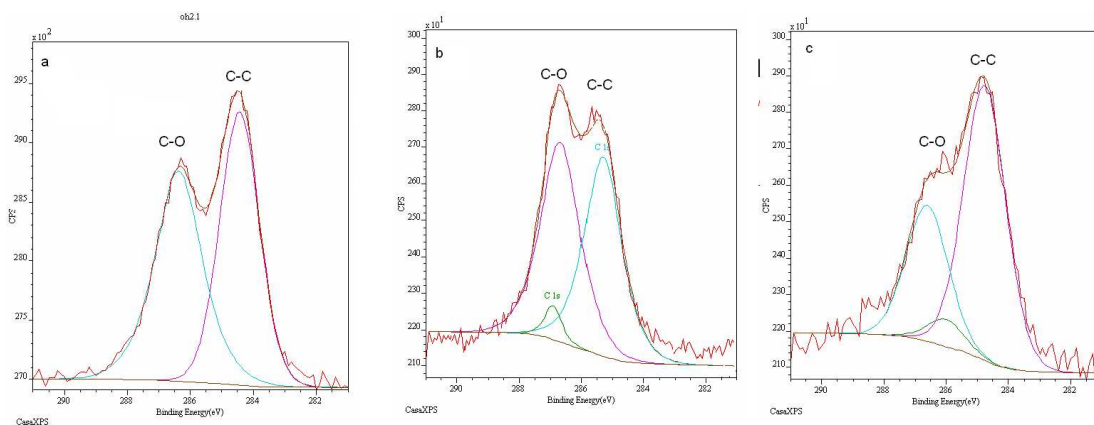


Figure 5.2 High resolution XPS C1s spectra of pure SAMs of EG₃OH (a), EG₆NH₂ (b) and mixture SAM prepared by immersing into 1mM 1:1 mole ratio of EG₃OH and EG₆NH₂ thiol solution (c)

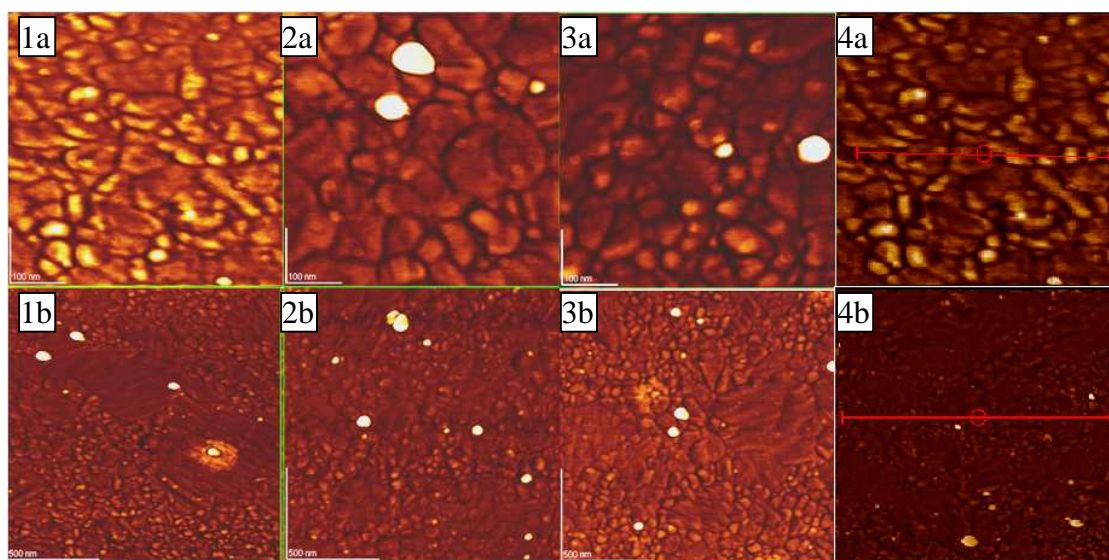


Figure 5.3 Phase contrast tapping-mode AFM images of SAMs prepared using ethanol with 3% TEA as solvent: SAM of HS(CH₂)₁₁EG₃OH (scan size 500nm², 1a and scan size 5μm², 1b), SAM of the mixture of HS(CH₂)₁₁EG₃OH and HS(CH₂)₁₁EG₆NH₂ with the ratio of 1:3 (scan size 500nm², 2a and scan size 5μm², 2b), SAM of the mixture of HS(CH₂)₁₁EG₃OH and HS(CH₂)₁₁EG₆NH₂ with the ratio of 3:1 (scan size 500nm², 2a and scan size 5μm², 2b), and SAM of HS(CH₂)₁₁EG₆NH₂ (scan size 500nm², 3a and scan size 5μm², 3b)

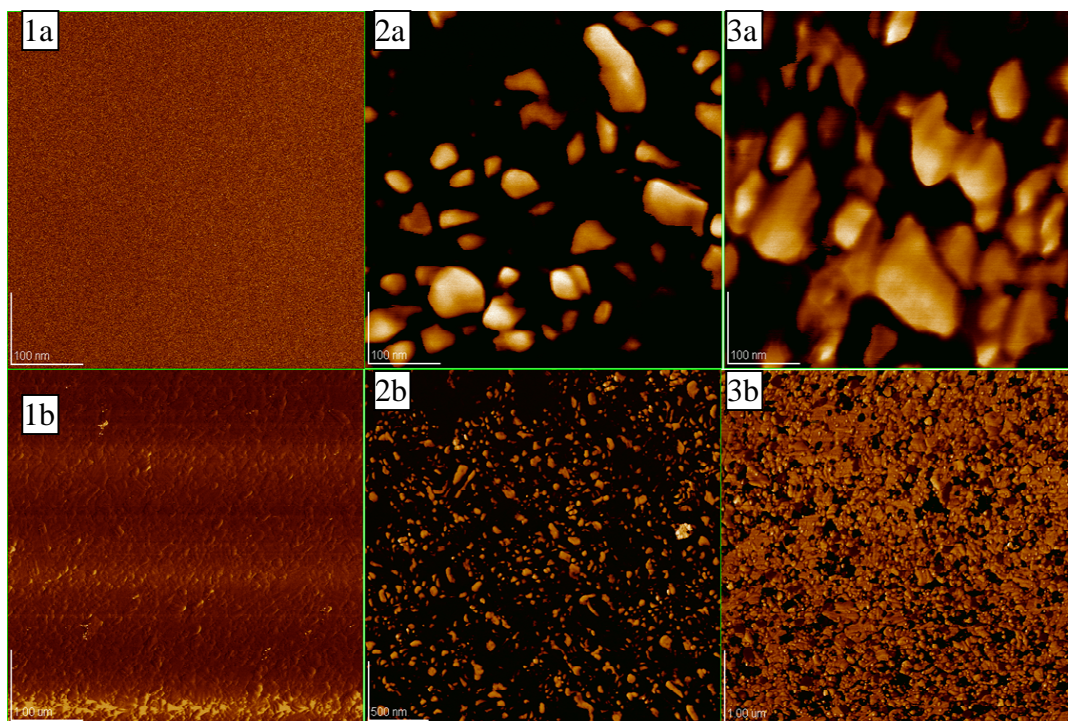


Figure 5.4 Phase contrast tapping-mode AFM images of SAMs prepared with THF as solvent: SAM of $\text{HS}(\text{CH}_2)_{11}\text{EG}_3\text{OH}$ (scan size 500nm^2 , 1a and scan size $5\mu\text{m}^2$, 1b), SAM of the mixture of $\text{HS}(\text{CH}_2)_{11}\text{EG}_3\text{OH}$ and $\text{HS}(\text{CH}_2)_{11}\text{EG}_6\text{NH}_2$ (scan size 500nm^2 , 2a and scan size $5\mu\text{m}^2$, 2b) and SAM of $\text{HS}(\text{CH}_2)_{11}\text{EG}_6\text{NH}_2$ (scan size 500nm^2 , 3a and scan size $5\mu\text{m}^2$, 3b)

Appendix 5-1: The Application and Operation Mode of AFM

In many research areas the possibility of analyzing surface properties with high resolution is becoming increasingly important. Atomic force microscopy (AFM) is one of the most powerful techniques for nanoscopic characterization of surfaces (48).

The AFM can operate in different modes, including static mode and dynamic mode (48). In static mode, also referred as the constant force mode, the tip is in permanent physical contact with the sample. The force between the tip and the sample surface, which is proportional to the cantilever deflection in z-direction, is kept constant via electronic feedback loop. Monitoring the signals received from the photodiodes and keeping the signal

at a given level via a feedback loop accomplishes the latter. The feed back system feeds its signal into the z-component of the piezo-scanner, which maintains the force to the cantilever at the given level through appropriate movement in z-direction. Image of the sample surface topography is created from the cantilever deflection. The interpretation of images acquired by contact mode is straightforward, but the contact mode can only be used to image hard and stable sample, which are not affected by the friction force components the tip applied to the sample (48).

In order to reduce frictional interaction and damage to sample, dynamic mode has been developed (37, 40). There are two common used dynamic modes, tapping mode and non-contact mode. In dynamic image mode, the cantilever oscillates in z-direction.

In tapping mode, the tip is forced to oscillate at certain frequency (generally 50~ 500 kHz in air and ~ 10 kHz in fluids) (36). When the surface is away from the surface, the amplitude the oscillation is in order of several tens of nanometer. If the oscillating tip moves towards the surface and begins to touch or in other word “tap” the surface, the amplitude reduces due to the lost of energy. The reduction of oscillation amplitude is used to measure surface topographic feature. The average cantilever deflections are used as input signal into the feed back loop similar to contact mode AFM to maintain a constant average applied force. For tapping mode, phase imaging can be performed at the same time as topographic imaging. The phase imaging mode is based on the fact that the interaction between tip and sample surface depend on not only surface topography but also other surface characteristics such as hardness, elasticity and adhesion (36, 40, 48). Variations in material property lead to the phase lag of the cantilever oscillation, relative to the signal sent to cantilever piezo oscillation. Besides

providing non-quantitative information about hardness, elasticity or surface adhesion, phase imaging can also act as contrast enhancement technique because phase imaging highlights edges (48). Fine features such as surface steps or edges, which can be obscured by rough topography, are revealed more clearly through phase imaging.

In non-contact mode, the cantilever tip is placed in the attractive force region and force gradients are detected (40). The amount of force applied by the AFM tip to the sample can be even more reduced with this mode. The force gradients can be detected either from shifting in resonance frequency of cantilever or the amplitude and the phase of the cantilever (40). Although, the operation non-contact mode is more complicated than tapping mode, the advantages of these approaches are the high sensitivity of gradient measurements and the small forces are applied to the sample attract more and more attention especially for biological and medical applications.

**Chapter 6. Affinity Interaction between Hexamer Peptide HWRGWV
Immobilized on Gold Surface with Human Immunoglobulin G by Quartz
Crystal Microbalance and Surface Plasmon Resonance**

Abstract

The hexamer peptide ligand HWRGWV binds specifically to the Fc fragment of immunoglobulin G (IgG). The affinity interaction between the human IgG (hIgG) and this short peptide ligand immobilized on a flat gold surface was studied by two complementary methods, quartz crystal microbalance (QCM) and surface plasmon resonance (SPR).

QCM and SPR sensors with a native gold surface film were first modified by adding amino-terminated pegylated thiols. A self-assembled monolayer (SAM) of HS(CH₂)₁₁EG₆NH₂ was formed on a clean gold surface by immersing in 1-mM thiol solution in ethanol with 3% tri-ethylene amine (TEA) for 24 hours. Then, Fmoc-protected HWRGWV was immobilized through its carboxyl terminal to the free amines on the surface of the SAM, followed by removal of the Fmoc group by using 20% piperidine in DMF for 1 hour. The success of the surface modification and peptide immobilization were evaluated by using x-ray photoelectron spectroscopy (XPS) and time of flight-second ion mass spectroscopy (ToF-SIMS).

The affinity of the immobilized peptide on the gold surface to hIgG was studied by measuring the frequency change by QCM and refractive index change by SPR due to protein adsorption in PBS buffer (pH7.4) on modified surfaces with and without immobilized peptide. In addition, the specificity of the ligand on the modified surface to hIgG was tested by comparing the adsorption behavior of hIgG from mammalian cell culture media containing 10% fetal calf serum (cMEM) with that from PBS buffer. The results showed that this hexamer peptide immobilized on gold surface has high affinity for hIgG binding in comparison to bovine serum albumin (BSA) and high specificity to hIgG adsorption even in

complex media such as cMEM. The QCM and SPR data were further analyzed to obtain the dissociation constant K_d , maximum binding capacity Q_{max} , association rate constant k_a , and dissociation rate constant k_d of the affinity interaction. The estimated values of these parameters obtained from QCM and SPR were compared and the effects of the overestimation of adsorbed protein mass by QCM on the parameter estimations were discussed. At the end of this study, the possibility to apply the peptide functionalized SPR sensor for quick IgG concentration determination was examined.

6.1 Introduction

Surface plasmon resonance (SPR) spectroscopy and the quartz crystal microbalance (QCM) method are both surface detection techniques with the capability of *in situ* monitoring of molecular adsorption at solid-liquid interfaces. These two methods have been used widely in the field of biological analysis in past decade (1-7). The merits of the SPR and QCM-based bioassays lie in the fact that the biomolecular binding interactions can be monitored without the use of molecular labels, thus shortening assay times while minimizing nonspecific interactions (8-14).

Currently, there is a trend to combine the use of these two techniques, since they can provide complementary information on a particular binding event (3, 15-16). These two methods are based on different physical principles. Each method is sensitive to different properties of the adsorbed material on the sensor surface. SPR spectroscopy is an optical technique that detects changes of refractive index close to the noble metal sensor surface. The measurement of SPR signal is proportional to the weight of adsorbed material and can be used to quantify the amount of adsorption (12-13, 17). When binding events occur on the

surface, the adsorbed molecules replace the solution close to the sensor surface. The difference between the refractive index of the adsorbed molecules and that of the buffer solution replaced can be detected by SPR. There is no difference between the molecules of solvent attached on the surface or entrapped inside of adsorbed layer and those in solution replaced by the adsorbed protein layer. Consequently, the mass adsorption measured by SPR is said to be a “dry mass” (12-13, 17).

QCM is an acoustic wave device. The signal change of QCM is not only affected by the mass associated with the sensor surface, including the solvent molecules associated with the adsorbed layer, but also by the viscoelastic properties of the adsorbed material, and the density and viscosity of the bulk liquid solution on the sensor surface (8-9, 18-20). For most macromolecular films such as protein and DNA, the mass uptake converted from the frequency changes recorded by QCM is always higher than the optical mass measured by SPR. The difference can be as high as a factor of 10, depending on the nature and conformation of the adsorbed molecules, and the liquid medium used (10, 20-24). The strengths and weaknesses of these two techniques have already been discussed in detail in studies of DNA assembly and hybridization (3), blood plasma coagulation (16), detection of enterotoxin (25), enzyme analysis (26), protein conformation analysis (15, 27), DNA-protein interaction (7), and protein-protein interaction (2). In general, SPR is more suitable for quantitative analysis of protein binding, a property which is essential for the investigation of thermodynamic and kinetic adsorption parameters. Although QCM is not a quantitative technique to the same extent as SPR, the dissipation factor of the QCM provides a qualitative measure of the viscoelastic properties of the adsorbed protein layer and the structure of the

layer adhered to the sensor surface (3). For instance QCM can detect the denaturation of hIgG adsorbed on hydrophobic surfaces by the direct measurement of the dissipation shifts caused by the conformation changes associated with the denaturation process (15).

In this study we employed both QCM and SPR to study the affinity interaction between human immunoglobulin (hIgG) in solution and the short peptide ligand HWRGWV immobilized on gold sensor surfaces. The data generated by these two methods were used to estimate the intrinsic thermodynamic and kinetic parameters of hIgG binding on sensors functionalized with peptide ligands. The importance of this work and our previous efforts spent on the understanding of these parameters of the affinity interactions between short ligands and target biomolecules were already discussed in Chapter 4. If the peptide immobilized on QCM and SPR sensor elements exhibits high affinity and specificity to hIgG adsorption, this technique could be used to develop a new method for real-time, on-line IgG concentration determination as well as a new platform for immunosensors. Because the peptide ligand HWRGWV binds to the Fc fragment of IgG molecule, it could also be used to properly orient the IgG molecules on a sensor surface, which is very important factor in maintaining high affinity activity of immobilized IgG for many applications (28-34).

The peptide can be physically or covalently attached to the surface, but previous studies with peptide ligands indicate that the orientation of peptide is critical to maintain the affinity to IgG binding (35). The peptide ligand needs to be covalently immobilized on the surface through its carboxyl terminal end. Therefore, the sensor surfaces of both SPR and QCM need to be prepared for peptide immobilization. The QCM sensor consists of a thin slice of a single crystal of quartz sandwiched between two metal electrodes, generally made from gold.

The SPR sensor is constructed with a metal surface deposited on a glass prism; and the surface plasmon is a longitudinal wave of charge density propagating along the interface of two media, a metal surface and a dielectric solution contacting the metal surface. Suitable metals include silver, gold, copper and aluminum of which silver and gold are more commonly used. In this study a gold surface was chosen to allow the use of both QCM and SPR techniques on the same sensor. The gold sensor surface was modified with a self-assembled monolayer (SAM) of HS(CH₂)₁₁EG₆NH₂ for peptide immobilization by the methods described in detail in Chapter 5. The optimized peptide immobilization conditions described in Chapter 4 were applied in this study. Two complementary surface analytical techniques, time of flight-secondary ion mass spectroscopy (ToF-SIMS) and X-ray photoelectron spectroscopy (XPS), were used to monitor the sensor functionalization processes.

6.2 Materials and Methods

6.2.1 Materials

The following chemicals and reagents were obtained from Sigma-Aldrich (St. Louis, MO): N,N-dimethylformamide (DMF, ACS reagent, 99.8%), anhydrous N,N-dimethylformamide (DMF), ethanol (200 proof, absolute, for molecular biology), triethyl amine (TEA, ACS reagent 99%), methanol (ACS reagents, 99.5%), piperidine (biotech grade, ≥99.5%), diisopropylethylamine (DIPEA), hydroxybenzotriazole (HOBt), trifluoroacetic acid (TFA, ACS reagents, ≥98%), anisole (≥99%), triisopropyl silane (TIPS, ACS reagents, ≥99%), acetic anhydride (ACS reagent, ≥98.0%), sodium acetate (ACS reagent, ≥99.0%), glycerin

(ACS reagent $\geq 99.5\%$), bovine serum albumin (BSA, $\geq 98\%$) and phosphate buffered saline (pH 7.4, monobasic sodium phosphate, dibasic sodium phosphate, sodium chloride 0.138 M, potassium chloride 0.0027 M). 2-(1H-Benzotriazole-1-yl)-1,1,3,3-tetramethyluronium tetrafluoroborate (TBTU) were purchased from Calbiochem-Novabiochem Corp. (San Diego, CA). Human immunoglobulin (hIgG purity 97%) was obtained from Equitech-Bio, Inc. (Kerrville, TX). Nitrogen gas, purity 99.99%, was obtained from National Welders Supply, Inc. (Raleigh, NC). A Millipore water purification system (Billerica, MA) was used to generate Deionized (DI) water (resistivity $> 16 \text{ M}\Omega\cdot\text{cm}$) and Milli-Q water (resistivity $> 18 \text{ M}\Omega\cdot\text{cm}$). The alkanethiol $\text{HS}(\text{CH}_2)_{11}(\text{CH}_2\text{CH}_2\text{O})_6\text{NH}_2$ was obtained from Prochimia Surfaces, Ltd. (Gdańsk, Poland). Peptide, Fmoc-His-Trp-Arg-Gly-Trp-Val-OH, was custom-synthesized using Fmoc chemistry by Peptides International, Inc. (Louisville, KY). All reagents were used as received.

6.2.2 Formation of SAM of $\text{HS}(\text{CH}_2)_{11}(\text{CH}_2\text{CH}_2\text{O})_6\text{NH}_2$

The native gold SPR sensor (KSV, Instruments OY, Helsinki, Finland) and the native gold QCM sensor (Q-Sense AB, Göthenburg, Sweden) were cleaned by an ultraviolet/ozone (UVO) cleaner (Model 42, Suprasil lamp, Jelight Co. Irvine, CA) for 20 minutes. The sensor was quickly immersed and kept in ethanol to prevent contamination from air, and then was dried by nitrogen stream before use. The cleaned sensor was modified by immersion in a thiol solution of $\text{HS}(\text{CH}_2)_{11}(\text{CH}_2\text{CH}_2\text{O})_6\text{NH}_2$ at a concentration of 1 mM in ethanol with 3% (v/v) tri-ethylene amine (TEA) for 24 hours. After that, the sensor was rinsed 5 times with 5

ml ethanol and sonicated for 5 minutes in ethanol and then rinsed three times with 5 ml ethanol.

6.2.3 Stability of SAM Under Peptide Immobilization and Protection Group

Deprotection Conditions

The modified sensor with SAM was placed into 5 ml one of following solutions, peptide immobilization solvent (DMF), Fmoc group deprotection solution (20% piperidine in DMF) and side chain deprotection solution (mixture of TFA/anisole/water/TIPS in the ratio of 88/5/5/2) for three different time periods: overnight, 1 hour and 2 hours respectively. After that, the sensors were sonicated in DMF solution for 5 minutes, and then rinsed with 5 ml DMF five times, and then dried with nitrogen and kept in a vial purged with nitrogen before being transported to an XPS sampling chamber for characterization. The XPS spectrum of narrow scan of S_{2p} of each sample was obtained and compared to those of intact SAM. The XPS experimental procedure used is described in detail in section 6.2.5).

6.2.4 Peptide Immobilization and Fmoc Group Deprotection

The Fmoc-protected peptide Fmoc-HWRGWV was dissolved in anhydrous DMF to a final concentration of 1 mg ml^{-1} . Then 10 equivalents of TBTU and HOBt and 20 equivalents of DIPEA based on the molar concentration of peptide were added into the peptide solution. A newly-modified sensor with a SAM of alkanethiol obtained by the method described in section 6.2.3 was placed into 5 ml of the above solution in a glass Petri dish. The dish was gently shaken and kept at room temperature for 2 hours or overnight (about 16 hours). The sensor was then rinsed 5 times with 5 ml of DMF, and put into a glass vial with 20 ml of DMF, and sonicated for 5 min, followed by rinsing with 5 ml of DMF 3 times and drying

with nitrogen flow. A solution of 20% piperidine in DMF was used to remove the Fmoc groups at the N-terminal ends of the attached peptides. The sensors remained in the deprotection solution for 1 hour. After that, the samples were rinsed with 5 ml of DMF 5 times, sonicated in 5 ml of DMF for 5 minutes, rinsed again with 5 ml of DMF 3 times and dried with nitrogen flow.

6.2.5 Characterization of the Modified Gold Surface by XPS

XPS was used in the examination of the stability of SAM under peptide immobilization conditions, and Fmoc group deprotection conditions and also for characterization of the peptide functionalized surfaces.

XPS studies were performed on an analytical axis ultra X-ray photoelectron spectrometer (Kratos Analytical Inc., Chestnut Ridge, NY). Monochromatic Al K α (1486.7 eV) was used as the X-ray source and it was operated at voltage and current conditions of 15kV and 8.9 mA respectively. The X-ray spot size was 400 μ m on the sample surface. The operation pressure of the sampling chamber was typically on the order of 10^{-9} Torr. The take-off angle, which is defined as the angle between the collection axis of the photoelectron analyzer and the sample plane was 90°. For survey scans, binding energies (BE) from 0 to 1200 eV were recorded; the pass energy was set as 100eV with an energy step of 1.0 eV and a dwell time of 100 ms. High resolution spectra were recorded at 200 eV pass energy with an energy step of 0.1 eV and a dwell time of 1.2 s. For the high-resolution spectra of C 1s, and N 1s, the average of 5 scans was recorded, and for spectra of S 2p the average of 12 scans was recorded. All peaks were calibrated with a reference of Au 4f at 84.0 eV in the survey scan and a C-C component at 285 eV for high-resolution scan. The data

were analyzed and fitted using the CasaXPS software suite (Casa Systems Inc. Andover, MA). The relative amounts of carbon, oxygen, nitrogen and gold were calculated based on the peak areas of each component identified by the position in the spectrum and the results presented in this study are the averages of three measurements obtained at different positions on the same sample.

6.2.6 Characterization of the Modified Gold Surface by ToF-SIMS

As a complement to XPS, ToF-SIMS was also employed to characterize the modified gold surfaces.

ToF-SIMS analysis of the samples was performed using an ION-TOF SIMS 5 instrument (ION-TOF GmbH, Münster, Germany). The operation of ToF-SIMS was the same as that described in Chapter 4. The pure peptide powder sample attached on the clean silica wafer with a stick tape made with polydimethylsiloxane was used as a positive control. Besides the positive control, three samples were collected after each modification step: the gold surface with SAM of $\text{HS}(\text{CH}_2)_{11}(\text{CH}_2\text{CH}_2\text{O})_6\text{NH}_2$ (Au-C₁₁EG₆NH₂), the gold surface with peptide immobilized on top of SAM of $\text{HS}(\text{CH}_2)_{11}(\text{CH}_2\text{CH}_2\text{O})_6\text{NH}_2$ before deprotection (Au-C₁₁EG₆NH-HWRGWV-Fmoc) and that after deprotection (Au-C₁₁EG₆NH-HWRGWV). The positive ion spectrum was collected for each sample. The mass scales were calibrated to the CH_3^+ , C_2H_3^+ , C_2H_5^+ , Au^+ and AuC_2H_4^+ peaks before further analysis.

6.2.7 Study of the Affinity Interaction between Peptide Ligand and hIgG by SPR

SPR-Navi device (KSV, Instruments OY, Helsinki, Finland) was used to monitor the adsorption of hIgG or bovine serum albumin (BSA) from PBS buffer or complete minimal essential medium (cMEM) on modified sensor surfaces. All experiments were performed at

room temperature and the flow rate was set at $10 \mu\text{l min}^{-1}$. The changes of SPR signals were converted to protein adsorption amounts. These data were used to carry out the thermodynamic and kinetic analysis by the same methods described in Chapter 4.

6.2.7.1 SPR Device Operation

The SPR sensors were modified by the methods described in section 6.2.4. The modified SPR sensor was installed into the sampling chamber. Pure ethanol, Milli-Q water, and then buffer were pumped through the chamber in this order. An initial scan spectrum of normalized reflected intensity vs. incidence angle (similar to that shown in Figure 6.1a) was first obtained by scanning the angle of incidence of the laser beam installed in this SPR device over a range of 39 to 79 deg. The normalized reflected intensity shows a sharp minimum at the resonance angle, which depends on the precise architecture of the metal-dielectric interface and is defined by the matching conditions for energy and momentum between the evanescent photons and the plasmon surface polaritons (36) (more details on the principle of SPR technique can be found in Chapter 2). Typically, the adsorption of proteins on the surface shifts the position of resonance to a higher angle (12-13, 36-37), as shown in Figure 6.1a. The adsorption process can be monitored under two different modes. One is the angular scan mode which is kept recording the change of reflected intensity over a range of incident angles. The other is the fixed angle scan mode, which monitors the intensity change at a certain fixed incident angle. For protein adsorption experiments in this study, the change of SPR response was generally less than 1 degree. Under this situation, the fixed angle scan mode was chosen because of its higher sensitivity. A fixed angle was determined by the system to be at the steep and nearly linear descending part of the SPR initial scan spectrum

and the normalized reflected intensity at this incidence angle was recorded continuously. After a stable baseline was acquired, the protein solution was loaded through a 200- μl sample loop and then the sample loop was connected to the flow of buffer or cMEM solution. During the adsorption process, the normalized reflected intensity was monitored as a function of time (as shown in Figure 6.1b). With a 200- μl sample loop and a flow rate of $10 \mu\text{l min}^{-1}$, the adsorption process lasted for 20 minutes. Within 20 minutes, generally the adsorption on the surface was able to reach equilibrium (the change of SPR response within 2 minutes was less than 5% of the total response to protein adsorption). In this study, the intensity change caused by protein adsorption was all within the linear range in the initial scan spectrum, in other words, the change of intensity (R_2-R_1) was proportional to the change of angle shift ($\delta\theta$), as illustrated in Figure 6.1a. As a result, the intensity change recorded in real time under fixed angle mode (R_2-R_1 illustrated in Figure 6.1b, same as that in Figure 6.1a) could be converted to angle shift ($\delta\theta$, in Figure 6.1a), by the slope of the curve around the chosen fixed incident angle in the initial scan spectrum. The angle shift measurement could be further quantitatively converted to refractive index (RI) change and then protein surface density by the method described below.

6.2.7.2 Quantification of SPR Measurements

A standard curve of SPR response vs. RI was obtained by using the following procedure. Glycerin was dissolved into Milli-Q water to final concentrations of 0, 0.3, 0.7, 1, 3, 5 and 10% (v/v). The RIs of these solutions are reported to be in the range of 1.333 to 1.345 (38). A gold SPR sensor was cleaned in the same way described in section 6.2.2 and installed into the SPR sample chamber right after the cleaning step. Milli-Q water was flowing continuously

through the sample chamber at a rate of $10\mu\text{l min}^{-1}$. After a stable baseline was obtained, the glycerin solution was introduced into the sample chamber and the SPR angle shift change was measured for each concentration. The SPR response was plotted against the refractive index values obtained for the glycerin solutions.

The change in RI needs to be converted further to protein adsorption amount by using an appropriate model describing the structure of adsorbed layers on top of the gold sensor surface. In this study the gold sensor surface was modified by SAM of $\text{HS}(\text{CH}_2)_{11}\text{EG}_6\text{NH}_2$ with or without peptide immobilized on it. So there is an adsorbed layer between the gold surface and the bulk solution, and after protein adsorption, there is one more layer of protein formed on the gold surface (as shown in Figure 6.2). Both the bulk solution and the layer of coating and bound protein on the sensor surface contribute to the RI measured by SPR. The effective RI (η_{eff}) measured by SPR can be calculated with the depth integral,

$$\eta_{\text{eff}} = \left(\frac{2}{l_d}\right) \int_0^{\infty} \eta(z) \exp\left(-\frac{2z}{l_d}\right) dz$$

$$\eta(z) = \begin{cases} \eta_b & z \in (0, d_b) \\ \eta_a & z \in (d_b, d_a) \\ \eta_s & z \in (d_a, \infty) \end{cases} \quad 6-1$$

where $\eta(z)$ is the index of refraction at height z , which equals to η_b , η_a or η_s (the refractive index of modification layer, adsorbed protein layer and solvent respectively) in different range. The l_d is decay length, which is of 25 to 50% of the wavelength of the light (17). For the instrument used in these studies l_d has a value of 240 nm (value provided by the manufacturer). For the adsorption on the modified sensor surface with a bilayer structure

shown in Figure 6.2, the change of effective RI ($\Delta\eta_{eff}$) caused by protein adsorption can be expressed as

$$\begin{aligned}\Delta\eta_{eff} &= \left(\frac{2}{l_d}\right) \left[\int_0^{d_a+d_b} \eta(z) \exp\left(-\frac{2z}{l_d}\right) dz - \int_0^{d_b} \eta(z) \exp\left(-\frac{2z}{l_d}\right) dz \right] \\ &= (\eta_a - \eta_s) \left[1 - \exp\left(-\frac{2d_a}{l_d}\right) \right]\end{aligned}\quad 6-2$$

where η_a , the RI of the adsorbed protein layer, has a value of 1.57 (17). The quantity η_s , the RI of the modified surface layer, has a value of 1.34 (17), and the quantity d_a is the thickness of the adsorbed protein layer. When d_a is much smaller than l_d , the above equation can be simplified as

$$d_a \cong \frac{l_d}{2} \frac{\Delta\eta_{eff}}{\eta_a - \eta_s} \quad 6-3$$

The adsorbed protein mass amount per unit sensor surface area (m_a/A) can then be estimated by the equation,

$$\frac{m_a}{A} \cong \rho_a \cdot d_a \cong \rho_a \frac{l_d}{2} \frac{\Delta\eta_{eff}}{\eta_a - \eta_s} = C \cdot \Delta\eta_{eff} \quad 6-4$$

where, ρ_a is the density of protein with a value of 1.35 g cm⁻³ (17). The calculated C ($\rho_a l_d / 2(\eta_a - \eta_s)$) value was 711 mg m⁻² RIU⁻¹ in this study.

6.2.7.3 Thermodynamics and Kinetics Analysis

The adsorption of hIgG or BSA on modified gold surfaces from PBS buffer or complex media mammalian cell culture media (complete minimum essential medium or cMEM) containing 10% fetal calf serum was recorded. The protein concentration samples were

within the range of 0.005 to 5 mg ml⁻¹. All the experiments were performed at least in duplicate. The measurements of adsorption amounts in equilibrium with protein solution with different concentrations were used to plot the isotherms and then the isotherms were fitted into a Langmuir model by the same method described in Chapter 4.

The association rate k_a and the dissociation rate k_d were obtained by nonlinear least squares regression fitting of SPR data using the two-step kinetics model described in Chapter 4. All the parameters have the same values as those described before in Chapter 4, except for the geometry of the sample chamber. For the SPR instrument, d , the inside diameter is 0.15 mm, and d_H , the hydraulic diameter of chamber, is 0.28 mm. Consequently, the estimated mass transfer coefficient k_m from the Sherwood number was 1.7×10^{-6} m s⁻¹ for SPR.

6.2.8 Study of the Affinity Interaction Between Peptide Ligand and hIgG by QCM

A commercial QCM-D apparatus (model E4, Q-Sense AB, Göthenburg, Sweden) was used to measure the changes in the resonance frequency (ΔF) and in the energy dissipation (ΔD) due to the protein adsorption process. The adsorption of hIgG or BSA on modified gold surfaces from PBS buffer was recorded until the adsorption reached equilibrium. The protein concentrations applied were in the range of 0.005 to 5 mg ml⁻¹. All the experiments were performed at least in duplicate. The operation of the QCM apparatus was the same as that described in Chapter 3. The ΔF data were converted to the adsorption amount by using the Sauerbrey equation (Equation 6-5) (39), with the knowledge that QCM tends to overestimate the adsorption amount, as discussed previously,

$$\Delta F_n = \frac{1}{nC} \frac{\Delta m}{A} \quad 6-5$$

Here, $\Delta m/A$ is the adsorption amount per surface area, ΔF_n is the frequency change of the overtone n and the mass sensitivity constant, C , is equal to $17.7 \text{ ng cm}^{-1} \text{ Hz}^{-1}$ (value from the instrument manufacturer).

The adsorption amounts calculated from QCM were used to perform the thermodynamic and kinetics analysis by the same methods described in Chapter 4 and the results were compared to those obtained from SPR experiments.

Along with the change of resonance frequency, ΔF_n , the change of dissipation, ΔD_n , was recorded as a function of time. Then, ΔD_n was analyzed by plotting the dissipation (ΔD_n) against the resonance frequency ($\Delta F_n/n$). The slope of the plots of ΔD vs. $\Delta F_n/n$ defined as K is a measure of the energy dissipation per unit mass added to the surface during the adsorption process. A more rigid and compact mass is expected to yield a small K value and *vice versa* (40). For studies related to adsorbed proteins, generally, significant changes in K value might be due to conformation changes of protein (2, 15, 18, 21, 41).

6.2.9 Regeneration of SPR sensor online

The SPR sensor was modified to immobilize peptide ligands by the methods described in sections 6.2.2 and 6.2.4. IgG adsorption experiments were performed as described in section 6.2.7, but instead of running the protein solution for 20 minutes, the adsorption step only lasted for 3 minutes in this experiment, and then inlet feed was changed back to buffer for rinsing for 10 minutes. After that, a wash was done with glycine-HCl buffer (pH 3) for 3 minutes and for a buffer rinse was applied for an additional 10 minutes. Then, a wash was done with 0.85% (v/v) H_3PO_4 aqueous solution for 3 min, followed by a rinse with buffer for 10 minutes. Finally, change was made to 2 M urea to wash for 3 minutes followed by rinsing

with buffer for 3 minutes before running a new round of protein injection. This process was repeated to see if the regeneration steps cleaned the surface sufficiently to recover the baseline of the sensor prior to introduction of the protein solution.

6.3 Results and Discussion

6.3.1 Immobilization of Peptide on SAM of $\text{HS}(\text{CH}_2)_{11}(\text{CH}_2\text{CH}_2\text{O})_6\text{NH}_2$

In chapter 4, the optimization of the peptide immobilization reaction on modified silica surface was discussed. The best condition obtained in these studies was applied to the gold surface modified with a SAM of $\text{HS}(\text{CH}_2)_{11}(\text{CH}_2\text{CH}_2\text{O})_6\text{NH}_2$. In short, the peptide was immobilized using TBTU combined with HOBt and DIPEA as coupling reagent and anhydrous DMF as solvent. The Fmoc group was deprotected by keeping in 20% piperidine in DMF for 1 hour. As mentioned in Chapter 4, the protection of the side chain was critical for the immobilization on APTES but not for that on APTES-PEG₃-NH₂. For the fully protected peptide, the side chain protective groups needed to be deprotected after immobilization by immersing the gold surface in a mixture of TFA/anisole/water/TIPS in the ratio of 88/5/5/2 for two hours. In this study, the suitability of the extension of peptide immobilization and deprotection methods developed for modified silica surface to modified gold surface was studied first, then the modified gold surfaces before and after peptide immobilization were characterized by XPS and ToF-SIMS.

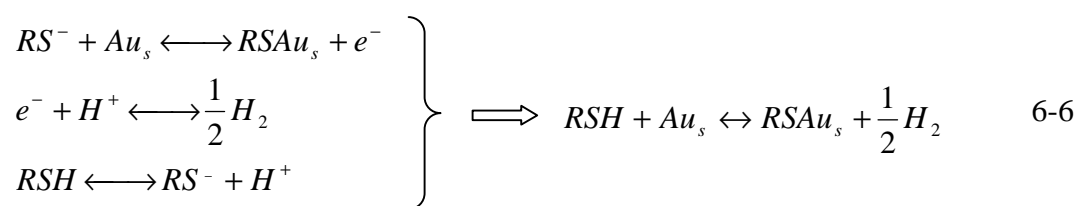
6.3.1.1 Stability of SAM under Peptide Coupling and Deprotection Reaction Conditions

It has been reported that the SAMs of alkanethiols such as octadecanethiol on gold slowly desorb from the surface when exposed to organic solutions such as tetrahydrofuran (42). The

peptide immobilization and deprotection steps used here all involved the use of organic solutions. Consequently, the stability of SAM under the conditions used for peptide immobilization and deprotection became the first concern. XPS was used to determine the extent of desorption of SAMs kept in solutions used for peptide immobilization and deprotection of both side groups and terminal amino groups. XPS has proven to be an efficient method to probe the chemical state of thiols on gold surfaces by monitoring the S_{2p} binding energy (BE) (43-45). In XPS spectra, S_{2p} sulfur peaks of both bound and unbound thiols have a doublet structure due to the presence of two states, the $S_{2p_{3/2}}$ and $S_{2p_{1/2}}$.

The BE state of $S_{2p_{1/2}}$ is always 1.2 eV higher than that of $S_{2p_{3/2}}$ and its peak area is smaller than that of $S_{2p_{3/2}}$. Typically, the $S_{2p_{3/2}}$ BE for unbound alkanethiols is between 163 and 164 eV. After assembly of these molecules on the gold surface to form S-Au bond, the $S_{2p_{3/2}}$ BE decreases to 162 eV (43). If the unbound thiol molecules physically adsorbed on the surface were oxidized by oxygen in the air, the S_{2p} BE of the oxidized sulfur species would, typically, be larger than 165 eV (46). In the spectrum of original SAM, as shown in Figure 6.3a, there were only peaks from bound thiolates, one at 163 eV for $S_{2p_{1/2}}$ and another relatively small one at 161.8 for $S_{2p_{3/2}}$. After immersion into the solution used for peptide immobilization and Fmoc deprotection, as shown in Figures 6.3b and 6.3c, these two peaks remained unchanged, while after immersion in the deprotection solution for side chains groups, as shown in Figure 6.3d, the intensity of these two peaks became much weaker, which indicated a lower amount of bound thiolates in the surface. There were no obvious peaks from unbound or oxidized thiols. The desorbed thiols should be removed from the surface by rinsing and sonication.

The narrow scan of sulfur peaks results indicated that the SAM on gold was unstable when exposed to the side chain deprotection solution, while the desorption of SAMs of $\text{HS}(\text{CH}_2)_{11}(\text{CH}_2\text{CH}_2\text{O})_6\text{NH}_2$ under the peptide immobilization and Fmoc group deprotection conditions was negligible. The instability of SAMs under the conditions used for deprotection of the side chains can be explained by a mechanism which is basically the reverse of the reaction for SAMs formation, as shown in the following equation (42),



As shown in Equation 6-6, the presence of H^+ favors the deprotection direction, and consequently, the SAM of alkanethiolate tends to be desorbed from gold surface with the presence of strong acid, TFA.

Based on the XPS results, the SAM was not stable under the conditions of side chain deprotection step. Hence, only the peptide without the side chain protection was used in the following experiments.

6.3.1.2 Characterization of the Modified Surfaces by XPS

Although no significant changes were observed after immersing the modified gold surface with SAMs of EG_6NH_2 in DMF overnight, the surfaces were exposed for 2 hours and 16 hours to peptide immobilization reaction conditions. XPS was also used to probe the presence of peptide after immobilization and also to study the effects of reaction time on

peptide linkage stability. Both survey scans and narrow scans of C1s and N1s regions were performed.

XPS survey scans were used to detect the elements expected from SAMs of thiol (C, O, N, S), peptide (C, O, N), and the substrate (Au). It was found out that the intensity of sulfur was too low to be detected for all the samples under the survey scan condition used in this study. The peaks from other elements were identified by the binding energy positions. The relative amounts of C, O, N and Au were calculated based on the peak area of each composition and the results are summarized in Table 6.2. As shown in Table 6.2, the atomic percentage of the substrate, Au, decreased from 21.8% to 19.9% after the immobilization of the peptide ligand for 2 hours, and it decreased further to 18.0% after extending the immobilization reaction time to 16 hours. This trend could be explained by the attenuation of the gold signal by the overlying SAM and immobilized peptide layers. It was reported that the intensities of x-ray photoelectrons from gold substrate decreased linearly as a function of film thickness for the SAMs of $\text{HS}(\text{CH}_2)_n\text{CH}_3$ (47-48). With the increase of immobilization time, the organic layer on gold became thicker, and consequently the intensity from Au was reduced. As shown in Table 6.2, the immobilization of peptide also changed the atomic percentages of the elements from the organic layers. In order to make the results more straightforward, the atomic percentages of these three elements C, O and N were normalized based on the percentage of C. These results are presented in comparison with the theoretical ratios of peptide molecules excluding hydrogen ($\text{C}_{56}\text{O}_9\text{N}_{12}$) and those of thiolate molecules ($\text{C}_{23}\text{O}_6\text{NS}$) of SAM in Table 6.3. As shown in Table 6.3, the ratios of C:O:N of SAM obtained from XPS were slightly different from the calculated stoichiometric ratios. Larger mole fractions were measured for

N and O by XPS. For well organized SAMs, the fragments of $-(\text{CH}_2)_{11}-$ are at the bottom of the layer and subjected to additional attenuation effects compared with the elements arising from the fragmentation of EG_6NH_2 (O and N). This leads to a deviation of experimental measurements from theoretical calculations. With the immobilization of the peptide on the surface, the fraction of oxygen decreased and that of nitrogen increased. In addition, with the lengthening of the peptide immobilization reaction time from 2 to 16 h, those differences became larger. These changes could be explained by the difference of the stoichiometric ratios of peptide from that of thiol, as shown in Table 6.3.

The binding energy measured by XPS is sensitive to the chemical surroundings of the target atom and high resolution narrow scans can distinguish the same element in different chemical states (49). For the SAMs of $\text{HS}(\text{CH}_2)_{11}(\text{CH}_2\text{CH}_2\text{O})_6\text{NH}_2$, there were three states of carbon atoms, C-C (BE = 285 eV), C-O (BE= 286.4 eV) and C-N (286.6 eV) (43). In the peptide, as shown in Figure 6.4, carbon could be in one of the following bonding arrangements: C-C, C-O, C-N, C=C (BE=284.8 eV (50)) and C=O (BE=288.5 eV (50)). The C1s narrow scan results are summarized in Figure 6.5, where it can be observed that before the immobilization of the peptide ligand, the C1s peak split into two components: one at 285 eV and the other at 286.6 eV, which should come from C-C bond, and the combination of C-O and C-N bonds of thiolates respectively (50). After peptide immobilization, as shown in Figure 6.5b, besides the main C1s peak including two components which were similar to those before peptide immobilization, a small peak appeared at the position of 288~289 eV. This new component should correspond to the C=O carbon of the peptide bond. The contribution from the carbon in C=C bond (BE=284.8 eV) was not apparent, since it is

almost at the same position of the peak for carbon in C-C bond (BE=285 eV). After removal of the Fmoc group, no significant change was observed, since all the C components exhibited by the peptide molecule also exist in the Fmoc moiety (C-C, C=C and C=O).

The BEs of N1s of the free primary amine and protonated amine are around 399.6 eV and 401.5 eV respectively (51). The N1s narrow scan spectra of the original SAM and those after peptide immobilization and Fmoc group deprotection are summarized in Figure 6.6. There is an obvious peak around 399.6 eV related to free amine group, while the peak for protonated amine at position of 401.5 eV was less significant. The BE of the amide in the peptide chain is around 400.1 eV (52). The amide peak from the free amine, and that of the amide, overlap due to the resolution limitations of the XPS. After immobilization of the peptide on top of SAM, it was observed that the central position of the main N1s peak shifted from 399.6 eV to 400.1 eV, and the small peak around 401.5 eV disappeared. After the deprotection step, the main N1s peak was similar as that before deprotection step and at the same time the small peak from the protonated amine shows up again but still with low signal strength. In summary, the changes of atomic percentages measured by the survey scan and the profiles of C1s and N1s peaks recorded narrow scans were explainable by a successful peptide immobilization process.

6.3.1.3 Characterization the Modified Surface by ToF-SIMS

Although XPS has been more widely used in the characterization of thin films on solid surfaces, ToF-SIMS is more chemically selective than XPS(53). XPS was employed in this study to further confirm the presence of peptide on the gold surface after immobilization.

There were three samples collected for ToF-SIMS characterization, Au-C₁₁EG₆NH₂, Au-C₁₁EG₆NH-HWRGWV-Fmoc and Au-C₁₁EG₆NH-HWRGWV. In addition, the free peptide ligand, HWRGWV, was used as a positive control. According to the ToF-SIMS experimental results of the peptide functionalized silica surfaces described in Chapter 4, positive spectra can provide sufficient information to prove the presence of peptide on the surface, and in this study only positive spectra were collected.

The peaks associated with fragments of peptide identified from the positive control experiments, described in detail in Chapter 4, were used as reference peaks to judge the presence of peptide samples on Au-C₁₁EG₆NH₂, Au-C₁₁EG₆NH-HWRGWV-Fmoc and Au-C₁₁EG₆NH-HWRGWV. These peaks include *m/z* 43, 59, 73, 100, 112 for Arg, *m/z* 81, 82, 110 for His, *m/z* 130, 159, 170 for Trp, *m/z* 41 for Gly, *m/z* 43, 100 for Val, *m/z* 165, 178, 179, 180 for Fmoc group, *m/z* 202 for fragment of Gly-Trp (CH₃-CO-NH⁺=CH-CH₂-C₈H₆N), and *m/z* 281 for fragment of His-Trp (C₃H₄N-C₂H₄-CO-NH⁺=CH-CH₂-C₈H₆N). The results are summarized in Figure 6.7.

As shown in Figure 6.7, the peaks from Au⁺ *m/z* 197 and AuC₂H₄⁺ *m/z* 225 appeared in the spectra for all three samples as expected and these two peaks were used for calibration of the mass scales. The characteristic OEG fragments, including CH₃O⁺ *m/z* 31, C₂H₃O⁺ *m/z* 43, C₂H₅O⁺ *m/z* 45, C₃H₇O⁺ *m/z* 59 (54), and those from nitrogen-containing fragments, including NH₄⁺ *m/z* 18, CH₂N⁺ *m/z* 28, CH₄N⁺ *m/z* 30, C₂H₄N⁺ *m/z* 42, C₂H₅N⁺ *m/z* 43 (55), were present in all three samples with significant intensity. But the relative intensities varied from sample to sample and the most obvious change was that the main peak from the OEG fragment at *m/z* 45 diminished after immobilization of the peptide. The most important

differences came from reference peaks from peptide fragments that were only found in the spectra of the sample with immobilized peptides (Figure 6.7 1-3b and 1-3c). In addition, the peaks from the Fmoc group disappeared completely after the deprotection step (Figure 6.7 2c).

The ToF-SIMS spectra provided direct evidence that peptide was present on the surface after the immobilization step and that the deprotection step was efficient.

6.3.2 Study of Protein Adsorption on the Modified Surface with and without Peptide by SPR and QCM

SPR and QCM were used to investigate the adsorption of hIgG adsorption on modified gold surfaces with peptide ligand HWRGWV.

6.3.2.1 Quantification of SPR Responses

The QCM measurements could be quantitatively converted to adsorption amount by the Sauerbrey equation, although, as mentioned in Chapter 4, it was noticed that this relationship tended to overestimate the adsorption amount. In order to compare the results obtained from SPR to those obtained from QCM, a method to quantify SPR measurements must be developed. SPR machines generate responses expressed as angle shifts or changes of wave length. The instrument used in these experiments use angle shift measurements. The angle shift is related to the refractive index (RI) changes happening close to the sensor surface. The RI change can be further converted to surface concentration of adsorbed molecules with the use of an appropriate model describing the structure of the adsorbed layer. Several papers have already addressed the quantitative interpretation of SPR signals in terms of adsorbed layer structural parameters (17, 37, 56-57). In general, these papers suggest that when the

thickness of the adsorption layer is much thinner than the decay length of the evanescent fields, the response of the SPR to reflective index (RI) change caused by adsorption can be approximately linear in most cases. According to the structure of IgG (23.5×4.4×4.4 nm) (33) and BSA (11.6×2.7×2.7 nm) (58), the thickness of an adsorbed protein monolayer should be less than 24 nm, which is much smaller than the decay length of 240 nm (value provided by the instrument manufacturer). Therefore, a simple linear relationship between adsorption amount and SPR response was expected. The magnitude of the slope can be thought as a sensitivity factor for the sensor and it can be obtained by the measurement of SPR response to a series of solutions with known RI (17).

The standard curve for the device employed in this study was obtained by the measuring the SPR response to changes of bulk solution from pure water to aqueous solutions of glycerin with concentrations ranging from 0.3 to 10% with the bare gold sensor surface. As shown in Figure 6.8, the slope (m) obtained from the linear regression was 110 degrees per refractive index unit (RIU). With this standard curve, the SPR responses can be translated to RI changes, which were further converted to protein surface concentration by the bilayer model described in section 6.2.7.2. This model indicated a linear relationship between adsorption amount per sensor surface area (m_a/A) and effective refractive index change ($\Delta\eta_{eff}$). With the linear standard curve of SPR response (ΔR) vs. RI, the protein surface density can be calculated from SPR response using the following equation,

$$\frac{m_a}{A} \cong C \cdot \Delta\eta_{eff} = \frac{C}{m} \Delta R = C' \Delta R. \quad 6-7$$

where C is equal to $711 \text{ mg m}^{-2} \text{ RIU}^{-1}$ as estimated in section 6.2.7.2. The slope m of the SPR response to RI had a value of 110 deg RIU^{-1} . As a result, C' , the reciprocal of the mass sensitivity of SPR was $6.46 \text{ mg m}^{-2} \text{ deg}^{-1}$.

6.3.2.2 Affinity and Specificity of hIgG Binding to HWRGWV Immobilized on Gold

Surface by SPR

The affinity of the immobilized peptide on gold surface was investigated by comparing the adsorption behavior of hIgG on the modified gold surface with and without peptide with that of bovine serum albumin (BSA). Isotherm curves for these proteins were obtained by measuring the difference between baseline before protein adsorption and that after equilibrium was reached, as shown in Figure 6.9, and then the isotherm curve was fitted into Langmuir equation to estimate the dissociation constant, K_d and the maximum binding capacity Q_{max} ,

$$[\text{Protein} - \text{Peptide}]_{\text{surface,eq}} = \frac{Q_{\text{max}} \times [\text{Protein}]_{\text{solution,eq}}}{K_d + [\text{Protein}]_{\text{solution,eq}}} \quad 6-8$$

When using the surfaces without peptide ligands (Eg_6NH_2), the proteins were mainly attracted by electrostatic forces between amine groups on the surface and negatively charged patches on the protein molecules. The dissociation constants of IgG and BSA adsorption on a surface without peptide ligands were both in the order of 10^{-5} M (as shown in Table 6.3). As shown in Figure 6.9, after immobilization of peptide ligands on the sensor's surface, the adsorbed amount of BSA was clearly reduced, presumably due to the lower charge density on the surface. On the other hand, the adsorbed IgG was noticeably increased due to the affinity interaction of the protein to the peptide ligands. As shown in Table 6.3, the

dissociation constant dropped slightly for BSA adsorption, while it dropped by two orders of magnitude for hIgG adsorption. These results indicated that the immobilized peptide ligands had high affinity to hIgG.

The specificity of immobilized peptide ligands to hIgG was studied by comparing the IgG adsorption behavior from mammalian cell culture media containing 10% fetal calf serum (cMEM) to that from PBS buffer. As indicated in Figure 6.10, the isotherm of hIgG adsorption on peptide functionalized gold surface from cMEM was very close to that obtained from PBS buffer. The adsorption to hIgG was not significantly affected by the presence of a complex medium.

6.3.2.3 Comparison of Isotherms Obtained by QCM and SPR

In Chapter 4, the reasons behind the overestimation of protein adsorption by QCM were discussed in detail, and how the accuracy of both thermodynamic and kinetic parameters were affected. Here, parallel experiments were performed to quantify the extension of the overestimation.

The isotherms of hIgG and BSA adsorption on modified gold surface with and without peptide ligands were obtained using QCM and summarized in Figure 6.11. In general, the shapes of the isotherms were similar to those obtained with SPR under the same conditions (as shown in Figure 6.9) and the immobilization of peptide on the surface also enhanced the amount of hIgG adsorption and suppressed the nonspecific binding to BSA. However, the absolute adsorption amounts were significantly higher than those obtained with SPR for all four isotherms. As shown in Table 6.4, the protein adsorption amount estimated from QCM measurement was about 2.6~6.2 times of that obtained with SPR within the protein

concentration range of 0.005~5 mg ml⁻¹, and the amount of overestimation increased with decreased protein concentration. This trend was consistent with the discussion of the overestimation reasons and effects included in Chapter 4. The lower the protein surface density, the more space available between protein molecules for solvent, which is one of main contributions to the overestimation of mass adsorption by QCM.

The dependence of the overestimation on protein concentration led to a bias in the calculation of thermodynamic parameters. As shown in Table 6.3, the binding capacity Q_{max} values were overestimated and dissociation constant values K_d values were underestimated for all experiments by QCM.

As mentioned in section 6.1, the SPR's measurements relate to the “dry mass” and provide relatively reliable data for kinetics and thermodynamics analysis. Therefore, we compared only those parameters obtained from SPR with those of same ligand immobilized onto polymethacrylate-based chromatography resins.

It was found that the dissociation constant K_d for hIgG adsorption on peptide functionalized gold surface obtained by SPR was 1.83 μM, which is well within the range of values from chromatography resins (0.95~30 μM depending on the peptide density) (59). As mentioned in Chapter 4, a monolayer of unperturbed hIgG molecules would give surface concentrations of 2.4~13 mg m⁻². The binding capacity Q_{max} measured by SPR was 4.15 mg m⁻², which is reasonable and also very close to the value observed for chromatography resins (4.4~5.3 mg m⁻², slight increase with increased peptide density) (59).

6.3.2.4 Kinetics analysis

SPR and QCM offer *in situ* monitoring of dynamic surface events, and consequently have the capability of determining rates of adsorption and desorption for a range of surface interactions (13, 37, 57).

The intrinsic adsorption and mass transport processes occurring inside of SPR and QCM chambers can be described by a two-step kinetic model, as mentioned in chapter 4. The adsorption rate constant (k_a) was fit to the kinetic data by using a nonlinear least squares regression analysis described in section 4.2.6.2. The raw data and fitting lines are shown in Figures 6.12 and 6.13, and the k_a and k_d values are summarized in Table 6.5. In this analysis, estimated values of the mass transfer coefficient and the equilibrium dissociation constant and maximum binding capacity were used in the equations in section 4.2.6.2 so that only one parameter needed to be fit to the data. The rate constant for desorption was estimated from the relationship between the equilibrium dissociation constant as the ratio of the desorption rate constant to the adsorption rate constant. As shown in Figures 6.12b and 6.13, for all SPR and QCM experiments, the calculated protein concentration near the sensor surface (C_s) was noticeably lower than that in bulk solution, C_b . The difference was more obvious at low protein concentrations and at the initial stage of adsorption. These results indicate that the transport of the protein from bulk to surface limited the adsorption rate and it was necessary to include the mass transport equation into the kinetic model to obtain reasonable estimates of the intrinsic association and dissociation rates. The sensitivity of the estimation of kinetics rates on transfer coefficient k_m was tested by comparing the results obtain with k_m estimated from equation 4-6 (60) and equation 4-7 (61). These two equations are both valid for the experimental conditions of SPR and QCM in this study.

The k_m values estimated with equation 4-7 were 1.47 times of those obtained with equation 4-6. It was found that the estimation of kinetics parameters wasn't affected by increasing k_m value by 1.47 times. The kinetics analyses of both QCM and SPR data were not sensitive to the choice of k_m . As shown in Figures 6.12a and 6.13, the deviations between fitting lines and experimental data for the QCM experiment were much larger than those for the SPR experiment. In addition, as shown in Table 6.5, only the estimated association rate constant values obtained from QCM data shown significant dependence on protein concentration. These discrepancies between fitting lines and QCM experimental results and unexpected dependence of association rate estimation on protein concentration were also observed in the kinetic analysis of QCM data in the study of the affinity interactions between hIgG and the peptide ligand immobilized on silica surface. The possible reasons were already discussed in detail in Chapter 4. In short, the QCM overestimation of the mass absorbed that results from measuring the solvent present in the protein layer causes the values of K_d to be significantly lower than those measured by SPR and results in fits of adsorption rate constants which depend strongly on protein concentration.

All in all, both kinetics and thermodynamics parameters obtained from SPR data analysis were more reliable than those obtained from QCM experiments. The adsorption rate constant and desorption rate constant estimated by SPR have average values of $0.68 \text{ m}^3 \text{ mol}^{-1} \text{ s}^{-1}$ and 1.24 s^{-1} , which are both in the similar orders as those obtained with chromatography techniques for other peptide ligand and protein affinity interactions (62).

Although QCM was not as quantitative as SPR for measurement of adsorbed amount, the dissipation measurements of QCM provide additional information on the state of the

adsorbed protein layers. As shown in Figure 6.14, the slope of ΔD vs. ΔF for hIgG adsorption on $\text{HS}(\text{CH}_2)_{11}(\text{CH}_2\text{CH}_2\text{O})_6\text{NH}_2$ without peptide was slightly larger than that of SAM with peptide. The slope of the plot of ΔD vs. $\Delta F_n/n$ was defined as K , which is a measurement of the energy dissipation per unit mass added to the surface during the adsorption process. A rigid and compact mass is expected to yield a small K value and *vice versa* (40). This difference in the slope shown in Figure 6.14 means that the adsorbed hIgG packed more rigidly on top of SAM with peptide than that without peptide. In other words, the association of adsorbed IgG molecules with the surface with peptide ligand is relatively stronger. As also shown in Figure 6.14, the plots of D vs. F for hIgG adsorption on SAMs of $\text{HS}(\text{CH}_2)_{11}(\text{CH}_2\text{CH}_2\text{O})_6\text{NH}_2$ with and without peptide ligand were almost straight lines. The nearly linear relationship suggests that no obvious conformation changes occurred during the adsorption of IgG to these surfaces, which means that the protein molecules adsorbed to the surfaces were intact after being adsorbed onto the surfaces. For the surface with peptide, the curve of ΔD vs. ΔF was not a perfect straight line; it curved slightly downwards with increasing frequency (increasing mass adsorption). The decrease in the slope of ΔD for the IgG adsorption on the modified gold surface with peptide was also observed before for the modified silica surface with peptide ligand (Chapter 4). The possible reason was also discussed in Chapter 4. In short, with the increase of protein surface density along with the adsorption process, water embedded in protein layer or PEG layers could be expelled and the protein molecules packed more rigidly on surface. This trend was not observed for the adsorption on surface without peptide, which may indicate that the surface density of protein was not high enough to form more compact structure.

6.3.3 The Application of Peptide Functionalized SPR sensor for IgG Concentration

Determination

As mentioned in section 6.1, if the peptide immobilized on the gold sensor surface still has high affinity and specificity to hIgG binding, it could be of use in making real-time on-line measurements of IgG concentration. Preliminary experiments were carried out to test the possibility.

Although it was possible to determine the hIgG concentration by the isotherm curve (63), it could take up to a few hours for the adsorption to reach equilibrium. The initial slope of the SPR or QCM signal, which is related to the initial association rate, has been used to quantify the concentration of bacterial (64) and proteins (65-66) in solution. Plots of the initial slope of SPR and QCM signals vs. hIgG concentration are presented in Figure 6.15 and 6.16. As shown in Figure 6.15 and 6.16, the initial slopes of SPR and QCM signals were both directly proportional to the hIgG concentrations over approximately a 2 log range of concentration for IgG adsorption from both PBS buffer and cMEM. With this relationship, the hIgG concentration can be determined within 2 minutes by the measurements of initial slopes of QCM or SPR signals in concentration ranges from approximately 0.02 to 5 mg/ml.

The other important issue for the application of hIgG concentration determination is the reusability of the sensor. Considering the costs of the sensor, the surface modification and the peptide immobilization processes, simple IgG elution and sensor regeneration methods could be a critical issue for the future application of this peptide ligand base biosensor for IgG concentration determination.

Bound hIgG on peptide on chromatography resins can be eluted with phosphate buffer at pH 4.0 (59). However this elution condition is not strong enough for the elution of the adsorbed IgG from the peptide immobilized on gold surfaces. Almost no IgG molecules can be removed from the surface by PB buffer at pH 4.0. Harsher elution conditions were tried. As shown in Figure 6.17, washing with glycine-HCl pH 3.0 buffer can partially remove adsorbed IgG, and most of IgG can be eluted by 0.85% H_3PO_4 solution (pH~1.7). 2M urea was used after the elution step with H_3PO_4 solution to further clean the sensor surface. With this elution and cleaning step the SPR signal returned back the baseline before the adsorption step and the re-adsorption of hIgG was very close to that of the first run. For additional proof of principle studies these cycles would have to be repeated to determine the maximum number of cycles of use of the sensor in real applications using cell culture fluids and other complex media.

6.4 Conclusions

In this study, a new method to immobilize small peptides on gold surfaces was developed and the modified gold surfaces were characterized by both XPS and ToF-SIMS. SPR spectroscopy and QCM techniques were used for the study of the affinity interaction between immobilized peptide ligand and hIgG. Both SPR and QCM results show that the immobilized peptide on gold surfaces still kept high affinity and specificity to hIgG binding. Through the parallel measurements, it was possible to demonstrate that SPR is more suitable for quantitative analysis of the protein binding, which is essential for the investigation of thermodynamics and kinetics parameter of the hIgG adsorption on modified surface with and without peptide ligands. Preliminary results indicate that the peptide functionalized SPR

sensor might be a good tool to measure on-line and in real-time the protein concentration in process streams.

References:

1. Tamerler C, Oren EE, Duman M, Venkatasubramanian E, & Sarikaya M (2006) Adsorption kinetics of an engineered gold binding peptide by surface plasmon resonance spectroscopy and a quartz crystal microbalance. *Langmuir* 22(18):7712-7718.
2. Su XD & Zhang H (2004) Comparison of surface plasmon resonance spectroscopy and quartz crystal microbalance for human IgE quantification. *Sensors and Actuators B-Chemical* 100(3):309-314.
3. Su XD, Wu YJ, & Knoll W (2005) Comparison of surface plasmon resonance spectroscopy and quartz crystal microbalance techniques for studying DNA assembly and hybridization. *Biosensors & Bioelectronics* 21(5):719-726.
4. Fang JJ, Wang P, Du XB, & Zhu DM (2009) Detailed analysis of quartz crystal microbalance and surface plasmon resonance spectroscopy in probing molecular adsorption onto solid-liquid interfaces. *Journal of Physical Chemistry C* 113(36):16121-16127.
5. Graneli A, Edvardsson M, & Hook F (2004) DNA-based formation of a supported, three-dimensional lipid vesicle matrix probed by QCM-D and SPR. *Chemphyschem* 5(5):729-733.
6. Neff JA, Tresco PA, & Caldwell KD (1999) Surface modification for controlled studies of cell-ligand interactions. *Biomaterials* 20(23-24):2377-2393.
7. Su XD, Wu YJ, Robelek R, & Knoll W (2005) Surface plasmon resonance spectroscopy and quartz crystal microbalance study of MutS binding with single Thymine-Guanine mismatched DNA. *Front. Biosci.* 10:268-274.

8. Kosslinger C, *et al.* (1992) A quartz crystal biosensor for measurement in liquids. *Biosensors & Bioelectronics* 7(6):397-404.
9. Niikura K, Nagata K, & Okahata Y (1996) Quantitative detection of protein binding onto DNA by using a quartz-crystal microbalance. *Chemistry Letters* (10):863-864.
10. Su XD, Chew FT, & Li SFY (2000) Design and application of piezoelectric quartz crystal-based immunoassay. *Analytical Sciences* 16(2):107-114.
11. O'Sullivan CK & Guilbault GG (1999) Commercial quartz crystal microbalances - theory and applications. *Biosensors & Bioelectronics* 14(8-9):663-670.
12. Rich RL & Myszka DG (2000) Advances in surface plasmon resonance biosensor analysis. *Current Opinion in Biotechnology* 11(1):54-61.
13. Homola J, Yee SS, & Gauglitz G (1999) Surface plasmon resonance sensors: review. *Sensors and Actuators B-Chemical* 54(1-2):3-15.
14. Melendez J, *et al.* (1996) A commercial solution for surface plasmon sensing. *Sensors and Actuators B-Chemical* 35(1-3):212-216.
15. Zhou C, *et al.* (2004) Human immunoglobulin adsorption investigated by means of quartz crystal microbalance dissipation, atomic force microscopy, surface acoustic wave, and surface plasmon resonance techniques. *Langmuir* 20(14):5870-5878.
16. Viking TP, *et al.* (2000) Comparison of surface plasmon resonance and quartz crystal microbalance in the study of whole blood and plasma coagulation. *Biosensors & Bioelectronics* 15(11-12):605-613.
17. Jung LS, Campbell CT, Chinowsky TM, Mar MN, & Yee SS (1998) Quantitative interpretation of the response of surface plasmon resonance sensors to adsorbed films. *Langmuir* 14(19):5636-5648.
18. Rodahl M, Hook F, Krozer A, Brzezinski P, & Kasemo B (1995) Quartz-crystal microbalance setup for frequency and Q-factor measurements in gaseous and liquid environments. *Review of Scientific Instruments* 66(7):3924-3930.

19. Rickert J, Brecht A, & Gopel W (1997) Quartz crystal microbalances for quantitative biosensing and characterizing protein multilayers. *Biosensors & Bioelectronics* 12(7):567-575.
20. Hook F, Rodahl M, Brzezinski P, & Kasemo B (1998) Measurements using the quartz crystal microbalance technique of ferritin monolayers on methyl-thiolated gold: Dependence of energy dissipation and saturation coverage on salt concentration. *Journal of Colloid and Interface Science* 208(1):63-67.
21. Hook F, *et al.* (2001) Variations in coupled water, viscoelastic properties, and film thickness of a Mefp-1 protein film during adsorption and cross-linking: A quartz crystal microbalance with dissipation monitoring, ellipsometry, and surface plasmon resonance study. *Analytical Chemistry* 73(24):5796-5804.
22. Hook F, *et al.* (2002) A comparative study of protein adsorption on titanium oxide surfaces using in situ ellipsometry, optical waveguide lightmode spectroscopy, and quartz crystal microbalance/dissipation. *Colloids and Surfaces B-Biointerfaces* 24(2):155-170.
23. Choi KH, *et al.* (2003) Investigation of protein adsorption with simultaneous measurements of atomic force microscope and quartz crystal microbalance. *Journal of Vacuum Science & Technology B* 21(4):1433-1436.
24. Stadler H, Mondon M, & Ziegler C (2003) Protein adsorption on surfaces: dynamic contact-angle (DCA) and quartz-crystal microbalance (QCM) measurements. *Analytical and Bioanalytical Chemistry* 375(1):53-61.
25. Spangler BD, Wilkinson EA, Murphy JT, & Tyler BJ (2001) Comparison of the Spreeta (R) surface plasmon resonance sensor and a quartz crystal microbalance for detection of Escherichia coli heat-labile enterotoxin. *Analytica Chimica Acta* 444(1):149-161.
26. Turon X, Rojas OJ, & Deinhammer RS (2008) Enzymatic kinetics of cellulose hydrolysis: A QCM-D study. *Langmuir* 24(8):3880-3887.
27. Reimhult E, Larsson C, Kasemo B, & Hook F (2004) Simultaneous surface plasmon resonance and quartz crystal microbalance with dissipation monitoring measurements

- of biomolecular adsorption events involving structural transformations and variations in coupled water. *Analytical Chemistry* 76(24):7211-7220.
28. Lu B (1995) Oriented immobilization of Fab' fragment on silica surfaces. *Analytical Chemistry* 67(1):83-97.
 29. Kwon Y, Han ZZ, Karatan E, Mrksich M, & Kay BK (2004) Antibody arrays prepared by cutinase-mediated immobilization on self-assembled monolayers. *Analytical Chemistry* 76(19):5713-5720.
 30. Bae YM, Oh BK, Lee W, Lee WH, & Choi JW (2005) Study on orientation of immunoglobulin G on protein G layer. *Biosensors & Bioelectronics* 21(1):103-110.
 31. Starodub NF, Pirogova LV, Demchenko A, & Nabok AV (2005) Antibody immobilisation on the metal and silicon surfaces. The use of self-assembled layers and specific receptors. *Bioelectrochemistry* 66(1-2):111-115.
 32. Lu B, Xie JM, Lu CL, Wu CG, & Wei Y (1995) Oriented immobilization of Fab' fragments on silica surfaces. *Analytical Chemistry* 67(1):83-87.
 33. Buijs J, Lichtenbelt JWT, Norde W, & Lyklema J (1995) Adsorption of monoclonal IgGs and their F(ab')(2) fragments on polymeric surfaces. *Colloids and Surfaces B-Biointerfaces* 5(1-2):11-23.
 34. Caruso F, Rodda E, & Furlong DN (1996) Orientational aspects of antibody immobilization and immunological activity on quartz crystal microbalance electrodes. *Journal of Colloid and Interface Science* 178(1):104-115.
 35. Yang H, Gurgel PV, & Carbonell RG (2005) Hexamer peptide affinity resins that bind the Fc region of human immunoglobulin G. *Journal of Peptide Research* 66:120-137.
 36. Green RJ, *et al.* (2000) Surface plasmon resonance analysis of dynamic biological interactions with biomaterials. *Biomaterials* 21(18):1823-1835.

37. Mullett WM, Lai EPC, & Yeung JM (2000) Surface plasmon resonance-based immunoassays. *Methods* 22(1):77-91.
38. Vogel HJ ed (2001) *Calcium-binding protein protocols: methods and techniques* (Humana Press Inc., Totowa, NJ), p 103.
39. Sauerbrey G (1959) Verwendung von schwingquarzen zur wagung dunner schichten und zur mikrowagung. *Zeitschrift Fur Physik* 155(2):206-222.
40. Rodahl M, *et al.* (1997) Simultaneous frequency and dissipation factor QCM measurements of biomolecular adsorption and cell adhesion. *Faraday Discussions*:229-246.
41. Voros J (2004) The density and refractive index of adsorbing protein layers. *Biophysical Journal* 87(1):553-561.
42. Schlenoff JB, Li M, & Ly H (1995) Stability and self-exchange in alkanethiol monolayers. *Journal of the American Chemical Society* 117(50):12528-12536.
43. Ishida T, *et al.* (1998) High resolution x-ray photoelectron spectroscopy measurements of octadecanethiol self-assembled monolayers on Au(111). *Langmuir* 14(8):2092-2096.
44. Flynn NT, Tran TNT, Cima MJ, & Langer R (2003) Long-term stability of self-assembled monolayers in biological media. *Langmuir* 19(26):10909-10915.
45. Schoenfisch MH & Pemberton JE (1998) Air stability of alkanethiol self-assembled monolayers on silver and gold surfaces. *Journal of the American Chemical Society* 120(18):4502-4513.
46. Castner DG (1996) X-ray Photoelectron Spectroscopy Sulfur 2p Study of Organic Thiol and Disulfide Binding Interactions with Gold Surfaces. *Langmuir* 12:5083-5086.

47. Laibinis PE, Bain CD, & Whitesides GM (1991) Attenuation of photoelectrons In monolayers of normal-alkanethiols adsorbed on copper, silver, and gold. *Journal of Physical Chemistry* 95(18):7017-7021.
48. Bain CD & Whitesides GM (1989) Attenuation lengths of photoelectrons in hydrocarbon films. (Translated from English) *Journal of Physical Chemistry* 93(4):1670-1673 (in English).
49. Barr TL (1991) Advances in the application of X-ray photoelectron spectroscopy. 1. foundation and established methods. *Critical Reviews in Analytical Chemistry* 22(1-2):115-181.
50. Cheng F, Gamble LJ, & Castner DG (2008) XPS, TOF-SIMS, NEXAFS, and SPR Characterization of Nitrilotriacetic Acid-Terminated Self-Assembled Monolayers for Controllable Immobilization of Proteins. *Analytical Chemistry* 80:2564-2573.
51. Martin HJ, Schultz KH, Bumgardner JD, & B. WK (2007) XPS study on the use of 3-aminopropyltriethoxysilane to bond chitosan to a titanium surface. *Langmuir* 23(12):6645-6651.
52. Xiao SJ, Textor M, Spencer ND, & Sigrist H (1998) Covalent attachment of cell-adhesive, (Arg-Gly-Asp)-containing peptides to titanium surfaces. *Langmuir* 14(19):5507-5516.
53. Belu AM, Graham DJ, & Castner DG (2003) Time-of-flight secondary ion mass spectrometry: techniques and applications for the characterization of biomaterial surfaces. *Biomaterials* 24(21):3635-3653.
54. Kingshott P, Wei J, Bagge-Ravn D, Gadegaard N, & Gram L (2003) Covalent attachment of poly(ethylene glycol) to surfaces, critical for reducing bacterial adhesion. *Langmuir* 19(17):6912-6921.
55. Cheng F, Gamble LJ, & Castner DG (2008) XPS, TOF-SIMS, NEXAFS, and SPR characterization of nitrilotriacetic acid-terminated self-assembled monolayers for controllable immobilization of proteins. *Analytical Chemistry* 80(7):2564-2573.

56. Yu F, Yao DF, & Knoll W (2003) Surface plasmon field-enhanced fluorescence spectroscopy studies of the interaction between an antibody and its surface-coupled antigen. *Analytical Chemistry* 75(11):2610-2617.
57. McDonnell JM (2001) Surface plasmon resonance: towards an understanding of the mechanisms of biological molecular recognition. *Current Opinion in Chemical Biology* 5(5):572-577.
58. Norde W & Anusiem ACI (1992) Adsorption, desorption and readsorption of proteins on solid surfaces. *Colloids and Surfaces* 66(1):73-80.
59. Yang H, Gurgel PV, & Carbonell RG (2009) Purification of human immunoglobulin G via Fc-specific small peptide ligand affinity chromatography. *Journal of Chromatography A* 1216.
60. Wilk J (2009) Experimental investigation of convective mass/heat transfer in short minichannel at low Reynolds numbers. *Experimental Thermal and Fluid Science* 33(2):267-272.
61. Acosta RE, Muller RH, & Tobias CW (1985) Transport process in narrow (capillary) channels. *AIChE Journal* 31(3):473-482.
62. Wang GQ & Carbonell RG (2005) Characterization of a peptide affinity support that binds selectively to staphylococcal enterotoxin B. *Journal of Chromatography A* 1078(1-2):98-112.
63. Roach P, Shirtcliffe NJ, Farrar D, & Perry CC (2006) Quantification of surface-bound proteins by fluorometric assay: comparison with quartz crystal microbalance and amido black assay. *Journal of Physical Chemistry* 110:20572-20579.
64. Poitras C & Tufenkji N (2009) A QCM-D-based biosensor for E. coli O157:H7 highlighting the relevance of the dissipation slope as a transduction signal. *Biosensors and Bioelectronics* 24:2137-2142.
65. Meyer MHF, Hartmann M, & Keusgen M (2006) SPR-based immunosensor for the CRP detection—A new method to detect a well known protein. *Biosensors and Bioelectronics* 21(10):1987-1990.

66. Cosnier S, Perrot H, & Wessel R (2001) Biotinylated polypyrrole modified quartz crystal microbalance for the fast and reagentless determination of avidin concentration. *Electroanalysis* 13(11):971-974.

Table 6.1 XPS atomic percentage of SAM of HS(CH₂)₁₁(CH₂CH₂O)₆NH₂ before and after peptide immobilization (mean ± standard deviation)

	Binding Energy (eV)	EG ₆ NH ₂	after 2 hours peptide immobilization	after 16 hours peptide immobilization
C(1s)	285	58 (1.4)	60.09 (1.6)	60.6 (1.3)
O(1s)	532	16.9 (1.2)	15.7 (1.2)	14.2 (0.8)
N(1s)	400	3.23 (0.4)	4.26 (0.6)	6.23 (0.6)
Au(4f)	83	21.8 (1.0)	19.9 (0.8)	19.0 (1.2)

Table 6.2 Comparing the normalized XPS atomic percentage of the elements excluding that of substrate with calculated stoichiometric ratios

	Stoichiometric ratio of SAM	Stoichiometric ratio of peptide	SAM	Ratios after 2 hours immobilization	Ratios after 16 hours immobilization
C(1s)	1	1	1	1	1
O(1s)	0.26	0.16	0.29	0.26	0.23
N(1s)	0.04	0.21	0.06	0.07	0.1

Table 6.3 Comparing the dissociation constant and maximum capacity of the BSA and hIgG adsorption on gold surfaces measured by QCM and SPR

Surfaces	Protein	QCM			SPR		
		K_d , μM	Q_{max} , mg m^{-2}	R^2	K_d , μM	Q_{max} , mg m^{-2}	R^2
EG ₆ -NH ₂	hIgG	38	4.07	0.91	59.3	1.34	0.92
	BSA	52.1	2.96	0.9	62.5	1.12	0.89
EG ₆ NH ₂ -HWRGWV-NH ₂	hIgG	0.53	12.5	0.97	1.83	4.15	0.99
	BSA	31	0.02	0.91	35.4	0.64	0.93

Table 6.4 The ratios of protein adsorption amounts estimated from QCM data to those estimated from SPR data

Protein concentration, mg ml ⁻¹	Surface: EG ₆ NH ₂		Surface: EG ₆ NH ₂ -HWRGWV	
	hIgG	BSA	hIgG	BSA
0.005	5.5	3.1	6.2	2.9
0.02	5.5	3.1	5.7	3.3
0.5	5.3	3.1	3.5	3.2
1	5.2	3.1	3.3	3.1
2.5	4.8	3.0	3.1	2.8
5	4.4	2.9	3.1	2.6

Table 6.5 Comparing the kinetic parameters k_a and k_d obtained by QCM and SPR

IgG Concentration mg ml ⁻¹	QCM		SPR	
	k_a , m ³ mol ⁻¹ s ⁻¹	k_d , s ⁻¹ × 10 ³	k_a , m ³ mol ⁻¹ s ⁻¹	k_d , s ⁻¹ × 10 ³
0.005	0.81	4.3	0.77	1.40
0.02	0.72	3.8	0.71	1.30
0.1	0.48	2.5	0.69	1.26
0.5	0.15	0.80	0.55	1.00
1	0.12	0.64	0.91	1.66
2.5	0.11	0.58	0.61	1.12
5	0.11	0.58	0.54	0.99

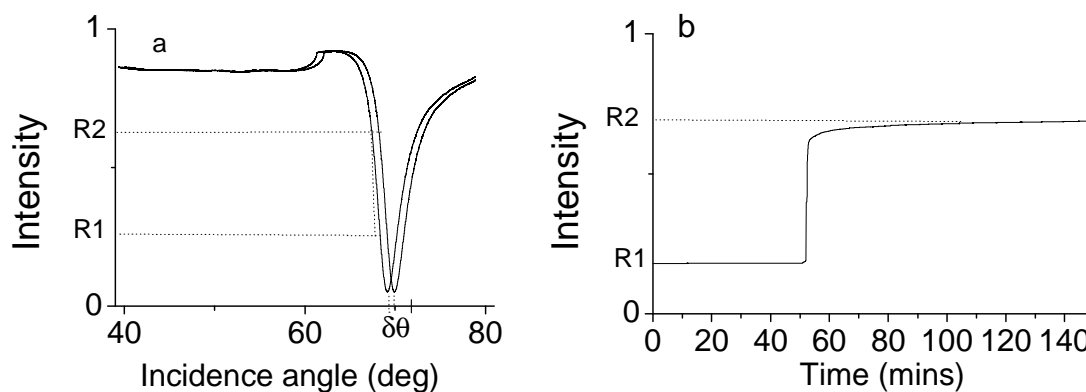


Figure 6.1 (a) A schematic change of reflected intensity vs. angle curve during protein adsorption process obtained with SPR. The angle θ at minimum reflected intensity in the initial scan spectrum was around 69 deg for the sensor stabilized in buffer solution, while the adsorption of protein to this sensor surface caused the shift of the minimum position by $\delta\theta$. (b) A schematic reflected intensity vs. time curve obtained with the SPR under fixed angle mode

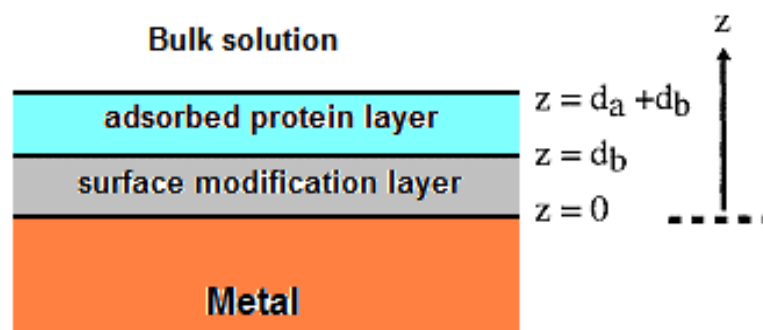


Figure 6.2 The schematic diagram of the bilayer structure of protein adsorption on modified gold surface

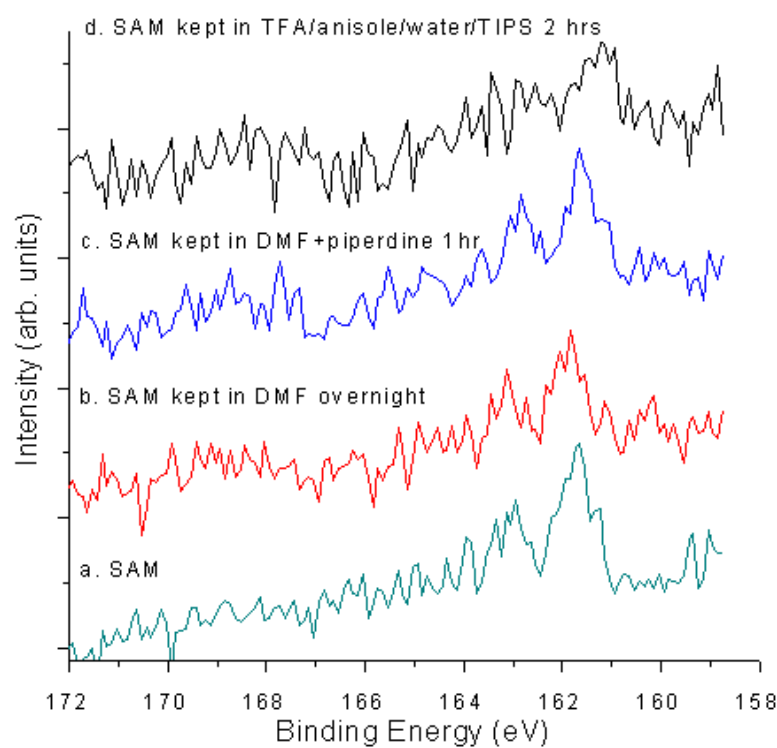


Figure 6.3 The spectrum of narrow scan of sulfur peaks of SAM of $\text{HS}(\text{CH}_2)_{11}(\text{CH}_2\text{CH}_2\text{O})_6\text{NH}_2$ right after preparation (a) after keeping in DMF overnight (b) after keeping in solution for deprotection of Fmoc group for 1 hour (c) after keeping in solution for deprotection of side chains (d)

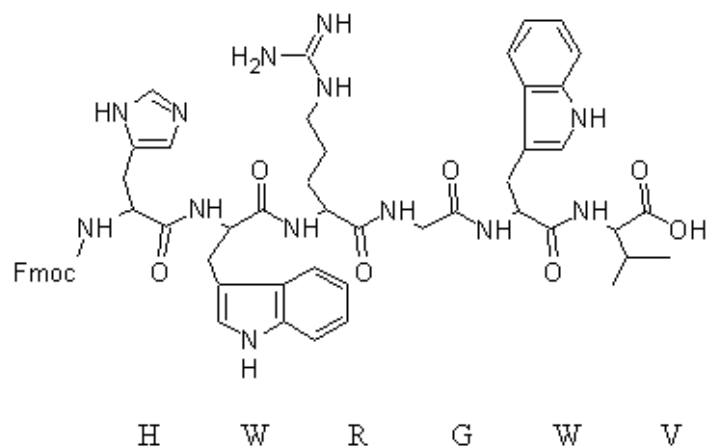


Figure 6.4 Structure of hexamer peptide ligand HWRGWW

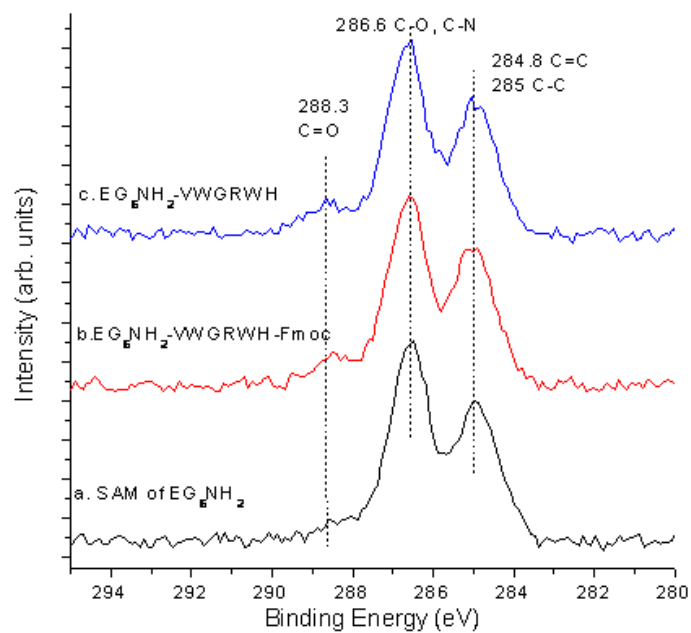


Figure 6.5 The spectrum of C1s narrow scan of the SAM of HS(CH₂)₁₁(CH₂CH₂O)₆NH₂ right after preparation (a) after peptide immobilization (b) after deprotection of Fmoc group (c)

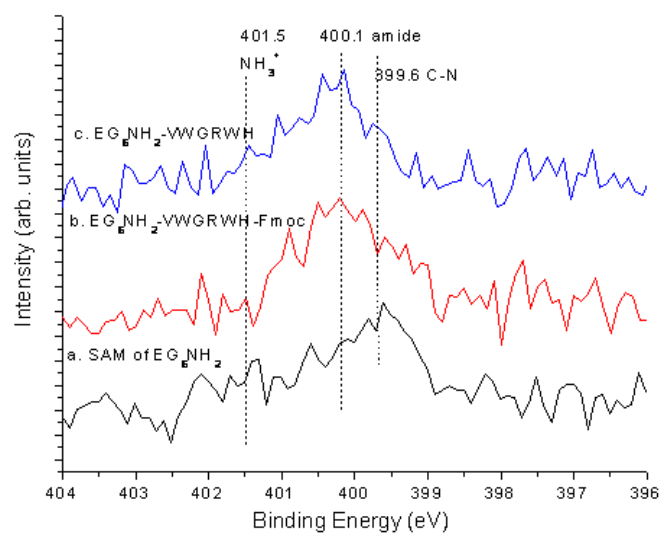
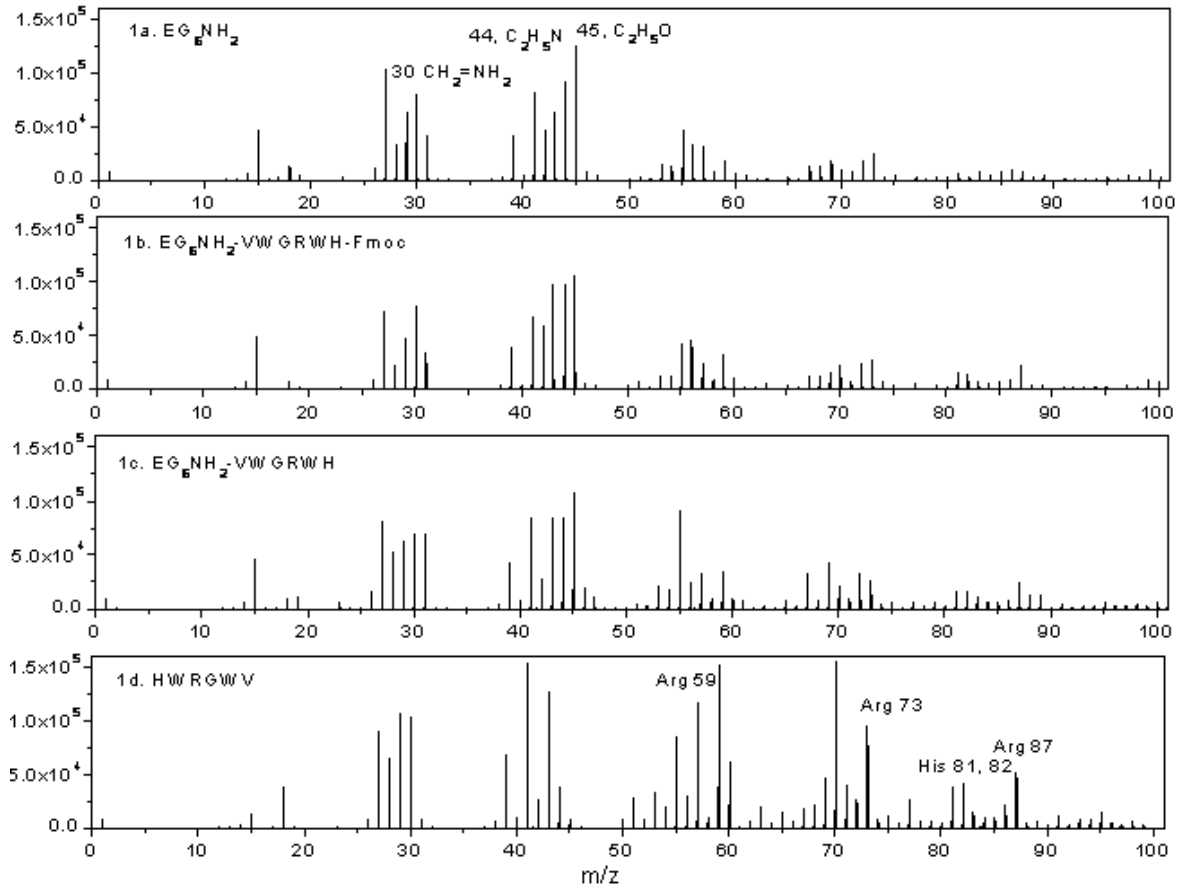
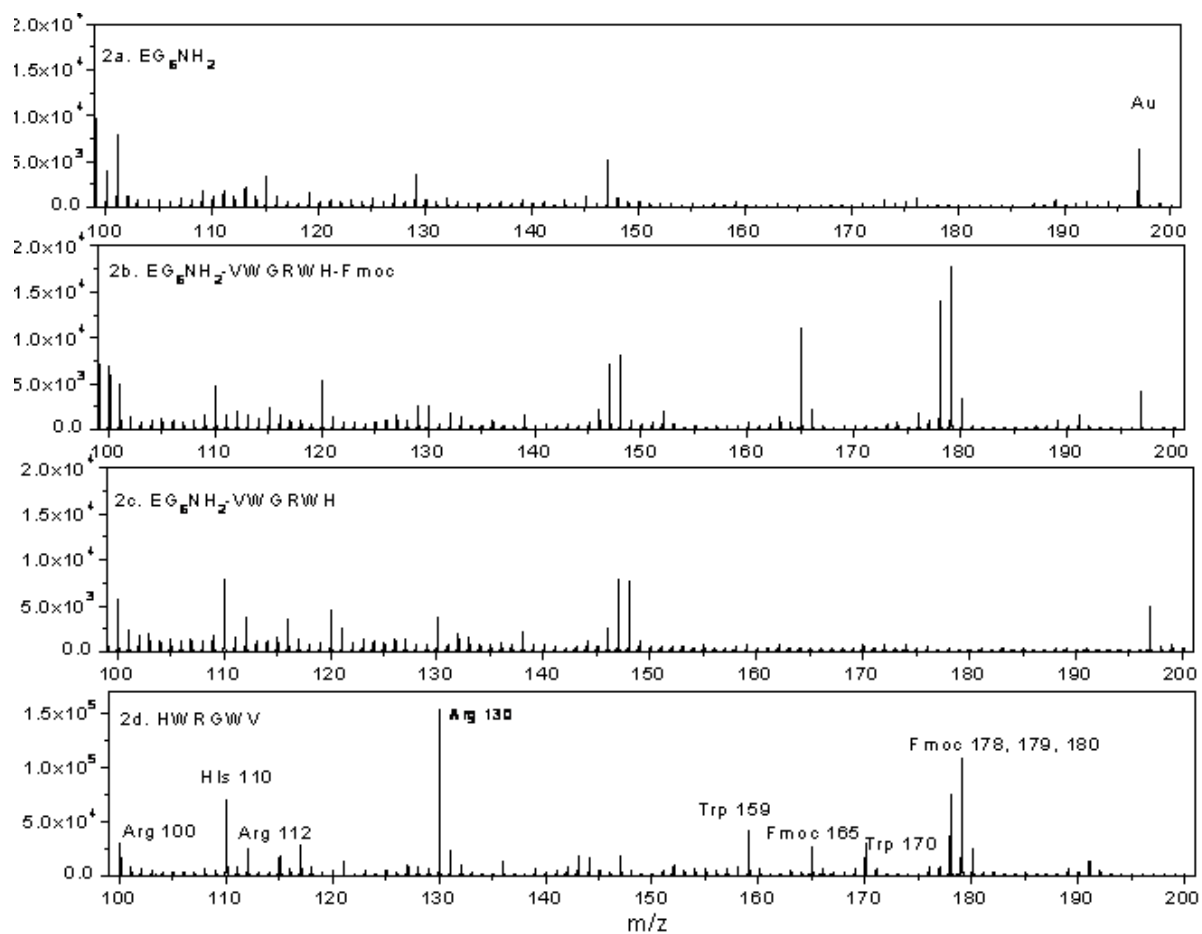
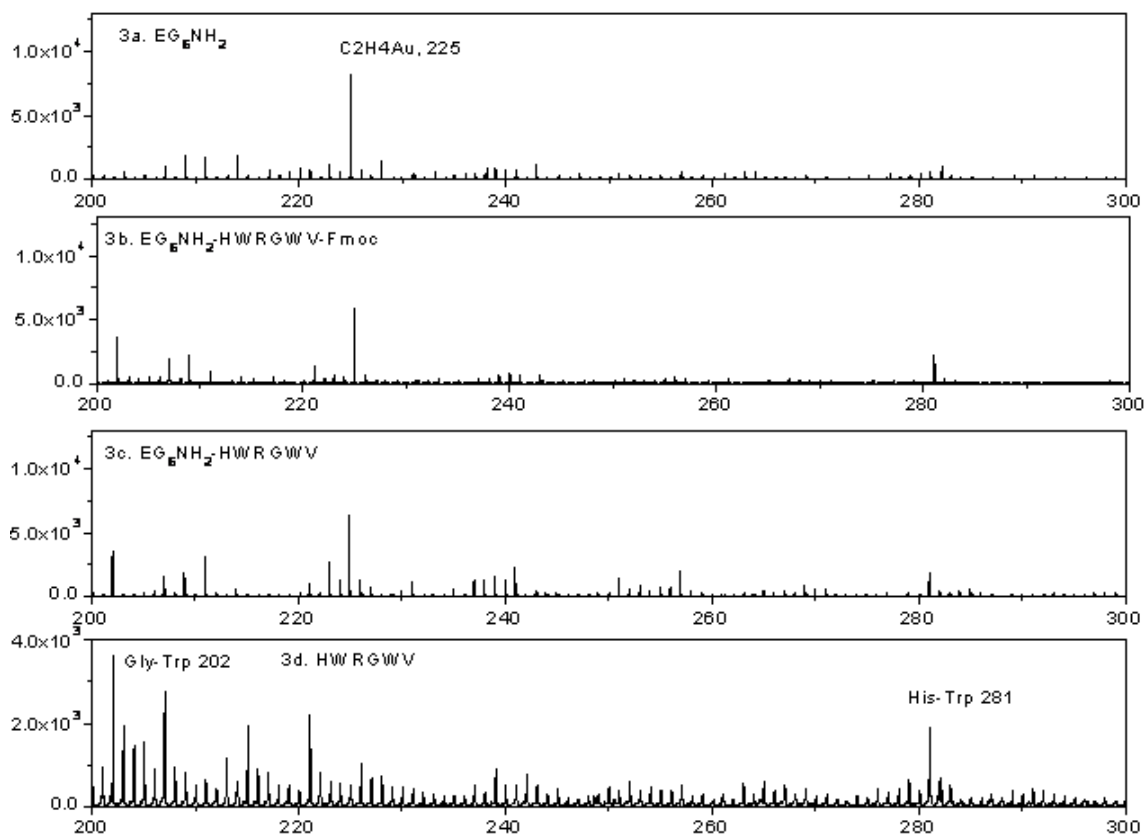


Figure 6.6 The spectrum of N1s narrow scan of the SAM of $\text{HS}(\text{CH}_2)_{11}(\text{CH}_2\text{CH}_2\text{O})_6\text{NH}_2$ right after preparation (a) after peptide immobilization (b) after deprotection of Fmoc group (c)

Figure 6.7 ToF-SIMS spectra of samples SAM of $\text{HS}(\text{CH}_2)_{11}(\text{CH}_2\text{CH}_2\text{O})_6\text{NH}_2$ (a) SAM with the immobilized peptide before deprotection of Fmoc group (b) SAM with the immobilized peptide after deprotection of Fmoc group (c) and pure peptide HWRGWV (d) within the range of m/z 0~100 (1a~1d), 100~200(2a~2d), 200~300 (3a~3d)







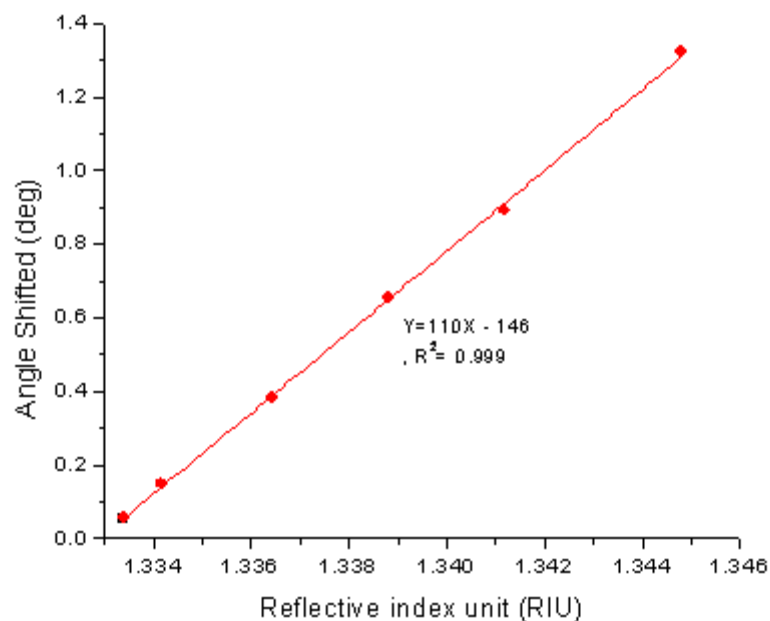


Figure 6.8 SPR calibration curve obtained with the measurement of SPR response to a series of glycerin aqueous solution with concentration range within 0.3~10% (v/v)

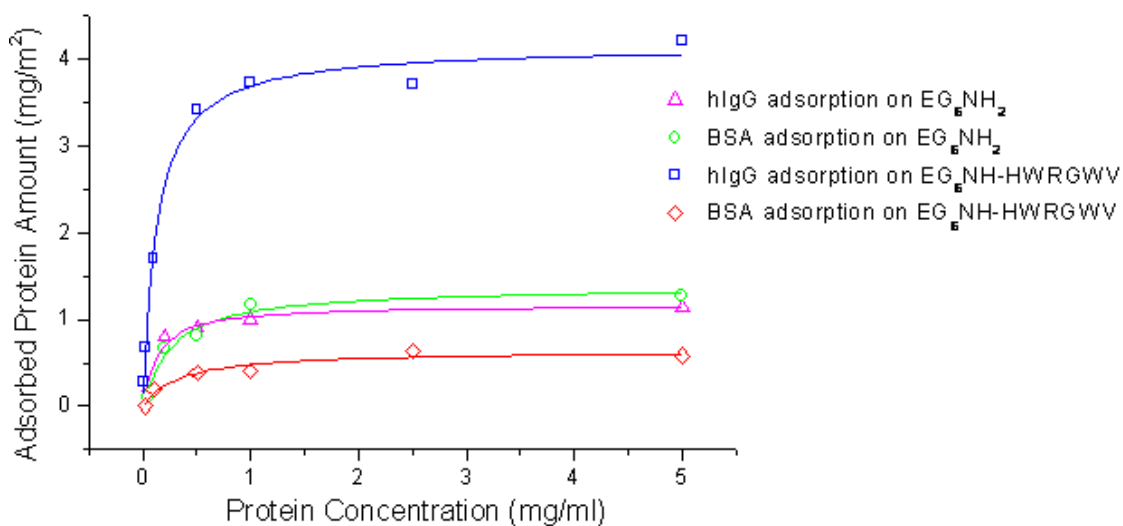


Figure 6.9 Isotherm of hIgG and BSA adsorption from PBS buffer on modified gold with and without peptide obtained by SPR

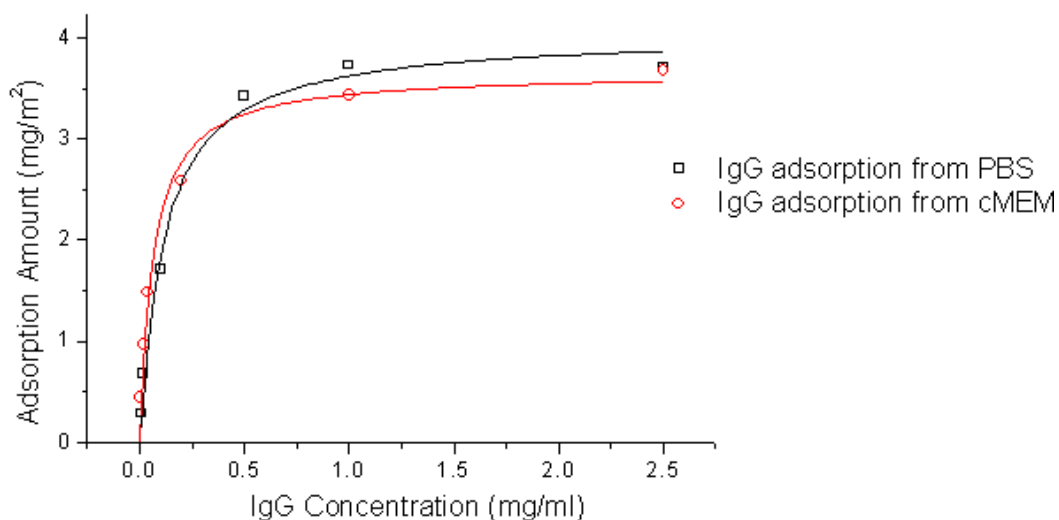


Figure 6.10 Comparing of the isotherm of hIgG adsorption from PBS buffer and that from cMEM by SPR

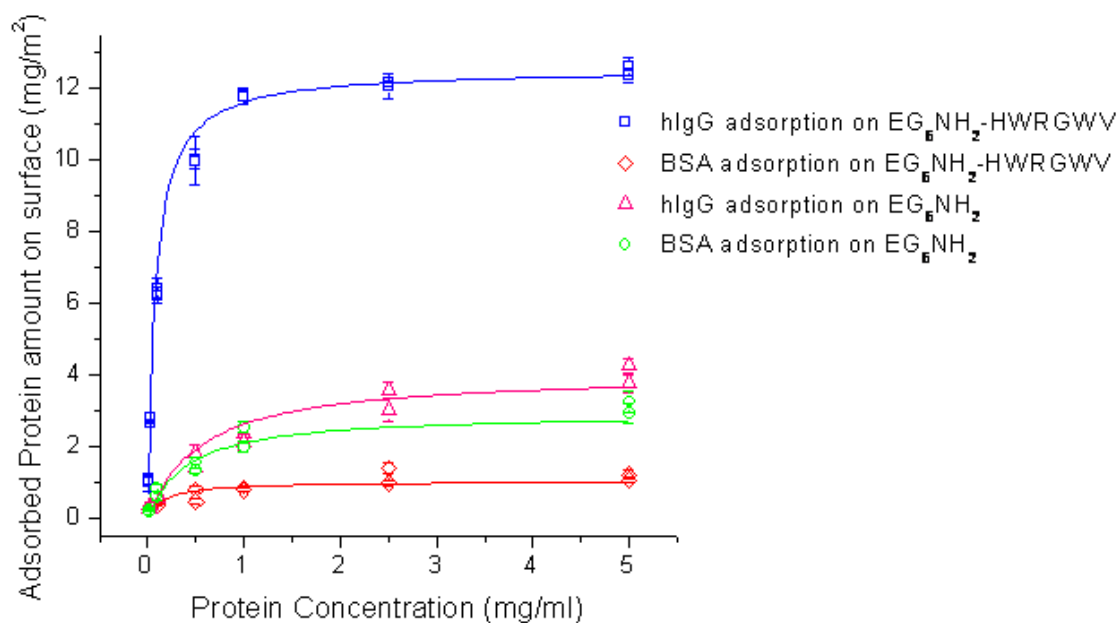


Figure 6.11 Isotherm of hIgG and BSA adsorption on modified gold with and without peptide obtained by QCM; the adsorption amounts were calculated from the average of frequencies changes recorded by 5th, 7th, 9th, 11th, 13th overtones and the error bar indicated the variation coming from difference overtones

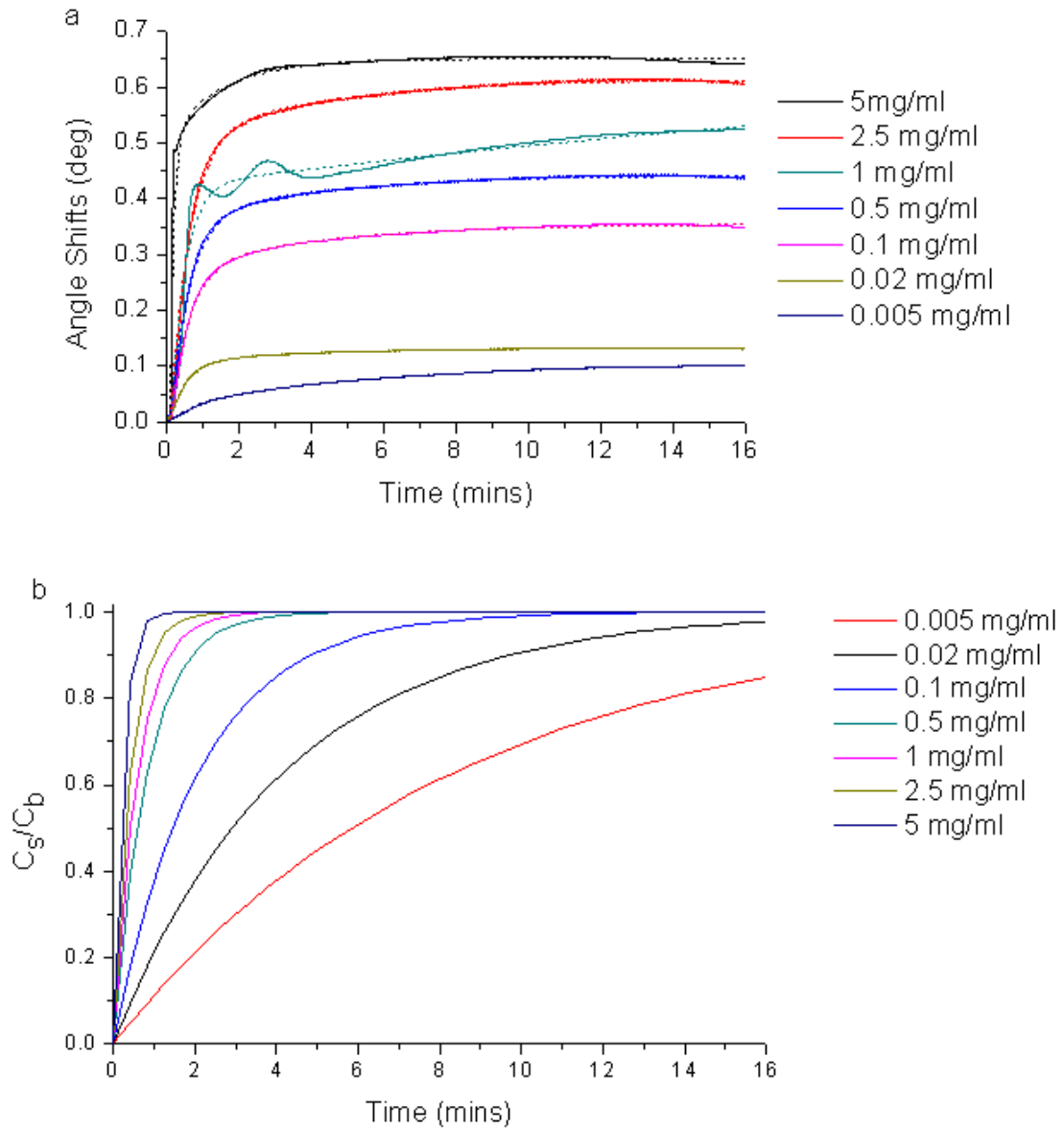


Figure 6.12 Kinetics fitting of hIgG adsorption on SPR sensor modified with peptide HWRGWV. Figure a: SPR response data (solid line) and fitting result (dot line); Figure b: modeling of the normalized protein concentrations close to sensor surface (C_s/C_b)

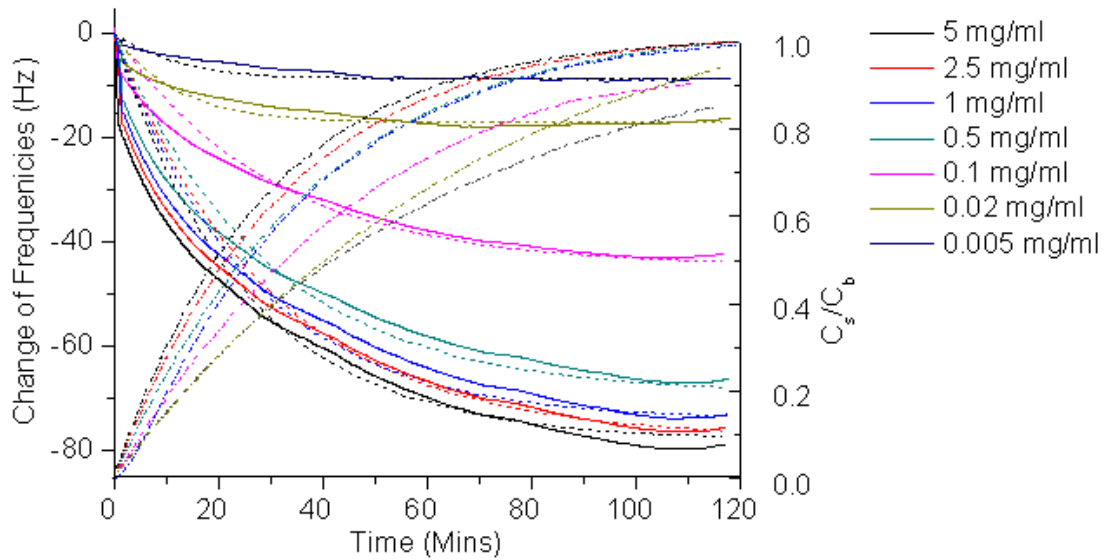


Figure 6.13 Kinetics fitting of hIgG adsorption on QCM sensor modified with peptide HWRGWV. QCM experiment data (solid line), fitting result (dot line) and modeling of the normalized protein concentration close to sensor surface (C_s/C_b)

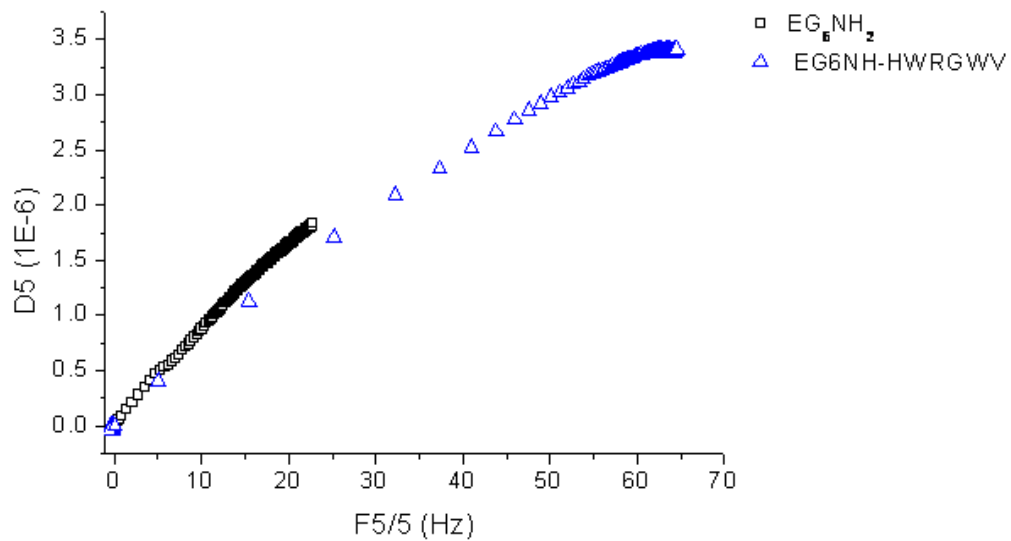


Figure 6.14 Correlation between dissipation ($D5$) and frequency changes ($F5/5$) of hIgG adsorption from 1 mg ml^{-1} solution on top of SAM of $\text{HS}(\text{CH}_2)_{11}(\text{CH}_2\text{CH}_2\text{O})_6\text{NH}_2$ with and without peptide ligand

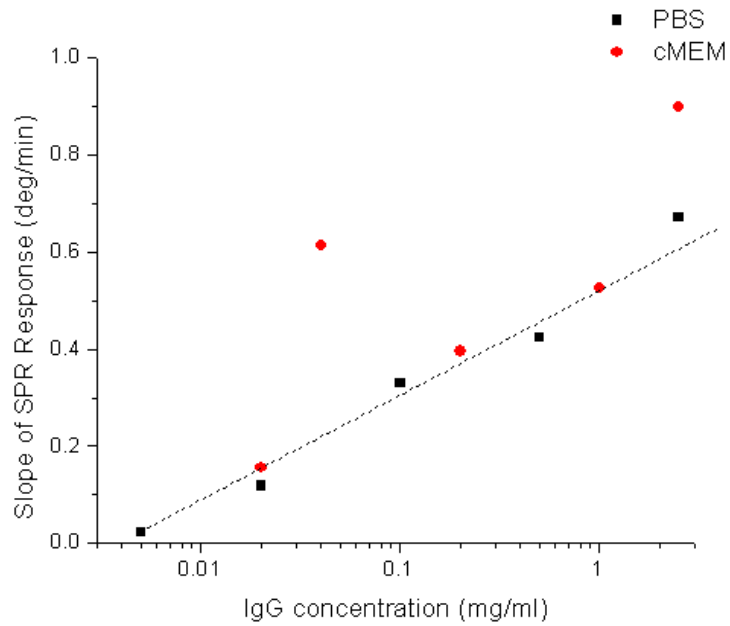


Figure 6.15 The relationship between initial slope of SPR response and hIgG concentrations

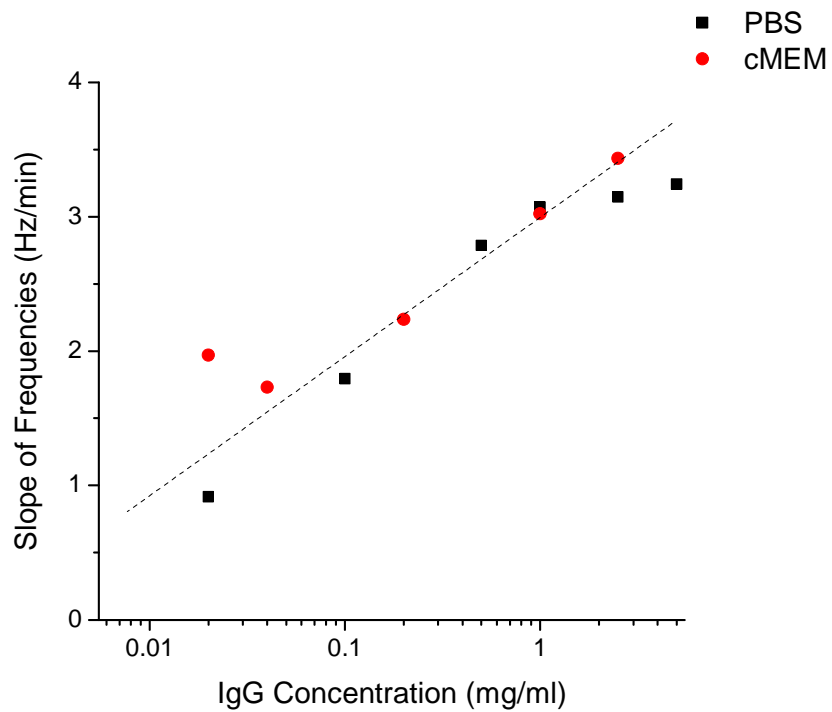


Figure 6.16 The relationship between initial slope of QCM response and hIgG concentrations

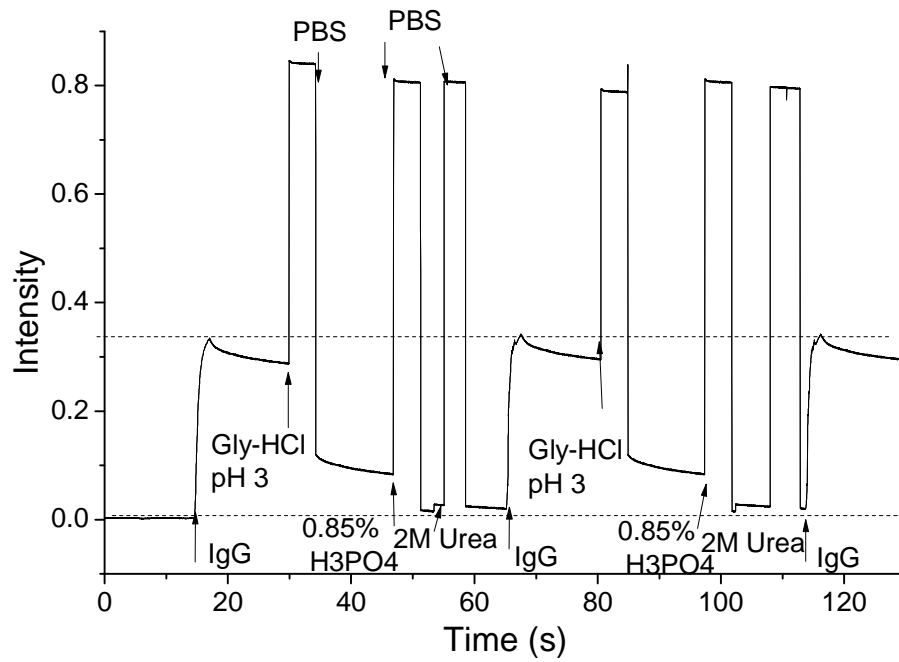


Figure 6.17 Regeneration of peptide functionalized SPR sensor for hIgG detection

Chapter 7. Conclusions and Recommendations for Future Work

7.1 Conclusions

7.1.1 Modification of Silica Surface

A new method is presented to modify silica surfaces with PEG chains terminated with amine groups. This kind of construct can be used to immobilize biomolecules, allowing for its use in fundamental studies of surface interactions between immobilized biomolecules and their targets with low nonspecific binding background. The spectra of time-of-flight secondary ion mass spectroscopy (ToF-SIMS) of the modified surface provided direct evidence that the silica surface was modified as desired. The density of amine groups estimated from thickness measurement by ellipsometry is approximately $2.74 \text{ chains nm}^{-2}$, which is significantly higher than that reported in previous literature similar applications. According to the contact angle titration and ToF-SIMS experiment results, the amine group at the end of PEG chains has higher activity than that at the end of APTES. The PEG chains with only three repeat units can significantly reduce bovine serum albumin (BSA) adsorption on the surface. The adsorption of BSA on the modified surface with PEG termination with free amine groups depends on the pH of the solution since the adsorption process is controlled to a great degree by charge-charge interactions.

7.1.2 Study the Affinity Interaction between Peptide Ligand HWRGWV Immobilized on Silica Surface and Immunoglobulin G (IgG) by Quartz Crystal Microbalance

A Quartz crystal microbalance (QCM) sensor with native silica surface was modified by the same method mentioned above and then hexamer peptide ligand HWRGWV was immobilized on it. The success of immobilization was proven by ToF-SIMS spectra. The

immobilization conditions were optimized. The highest peptide surface density estimated from the thickness measurement by ellipsometer is $0.88 \text{ chains nm}^{-2}$.

As suggested by QCM results, the peptide immobilized on the silica surface has high affinity and specificity to hIgG binding even in a complex medium such as complete mammalian cell culture medium (cMEM). Both thermodynamic and kinetic parameters of affinity interaction were obtained by analysis of QCM data. The dissociation constant, K_d , and the maximum binding capacity, Q_{max} have the values of $0.43 \text{ }\mu\text{M}$ and 14 mg m^{-2} respectively. The absolute values could deviate from true values due to the overestimation of the amount of protein adsorption by QCM. Rough estimates of the association rate constant k_a , and the dissociation rate constant k_d were also presented with evaluation of the effect of mass overestimation from the QCM method.

7.1.3 Modification of Gold Surface

Gold surfaces were modified by oligo(ethylene glycol)-terminated alkanethiols. The formation conditions of self assembled monolayers (SAMs) of $\text{HS}(\text{CH}_2)_{11}(\text{CH}_2\text{CH}_2\text{O})_6\text{NH}_2$ (EG_6NH_2) and $\text{HS}(\text{CH}_2)_{11}(\text{CH}_2\text{CH}_2\text{O})_3\text{OH}$ (EG_3OH) were studied. Ethanol with 3% of triethylene amine was found to be the best solvent for the formation of the SAMs of EG_6NH_2 . Both contact angle measurement and chemical force microscopy (CFM) results indicated that the SAMs of EG_6NH_2 formed by immersing into 1 mM thiol solution with ethanol with 3% of TEA as solvent for 1 day were more uniform than those formed in ethanol or THF for the same formation time. The formation of SAMs of EG_3OH is not as sensitive to the solvent conditions. Mixed SAMs of EG_6NH_2 and EG_3OH were formed under the best conditions for the formation of pure SAM. An attempt was made to quantify the amine group density on the

surface by radio labeling the amine group with [^{14}C]-formaldehyde, analyzing the XPS survey and narrow scan results. None of these methods were suitable for the quantization of amine group density. The CFM scan result indicated that no phase separation was present in the mixed monolayers on a scale of 10 nm when they were formed in ethanol with 3% of TEA. The uniform and even distribution of amine groups in the mixed SAM is favorable for the immobilization of peptides.

7.1.4 Study the Affinity Interaction between Peptide Ligand HWRGWV Immobilized on Gold Surfaces and IgG by Quartz Crystal Microbalance and Surface Plasmon Resonance

The gold surfaces of both QCM and surface plasmon resonance (SPR) sensors were modified with SAMs of EG_6NH_2 and the peptide ligand HWRGWV was immobilized using the best conditions obtained with silica surface modification experiments. The success of the peptide immobilization step was evident from the ToF-SIMS spectra of X-ray photoelectron spectroscopy (XPS).

Both SPR and QCM results showed that this hexamer peptide immobilized on gold surface has high affinity and specificity to hIgG adsorption even in complex media such as cMEM. Thermodynamic and kinetic parameters of this affinity interaction were obtained by the analysis of static and dynamic QCM and SPR data. The estimated values of Q_{max} and K_d by QCM in this study are close to those obtained with silica surface experiments discussed before and again the existence of mass adsorption overestimation lead to divergence from reasonable values. The estimated value of Q_{max} (4.15 mg m^{-2}) by SPR is close to that of chromatography resins with the same peptide ($4.3 \sim 5.3 \text{ mg m}^{-2}$, variable with peptide density)

and the K_d value (1.83 μM) from SPR experiment is also within the range of that obtained with chromatography resin (0.95~30 μM , vary with peptide density). The kinetic parameters obtained from the fitting of the kinetics model to SPR data is more reliable than those obtained with QCM data. The QCM parameters exhibit relatively large deviations between fitting lines and experiment data, and the association rate constants showed a strong dependence on hIgG concentration. The association and dissociation rate constants estimated by SPR have the values of $0.68 \text{ m}^3 \text{ mol}^{-1} \text{ s}^{-1}$ and $1.24 \times 10^3 \text{ s}^{-1}$ respectively, which are similar orders to those obtained with chromatography techniques for other peptide ligand and protein affinity interactions (1). Finally, the feasibility of using the peptide functionalized SPR and QCM sensors to quickly determine IgG concentration from the initial slopes of the system response was proven.

7.2 Recommendations for future work

7.2.1 Characterization of the Peptide Ligands

In this thesis, the methods for peptide characterization with QCM and SPR were developed and applied to probe the affinity interaction between the hexamer peptide ligand HWRGWV and hIgG under one condition (room temperature for SPR experiment or 25 °C for QCM experiment, PBS buffer, pH 7.4). In order to deepen the understanding of affinity interaction between this peptide and IgG, the variation of adsorption behavior with solvent environment need to be quantified by the same methods. The binding temperature has a direct relation with the binding mechanism, with hydrophobic interactions increasing as temperatures increase, and ionic interactions decreasing as temperature increases, the

determination of binding isotherms at various temperatures can provide some insight into the binding mechanism between the modified surfaces and the target proteins (2). These temperature-dependent isotherm measurements will provide an opportunity to determine the change in free energy of adsorption, as well as the change in entropy and enthalpy of adsorption (3). In addition, the effects of pH and ionic strength on affinity interaction will also help to understand the affinity interaction nature of the ligand-protein adsorption mechanism (3). Increasing ionic strength can enhance hydrophobic interaction and reduce ionic interactions. The change of pH directly affects ionization of charged residues on both peptide ligand and target protein. The sensitivity to the change of pH is an index of the contribution of ion charge-charge force in the affinity interaction. All these studies will provide information to improve previous molecular docking calculations using the HADDOCK software. Finally, ligand density can also affect the interactions between the peptide ligands and the target protein. Previously studies with chromatography resin indicated that the affinity and specificity depended on peptide density (4). Peptide density can be controlled by using the two components of SAMs on gold surfaces: EG₆NH₂ and EG₃OH. Variation of the ratio of EG₆NH₂ and EG₃OH in thiol solution for the formation of SAM can lead to different densities of amine group for peptide immobilization. XPS could be used to probe the change of peptide density with the variation of amine group density.

7.2.2 Application of the Biosensor Functionalized with Fc-specific Binding Peptide Ligand

As shown in Chapter 6, the IgG concentration could be quickly determined from the initial slope of SPR signals. The peptide-functionalized surface can be regenerated by a

combination of 0.85% H₃PO₄ and 2 M urea. However, the peptide based biosensor still need to be tested further for stability, sensitivity and repeatability under various conditions to proven its capability to be an alternative method for IgG concentration determination for the application of process analysis and control as well as medical diagnostics. These studies should include comparisons of the HWRGWV ligand to immobilized protein A and capture of hIgG from mammalian cell culture media in order to provide a more realistic scenario for biosensor performance.

Fc-specific binding peptide ligand can not only capture IgG, but also orient IgG on solid surfaces to leave the fraction of the IgG molecule responsible for interaction with its epitope free to react. As mentioned in Chapter 2, the right orientation of IgG is critical for the sensitivity and repeatability of immunosensor (5-9). The performance of immunosensor based peptide ligands HWRGWV should be compared with that based on other IgG affinity ligands for antigen detection. Previously, a similar study was reported by Jung and his colleagues for the detection of C-reactive protein using SPR sensor with oriented IgG by three IgG affinity ligands, including, linear peptide ligand HWRGWV, branched peptide (GTT)₄K₂KG (TG19318) and cyclic peptide, DCAWHLGELVWCT (10). Unfortunately, Jung and his colleagues added glycine at the N terminal end and Serine at C terminal end of this linear peptide ligand HWRGWV in their study and they claimed that this peptide cannot capture IgG well under the experiment condition applied in their study. In fact, Yang emphasized early that the binding strength of the peptide ligand HWRGWV to HIgG depends on the entire sequence of the peptide and the histidine side chain plays a very important role in the protein-ligand interaction (11). Any variation, especially those blocking

the histidine at the N-terminal could greatly reduce the affinity to IgG binding. Although Jung and his colleagues' conclusion on the peptide ligand HWRGWV is incorrect, their work demonstrated that antibodies captured by the peptide ligand had higher antigen binding capacity compared with randomly immobilized antibodies. In future work, the peptide ligands HWRGWV should be compared with protein A or protein G and ligands such as A2P, TG19318, for IgG oriented immobilization for the application of immunosensor and the effects of anchor ligands on the stability, sensitivity and repeatability we be studied systemically.

7.2.3 Application of the methodology developed in this study for the study of other peptide ligand

The surface modification, peptide immobilization, QCM and SPR data analysis methods developed in this research could be applied to the studies of other peptide ligands identified in our group, which may provide an alternative perspective and addition information for the understanding the affinity interaction between these peptide ligands and their target biomolecules.

References:

1. Wang GQ & Carbonell RG (2005) Characterization of a peptide affinity support that binds selectively to staphylococcal enterotoxin B. *Journal of Chromatography A* 1078(1-2):98-112.
2. Gunter Z & Sherma J (1973) *CRC handbook of chromatography: general data and principles* (CRC Press, Inc., Boca Raton, Florida) p 89.

3. Wang G, Salm JR, Gurgel PV, & Carbonell RG (2005) Small peptide ligands for affinity separations of biological molecules. *Chemical Engineering*, eds Gal'an MA & del Valle EM (John Wiley & Sons, Ltd., New York, NY).
4. Yang H, Gurgel PV, & Carbonell RG (2009) Purification of human immunoglobulin G via Fc-specific small peptide ligand affinity chromatography. *Journal of Chromatography A* 1216.
5. Cha T, Guo A, Jun Y, Pei DQ, & Zhu XY (2004) Immobilization of oriented protein molecules on poly(ethylene glycol)-coated Si(111). *Proteomics* 4(7):1965-1976.
6. Caruso F, Rodda E, & Furlong DN (1996) Orientational aspects of antibody immobilization and immunological activity on quartz crystal microbalance electrodes. *Journal of Colloid and Interface Science* 178(1):104-115.
7. Lu B, Smyth MR, & Okennedy R (1996) Oriented immobilization of antibodies and its applications in immunoassays and immunosensors. *Analyst* 121(3):R29-R32.
8. Lu B, Xie JM, Lu CL, Wu CG, & Wei Y (1995) Oriented immobilization of Fab' fragments on silica surfaces. *Analytical Chemistry* 67(1):83-87.
9. Rao SV, Anderson KW, & Bachas LG (1998) Oriented immobilization of proteins. *Mikrochimica Acta* 128(3-4):127-143.
10. Jung Y, *et al.* (2008) Controlled antibody immobilization onto immunoanalytical platforms by synthetic peptide. *Analytical Chemistry* 274(99-105).
11. Yang H, Gurgel PV, & Carbonell RG (2005) Hexamer peptide affinity resins that bind the Fc region of human immunoglobulin G. *Journal of Peptide Research* 66:120-137.